Geosynthetics '99

"Specifying Geosynthetics and
Developing Design Details"

GEOSYNTHETICS
99
CONFERENCE
Boston, Massachusetts USA

Conference Proceedings

April 28-30, 1999

Organized by:

IFAI
Industrial Fabrics Association International

NAGS
North American Geosynthetics Society

GMA
Geosynthetic Materials Association

under the auspices of
IGS
International Geosynthetics Society

Table of Contents

PERFORMANCE OF TWO MUNICIPAL SOLID WASTE LANDFILL COVERS

CYNTHIA A. FINLEY
UNIVERSITY OF TEXAS AT AUSTIN
USA

ROBERT D. HOLTZ
UNIVERSITY OF WASHINGTON
USA

ABSTRACT

The conditions of the components of two municipal solid waste landfill covers were observed by excavating test pits in the covers. Soil and geotextile samples were obtained for laboratory testing. The drainage layer soils were found to generally meet granular filter criteria for the overlying vegetative soil, indicating that a geotextile filter was not strictly necessary. Although the permittivity of the geotextile filters had decreased since the time of installation, the permittivities were generally still high enough to meet geotextile filter criteria.

The finite difference code FLAC (Fast Lagrangian Analysis of Continua) was used to model differential settlements in the landfill covers. Relationships between settlement characteristics and the resulting geomembrane strain were developed, then used to evaluate two areas of differential settlement in the landfill covers. The geomembrane strains were found to be below yield strains. A general design method for other cover conditions was also developed with FLAC.

INTRODUCTION

When municipal solid waste landfills are closed, a final cover must be placed over the waste. The primary purposes of a final cover are to control the runoff of surface water into drainage facilities and minimize the infiltration of water into the waste, which reduces the amount of leachate produced by the landfill. The cover also controls waste odors, keeps vectors such as birds and rodents out of the waste, and provides an aesthetically pleasing appearance to the landfill.

Modern landfill covers generally consist of five layers that serve specific purposes. The first layer above the waste is a gas collection system which controls the movement of waste-produced gases. Above this is a barrier to prevent infiltration of water into the waste, then a drainage layer to prevent water build-up on the barrier. A protective layer of soil covers the

drainage layer, and a cover soil provides a medium for vegetative growth. Typically, geomembranes are used in the barrier layer, and geotextiles are used as a filter above the drainage layer.

Since the use of composite covers containing geosynthetics is relatively recent, the long-term performance of these covers is not yet fully understood. Potential problems exist that could impair the performance of cover components. The geotextile filter or drainage layer may become clogged, leading to instability of the cover slopes. Damage to the cover components - especially the geosynthetics - may result from differential settlement of the landfill waste. Although the settlement behavior of municipal solid wastes has been studied extensively, there has been little research into the effects of these settlements on the cover components.

This research is a follow-up to Reitz (1995) and Reitz and Holtz (1997). Additional details about this research may be found in Finley (1997).

DESCRIPTION OF LANDFILLS

Two landfills were selected for this study, the Purdy Landfill and the Hidden Valley Landfill, both located in Pierce County, Washington. These landfills were chosen because final composite covers utilizing soil, geotextiles, and geomembranes existed over the Purdy Landfill and portions of the Hidden Valley Landfill. Also, differential settlements of waste have occurred at both landfills, requiring some portions of the final covers to be replaced.

The 6.1-ha Purdy Landfill began receiving municipal solid waste in 1960. Filling ceased in 1989, when a temporary geomembrane cover was placed over the landfill. Construction of the final cover began in March 1990 and was completed in September 1990. Waste filling began at the 29.1-ha Hidden Valley Landfill in the mid-1960s. Construction of a final cover over one portion of the landfill, the North Area Closure, began in June 1989 and was completed in October 1989. A final cover was constructed over another portion of the landfill, the Southwest Closure, in 1992. Other areas of the landfill are still active.

According to design specifications and construction reports, the final covers of both landfills consist, from the waste up, of a 10-cm to 30-cm sandy foundation layer, a 1.5-mm (60-mil) high-density polyethylene (HDPE) geomembrane, a 30- to 46-cm sand or gravel drainage layer, a nonwoven, polypropylene, heat-bonded geotextile filter, a 20- to 30-cm sandy vegetative soil layer, and topsoil.

Before the final cover was constructed on the Purdy Landfill, the northeastern portion of the landfill was filled quickly so that the construction could begin. The waste in this area was not compacted well and did not experience much settlement under its own weight before the cover was placed over it. However, large settlements later occurred in this area, requiring the construction of a new final cover on this part of the landfill. No measurements of the settlements were available. Dense fill, consisting of sand with some gravel and fines, was

placed over this portion of the landfill to bring it back to the original required foundation grade for the cover and to induce further settlement of the waste before construction of the new cover. At the time of the field investigation, the dense fill was in place and construction of the new cover was ready to begin.

The southern portion of the Purdy Landfill cover has experienced differential settlements that have not been severe enough to require cover repairs. No information is available regarding the magnitude of these settlements.

The settlements experienced at the Hidden Valley Landfill were found by comparing the contours of the final grading plan with those of an aerial survey conducted in May 1995. The total settlement of the North Area Closure was approximately 0.3 to 0.6 m, while differential settlements ranged from 0.6 to 1.5 m. In the Southwest Closure portion of the landfill, total settlements were approximately 0.5 to 0.9 m, and differential settlements ranged from 0.6 to 1.2 m. In the southwestern portion of this cover, the slope in one area was reduced in inclination from 4.2:1 to 6.2:1. The cover in this area was subsequently replaced in early 1996.

FIELD INVESTIGATIONS

A total of eight test pits were excavated, with two test pits in each landfill cover section. The test pits were excavated in May and July of 1996. Test Pits 1 through 4 were excavated at the Purdy Landfill, with Test Pits 1 and 2 located in the northeastern portion where excessive settlements had occurred and Test Pits 3 and 4 located on the southern slope where smaller differential settlements had occurred. Test Pits 5 and 6 were located in the North Area Closure of the Hidden Valley Landfill, and Test Pits 7 and 8 were located in the Southwest Closure. Test Pits 5, 6, and 7 were in areas where differential settlements had occurred, and Test Pit 8 was in the area where settlement problems necessitated a new cover in 1996.

The procedure for excavating test pits followed the procedure used in Reitz (1995) and Reitz and Holtz (1997). Photographs were taken during the excavation and the conditions found were recorded. Disturbed samples were taken of the topsoil, the top of the vegetative soil layer, and the bottom of the vegetative soil layer immediately above the geotextile filter. The condition of the geotextile was observed and a sample was cut from it. Samples of the drainage layer soils were taken from immediately below the geotextile and immediately above the geomembrane. The geomembrane was uncovered, if possible, and its condition observed. If the geomembrane could not be uncovered, the second sample of the drainage layer was taken at the maximum excavation depth.

LABORATORY TESTING

Water content and grain size analyses were performed on each soil sample in accordance with ASTM D 2216 and ASTM D 422, respectively. The water content was determined in order to develop soil-moisture profiles of the landfill covers. The grain size analyses were used to

classify the soils, to evaluate the filtering capability of the drainage materials, and to determine if the drainage layers had become clogged since construction of the landfill covers.

Permittivity tests were conducted on each geotextile sample to determine the degree of clogging that had occurred since installation. The tests were performed in general accordance with ASTM D 4491, although a different permeameter was used as allowed by the standard. The permeameter and testing procedure are described in Christopher and Holtz (1985).

RESULTS

Field Observations

In Test Pits 1 through 4, excavated at the Purdy Landfill, the field conditions of the covers were similar to the conditions outlined in the construction reports. However, the thicknesses of the soil layers in the field were much greater than those given in the reports, probably due to inaccuracies in the construction process. The geotextiles in these test pits appeared somewhat clogged with fine-grained sand, especially in Test Pits 1 and 2. Permittivity tests were subsequently conducted to supplement this visual observation of geotextile clogging. The geotextiles in Test Pits 1 and 2 also had more noticeable indentations from the drainage layer than those in Test Pits 3 and 4, probably due to the additional fill placed over the northeastern portion of the cover. No rips or tears were evident in the geotextiles, but they appeared to be blinded by a thin layer of fine sand covering the surface. The geomembrane uncovered in Test Pits 1 and 2 was covered with a thin layer of wet, fine-grained soil and did not appear damaged. Caving of the drainage layers prevented the excavation of Test Pits 3 and 4 from extending all the way to the geomembrane.

The field conditions encountered in Test Pits 5 through 8, excavated in the Hidden Valley Landfill, were quite different from those specified in the construction reports and design specifications. The vegetative layers were thicker than specified, and cobbles in Test Pits 5, 6, and 7 far exceeded the maximum particle size specified for that layer. The drainage layers found in the field, although free-draining as required, consisted of sandy gravel instead of the specified sand with some small gravel. In Test Pits 5, 6, and 7, the geotextile did not appear damaged or clogged, although some fine-grained soil particles were embedded near the surface. Only a very small amount of fine-grained soil particles were embedded in the geotextile in Test Pit 8. Caving occurred in the drainage layers of all the test pits in the Hidden Valley Landfill, so the geomembrane could not be uncovered in any of the test pits.

Drainage Layer Clogging

In order to determine if the drainage layers had experienced clogging, three criteria were used. All three criteria were based on the results of the grain size analyses conducted on the samples taken from the top and bottom of the drainage layers. First, the gradations of the samples from the top and the bottom of the drainage layer were compared. If the gradations

were similar, then either no clogging was indicated or the drainage layer was clogged equally throughout its depth. Second, the grain size distributions of the samples were compared to the gradation specifications and conformance tests for the drainage layers to see if any changes in gradation had occurred. Third, the hydraulic conductivity of the drainage layer soils was estimated with Hazen's approximation and compared to the hydraulic conductivity specifications. This final criteria is probably the most important, since it indicates how well the drainage soil is performing its design function.

The results of the drainage layer clogging analysis are summarized in Table 1. In all test pits where drainage layer samples were available from both the top and bottom of the layer, the gradations at each location were similar. Clogging was therefore not indicated with this criteria. Conformance tests confirmed that the drainage layer soils met the specifications at the time of construction. The drainage layer samples were found to still meet the gradation specifications, except that the maximum specified particle size in the Southwest Closure of the Hidden Valley Landfill was exceeded. However, the amount of fine particles remained within the specification of 0 to 3 percent fines, so clogging was not indicated. The conformance test results for the hydraulic conductivity of the drainage layer soils for the Purdy Landfill ranged from 0.1 to 0.3 cm/s, and a minimum hydraulic conductivity of 0.1 cm/s was specified for the Hidden Valley Landfill covers. The estimated values were all above the specified and conformance test values, indicating that no measurable clogging had occurred.

Geotextile Clogging

The procedure used for determining geotextile clogging followed that of Metcalfe, Holtz, and Allen (1995) and Reitz and Holtz (1997). Specimens from the undisturbed geotextiles were

Table 1 – Summary of drainage layer clogging criteria analysis.

Landfill	Test Pit Location	Test Pit Number	Sample Location within Layer	Comparable Gradations within Layer?	Generally Meets Gradation Specs?	Estimated Hydraulic Conductivity (cm/s)	Meets Hydraulic Conductivity Specs?
Purdy	northeastern area	1	top	N/A	yes	2.0	yes
		2	top	yes	yes	0.6	yes
		2	bottom		yes	7.3	yes
	southern area	3	top	yes	yes	2.6	yes
		3	bottom		yes	0.8	yes
		4	top	N/A	yes	3.2	yes
Hidden Valley	North Area Closure	5	top	yes	N/A	4.4	yes
		5	bottom		N/A	4.4	yes
		6	top	yes	N/A	N/A	N/A
		6	bottom		N/A	4.4	yes
	Southwest Closure	7	top	yes	yes	9.0	yes
		7	bottom		yes	4.4	yes
		8	top	N/A	yes	2.0	yes

subjected to five successive permittivity test runs. The specimens were then washed to remove soil particles and subjected to another five permittivity test runs. The increase in permittivity between the washed and unwashed specimens was used to measure the degree of clogging of the geotextile that had occurred since the time of installation.

Four test specimens were cut from the geotextile sample taken from each test pit. Each unwashed specimen was subjected to five successive permittivity test runs to find the approximate permittivity of the undisturbed geotextile in the field. The specimens were then hand washed to remove as much of the soil as possible, then subjected to another five successive permittivity test runs to approximate the original permittivity of the geotextile.

In all but three cases, the first test run of the unwashed specimen gave the lowest permittivity value, with the values increasing for each successive run. Generally, the washed permittivity values were very similar for each test run. Patterns of increasing permittivity for unwashed geotextiles and constant permittivity for washed geotextiles were also found by Metcalfe (1993), Metcalfe, Holtz, and Allen (1995), Reitz (1995), and Reitz and Holtz (1997). As water flows through the geotextile specimens during the unwashed permittivity tests, the soil particles dislodge and the geotextiles approach a washed condition. This was evident not only in the permittivity values but also in the appearance of the specimens before and after the five unwashed test runs. The permittivity found with the first test run is therefore the most appropriate approximation of the undisturbed geotextile condition.

The average permittivity values of the specimens tested from each test pit are shown in Figure 1. The average of the first test runs of the unwashed geotextile specimens are compared
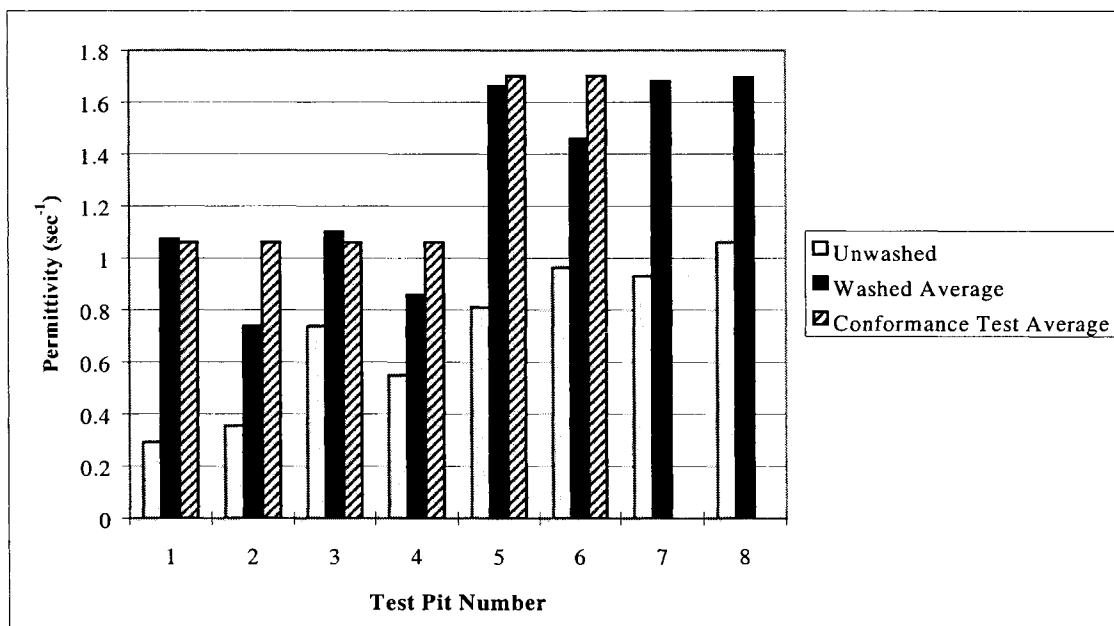

Figure 1 – Average permittivity test results for each test pit.

to the washed permittivity averages and the conformance test averages. (No design specifications or conformance test values were available for the permittivities of the geotextiles used in the Southwest Closure of the Hidden Valley Landfill, where Test Pits 7 and 8 were located.) Since the permittivities of the unwashed samples, representing the field conditions, are lower than the permittivities of the washed tests and the conformance tests, it appears that the geotextile permittivity has decreased in the field since the time of installation, possibly due to clogging.

Granular Filter Analysis

The Terzaghi (1922) granular filter criteria were applied to the results of the grain size analyses in order to determine if the drainage layer would adequately act as a granular filter for the vegetative soil. The grain size information from the samples taken nearest the geotextile, which were the samples from the bottom of the vegetative layer and the top of the drainage layer, were used in the analysis. With the Terzaghi criteria, the $D_{15, filter}/D_{85, soil}$ must be less than 4 to 5 for retention of the soil and the $D_{15, filter}/D_{15, soil}$ must be greater than 4 to ensure that the hydraulic conductivity of the filter will be greater than that of the overlying soil.

The results of the granular filter criteria are shown in Table 2. The drainage layer soils qualified as filters for the vegetative soil in Test Pits 1 through 4, all located at the Purdy Landfill. Of the test pits located at the Hidden Valley Landfill, only Test Pit 6 met both filter criteria. For the other test pits, the soil samples taken from the bottom of the vegetative layer and the top of the drainage layer had very similar grain size distributions, especially for grain sizes less than 10 mm. Although the drainage layer soils met the criterion for retention, the hydraulic conductivity was not sufficiently greater than that of the vegetative soil to qualify as a granular filter. However, the hydraulic conductivity of the drainage layer soils in these test pits was estimated to range from 2.0 to 9.0 cm/s. This hydraulic conductivity should be high enough to insure that no hydraulic pressure builds up in the vegetative soil layer, therefore satisfying the intent of the permeability criterion.

Table 2 – Summary of granular filter analysis for retention and clogging resistance criteria.

Landfill	Test Pit Location	Test Pit Number	D_{15} filter/ D_{85} soil	Retention criterion met?	D_{15} filter/ D_{15} soil	Permeability criterion met?
Pur	northea	1	0.2	yes	10.7	yes
	area	2	0.1	yes	6.8	yes
	souther	3	0.1	yes	10.8	yes
	area	4	0.2	yes	10.4	yes
Hid	North	5	0.2	yes	1.1	no
Vall	Closure	6	0.3	yes	56.4	yes
	Southw	7	0.1	yes	0.8	no
	Closure	8	0.1	yes	2.5	no

Geotextile Filter Analysis

The Christopher and Holtz (1985) and Holtz, Christopher, and Berg (1995) geotextile filter criteria were applied to the geotextiles used in the covers of the Purdy and Hidden Valley Landfills. The results are summarized in Table 3. In the evaluation of the retention and clogging resistance criteria, the grain size distributions of the samples taken from the bottom of the vegetative soil layer were used, since this was the soil immediately above the geotextile. The retention criterion requires that the apparent opening size (AOS) of the geotextile be less than or equal to the coefficient B multiplied by the D_{85} of the overlying soil, where B depends on the coefficient of uniformity, C_u, of the soil. This criterion was met for all the geotextiles for which it could be evaluated. The clogging resistance criterion requires that the AOS be greater than or equal to 3 times the D_{15} of the overlying soil. This criterion was not met for any of the geotextiles for which it could be evaluated.

The geotextile filter criteria require that the permittivity of the geotextile be greater than or equal to 0.5 sec^{-1} for soils with a fines content of less than 15 percent. Despite the apparent clogging that occurred in the geotextiles during their use in the landfill covers, the unwashed geotextiles generally still met this permittivity requirement, as shown in Figure 1. The exceptions were Test Pits 1 and 2, which were located in the northeastern portion of the Purdy Landfill where excessive settlements had occurred and fill had been placed over the cover.

MODELING DIFFERENTIAL SETTLEMENTS WITH FLAC

The computer program FLAC (Itasca Consulting Group, Inc., 1992) was used to model the effects of waste voids beneath composite landfill covers. Relationships between the geomembrane deflection, the strains in the geomembrane, and the settlement patterns of the soil surface were examined for the Purdy and Hidden Valley Landfills. A general design method for composite covers spanning voids was also developed.

Table 3 – Summary of geotextile filter analysis for retention and clogging resistance.

Landfill	Test Pit Number	Specified AOS (mm)	D_{85} (mm)	C_u	B	BD_{85} (mm)	Retention Criterion Met?	$3D_{15}$ (mm)	Clogging Resistance Criterion Met?
Purdy	1	0.15 - 0.21	11	107	1.0	11	yes	0.62	no
	2	0.15 - 0.21	18	6.8	1.0	18	yes	0.75	no
	3	0.15 - 0.21	20	11	1.0	20	yes	0.78	no
	4	0.15 - 0.21	19	10	1.0	19	yes	0.84	no
Hidden Valley	5	0.13 - 0.18	25	1.1	1.0	25	yes	12	no
	6	0.13 - 0.18	20	56	1.0	20	yes	0.33	no
	7	not available	41	0.8	1.3	53	N/A	18	N/A
	8	not available	38	2.5	1.0	38	N/A	4.8	N/A

About the Program

FLAC is a two-dimensional, explicit finite difference code that simulates the behavior of structures made of soil, rock, or other materials that may show plastic flow after their yield limit. The materials are represented as a grid that is formed by elements. The grid may be adjusted to fit the shape of the structure being modeled, and if the large-strain mode of the program is used, the grid deforms as the material moves. A two-dimensional plane strain case is assumed by the program. Interfaces may be specified between portions of the grid to model planes where slip and separation may occur.

The process of running a simulation using FLAC begins with the generation of a grid and adjustments to the grid to form the desired shape for the problem being modeled. The boundary and initial conditions are set, then the constitutive laws and properties of the materials represented by the grid are defined. After the model is brought to initial force equilibrium, alterations may be performed. Types of alterations that may be made include excavating material, applying forces, and changing boundary conditions. The response of the model to these alterations is found by stepping to a solution.

Modeling Procedure

In order to model settlement conditions for the Hidden Valley and Purdy Landfills, it was necessary to determine appropriate material properties to be used in the model for each cover component. These material properties are summarized in Table 4. For the soil layers, the thickness and density were based on observations made during the excavation of the test pits in the covers. The elastic modulus and Poisson's ratio, which were used to calculate the shear modulus and bulk modulus, were estimated using the values suggested by Bowles (1988). For the geosynthetics, the thickness, density, and elastic modulus were based on the average conformance test results contained in the construction reports for the landfills. The values for Poisson's ratio were based on the recommendations of Giroud (1992).

A layer representing the landfill waste was placed beneath the cover components and modeled as a stiff Mohr-Coulomb material with cohesion, which prevented significant further

Table 4 – Properties used in FLAC analysis of Purdy and Hidden Valley Landfill covers.

Component	Material Type	Thickness (m)	Density (kg/m3)	Bulk Modulus (Pa)	Shear Modulus (Pa)	Friction Angle (deg)	Cohesion (Pa)
Topsoil	Mohr-Coulomb	0.2	1350	8.0E+07	2.9E+07	30	0
Vegetative Soil	Mohr-Coulomb	0.98	1600	1.1E+08	3.7E+07	35	0
Geotextile	Elastic	0.0025	105	6.7E+06	2.2E+06	N/A	N/A
Drainage Layer	Mohr-Coulomb	0.68	1800	1.7E+08	5.7E+07	40	0
Geomembrane	Elastic	0.0015	1000	3.7E+08	3.8E+08	N/A	N/A
Waste	Mohr-Coulomb	0.65	2000	5.0E+09	5.0E+09	40	1.0E+10

settlements of the supporting waste. Interfaces between the geosynthetics and the soil were also modeled so that the geosynthetics could move relative to the soil. The friction angle of the interface was assumed to be two-thirds of the friction angle of the neighboring soil.

To represent differential waste settlement in the model, a portion of the waste layer was changed to a null material after initial equilibrium was reached, forming an infinitely long void in the waste. A typical model grid after the void was made is shown in Figure 2. Symmetry of the model was used, so one vertical boundary passed through the center of the void, as shown in Figure 2. The gridpoints on this boundary were allowed to move in the vertical direction, but not in the horizontal direction. Each element of the grid is approximately 0.05 m high, except for the elements of the grid representing geosynthetics, which had a height equal to the geosynthetic thickness. The element width was 0.05 m in the area of the void, gradually becoming wider as the distance from the void increased. The element width could be increased away from the void since the primary area of interest of the model was in the vicinity of the void. The increased element width and the use of symmetry reduced the elements in the grid, therefore reducing the solution time of the model.

Five void widths in the landfill waste were modeled for the average cover conditions of the Purdy and Hidden Valley Landfills. The void widths modeled were 1.0, 1.5, 2.0, 2.5, and 3.0 m, and each void was infinitely long. After the void was placed in the waste, the response of
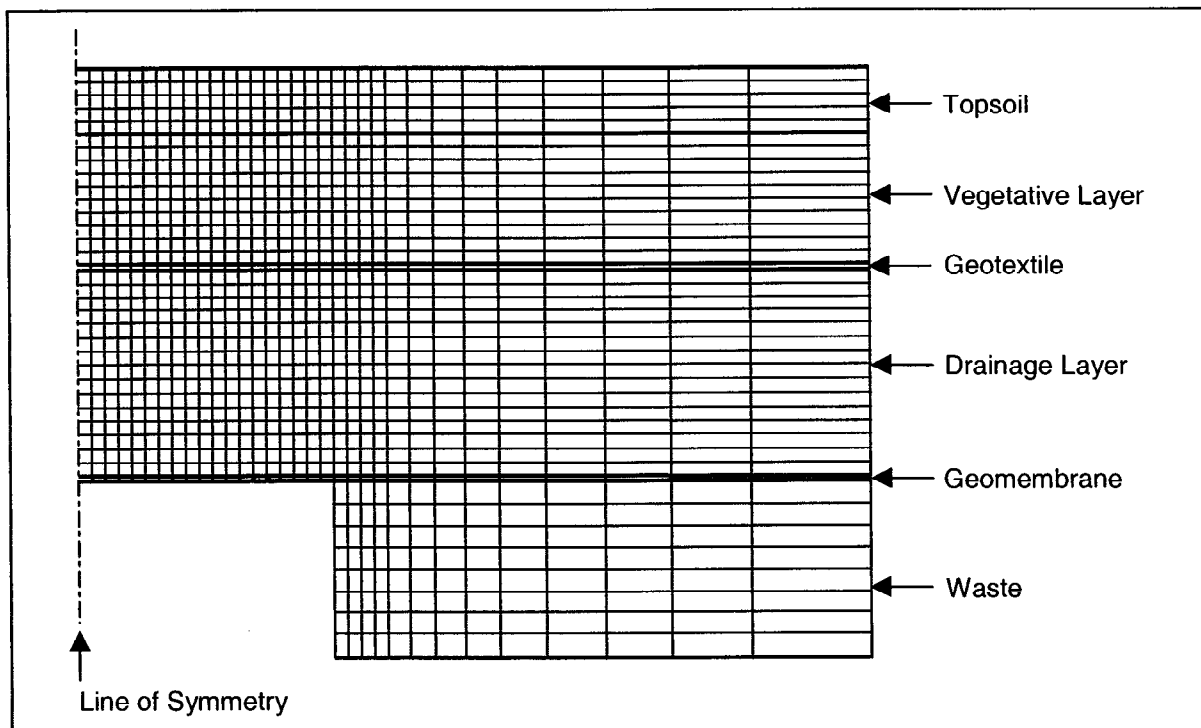

Figure 2 – A typical FLAC grid after initial equilibrium is reached and a void is placed in the waste.

the modeled cover was found by stepping to equilibrium again. The vertical and horizontal displacements of the geomembrane and cover surface were monitored for each void width, and the geomembrane strain was calculated from these displacements.

Results

The maximum vertical displacement of the cover components occurred in the center of the infinitely long void, at the line of symmetry. This maximum vertical displacement is referred to as the settlement depth. The settlement width is defined as the distance between the points where the vertical displacement of a cover component is 10 percent of the settlement depth of that component. In order to evaluate geomembrane strains based on settlement characteristics visible from the top of the cover, the geomembrane strain was compared to the settlement depth and settlement width at the surface of the cover. The surface settlement width divided by the surface settlement depth is related to the geomembrane strain as shown in Figure 3.

Both the Hidden Valley and Purdy Landfills have experienced differential settlements of the final covers. Contour maps were available for the Hidden Valley Landfill, so the differential settlements could be quantified. In the vicinity of Test Pits 5 and 6 in the North Area Closure, there are two areas of differential settlements for which the two-dimensional plane strain case modeled by FLAC may be applied. These two areas of differential settlement have surface settlement widths of 3.7 m and 5.5 m and surface settlement depths of 0.15 m and 0.55 m,
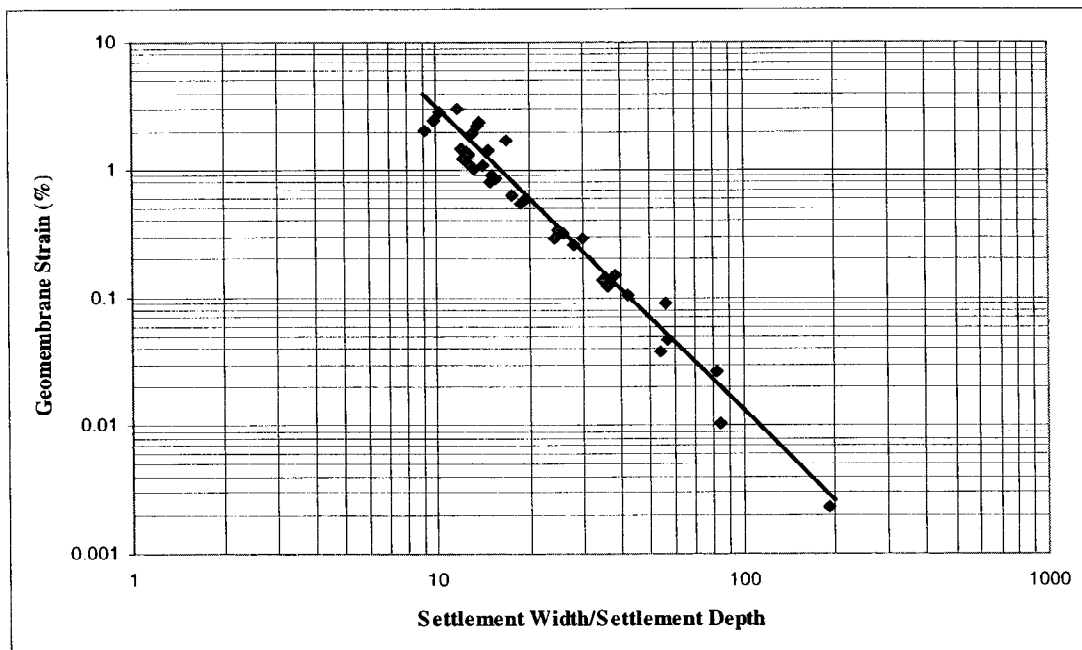

Figure 3 – Relationship between surface settlement characteristics and geomembrane strain for Purdy and Hidden Valley Landfills.

respectively. This results in a surface settlement width to surface settlement depth ratio of 25 for the first case and 10 for the second case. Using Figure 3, the geomembrane strain is approximately 0.25 percent for the first case and 2.5 percent for the second case. The method described by Giroud (1992) may then be used to correlate this plane-strain value with the uniaxial allowable strain as found in the conformance tests for the geomembranes. Using a Poisson's ratio of 0.5 for the geomembrane, as recommended by Giroud (1992), the corresponding uniaxial strain is 0.75 times the plane-strain value. The resulting uniaxial strain values of 0.19 percent for the first case and 1.9 percent for the second case are well below the average yield for strain of 19.0 percent for the HDPE geomembranes as found in the conformance tests for the landfill covers.

General Design Method

In order to develop a general design method for geomembranes in landfill covers overlying voids in the waste, landfill cover settlements were modeled with FLAC for soil conditions other than those encountered at the Purdy and Hidden Valley Landfills. The density and thickness of the cover soil layers were varied, and the corresponding geomembrane deflections and strains were found. The other soil properties were not varied, since they are typical of soils used in landfill covers. The geomembrane yield strength was also varied by changing the thickness of the geomembrane. The other geosynthetic properties were not changed since they are also considered typical for HDPE geomembranes and nonwoven geotextile filters used in landfill covers.

The cover conditions and void width were found to be related to the geomembrane strain as shown in Figure 4. The geomembrane strain may be found for different geomembrane yield
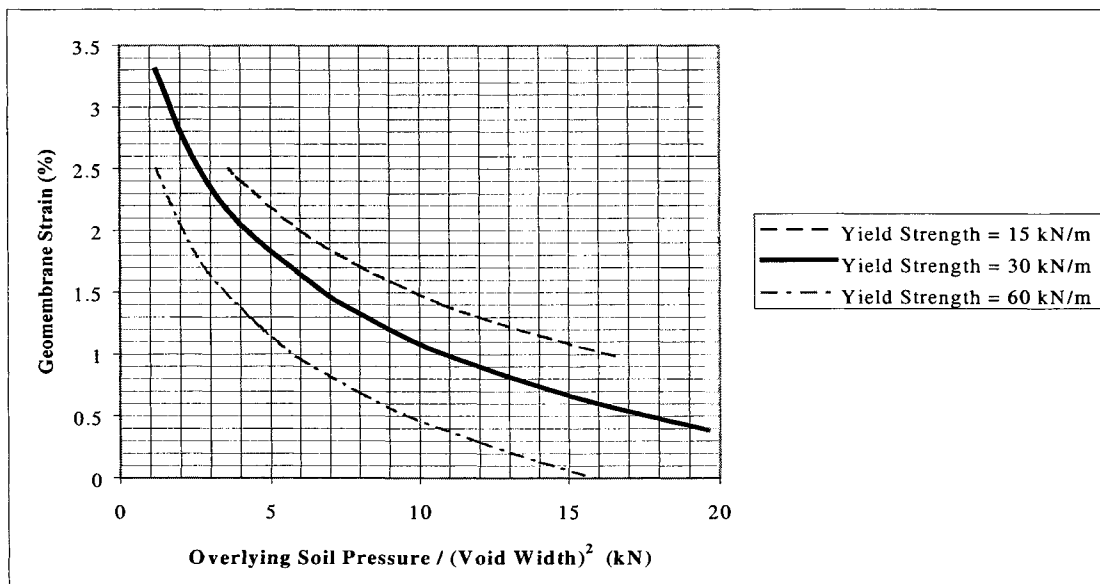

Figure 4 – Design of geomembranes in landfill covers to span voids in waste.

strengths by determining the value of the overlying soil pressure and dividing by the square of the void width.

Limitations of Evaluation Method

Although the results of FLAC models are useful for estimating geomembrane strains, there are certain limitations to this evaluation method. The geomembrane strains calculated were below yield values, but the evaluation is only for an intact, undamaged geomembrane. No consideration was made for seams, which tend to be weaker than geomembrane panels, or imperfections in the geomembrane, which can lead to tearing of the geomembrane at smaller strain values. The behavior of the geomembrane under a constant load with increasing time was not considered, either. FLAC contains a method for analyzing creep; however, the creep and stress relaxation characteristics of geomembranes are not yet fully understood. Also the effects of differential settlements on the drainage patterns of the landfill cover should be considered when determining acceptable strains and deformations of the geomembrane.

CONCLUSION

Field exploration and laboratory tests indicated that the components of the Purdy and Hidden Valley Landfill covers were in good condition and their characteristics generally met those described in the specifications and construction reports for the covers. The drainage layer soils had not experienced any measurable clogging since construction. In addition, the drainage layer soils generally met the granular filter criteria for the overlying vegetative soil, so a geotextile filter may not be necessary between the two layers. The permittivities of the geotextiles had decreased since the time of installation, but the permittivities were still high enough to meet geotextile filter criteria. The geomembranes uncovered in the test pits appeared to be in good condition, with no rips or tears.

From the results of differential settlement modeling with the computer program FLAC, relationships between the surface settlement characteristics and the geomembrane strain were found for the Purdy and Hidden Valley Landfill covers. Differential settlements at two locations in the Hidden Valley Landfill cover were evaluated with this method, and the geomembrane strains were found to be well below yield strains. A general design method for other landfill cover conditions was also developed with FLAC.

ACKNOWLEDGMENTS

REFERENCES

Bowles, J.E. (1988) Foundation Analysis and Design, 4th Ed., McGraw-Hill, Inc., New York, pp. 97-100.

Christopher, B.R., and Holtz, R.D. (1985) Geotextile Engineering Manual, Report No. FHWA-TS-86/203, Federal Highway Administration, Washington, D.C., 1044 pp.

Finley, C.A. (1997) "Performance of Municipal Solid Waste Landfill Covers", Master of Science Thesis, University of Washington, Seattle, WA.

Giroud, J.P. (1992) "Biaxial Tensile State of Stress in Geosynthetics", Geotextiles and Geomembranes, Vol. 11, No. 3, pp. 319-325.

Holtz, R.D., Christopher, B.R., and Berg, R.R. (1995) Geosynthetic Design and Construction Guidelines, National Highway Institute, Federal Highway Administration, Publication No. FHWA HI-95-038, McLean, VA, pp. 27-38.

Itasca Consulting Group, Inc. (1992) FLAC: Fast Lagrangian Analysis of Continua, Version 3.2, Vol. 1-3, Minneapolis, MN.

Metcalfe, R.C. (1993) "Performance of Geotextile Separators in Western Washington", Master of Science Thesis, University of Washington, Seattle, WA.

Metcalfe, R.C., Holtz, R.D., and Allen, T.M. (1995) "Field Investigations to Evaluate the Long-Term Separation and Drainage Performance of Geotextile Separators", Proceedings of Geosynthetics '95 Conference, Vol. 3, Nashville, TN, pp. 951-962.

Reitz, L.J. (1995) "Performance of Geosynthetics in Landfill Covers", Master of Science Project Report, University of Washington, Seattle, WA.

Reitz, L.J., and Holtz, R.D. (1997) "Performance of Geotextiles in Landfill Covers", Proceedings of Geosynthetics '97 Conference, Vol. 1, Long Beach, CA, pp. 413-424.

Terzaghi, K. (1922) "Der Grundbuch an Stauwerken und seine Verhutung", Die Wasserkraft, Vol. 17, No. 24, pp. 445-449; reprinted in From Theory to Practice in Soil Mechanics, John Wiley and Sons, Inc., New York, NY, pp. 114-118 (as cited by Terzaghi, Peck, and Mesri, 1996).

Terzaghi, K., Peck, R.B., and Mesri, G. (1996) Soil Mechanics in Engineering Practice, 3rd Ed., John Wiley and Sons, Inc., New York, NY, pp. 81-82.

EVALUATION OF AN EXISTING COMPOSITE COVER OVER STEEP LANDFILL SLOPES

ROBERT J. GRILLO, P.E., SR. ENGINEER
CMA ENGINEERS, INC., USA

PAUL F. BURNS, P.E., SR. ENVIRONMENTAL ENGINEER
WASTE MANAGEMENT, INC., USA

ABSTRACT

This paper presents the results of an evaluation of the stability and hydraulic performance of a landfill cover built over 2.5 horizontal to 1 vertical (2.5H:1V) sideslopes. The evaluation consisted of excavating a section of the cover, and testing a geosynthetic clay liner and a compacted clay liner. The purpose of the evaluation was to assess the performance of the cover after three years of service. Data are presented on the moisture content and internal shear strength of the GCL, and the moisture content and hydraulic conductivity of the compacted clay layer.

Test results indicate that the internal shear strength of the GCL has not degraded, and that the cover is stable with an acceptable factor of safety. The cover has not visibly weathered, deteriorated, clogged or shown evidence of slippage. The clay layer has not dried or exhibited a substantial increase in hydraulic conductivity.

INTRODUCTION

This paper presents the results of field observations and a laboratory testing program to evaluate the stability and hydraulic performance of a landfill cover at a commercial landfill site in central Maine. The cover was built over 2.5 horizontal to 1 vertical (2.5H:1V) sideslopes and incorporates a unique barrier layer consisting of a geomembrane, geosynthetic clay liner (GCL), and compacted clay. The landfill accepts primarily incinerator ash from waste-to-energy plants, with lesser amounts of wastewater treatment plant sludges, demolition debris, and other non-hazardous industrial wastes.

The evaluation consisted of excavating a section of the cover and observing its overall condition; testing for any degradation of the GCL internal shear strength due to creep, construction stresses, weathering, or other mechanisms; and assessing the effects of desiccation and freeze-thaw cycles on the hydraulic conductivity of the clay. The purpose of the evaluation was to assess the performance of the cover after three years of service, in consideration of the unusual cover section, steep sideslopes, and plans to grade and close other landfills on the site in a similar manner.

PROJECT BACKGROUND

The owner had applied for a permit to expand the landfill to accommodate the incoming waste stream for a period of several years. Shortly thereafter, the remaining permitted disposal capacity and the schedule for receiving the permit and constructing the first expansion phase was evaluated. The evaluation indicated that the site would run out of capacity several months before the new landfill cells could be brought on line. The landfill management identified steepening two 15-meter high and 122-meter wide sideslopes of the existing landfill, to 2.5H:1V from 3H:1V, as a safe and effective way to gain the needed capacity in the available time. Since steepening the slopes would not involve expanding the landfill footprint or increasing its height, the Maine Department of Environmental Protection (MEDEP) considered this modification to be a minor revision to existing permits. The project, however, required a variance from regulations limiting landfill sideslopes to 3H:1V. Gaining regulatory approval for the variance required thorough evaluations demonstrating that the cover would be stable.

Pre-design evaluations indicated that a geomembrane and clay composite cover section typically required by Maine regulation would not have a sufficiently high veneer stability factor of safety. Stability calculations using laboratory direct shear test results indicated a factor of safety of about 1.2 for the textured geomembrane/clay interface, which is less than the 1.5 value required by the regulations. An alternative design had been developed that substituted a GCL for the upper foot of clay. Figure 1 presents schematic cross sections of the regulation cover and the alternative GCL cover design.

Calculations based on design and pre-construction laboratory direct shear testing indicated factors of safety of 1.5 or greater for the alternative design. The stability calculations were based on using large displacement, or residual shear strength data. The landfill cover

was installed in 1995 and has performed satisfactorily since that time. The field work and laboratory testing program reported herein were completed in June and July, 1998.
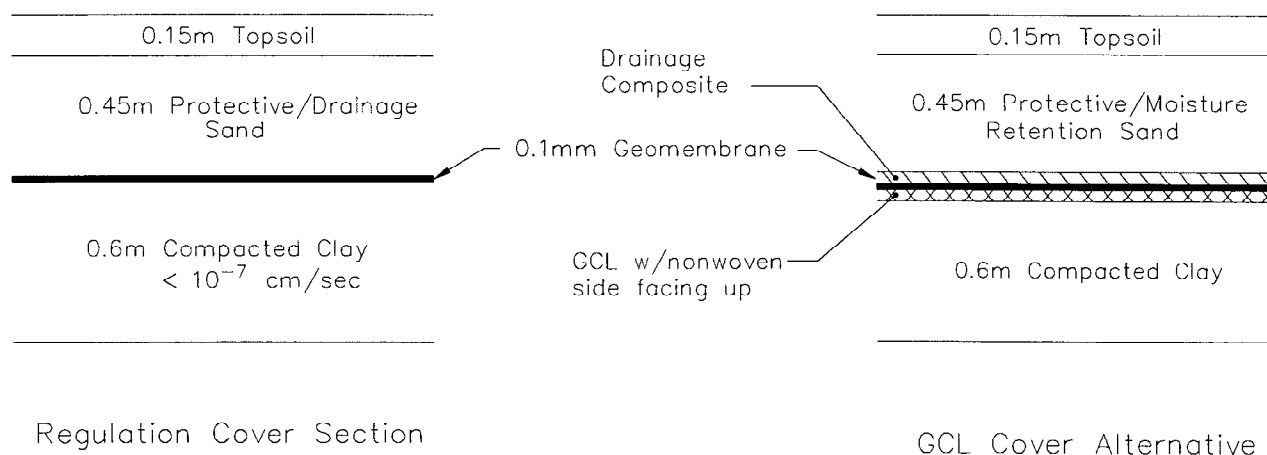

Figure 1. Cover System Schematics

COVER EXCAVATION AND OBSERVATIONS

The test excavation area was located near the middle of a 122-meter wide slope to avoid sampling areas subject to end effects. The test area was located about 3 meters above the base portion of the slope that is buttressed by the access road. Over an approximately 2 meter square area, 0.6 meters of soil covering the geosynthetic layers were removed using a backhoe equipped with a smooth-edged bucket. Next, the individual geosynthetic layers were cut and inspected, and three samples of the GCL were collected for laboratory testing. After inspecting the clay surface, four test holes were excavated through the 0.3 meter thick clay layer and twelve clay samples were obtained for water content testing. Using the backhoe bucket, three Shelby tubes were pushed to obtain undisturbed samples of the clay.

The cover system components appeared to be in good condition, without any visible indications of weathering, deterioration or slippage. No evidence of clogging of the geotextile fabric that separates the protective sand layer from the geonet drainage core was observed, as silt particles had not migrated to the fabric surface. Silt or sand particles were not present within the geonet drainage core itself. There was no evidence of slippage among any of the interfaces. There was also no evidence that bentonite had migrated beyond the carrier fabrics up to the geomembrane surface or down to the clay. The

GCL appeared to be uniformly hydrated and it was about 10 millimeters (mm) thick. The clay surface was not desiccated, and there was not any free water or indications that the clay surface was over-saturated. The clay layer was moist throughout, and there were no obvious cracks that could have been caused by desiccation or freeze-thaw effects.

LABORATORY TESTING PROGRAM

Three GCL samples were tested for internal shear strength. Two of the samples were tested at their field moisture contents to simulate current field conditions. The third GCL sample was soaked for 24 hours under the applied test load to provide comparative test data for the pre-construction direct shear tests for which the GCL samples were also soaked for 24 hours. The GCL samples were sheared under a single normal stress equal to the actual field overburden stress of 11.5 kilopascal (kPa). Except as noted above, the direct shear test procedures and parameters followed as part of this work duplicated those used during pre-construction direct shear testing. The laboratory conducted each test with the top fabric shearing in the downslope direction. The pre-construction testing was performed on GCL samples provided by the manufacturer just prior to the start of construction.

The direct shear tests were performed in general accordance with ASTM D5321. Each sample was sheared at a faster strain rate (0.5 mm/minute) than is specified by the standard, however, to save time and lower costs. It has been the authors' experience that strain rates in the range of 0.5 mm/minute are commonly specified by designers for this type of application.

The middle 0.15 meter portions of the three undisturbed clay samples were tested for hydraulic conductivity (ASTM D5084), water content (ASTM D2216) and dry unit weight. Water content testing was performed on twelve clay samples, with three samples each tested from the clay surface, from depths of 0.1 meter and 0.2 meters, and from the bottom of the clay layer.

RESULTS AND DISCUSSION

<u>GCL Testing</u>

Figure 2 presents the recent and pre-construction GCL internal strength test results. Figure 2 includes both peak strength values and large displacement, or residual, values. As indicated earlier, the large displacement values were used as the basis for design.

Table 2 summarizes the GCL water content conditions and shear strength values during the recent and pre-construction test programs. The data identified as 1998 refer to the recent testing on three-year-old samples excavated from the cover, and the data identified as 1995 refers to the pre-construction test results on samples provided by the manufacturer. The strength data reported for the 1995 samples were obtained from the peak and large displacement strength envelopes at the long-term static normal pressure of 11.5 kPa, as presented in Figure 2. The design shear strength reported in Table 2 is the value required for a factor of safety of 1.5 under long-term static loading conditions.

Table 2. GCL Water Content and Internal Shear Strength Test Results

Sample	Water Content, Initial/Final, 0/0	Strength, kPa Large Disp./Peak	Design Shear Strength, kPa, for F.S = 1.5
1998 @ field w%	82.1/78.7	11.2/20.8	6.8
1998 @ field w%	83.3/81.1	10.7/20.0	6.8
1998 soaked	79.7/86.4	10.4/19.2	6.8
1995 soaked (3 samples)	9.0/101 to 113 (range of 3 samples)	8.7/17.6	6.8

The three-year-old GCL samples obtained from the field have higher peak and large displacement internal shear strengths than the manufacturer-supplied GCL samples tested prior to construction. The test results indicate that no reduction in the internal shear strength of the GCL has occurred over the three years that the GCL has been in service on the steep slideslopes. The peak strength data also indicate that stresses in the field have not exceeded the peak internal strength of the GCL. If this were the case, the authors would expect that the recent test results for peak strength would be closer to residual strength values because at least some of the reinforcing fibers that contribute to the peak strength would have been broken or been pulled out of the carrier fabrics.
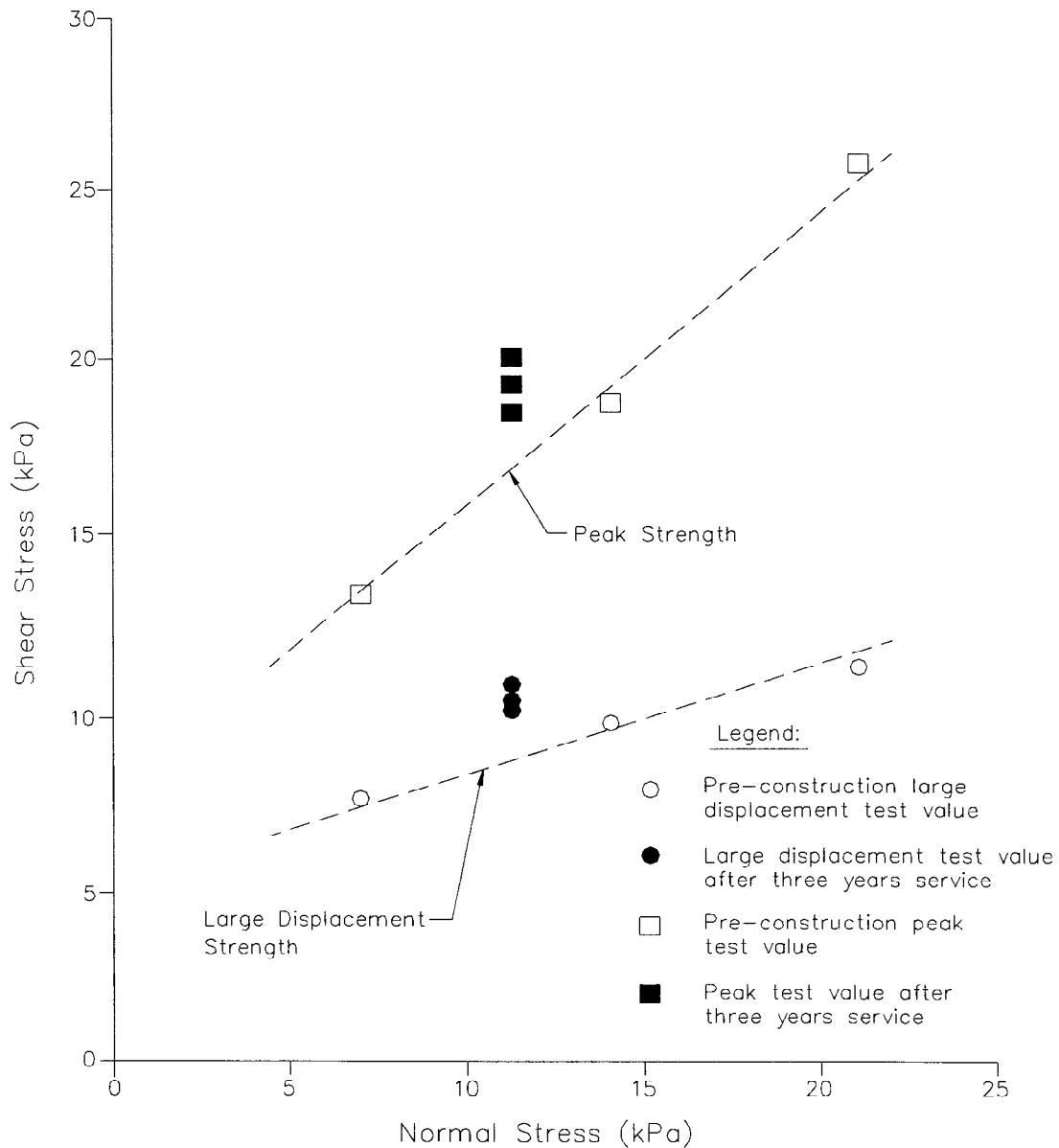
Figure 2. GCL Internal Strength Test Results

The data in Table 2 indicate that there is an inverse relationship between the GCL water content and internal shear strength. For both peak and large displacement test results, shear strengths are higher for GCLs tested at lower water contents.

The pre-construction tests were performed on samples provided by the manufacturer. These samples were provided in an essentially dry condition (9% moisture content), then soaked for 24 hours under the applied normal stress prior to testing. This procedure yielded GCL

moisture contents in the range of 101 to 113 percent. The field moisture contents of the GCL samples obtained three years after installation ranged from 79.7 to 83.3 percent. These data indicate that from a strength perspective, the pre-construction test procedures were conservative in that they resulted in higher GCL moisture contents and lower internal shear strengths than has actually occurred in the field. It is unclear why the 3-year old field sample hydrated from a field moisture content of 79.7% to only an 86.4% after soaking for 24 hours, when the manufacturer-supplied "dry" GCL samples hydrated to greater than 100 percent moisture contents under similar conditions.

Compacted Clay

The locally available clay is from the Presumpscot Formation, a low plasticity clay of glacial marine origin. Figure 3 presents the results of water content testing of the compacted clay layer three years after closure construction.
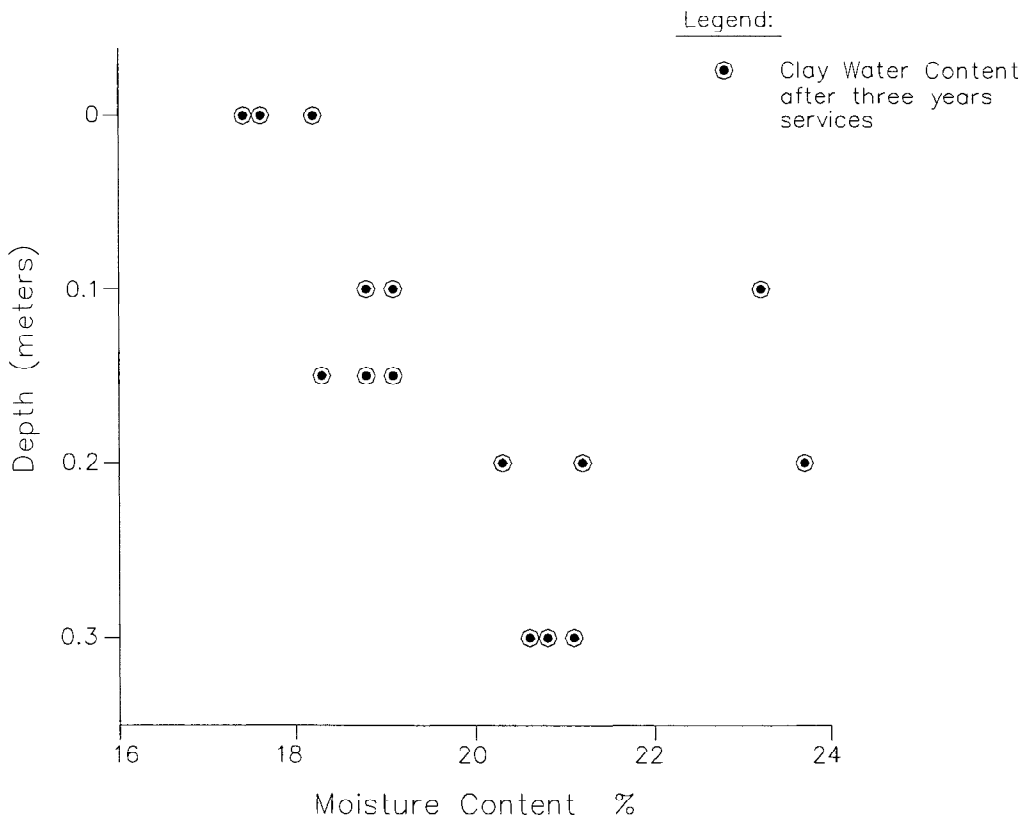

Figure 3. Clay Layer Water Contents

The water contents at the clay surface are drier than the clay at depth. This drying of the clay surface is likely due to migration of the clay pore water up into the adjacent GCL under flow gradients created by the hydrating bentonite in the GCL core. It is not likely that the clay surface dried through evaporation to the atmosphere because the HDPE geomembrane that overlies the GCL was placed immediately after completion of the clay layer, and after construction the geomembrane provides a barrier to upward moisture migration.

The authors believe that this drying process strengthens the GCL-clay interface by desiccating and strengthening the clay surface. Pre-design laboratory testing on a textured geomembrane-clay interface yielded a shear strength of about 5 kPa at a normal stress of 11.5 kPa, whereas testing of a GCL-clay interface yielded a much higher shear strength of about 7.2 kPa at the same normal stress. Due to the nature of the textured geomembrane-clay interface, the strength of this interface is essentially equal to and limited by the strength of the clay. When testing this interface, the failure plan was observed to pass mostly through the clay, and to a lesser extent along the geomembrane/clay interface at the higher points in the textured geomembrane surface. The higher GCL-clay interface strength must therefore be attributable, at least in part, to a strengthening of the clay surface as the clay dries.

Overall the clay layer appears to be wetter now than when it was placed three years ago. Construction quality control records indicate the clay layer was placed at moisture contents ranging from 15.2 to 19.6 percent and averaging 17.2 percent. The recent test results indicate the moisture contents now range from 17.6 to 23.7 percent, and average 20.2 percent. The differences in reported moisture contents over the three year period could be due to differences in the test methods (field nuclear moisture testing during construction (ASTM D3017)versus oven drying in the laboratory (ASTM D2216)). Alternatively, the data could represent an actual moistening of the clay resulting from a humid environment within the landfill. Regardless, the data indicate that the clay layer has not dried over the three-year period.

Figure 4 is a plot showing the moisture-density data from the closure construction and the recent testing, and the relationship between moisture, dry unit weight and hydraulic conductivity of the compacted clay. The moisture-density acceptance zone was developed prior to construction and is based on extensive laboratory hydraulic conductivity testing of field-compacted clay samples from test fills and samples re-compacted in the laboratory. Clay compacted to moistures and dry unit weights within the acceptance zone have hydraulic

conductivities in the 10^{-8} cm/sec range. Clay compacted to less than a 78% saturation level, outside the acceptance zone, have hydraulic conductivities greater than 10^{-7} centimeters per second (cm/sec).

For the closure construction project, the clay layer was compacted to structural criteria, rather than hydraulic conductivity criteria, in consideration of the barrier properties of the GCL. Regardless, construction quality control records indicate that the clay layer, for the most part, was compacted to moisture/density values resulting in as-placed hydraulic conductivities in the 10^{-8} cm/sec range based on the acceptance zone criteria shown on Figure 4.
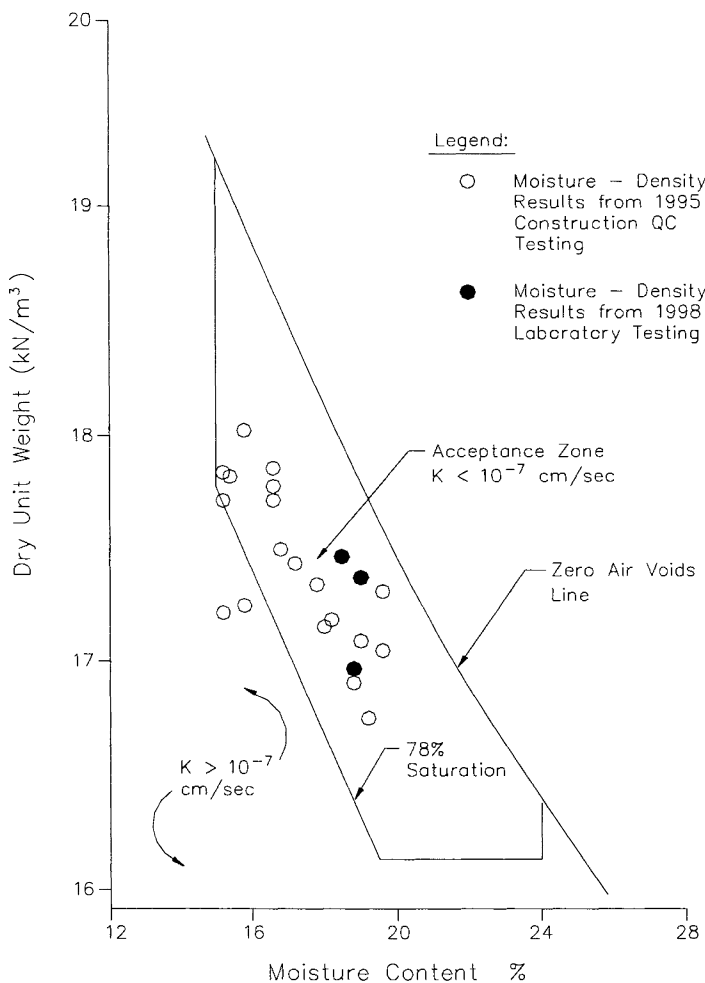

Figure 4. Moisture-Density and Hydraulic Conductivity Relationships

Clay moisture and density measured from three undisturbed tube samples taken as part of this study indicate the clay layer should have a hydraulic conductivity in the 10^{-8} cm/sec range based on the acceptance

zone. Laboratory tests on these samples indicate hydraulic conductivities of 9.7×10^{-8}, 1.2×10^{-7}, and 1.4×10^{-7} cm/sec. These values are about a half an order of magnitude higher than would be expected based on the moisture-density and hydraulic conductivity relationships developed for this soil. These slightly higher than expected hydraulic conductivity values could be attributed to either normal variations in the data that are typical of this type of soil and testing, or an actual slight increase in hydraulic conductivity due to minor effects of freeze-thaw. Overall the data indicate that after three years in service, the clay layer continues to provide an effective barrier to cover leakage.

CONCLUSIONS

1. The unique composite cover design on 2.5H:1V slopes remains stable with an acceptable factor of safety after being in service for three years. The cover has not visibly weathered, deteriorated, clogged or shown evidence of slippage. There were no indications that the favorable performance observed to date will not be maintained for the foreseeable future.

2. The internal strength of the GCL has not degraded after the GCL has been in service on the steep slopes for three years. The data further indicate that stresses have not exceeded the peak internal strength of the GCL. The design assumption that large displacement shear strength values would control stability, while not necessarily inappropriate, was conservative in this instance.

3. For this design and for these field conditions, the 24-hour soaking criteria for testing GCL shear strengths in the laboratory provided conservative shear strength results. The test results indicate an inverse relationship between GCL water content and internal shear strength.

4. The bentonite in the GCL was hydrated by pore water from the underlying compacted clay layer. This process, in effect, dried and strengthened the clay surface. As a result, the GCL-clay interface shear strength is higher than would be otherwise expected based on the strength of the clay itself.

5. The hydraulic conductivity of the compacted clay layer has not substantially been degraded over the three years that the cover has been in service. Considering that the clay layer is not drying out - in fact it appears to be wetter than when it was originally

placed - the clay layer will likely remain an effective barrier layer for several more years, or longer.

RECOMMENDATION

1. Given the sensitivity of GCL shear strength to the water content at which it is tested, designers should exercise caution in selecting soaking criteria to avoid use of unconservative design strength values. More data on actual field moisture contents of GCLs in service is needed to assist designers in specifying this test parameter.

ACKNOWLEDGMENTS

REFERENCES

ASTM D5321   Standard Test for Determining the Coefficient of Soil and Geosynthetic or Geosynthetic and Geosynthetic Friction by the Direct Shear Method

ASTM D5084   Standard Test Method for Measurement of Hydraulic Conductivity of Saturated Porous Materials Using a Flexible Wall Permeameter

ASTM D2216   Standard Test Method for Laboratory Determination of Water (Moisture) Content of Soil and Rock

ASTM D3017   Standard Test Method for Water Content of Soil and Rock in Place by Nuclear Methods (Shallow Depth)

DESIGN OF A GAS PRESSURE RELIEF LAYER BELOW A GEOMEMBRANE COVER TO IMPROVE SLOPE STABILITY

Richard Thiel
Thiel Engineering, USA

ABSTRACT

Pore pressures generated by landfill gas underneath a geomembrane final cover can significantly reduce the effective normal stress on the lower geomembrane interface to the point of creating a cover veneer instability. An estimation of gas flux from the landfill surface can allow a gas-relief layer to be designed using Darcy's law for gas flow through a porous medium. The methodology incorporates knowledge of the gas transmissivity of a chosen medium to design a spacing for highly-permeable strip drains. The strip drains in turn would discharge the gas either to vents or an active gas collection system. The gas-relief layer typically consists of sand or a geonet-composite. Limited testing of nonwoven-needlepunched (NWNP) geotextiles indicates that these materials may also be acceptable for gas relief in some designs. However, more testing is recommended before using NWNP geotextiles alone in this application. A failure case histories is presented that supports the design theory recommended in the paper. The greatest assumption in the proposed methodology concerns the estimation of gas flux. More work is needed in this regard. However, the basic concept of providing a gas-relief layer with intermittent highly-permeable strip drains is recommended as a prudent engineering measure for landfill final covers incorporating geomembrane barriers.

INTRODUCTION

Recent landfill cover slope stability failures have been attributed to excess gas pore pressures below the geomembrane. Soil mechanics methods provide all the tools necessary to address this issue. However, what has been lacking to date are recognition of gas pressures as a design issue, and a design methodology to account for gas pressures and gas relief. The primary steps recommended in this paper to incorporate gas pressures in a landfill cover design are: (1) estimate the maximum gas flux that may need to be removed from below the landfill cover; (2) perform slope stability analyses to estimate the maximum allowable gas pressure; and (3) design a vent system below the cover that will evacuate the assumed gas flux under the estimated maximum allowable driving pressure. Each of these three steps are described in detail in this paper.

ESTIMATING GAS FLUX

The mass flux of gas from the surface of a landfill will be site specific. It will also vary spatially and temporally at a given landfill. The amount of gas will depend on the waste type, age, temperature, moisture, other avenues of gas extraction or venting, barometric pressure, etc. For purposes of slope stability design, estimates of the maximum gas flux, rather than the average, are recommended. One way to estimate the gas flux is to use a computer model for landfill gas generation, such as the EPA's Clean Air Act model. The upper bound estimate of landfill gas generation should be used. The gas flux would then be calculated as the estimated gas generation rate divided by the landfill area under consideration.

An alternate, simplistic method to estimate gas flux (for example, see Richardson, 1998) is to assume a gas generation rate per unit mass of waste, multiply by the mass of waste under consideration, and divide by the area. The literature reports landfill gas generation rates up to 0.6 standard cubic feet per wet pound of waste per year (ft^3/lb/yr) (0.037 m^3/kg/yr) (Pacey, 1997). However, this value is exceptionally high and is reported for controlled landfills in an enhanced decomposition mode. For closures at municipal solid waste landfills on the west coast of the United States, where cell closure occurs at the end of a cell's life, the author has used a gas generation rate of 0.1 ft^3/lb/yr (6.24×10^{-3} m^3/kg/yr) for purposes of cover design. However, estimation of the gas generation rate is very site specific, and the designer is encouraged to consult someone experienced in landfill gas considerations for estimates of gas flux for a particular project.

SLOPE STABILITY CALCULATIONS INCORPORATING GAS PRESSURES

Several papers describing landfill cover veneer slope stability have been presented in the literature (for example Koerner and Soong, 1998; Kavazanjian, 1998; Giroud et al, 1995; Thiel and Stewart, 1993). In these papers different considerations for cover slope stability are presented and developed, including infinite slope approaches, seepage forces, seismic forces, toe buttressing forces, tapered slopes, and slope reinforcement. It is left to the individual practitioner to select the model most appropriate for a given situation to develop the design. In the interests of brevity, the slope stability equations used in this paper for the development of gas pressure considerations will be limited to non-reinforced, static, infinite-slope conditions. However, the principles developed herein to include gas pressures in a stability analysis could easily be combined with other models as well.

Because of the hydraulic break provided by the barrier geosynthetic (assumed to be a geomembrane), seepage forces that may occur in the cover soils above the geomembrane have no influence on the stability of the interface below the geomembrane. Therefore, separate slope stability analyses are required for the geomembrane's upper and lower interfaces. The stability analysis presented herein would only be for the lower interface, where the gas pressures would potentially occur.

The general equation for the factor of safety of an infinite-slope section experiencing pore pressures from below (gas or water) can be formulated as (see Giroud et al, 1995, Eqn 38, for derivation of similar equation):

$$FS = \frac{\overline{a} + [h\gamma \cos\beta - u_g] \tan\overline{\phi}}{h\gamma \sin\beta} \quad\quad (1)$$

where: h = cover soil thickness above the geomembrane and perpendicular to the slope; γ = average unit weight of cover soil above geomembrane; β = slope angle; u_g = gas pore pressure on lower side of geomembrane; $\overline{a}$ = effective adhesion parameter for the lower geomembrane interface; $\overline{\phi}$ = effective friction parameter for the lower geomembrane interface.

Presuming that the material properties and geometry are fixed for a specific design, the designer must then select a minimum allowable factor of safety, FS_{allow}, and calculate a maximum allowable gas pressure, $u_{(g-allow)}$. Note that the most common unit for measuring landfill gas pressures in the United States is "inches of water column," where one inch of water = 5.2 psf = 0.036 psi (249 Pa).

DESIGNING THE GAS PRESSURE RELIEF SYSTEM

For purposes of the model proposed in this paper, the surface gas relief layer is assumed to be composed of the following three primary elements:

- a blanket gas-relief layer
- a series of parallel trenches or strip drains (the term 'strip drains' is used in the remainder of the paper), at a regular spacing (D), that collect gas from the gas-relief layer, and are more permeable than the gas-relief layer to allow the gas to be conveyed to the outlets
- outlet points for the strip-drains

Figure 1(a) shows a typical landfill slope cross section, with an emphasis on the gas collection layer below the barrier layer. In the cross section two benches are shown (which could just as well be the crest and toe of slope for short landfills). Strip drains, which could be perforated pipes, gravel filled trenches, or geosynthetic highway edge drains, are shown running longitudinally along the benches. The distance D is defined as the slope distance between the strip drains. Figure 1(b) shows a schematic plan view of the strip-drain layout for this situation, and also indicates that outlet points (in this case vents to the atmosphere) would be intermittently located along the strip drains to relieve the collected gas.

In the event that the strip-drain spacing between benches is found to be inadequate, additional strip drains could be connected in the slope direction between benches. This is illustrated in Figure 1(c) where the spacing D is now defined as the distance between the drains running up and down the slope. In this case the strip drains along the benches would serve as headers.

The derivation of the relationship between the strip drain spacing (D), incoming gas flux rate, gas transmissivity of the gas-relief layer, and pressure in the gas relief layer is similar to the design of the drainage layer and drainage layer outlets in the cover above the

Cover soil layers (may include drainage, vegative, topsoil, and erosion control elements).

Gas—relief layer (may be granular soil or geosynthetic).

Gas vent (typ.)

Barrier layer (geomembrane with or without GCL or low permeability soil layer)

Waste

General soil cover over waste

Strip drains or benches (may consist of perforated pipes, gravel, trenches or highway edge drains)

(a)

Strip drain (typ)

D (measured along gas relief layer)

Gas vent (typ)

Bench or crest

Slope

Bench
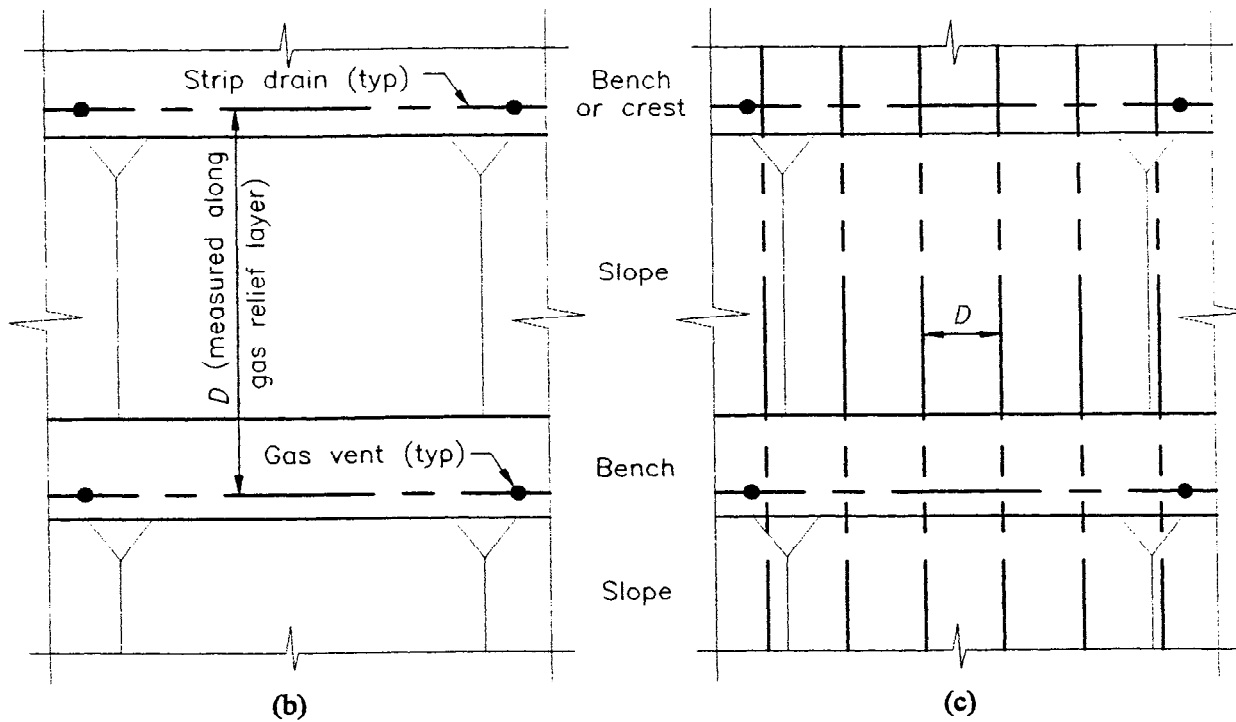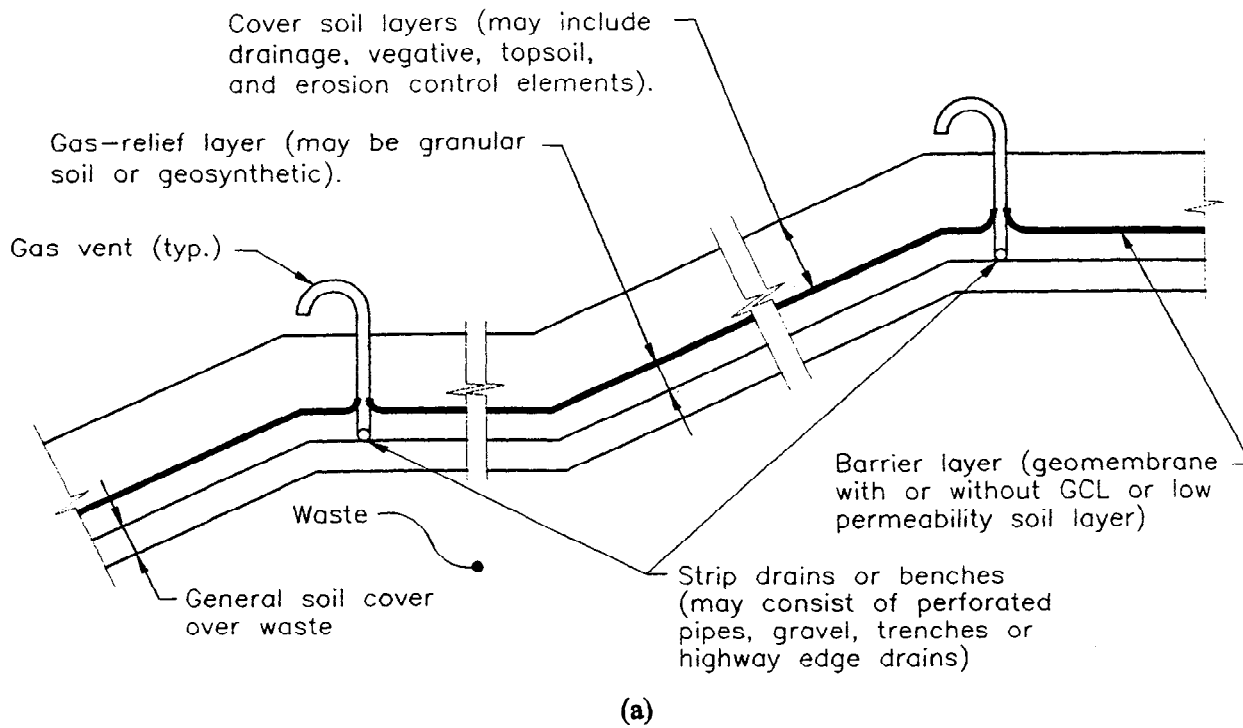
Slope

D

(b)

(c)

Figure 1. Schematic Showing Design Elements of Gas Relief Layer: (a) Side View of Final Cover with Gas-Relief Layer and Strip Drains; (b) Plan View of Strip Drain Layout on Benches Only; (c) Plan View of Strip Drain Layout on Slopes and Benches.

geomembrane as presented by Thiel and Stewart (1993). The derivation is based on Darcy's law, which applies to fluid flow in porous media where the flow is laminar. A discussion of the applicability of laminar flow to the gas-relief layer is presented in Thiel (1999). The derivation steps are as follows:

1. Consider a unit-width surface area between strip drains, as shown in Figure 2(a). Figure 2(b) illustrates a cross-section between two strip drains, showing the gas flux coming uniformly into the gas-relief layer from the waste below. Ideally, the gas flow is symmetric about the centerline between the strip drains, and we need only consider the half-distance, L, where $L = D/2$. The figure identifies the variable distance 'x' beginning at one of the strip drains, and increasing towards the centerline.

2. Figure 3 illustrates how the volume of gas being carried in the gas-relief layer would vary linearly from zero at $x=L$, to a maximum value at $x=0$. The volume of gas per unit width can be written in terms of the gas flux as

$$Q_x = \phi_g(L - x) \qquad (2)$$

   where Q_x is the gas discharge flow rate per unit width at any point x in the gas-relief layer.

3. The flow of gas in the gas-relief layer can be assumed to follow Darcy's law, which can be written in terms of the pressure gradient as follows:

$$Q_x = \left(\frac{k_g}{\gamma_g}\right) \cdot A \cdot \left(\frac{du}{dx}\right) = \left(\frac{k_g}{\gamma_g}\right) \cdot (t \times 1) \cdot \left(\frac{du}{dx}\right) = \left(\frac{k_g \cdot t}{\gamma_g}\right)\left(\frac{du}{dx}\right) \qquad (3)$$

   where k_g=gas permeability of the gas-relief layer; γ_g=the gas unit weight; A=cross-sectional flow area which is the thickness of the layer (t) times a unit-width; and du/dx is the pressure gradient.

4. Since we can define the gas transmissivity (Ψ_g) of the gas-relief layer as the permeability times the thickness:

$$\Psi_g = k_g \cdot t \text{ (gas transmissivity of the gas relief layer)} \qquad (4)$$

   we can combine equations (2), (3), and (4) as:

$$\phi_g(L - x) = \frac{\Psi_g}{\gamma_g}\frac{du}{dx} \qquad (5)$$

5. Equation (5) can be rearranged to solve for 'u' by integrating in terms of 'x' as:

$$u_x = \frac{\phi_g \gamma_g}{\Psi_g}\int_0^x (L - x)dx = \frac{\phi_g \gamma_g}{\Psi_g}\left(Lx - \frac{x^2}{2}\right) \qquad (6)$$

   where 'u_x' is the gas pressure at any distance 'x' from a strip drain.
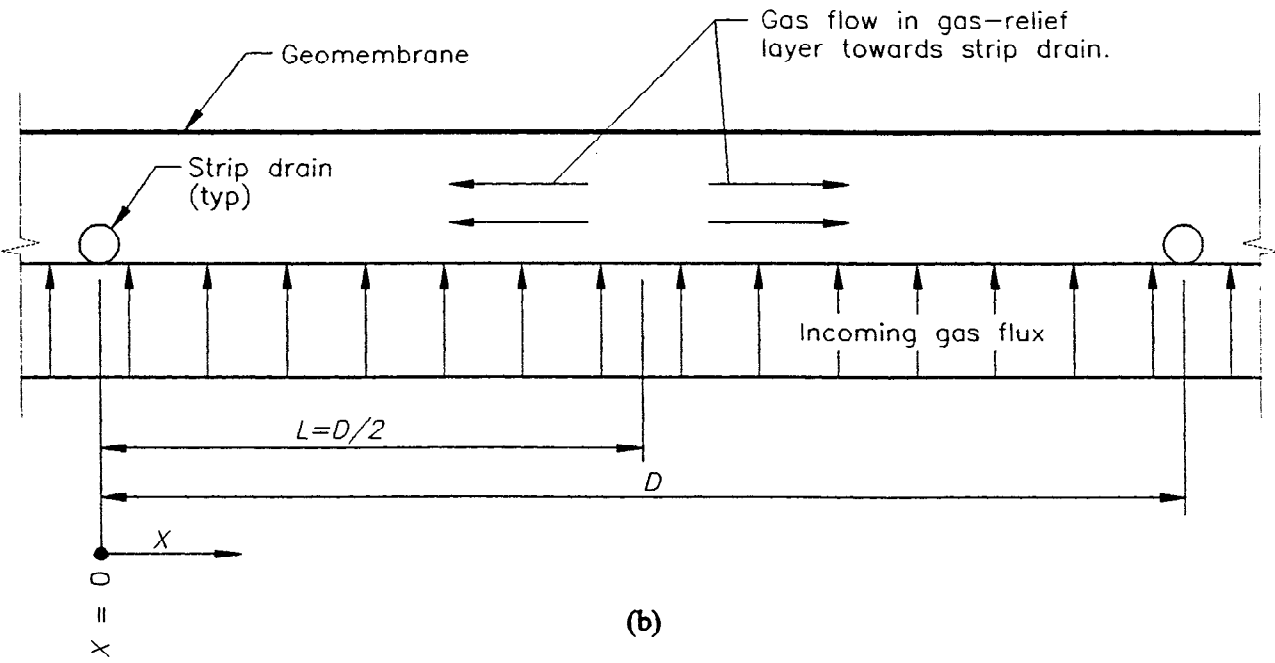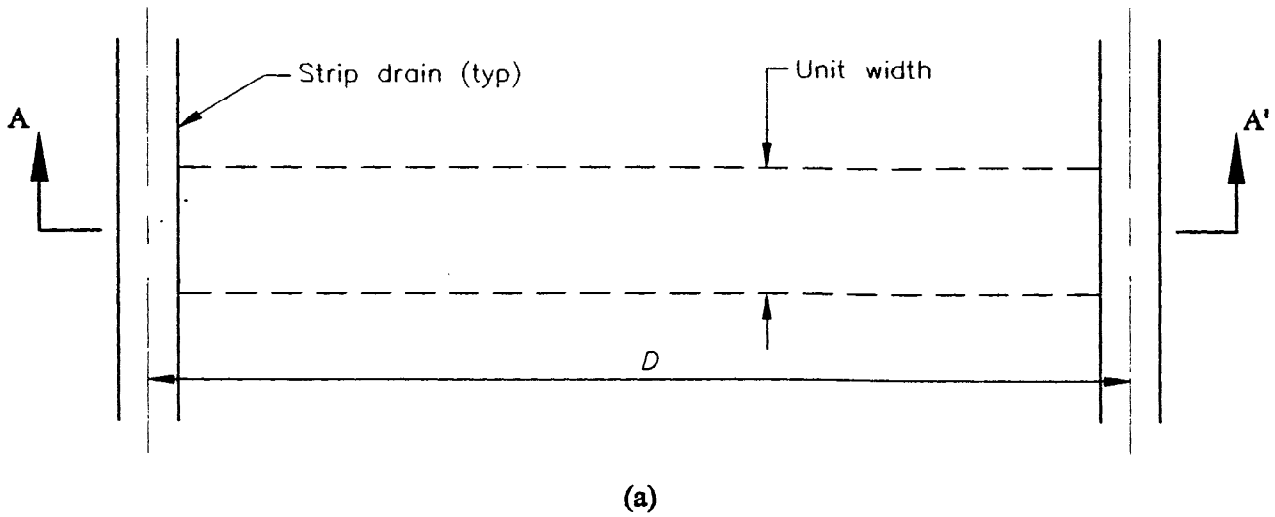
Figure 2. Model of Gas Flow to Strip Drains: (a) Plan; (b) Section
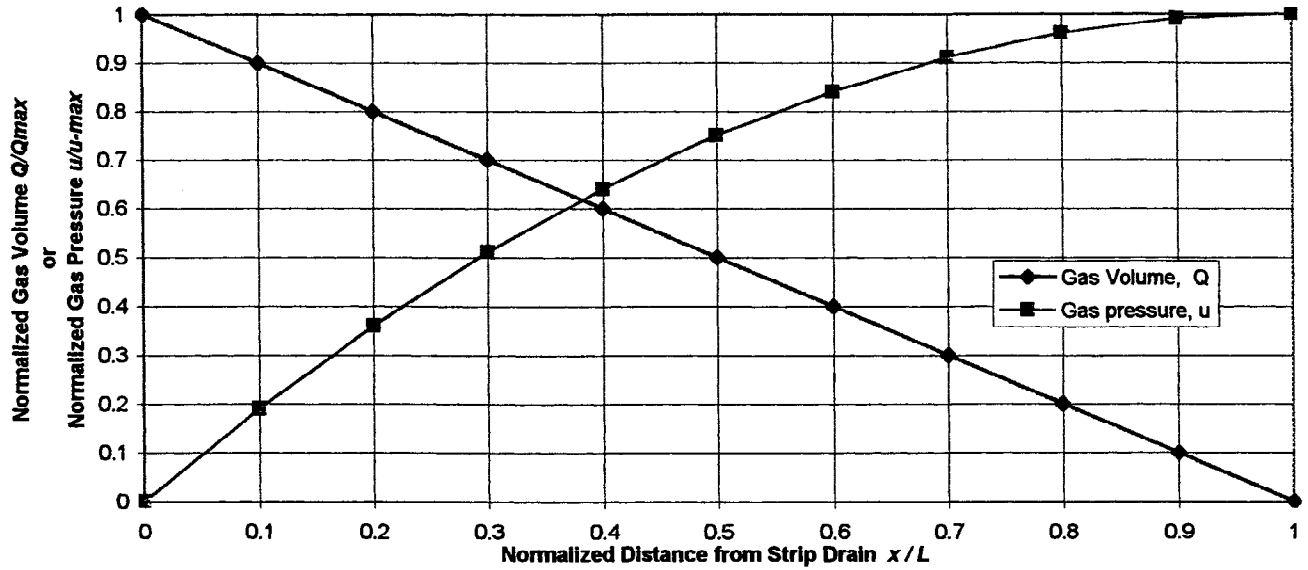
Figure 3. Normalized Gas Pressure and Volume vs. Distance From Strip Drain

The gas pressure is plotted in Figure 3 as a function of distance from the strip drain. From Figure 3, and Equations (5) and (6), we can observe the following:

- The pressure gradient, du/dx, varies linearly with distance x. It is a maximum at $x=0$ (where the gas volume is greatest), and is zero at $x=L$ (where there is essentially no gas flow).

- The pressure varies as a polynomial function of distance. It is zero at $x=0$ (that is, it is at the backpressure value in the strip drain). The maximum pressure at $x=L$ is:

$$u_{max} = \frac{\phi_g \gamma_g}{\Psi_g}\left(\frac{L^2}{2}\right)$$

(7a)

or in terms of the strip-drain spacing, D:

$$u_{max} = \frac{\phi_g \gamma_g}{\Psi_g}\left(\frac{D^2}{8}\right)$$

(7b)

Using Equation (7b), the distance D can be written in terms of the maximum pressure as:

$$D = \sqrt{\frac{8 u_{max} \Psi_g}{\phi_g \gamma_g}}$$

(8)

It is important to note that the gas pressure calculated in the above equations would be additive to whatever back-pressure exists in the strip drain system. The backpressure value would be the pressure relative to atmospheric pressure that exists at $x=0$. The author estimates that the back pressure should be no more than 1 inch water column (249 Pa) for well designed passive vent systems. If the vents are connected to an active (suction) gas collection system, a negative value may exist for the backpressure, depending on the suction pressure.

USING INTRINSIC PERMEABILITY TO COMPARE AIR AND WATER TRANSMISSIVITY

Use of Equations (7) or (8) requires the designer to select, or back-calculate, the value of transmissivity, Ψ_g, of the gas-relief layer. However, little if any testing or manufacturer data are available regarding the gas transmissivity of soils or geosynthetics. Therefore, the design will usually have to resort to assuming or specifying an equivalent hydraulic (water) transmissivity. In theory, the gas transmissivity can easily be calculated from the water transmissivity using the concept of intrinsic permeability.

Intrinsic permeability is characteristic of the medium in question, and entirely independent of the nature of the fluid. The principle of intrinsic permeability is considered valid for granular soils, and probably most geosynthetic drainage layers, but would not hold for silts and clays where the polarity of the fluid and electro-osmotic potentials begin to have a significant influence on the measured flow rates. (See, for example, Lambe and Whitman, 1969, pp 287-289; McWhorter and Sunada, 1977, pp 65-71; or for an excellent analytical and historical discussion Muskat, 1937). The formulation of Darcy's law in terms of intrinsic permeability is:

$$Q = K \cdot \frac{\gamma_f}{\mu_f} \cdot i_f \cdot A \tag{9}$$

where Q = flow rate; K is the intrinsic permeability with units of L^2; γ_f = unit weight of the fluid; μ_f = dynamic viscosity of the fluid; i_f = the fluid gradient, and A is the cross-sectional area of the flow medium. The relationship between the standard civil engineering coefficient of permeability and the intrinsic permeability can be written as:

$$k_f = K \cdot \frac{\gamma_f}{\mu_f} \tag{10}$$

where k_f is the standard civil engineering coefficient of permeability for a given fluid.

Since K is a constant independent of the fluid, the ratio between the coefficients of permeability for two different fluids (denoted by subscripts 1 and 2) can be determined as

$$\frac{k_1}{k_2} = \frac{\mu_2}{\mu_1} \cdot \frac{\gamma_1}{\gamma_2} \tag{11}$$

Using Equation (11), the design of a gas-relief layer can now be accomplished by converting the required gas transmissivity to a required hydraulic (water) permeability. All that

is required are physical properties of density and viscosity for the fluids of concern. These are easily obtained from published literature.

GAS PERMEABILITY IN PARTIALLY SATURATED SOILS

If the gas-relief layer is a granular soil, it is reasonable to assume that the soil will be holding a certain amount of capillary water either due to rain during construction, or from condensate underneath the geomembrane. Note that condensate water will be prevalent under landfill covers due to landfill gas, which is generally saturated. Since the bottom of the gas-relief layer is not a water table (hopefully!), a sand in this application would probably be at or above its field capacity. Guidance on the field capacity for typical sands can be found in the reference documents for the HELP computer program (Schroeder et al, 1994).

The reduction in gas permeability due to partial saturation of the sand layer can be estimated using the Brooks and Corey (1964, as reported by Fredlund and Rahardjo, 1993) relationship:

$$k_g = k_d \left(1 - S_e\right)^2 \left(1 - S_e^{(2+\lambda)/\lambda}\right) \tag{12}$$

where: k_g = gas coeff of permeability under given moist conditions

k_d = coeff of permeability to air for a dry soil ($S=0$)

λ = pore size distribution index (typical values range from 2 for porous rocks, 4 for natural sand deposits, to infinity for uniform spheres)

$$S_e = \text{effective degree of saturation} = \frac{S - S_r}{1 - S_r} \tag{13}$$

S_r = residual degree of saturation at which point an increase in matric suction does not produce an appreciable change in the degree of saturation (S). Typical values for residual saturation are presented by Schroeder et al (1994, pg 13, Figure 2).

For example, the author investigated the air transmissivity of a moist fine sand that was used as the gas-relief layer for a cover system that failed (see Failure Case History, later). The water permeability had previously been measured as 6×10^{-3} cm/s. Using the Equations (11) and (12) with appropriate input values for the field-exhumed sand sample, the author calculated that the air permeability of the moist sample would be 7.2×10^{-5} cm/s. The laboratory-measured value of the air permeability was found to be 8×10^{-5} cm/s, which is in excellent agreement with the theoretically calculated value. It is worthwhile noting that the ratio of k_g/k_d was 0.18. That is, the gas permeability of the sand was reduced by over 80% due to the presence of field moisture!

Using typical values of moisture field capacity for sands presented by Schroeder et al (1994), and going through the same calculations above, indicates that the gas permeability of a typical sand would be reduced by 25-50%. The example described above, derived from actual field data, showed a considerably greater reduction because the field moisture content

was greater than the static-drained field capacity. This was probably due to rains during construction, and the constant presence of moisture due to saturated landfill gas. Coarser sands will be less saturated and retain better gas permeability. Based on the limited field experience discussed in the preceding paragraph, and the limited data presented by Schroeder et at (1994), the following preliminary recommendations are put forward until more data is available:

1. For fine sands containing less than 10-15 percent fines, the field-gas permeability can be taken as the dry-gas permeability reduced by a factor of 5 to 10 to account for the presence of field-moisture.

2. For clean medium and coarse sands, the field-gas permeability can be taken as the dry-gas permeability reduced by a factor of 2 to account for the presence of field-moisture.

FAILURE CASE HISTORY

A sliding failure occurred during construction of a 15-acre (6 ha) final cover project. The slope on which the failure occurred was inclined at 4H:1V (25%, or 14 degrees), and was 60-feet (18 m) high with no benches. The cover system design consisted of the following elements, from bottom to top:

- Foundation soil over waste
- 1-foot (30 cm) thick gas relief layer consisting of a fine sand with a measured hydraulic conductivity of 0.006 cm/s.
- Geosynthetic clay liner (GCL) (needlepunched type, with slit-film geotextile carrier against geomembrane, and nonwoven geotextile carrier facing down)
- PVC geomembrane
- 1-foot (30 cm) drainage layer sand
- 1-foot (30 cm) vegetative soil
- 0.5 feet (15 cm) topsoil

The design also included vertical gas vents on a 200-foot (60 m) spacing each way. The wells consisted of 18-inch (45 cm) borings 15 to 60 feet deep (4.6 to 18.3 m), with 6-inch (15 cm) dia. slotted PVC pipe, backfilled with pea gravel around the pipe. Failure occurred after the following elements had been constructed:

- gas vents
- sand gas-relief layer
- GCL
- geomembrane
- 8 acres (3.2 ha) had just been covered with 1-2 feet (30-60 cm) of drainage sand

The observed failure mode was the geomembrane stretching and then tearing at the top of the slope. The sand on top of the geomembrane, and the geomembrane, slid downslope along the geomembrane/GCL interface. The GCL did not appear to be distressed. However,

a thin film of bentonite had extruded from the slit-film side of the GCL at the geomembrane interface.

As the failure progressed, and rain eroded portions of the top sand drainage layer, large gas bubbles formed in the geomembrane. Even the exposed GCL appeared to be uplifted by gas pressures. Subsequent installation of 12 gas probes monitored over a period of two months revealed an average gas pressure in the gas-relief layer of 6.8 inches of water (35.4 psf, or 1.7 kPa) in the nine most critical locations. Two of the probes reported average readings of over 10 inches of water column (2.5 kPa). The probe with the highest pressure averaged over the two months was 13.3 inches of water (69 psf, or 3.3 kPa), and had a single high reading of 16 inches of water (83.2 psf, or 4 kPa).

Shear strength testing was conducted on the PVC geomembrane/hydrated GCL interface over a normal load range of 50-250 lb/ft^2 (2.4-12 kPa). The samples were recovered from the field. The measured Mohr-Coulomb shear strength parameters were 16 degrees friction, and a y-intercept of 11 lb/ft^2 (0.5 kPa). The peak and post peak values were the same. Using the moist sand unit weight of 107 lb/ft^3 (17.3 kN/m^2), a gas pressure of 10 inches of water column (52 psf, or 2.5 kPa), and a sand layer thickness of 1 foot (30 cm) the factor of safety can be calculated from Equation (1) as:

$$FS = \frac{11psf + [1ft \cdot 107pcf \cdot \cos(14) - 52\ psf] \cdot \tan(16)}{1ft \cdot 107pcf \cdot \sin(14)} = 0.9999$$

This factor of safety is marginally less than one, which implies potential localized failure. It is useful to note that the factor of safety is extremely sensitive to the shear strength parameters, and assumed pore pressure. A discussion of these sensitivities is provided by Liu et al (1997). For example, ignoring the very small y-intercept of the Mohr-Coulomb envelope reduces the factor of safety to 0.57! Note that the practice of ignoring the y-intercept is a common practice and is often recommended in the literature (e.g. Koerner and Soong, 1998).

In this case history, no strip drains were provided in the gas-relief layer. We can use this opportunity, in hindsight, to calculate the improvement in factor of safety by installing strip drains. The original designer assumed a gas generation rate of 0.1 ft^3/lb/yr (6.24x10^{-3} m^3/kg/yr), which resulted in an estimated gas flux of 0.001 cfm/ft^2 (5x10^{-6} m^3/s/m^2) for this site. The air-permeability of the moist gas-relief layer was measured in the laboratory as 8x10^{-5} cm/s. The equivalent landfill gas permeability and transmissivity can be calculated from Equations (11) and (4) as:

$$k_g = k_{air} \frac{\mu_{air}}{\mu_{gas}} \cdot \frac{\gamma_{gas}}{\gamma_{air}} = 8(10)^{-5} \frac{cm}{s} \cdot \frac{1.79(10)^{-5}N - s/m^2}{1.32(10)^{-5}N - s/m^2} \cdot \frac{12.8N/m^3}{11.8N/m^3} = 1.2(10)^{-4} \frac{cm}{s}$$

$$\Psi_g = k_g \cdot t = 1.2(10)^{-4} \frac{cm}{s} \cdot 30cm = 3.6(10)^{-3} \frac{cm^2}{s} \left(3.6(10)^{-7} \frac{m^2}{s}, or\ 2.32(10)^{-4} \frac{ft^2}{min}\right)$$

Using Equations (1) and (7b), the variation in factor of safety with strip drain spacing (*D*) is graphically presented in Figure 4. The figure indicates a variation in FS from 1.4 with back-to-back strip drains (i.e. no gas pressure buildup), to *FS* = 1.0 with a strip drain spacing of 29 ft (8.8 m). The close strip-drain spacing required by this case history is caused by the poor transmissivity of the sand. One of the lessons learned in this case is that fine sands that may demonstrate relatively good hydraulic conductivity lose a lot of their gas permeability due to the presence of field moisture.
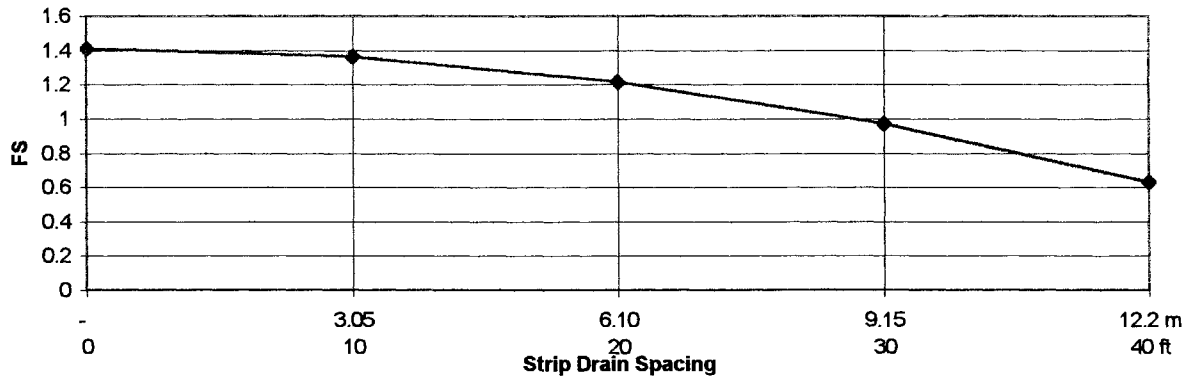

Figure 4. Solution for Case History

LABORATORY STUDY OF GAS TRANSMISSIVITY OF NWNP GEOTEXTILES

In specifying a gas-relief layer, it is tempting to consider use of a NWNP geotextile. However, there is very limited test data available regarding the in-plane air transmissivity (or permeability) of geotextiles. Koerner et al (1984) presented their interpretation of water and air transmissivity testing using a radial flow device. However, the data interpretation appears to have been flawed in that the authors did not take into account the gradient for the air testing. Therefore this reference is not able to be used without further evaluation of the raw data, which was not provided in the paper.

Weggel and Gontar (1993) used the same radial flow device as Koerner et al (1984) to study in-plane air flow through eight NWNP geotextiles. They provided a substantial amount of raw experimental data, and a relatively thorough derivation of the flow analysis. Their testing appears to have been outside of the laminar flow region as indicated by the trends in the test data. Their empirically derived relationship results in a dry-air transmissivity of a geotextile with a thickness of 145 mils (0.37 cm) (presumably a 16-oz/yd^2, or 540 g/m^2 material) of approximately 1x10^{-4} cfm/ft (1.5x10^{-7} m^2/s). This is about one-half the gas-transmissivity of the fine sand described in the failure case history.

Thiel (1999) provides radial air testing data on a suite of three NWNP polyester geotextiles, under both dry and wet conditions, all at a normal load of 1,000 psf (47.8 kPa). The tests were conducted at an average gradient of approximately 750. The tests results indicated the following:

- The wet specimens lost 25-33% of their transmissivity, compared to the dry specimens.
- Going from a 6 denier (6d) -16 oz/yd^2 (540 g/m^2) material to a 45d-32 oz/yd^2 (1,100 g/m^2) material resulted in an order-of-magnitude increase in transmissivity. The average dry transmissivity of the 6d-16 oz/yd^2 (540 g/m^2) material was found to be 6×10^{-4} cfm/ft (9×10^{-7} m^2/s). The average dry transmissivity of 45d-32 oz/yd^2 (1,100 g/m^2) material was found to be 6×10^{-3} cfm/ft (9×10^{-6} m^2/s).
- Using the theory of intrinsic permeability, the estimated in-plane water transmissivity of the 45d material is equivalent to that of a 1-ft (30 cm) thick layer of sand having a permeability of 4.7×10^{-2} cm/s.

The author is currently coordinating radial air and water testing of a 45d-32 oz/yd^2 (1,100 g/m^2) NWNP polyester material and a 6d-16 oz/yd^2 (540 g/m^2) NWNP polypropylene material. The testing purposes are (a) to verify that the theory of intrinsic permeability is valid for these geotextiles, and (b) to determine the materials' air transmissivity under dry and wet conditions. The tests are being conducted and analyzed in a fashion similar to that described by Weggel and Gontar (1993) and Thiel (1999). Typical preliminary results are summarized in graphical form on Figure 5. Preliminary conclusions from these test results are:

- The theory of intrinsic permeability appears to be valid. That is, the intrinsic permeability calculated from air and water tests on the same material is nearly the value. The graph shows this by illustrating that the dry-air transmissivity back-calculated from a water test is approximately the same value as the dry-air transmissivity determined from an air test. The dry-air transmissivity for the 45d-32 oz/yd^2 (1,100 g/m^2) material is approximately 8×10^{-3} cfm/ft (1.2×10^{-5} m^2/s). The dry-air transmissivity of the 6d-16 oz/yd^2 (540 g/m^2) material is approximately one-order of magnitude less, or 8×10^{-4} cfm/ft (1.2×10^{-6} m^2/s).

- The air transmissivity of a 45d-32 oz/yd^2 (1,100 g/m^2) material that has been wetted to field-capacity and stabilized under the air flow is approximately one-order of magnitude less than its dry-air transmissivity.

- The air transmissivity of a 6d-16 oz/yd^2 (540 g/m^2) material that has been wetted to field-capacity and stabilized under the air flow is approximately one-half order of magnitude less than its dry-air transmissivity.

It is the gas-transmissivity of a wet material that would be of primary interest to the design subject of this paper, since the field condition of a gas relief layer would generally be expected to be moist. The wet-air transmissivity of the 45d-32 oz/yd^2 (1,100 g/m^2) material is preliminarily estimated to be between 5×10^{-4} cfm/ft (1.2×10^{-6} m^2/s) and 1×10^{-3} cfm/ft (6×10^{-6} m^2/s). This is 3-6 times the wet-air transmissivity of the fine sand discussed in the case history.

The author advises caution in using any of the geotextile air-transmissivity values presented in this paper for actual designs. The test methodologies and data interpretations

Figure 5. Air Transmissivity of Selected NWNP Geotextiles - Preliminary Laboratory Results
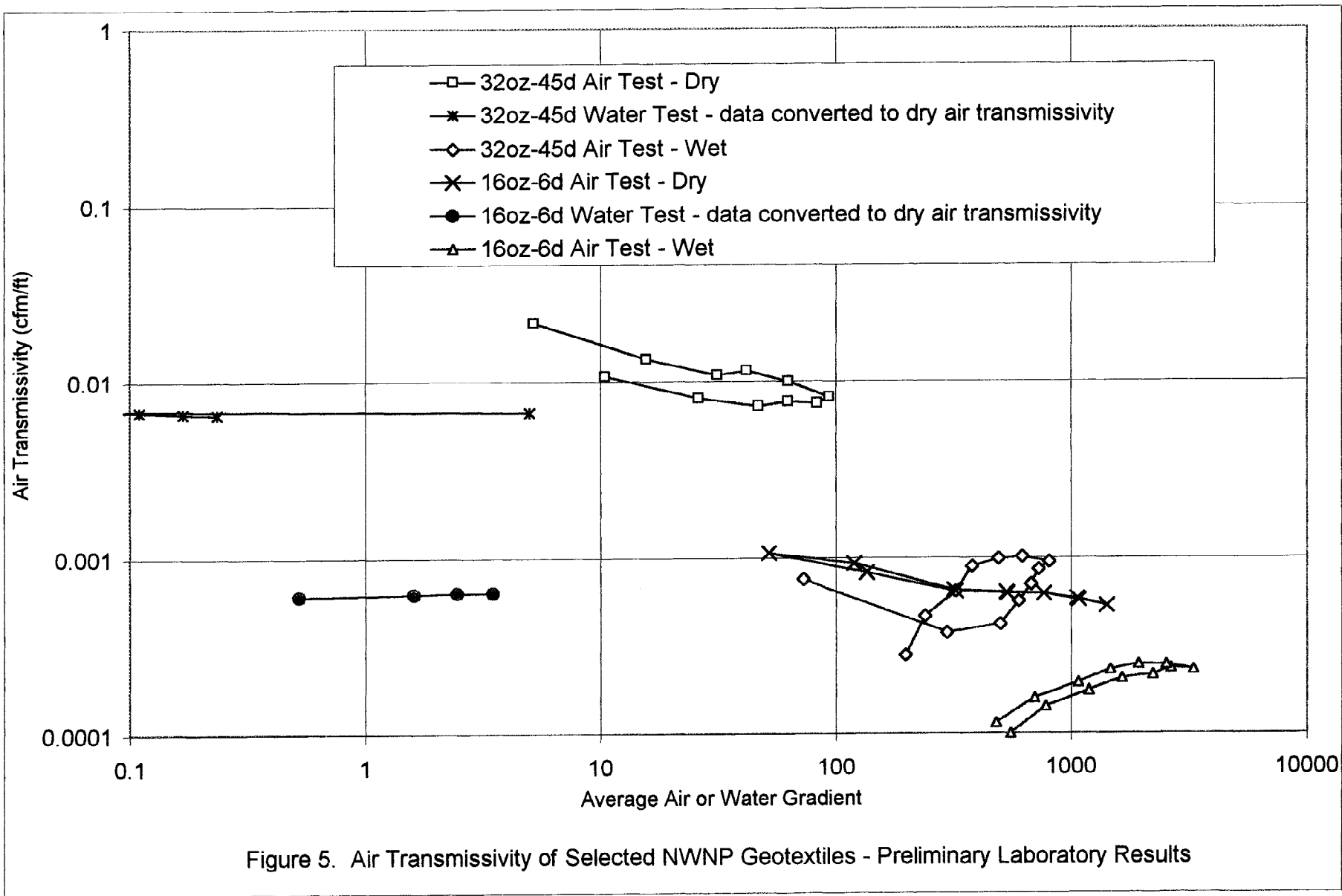
are non-standard at this point. The data is presented to illustrate the potential for using these materials, and the direction that laboratory testing studies need to go.

CONCLUSIONS

Slope stability of landfill covers incorporating geomembrane barriers can be compromised by pore pressures caused by landfill gas. This has been demonstrated by field failures in which gas pressures appeared to play a significant role.

Standard geotechnical and fluid mechanics engineering principles can be used to design final cover systems to accommodate potential landfill gas pressures. However, as is typical with many geotechnical problems, the basic input of field parameters to the analysis, in this case an estimation of the field gas pressures and volumes, is not an exact science, and involves educated assumptions and experience.

Calculations and experimental evidence from the literature suggests that landfill gas flow rates expected in gas-relief layers are generally expected to be laminar, and Darcy's law applies. The fluid-mechanics principle of intrinsic permeability can allow estimations of gas transmissivity and permeability to be made based on more well known, or more easily obtained, values for water.

Limited laboratory test data suggests that coarse, heavy (e.g. 45d-32 oz/yd^2 (1,100 g/m^2)) NWNP geotextiles may have adequate gas transmissivity under field conditions for many typical situations. However, industry testing and design experience in this regard is sparse.

RECOMMENDATIONS AND DISCUSSION

The theoretical solution to gas flow presented in this paper is undoubtedly more developed than the profession's ability to provide the basic input parameters to the model. To that extent, it may be found that the theoretical assumptions presented herein are incorrect when a more accurate understanding of landfill gas generation, flux, and flow mechanisms is attained. However, in lack of any other procedures available, the model presented in this paper is meant to serve as a starting point.

The key input parameter that needs more development is the assumed gas flux that might cause pressures below a landfill cover. To that end, additional gas flow measurements below installed covers would be useful. Gas pressure measurements, as described for the failure history, would also be very useful.

The industry is also in need of good, well documented test data for in-plane gas transmissivity. The testing should be performed at relatively low pressure gradients representative of landfill gas collection requirements, where the flow is laminar. However, higher gradient tests with non-laminar flow would be conservative in that they would result in lower transmissivity values. The testing should be performed not only for dry geotextiles, but also on wet geotextiles at a simulated field moisture capacity obtained from soaking the geotextile and then letting it drain. When possible, it would be useful to provide side-by-side

testing of air and water transmissivity in the laminar flow region to verify that the concept of intrinsic permeability can be applied to geotextiles. The geotextiles being tested should be fully described in terms of their mass per unit area, fiber size, initial thickness, and polymer type.

The model presented herein is probably conservative since many successful landfill covers have been constructed without explicit considerations for gas pressures. However, the author has witnessed several cover construction projects that, even though successful in the end product, experienced significant landfill gas problems during construction. Whether the design procedures presented in this paper are used, or some other method, the author believes that all parties involved with a landfill final cover will be well served if some degree of highly permeable strip drains and gas-relief layer are constructed below the barrier layer system.

ACKNOWLEDGEMENTS

REFERENCES

Fredlund, D.G., Rahardjo, H. (1993) Soil Mechanics For Unsaturated Soils, John Wiley & Sons, Inc., New York.

Geocomp, Inc. (1998) Personal communication with Ron Marsh, 1996-1999.

Giroud, J.P., Bachus, R.C. and Bonaparte, R. (1995) "Influence of Water Flow on the Stability of Geosynthetic-Soil Layered Systems on Slopes", Geosynthetics International, Vol. 2, No. 6, pp. 1149-1180.

Koerner, R. M., Bove, J.A., and Martin, J.P. (1984) "Water and Air Transmissivity of Geotextiles", Geotextiles and Geomembranes, Elsevier Applied Sciences Publishers, Inc., Vol. 1, pp 57-73.

Koerner, R.M., Soong, T.Y. (1998) "Analysis and Design of Veneer Cover Soils", Proceedings of the Sixth International Conference on Geosynthetics, Roseville, MN, IFAI, pp 1-26.

Kavazanjian, E. (1998) "Current Issues in Seismic Design of Geosynthetic Cover Systems", Proceedings of the Sixth International Conference on Geosynthetics, Roseville, MN, IFAI, pp 219-226.

Lambe, T.W., Whitman, R.V. (1969) Soil Mechanics, John Wiley & Sons, New York.

Liu, C.N., Gilbert, R.B., Thiel, R.S., Wright, S.G. (1997) "What Is An Appropriate Factor of Safety for Landfill Cover Slopes?", Proceedings of Geosynthetics '97, Roseville, MN, IFAI, pp 481-496.

McWhorter, D., Sunada, D. (1977) Ground Water Hydrology and Hydraulics, Water Resources Publications, Highlands Ranch, CO.

Muskat, M. (1937) The Flow of Homogeneous Fluids Through Porous Media, McGraw Hill, New York.

Pacey, J.G. (1997) "Insights to Enhanced Landfill Gas Generation", Proceedings to Sardinia '97 Sixth International Landfill Symposium, CISA, Vol. 1, pp 359-368.

Peck, R.B., Hanson, W.L., Thornburn, T.H. (1974) Foundation Engineering, 2nd Ed., John Wiley & Sons, Inc., New York.

Richardson, G.N., and Zhao, A. (1998) "Composite Drains for Side Slopes in Landfill Final Covers", Geotechnical Fabrics Report, Volume 16, No. 5, June/July 1998, pp. 22-25.

Schroeder, P.R., Dozier, T.S., Zappi, P.A., McEnroe, B.M., Sjostrom, J.W., and Peyton, R.L. (1994) The Hydrologic Evaluation of Landfill Performance (HELP) Model - Engineering Documentation for Version 3, USEPA.

Thiel, R.S., Stewart, M.G. (1993) "Geosynthetic Landfill Cover Design Methodology and Construction Experience in the Pacific Northwest", Proceedings of Geosynthetics '93, Roseville , MN, IFAI, pp 1131-1144.

Thiel, R.S. (1999) "Design Methodology for a Gas Pressure Relief Layer Below a Geomembrane Landfill Cover to Improve Slope Stability." Accepted for publication in Geosynthetics International. To be published in 1999.

Weggel, R., and Gontar, W.A. (1993) "In-Plane Air Flow Through Needle-Punched Nonwoven Geotextiles Under Normal Loading", Geotechnical Testing Journal, ASTM, Vol. 16, No.2, June 1993, pp 207-215.

INFLUENCE OF GEOSYNTHETIC PLACEMENT POSITION ON THE PERFORMANCE OF REINFORCED FLEXIBLE PAVEMENT SYSTEMS

Steven W. Perkins, Associate Professor
Muhannad Ismeik, Post-Doctoral Research Associate
Macgregor L. Fogelsong, Graduate Research Assistant
Department of Civil Engineering
Montana State University
USA

ABSTRACT

The use of geosynthetics for the design and construction of reinforced flexible pavements has been complicated by the importance of certain variables known to influence subsequent pavement performance. One such variable is the vertical placement position of the geosynthetic within the base course layer. Results of laboratory-scale model pavement experiments are presented which further show the importance of this design parameter. Two sections reinforced with the same geogrid product are compared to a similar section without geosynthetic reinforcement. Measurements of stress and strain in the pavement system layers are presented and used to quantify the system's mechanical response that was responsible for the levels of reinforcement benefit observed in the test sections.

INTRODUCTION

The successful use of geosynthetics (geogrids and geotextiles) for inclusion as a reinforcement member in the base course layer of a flexible pavement has been historically hampered by an inadequate understanding of how certain variables influence subsequent reinforcement benefit. One such variable that appears to critically influence reinforced pavement performance is the vertical placement position of the geosynthetic within the base course layer.

Studies that have directly examined the influence of placement position of the geosynthetic in the base course layer include Barksdale et al. (1989), Haas et al. (1988), Miura et al. (1990), Moghaddas-Nejad and Small (1996) and Webster (1993). Collective results from these studies indicate that optimal placement position of the geosynthetic is dependent on the magnitude of the applied load, the base course thickness and the strength of the subgrade soil. In general, it appears that as load magnitude increases, the optimal placement position of the geosynthetic becomes deeper in the base layer. For instance, Moghaddas-Nejad and Small (1996) used a light load (0.42 kN) and found that better performance (as determined by permanent deformation of the pavement surface) was achieved when a geogrid was placed in the middle of a thin (40 mm)

base layer as compared to placement at the bottom of the layer. On the other extreme, Webster (1993) applied a load of 130 kN and found better performance by placing the geogrid at the bottom of a 350 mm base as compared to the middle of the base. Figure 1 illustrates results from Webster (1993), where properties of the geogrid used are listed in Table 1. Results from Collin et al. (1996), where sections of varying base course thickness were used and where a geogrid was placed at the bottom of the base, showed that beyond a certain base course thickness, performance began to decrease. This suggests that reinforcement became less effective as the distance between the load and the geogrid exceeded a certain value, meaning that the geogrid was in a position where less load was experienced and less benefit could be derived by the reinforcement. Perkins and Ismeik (1997) have provided a more detailed summary and discussion of these studies.

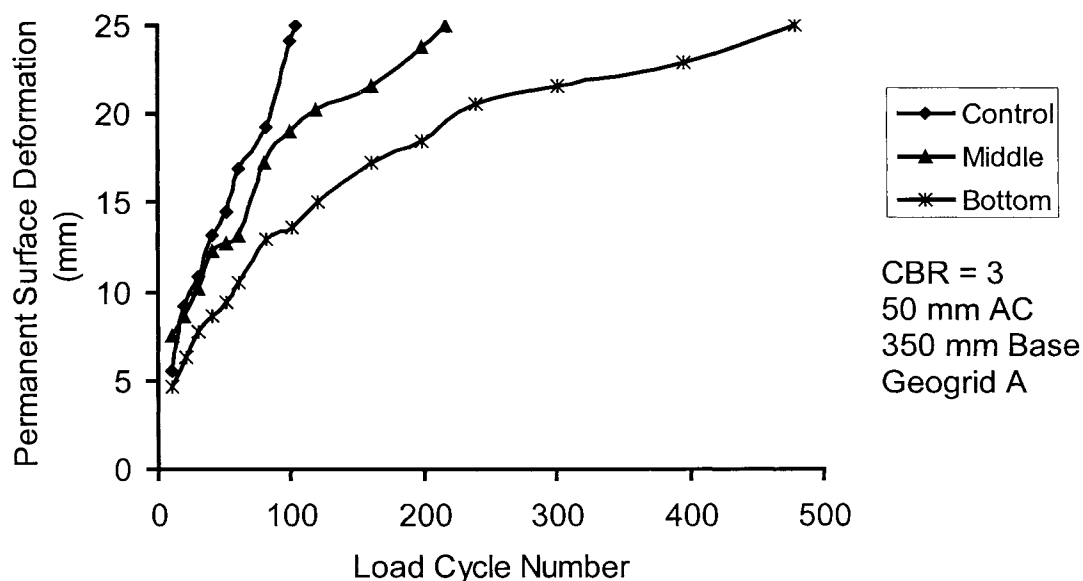Figure 1. Pavement Loading Results From Webster (1993)
(reproduced from Perkins and Ismeik, 1997)

Table 1. Geogrid Properties

Property	Geogrid A
Mass/Unit Area (g/m^2)	215
Wide-Width Tensile Strength at 5 % Strain (kN/m)	
Machine Direction	9
Cross-Machine Direction	13
Wide-Width Tensile Strength (kN/m)	
Machine Direction	13
Cross-Machine Direction	20

The majority of the studies noted above have provided information focusing primarily on the overall performance of the pavement system as described by surface rutting behavior. The focus of this paper is to present data on stress and strain response of test sections incorporating the geogrid described in Table 1 placed at two different positions in the base course layer. An examination of the stress and strain behavior illustrates mechanisms involved in reinforcement and the resulting effect on deformations in the base and subgrade layers.

PAVEMENT TEST FACILITY

The facility used to construct and load the test sections has been described by Perkins et al. (1998). Provided below is a summary of details concerning the test facility and specific details regarding the test sections reported in this paper.

Test Container and Loading Arrangement

Laboratory-scale pavement test sections were constructed in a reinforced concrete box having inside dimensions of 2 m by 2 m in plan and 1.5 m in height and shown in Figure 2.
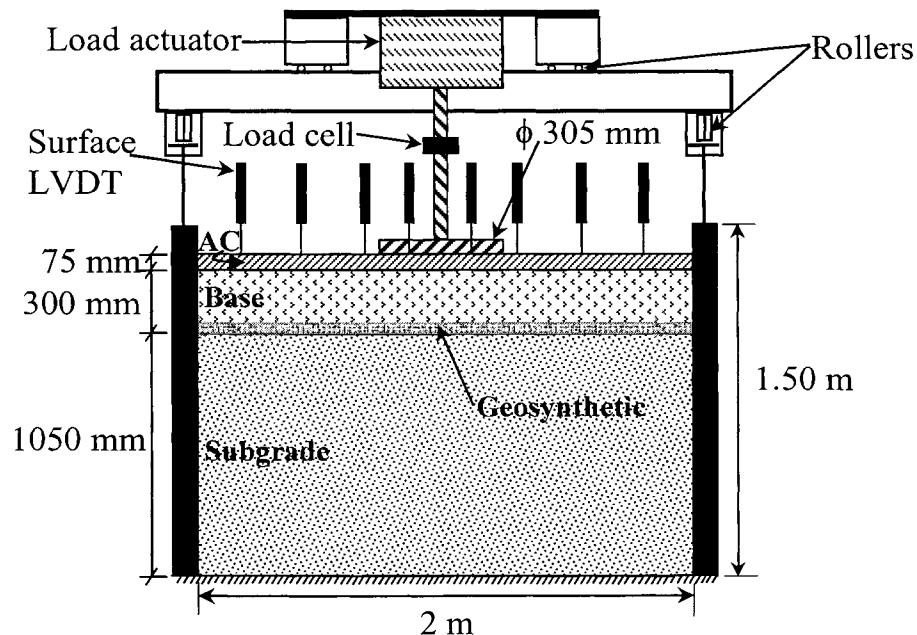

Figure 2. Schematic of Pavement Test Facility

A load frame consisting of several pairs of I-beams securely attached to the concrete box is used to support a load actuator. The load actuator consists of a pneumatic cylinder providing an average load of 40 kN. A load cell is used to monitor the load applied to a 305 mm diameter steel plate that rests on the pavement surface. A waffled rubber pad 4 mm in thickness is placed between the steel plate and the asphalt concrete (AC) surface to aid in distributing the load, resulting in an average plate pressure of 550 kPa. A binary regulator and a data

acquisition/control unit, which has been set to provide a flat-topped triangular load pulse with a period of approximately 1.5 seconds, controls the time-history of load.

A series of linear variable differential transducers (LVDT) are used to monitor both dynamic and permanent pavement surface deformations. The two LVDT's measuring deformation below the load plate extend through holes drilled in the load plate and the rubber pad and rest directly on the AC surface.

Pavement Layer Materials

Results from three tests are reported in this paper. Each test section was constructed with a hot-mix asphalt concrete with as-constructed properties of the material given in Table 2. A crushed stone aggregate was used for the base course material. The material classifies as A-1-a according to the AASHTO classification system and as a GW according to the Unified Soil Classification System with 100 % passing the 19 mm sieve. Specific gravity of the base course is 2.64. As-constructed properties of the base course aggregate are listed in Table 3.

Table 2. As-Constructed Properties of Asphalt Concrete

Section	Thickness (mm)	Bulk Density (kN/m^3)	Air Voids (%)	Asphalt Content (%)	Marshall Stability (lb)	Flow
1	78	23.1	3.3	6.8	2013	26
2	77	23.4	1.9	6.0	2480	20
3	75	22.9	4.3	6.6	1979	16

Table 3. As-Constructed Properties of the Base Course Aggregate

Section	Thickness (mm)	Dry Density (kN/m^3)	Water Content (%)	Degree of Saturation (%)
1	300	20.6	6.4	65.7
2	300	20.5	6.3	63.2
3	300	20.6	5.5	56.5

A high-plasticity natural clay with a specific gravity of 2.7 was used for the subgrade for the sections reported in this paper. The material has 100 % passing the number 200 sieve, a liquid limit of 100 % and a plastic limit of 40 %, classifying the material as an A-7-5 or a CH. Modified Proctor compaction tests result in a maximum dry density of 16.0 kN/m^3 occurring at a water content of 20 %. The clay was prepared by mixing to a target water content of 45 %. The clay was dumped and compacted in 75 mm lifts using a "jumping-jack" trench compactor. As-constructed properties of the subgrade for each test section are listed in Table 4. The subgrade CBR was determined from laboratory tests (ASTM, 1997) on unsoaked samples prepared to the same moisture content and dry density as that in the test box. Very little change in CBR was observed for water contents ranging from 43 to 46 %. These CBR values were verified in situ

using a Dynamic Cone Penetrometer. The Dynamic Penetration Index (DPI) of the subgrade soil was determined following construction. CBR values were estimated from the DPI using the correlation equation provided in MnROAD (1993). All pavement materials were completely removed and reconstructed for each test section. Excavation and sampling of the base course soil in all the test sections has shown that this subgrade did not intermix or pump with the base course aggregate in any of the test sections, which is expected given the plasticity of the clay.

Table 4. As-Constructed Properties of the Subgrade Soil

Section	Dry Density (kN/m^3)	Water Content (%)	Degree of Saturation (%)	CBR
1	11.4	44.8	91.4	1.5
2	11.4	45.1	92.0	1.5
3	11.5	44.2	91.6	1.5

A polypropylene biaxial geogrid was used in two of the test sections. The geogrid has an aperture size of 25 by 33 mm. Other properties of the geogrid are provided in Table 1. As reported in this paper and summarized in Table 5, section 1 was an unreinforced section. Section 2 contained geogrid A placed between the subgrade and the base course layer. Section 3 contained geogrid A placed within the base at 100 mm above the subgrade-base interface. The geogrid placement position was the only variable included in the test sections reported in this paper. Table 5 also provides values of the average load plate pressure and the standard deviation of this pressure for the duration of each of the test sections. As seen from data presented in Tables 2-5, as-constructed properties of the test sections and loading conditions were very similar between the sections. As such, it is believed that direct comparison of results from each test section can be performed with a high degree of confidence.

Table 5. Test Section Configuration, Average Applied Load and Standard Deviation

Section	Geogrid Type	Geogrid Position	Average Load (kPa)	Standard Deviation (kPa)
1	None	None	549	3.6
2	A	Base-Subgrade Interface	549	6.0
3	A	100 mm Above Base-Subgrade Interface	548	3.0

Instrumentation

An extensive array of instrumentation was used to quantify the mechanical response of the pavement sections. In addition to the load cell and surface LVDT's shown in Figure 2, stress cells, strain cells and strain gages were used to monitor response in the pavement layers. Stress cells, marketed by Dynatest, were used to measure total stress in the base and subgrade materials. Strain in the base and subgrade was measured using a LVDT mounted between rectangular end plates measuring 15 by 50 mm and 5 mm thick. The gage length between the

end plates was nominally 80 mm. Stress and strain cells were oriented in the base and subgrade soils to measure response in the vertical direction and in directions radial and tangential to the center of the applied load. These sensors were placed at different radial distances from the centerline of the applied load to establish the variation of response with radial distance. In the base layer, the instruments were concentrated towards the bottom of the base and above the geosynthetic layer and as close as possible to this layer. In the subgrade, the sensors were concentrated towards the top of the subgrade, however sensors were also placed at various depths throughout the layer. Bonded resistance strain gages were mounted to the geogrid materials at different locations. Similar to other sensors, these gages were oriented to measure strain in the radial and tangential directions.

RESULTS

Rut Deformation Behavior

Figure 3 shows the development of permanent rut deformation of the pavement surface directly beneath the load plate versus the applied load cycle number. Significant improvement is seen between sections 1 and 2 when geogrid A is placed at the bottom of the base course layer. Substantially more improvement is observed in section 3 by placing geogrid A 100 mm up into the base course layer. Sections 2 and 3 were not carried out to a rut depth of 25 mm due to time restraints. A Traffic Benefit Ratio (TBR), defined as the number of load cycles necessary to reach a given rut depth in the reinforced section divided by the number of load cycles necessary to reach this same rut depth in the unreinforced section, was computed for sections 2 and 3 for each 1 mm increment in rut depth with the results shown in Figure 4.

Figures 3 and 4 show that section 3 begins to show substantially improved performance over section 2 after 5 mm of rut depth. Beyond this level of deformation, the rate of rut depth development is much less for section 3. A closer examination of Figure 3 for rut depths less than 5 mm shows that while initial rut development is relatively rapid, the majority of the initial rutting does not take place within the first several load cycles. For instance, sections 1-3 reach a rut depth of 5 mm in 200, 3550 and 5750 cycles, respectively. This illustrates that initial rutting is not necessarily a function of the compression of freshly compacted material layers but is a mechanical response influenced by the presence of reinforcement. Figure 5 further illustrates this point by showing the dynamic surface deflection bowls for the three sections for the first load cycle. The lower dynamic deflection seen in sections 2 and 3 indicates that the reinforcement effectively increases stiffness of the pavement system immediately upon load application. Similar results are observed by examining the permanent deflection at the first load cycle. Figure 5 does not, however, show a good correspondence of dynamic deformation for the first load cycle for sections 2 and 3 and long-term rutting behavior. The dynamic center deflection of sections 2 and 3 approach the same value of 2 mm in approximately 20 load cycles and remain approximately equal to each other for the remainder of the test, further indicating that dynamic surface deformation is not necessarily a good indicator of long-term rutting

performance of the sections. Nevertheless, Figure 5 shows that reinforcement of the sections is immediate upon the first load application.
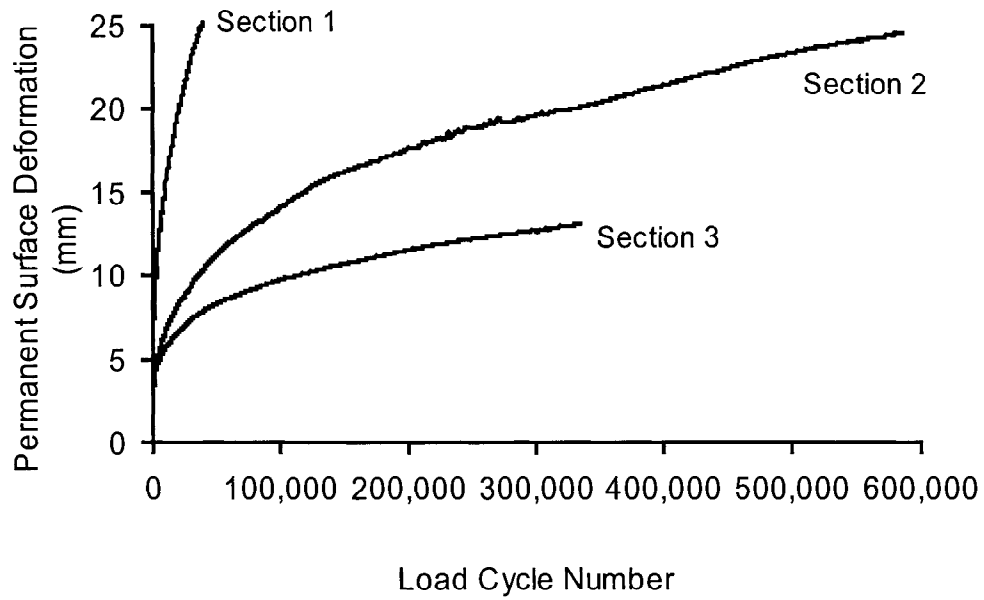

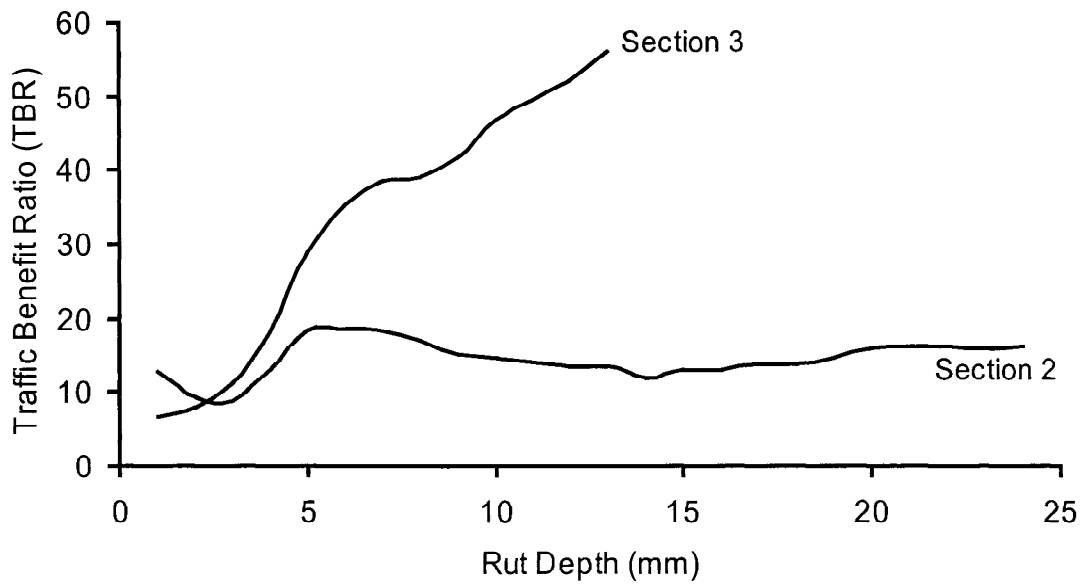Figure 3. Permanent Rut Deformation versus Load Cycle Number

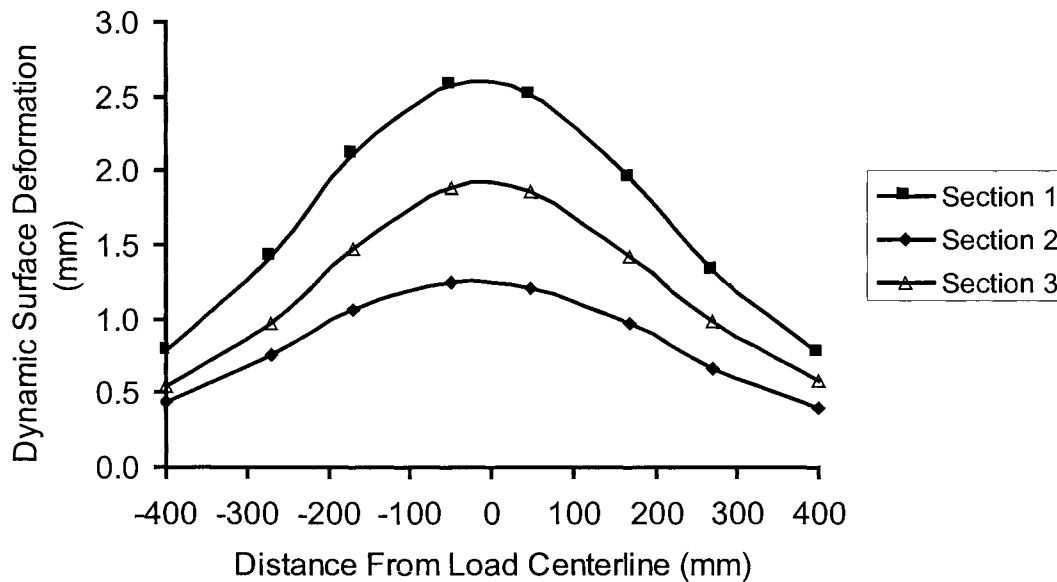Figure 4. Traffic Benefit Ratio versus Permanent Rut Deformation

Figure 5. Dynamic Surface Deformation Bowls for Load Cycle 1

Pavement Layer Response

Figure 6 shows a measure of permanent radial strain developed at the bottom of the base of sections 1-3. The gages were placed at a radius of 100 mm and at a depth of 325 mm below the pavement surface. In this position, the gages were 50 mm above the base course – subgrade interface. For section 3, the gage was 50 mm below the geogrid. The results show less extensional radial strain in the reinforced sections. The values from sections 2 and 3 are not necessarily comparable due to the different location of the gage relative to the reinforcement, but nevertheless, lower strains are seen in section 3 that had overall better performance.

Figure 7 shows a profile of radial strain in the bottom of the base versus radial distance from the load plate centerline at a depth of 325 mm below the pavement surface. Figure 7 was prepared from data corresponding to 40,000 load cycles where the unreinforced section had reached approximately 25 mm of rut depth. From Figures 6 and 7, a dramatic change in behavior of the bottom of the base can be seen between the reinforced and unreinforced sections. The reinforced sections show much less extension of the base below the load plate and much less compression or shoving of the base beyond the radius of the load plate. Similar results are seen for the first load cycle, illustrating that this effect is immediate upon load application. These figures clearly show the ability of the geogrid to restrain lateral motion of the base.

Figure 8 shows permanent radial strain developed in the geogrids in the machine (M) and cross machine (X-M) directions at a radius of 15 and 20 mm, respectively. Significant permanent strains are developed, with the greater strains being developed in the less stiff direction (i.e. machine direction) of the material. It is interesting to note that the strains developed in the geogrid in section 3 are lower than in section 2 while overall performance of section 3 was better. The dynamic strain developed in the geogrid of section 3 was also less than that developed in section 2. Dynamic strains ranging from 0.2 to 0.4 % resulted in calculated dynamic loads ranging from 1.3 to 2.6 kN/m being induced in the geogrids.
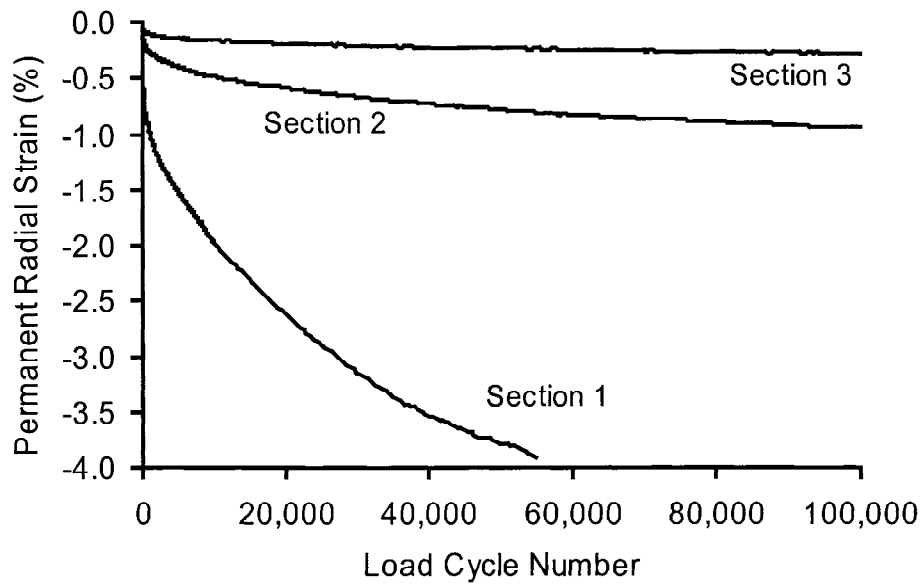
Figure 6. Permanent Radial Strain in the Bottom of the Base versus Load Cycle Number
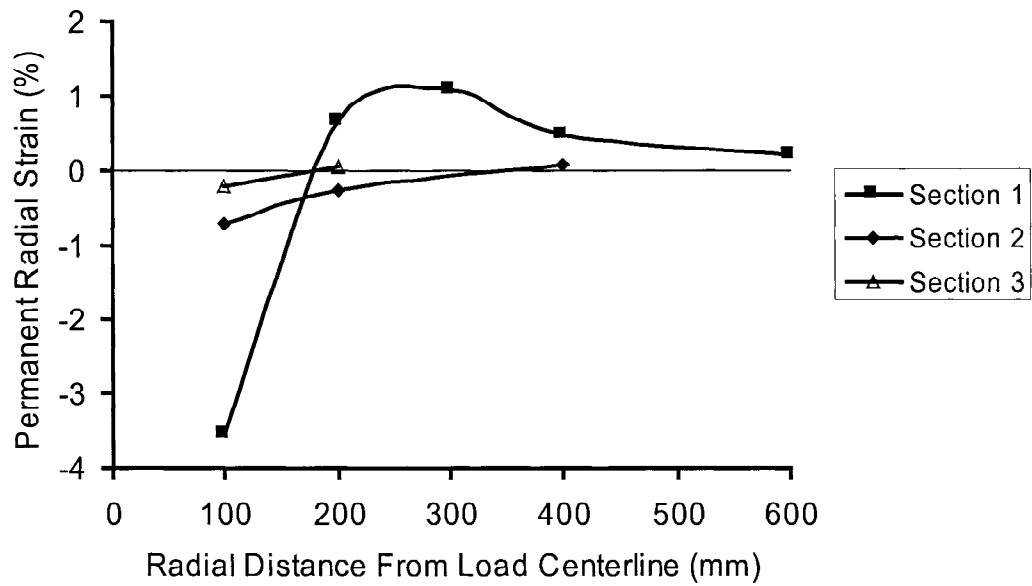(R=100 mm, Z=325 mm)

Figure 7. Permanent Radial Strain in the Bottom of the Base versus Radial Distance at Load
Cycle 40,000 (Z=325 mm)

Figure 9 shows a profile of permanent radial strain versus radial distance developed in the geogrids in the machine direction at load cycle number 7500. This load cycle number was selected since some foil gages became inoperable after this point in the test. This figure illustrates a profile of radial strain that is indicative of a lateral restraint mechanism of the base course soil.
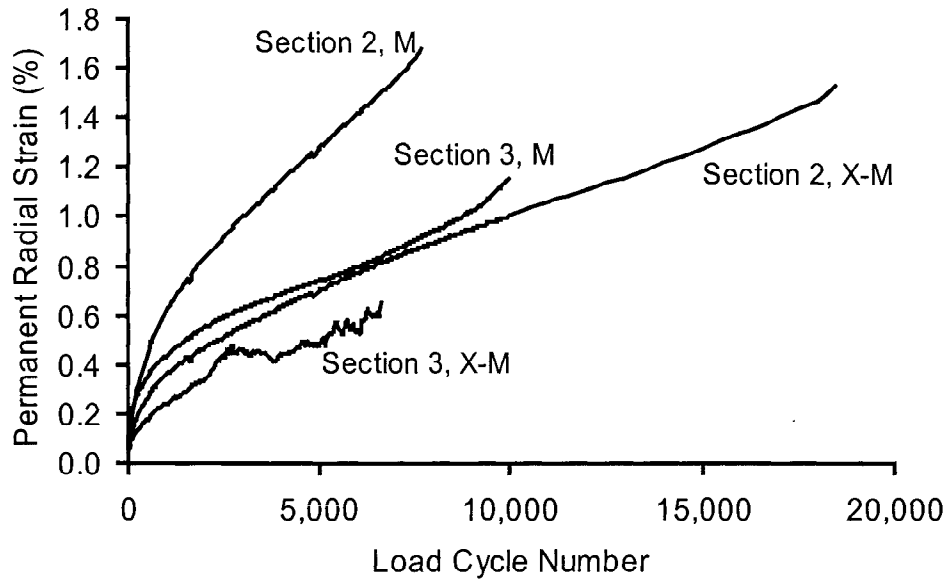
Figure 8. Permanent Radial Strain in the Geogrids in the Machine and Cross-Machine Directions at Radii of 15 and 20 mm, Respectively, versus Load Cycle Number
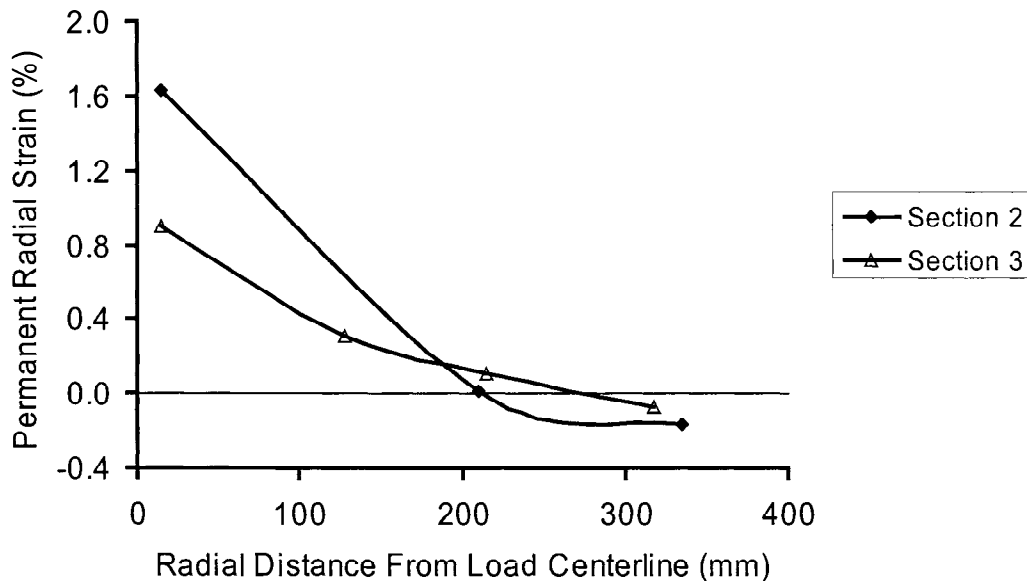
Figure 9. Permanent Radial Strain in the Geogrids versus Radial Distance at Load Cycle 7500
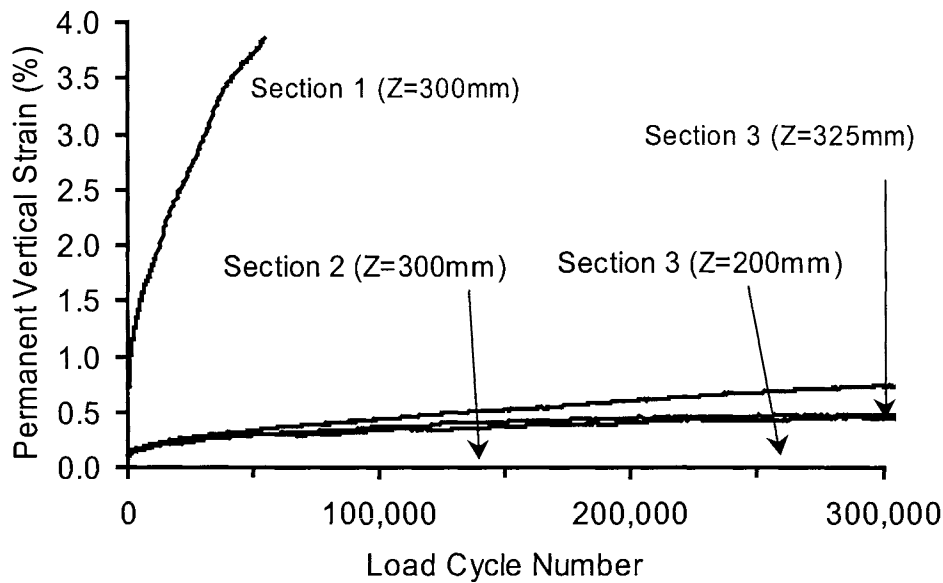
Figure 10. Permanent Vertical Strain in the Base versus Load Cycle (R=65mm)

The result of the mechanisms illustrated above is a reduction of vertical strain in the base course layer. Figure 10 shows the permanent vertical strain developed in the base layer at depths noted in the figure. The two gages for section 3 show vertical strain above and below the geogrid. A clear influence of lateral restraint of the base is seen on vertical strain.

CONCLUSION

Results from instrumented pavement test sections containing a geogrid located at the base course – subgrade interface and 100 mm up into the base course layer have illustrated significant improvement as compared to an unreinforced section. Furthermore, improved performance was seen by elevating the geogrid up in the base as compared to the section where the geogrid was at the interface. Traffic Benefit Ratios as high as 56 were observed for the section where the geogrid was elevated in the base. An examination of behavior for the first load cycle illustrated that improvement due to reinforcement was immediate. Dynamic behavior, however, was not capable of fully accounting for differences between the two geogrid sections.

Measurements of strain in the base course layer and on the geogrid materials has illustrated a significant influence of the geogrid on lateral movement of the base in the vicinity of the geogrid. Strain development in the geogrid layers has been illustrated and is responsible for restraint of lateral movement of the base course layer. These effects have been shown to reduce the permanent vertical strain developed in the base course layer. Movement of the geogrid up into the base course for this particular pavement system has resulted in further improvements in measures that have been shown to be attributable to reinforcement. Additional stress and strain measures made in the subgrade materials have also shown improvements due to reinforcement and are currently being examined.

ACKNOWLEDGEMENTS

REFERENCES

ASTM (American Society of Testing and Materials) (1997), "Standard Test Method for CBR (California Bearing Ratio) of Laboratory-Compacted Soils", ASTM Designation D 1883-94, *Annual Book of Standards*, Section 4, Vol. 4.08.

Barksdale, R.D., Brown, S.F. and Chan, F. (1989), *Potential Benefits of Geosynthetics in Flexible Pavement Systems*, National Cooperative Highway Research Program Report No. 315, Transportation Research Board, National Research Council, Washington DC, USA, 56p.

Collin, J.G., Kinney, T.C. and Fu, X. (1996), "Full Scale Highway Load Test of Flexible Pavement Systems With Geogrid Reinforced Base Courses" *Geosynthetics Intentional*, Vol. 3, No. 4, pp. 537-549.

Haas R., Wall, J. and Carroll, R.G. (1988), "Geogrid Reinforcement of Granular Bases in Flexible Pavements," *Transportation Research Record 1188*, TRB, National Research Council, Washington DC, USA, pp. 19 - 27.

Miura, N., Sakai, A., Taesiri, Y., Yamanouchi, T. and Yasuhara, K. (1990), "Polymer Grid Reinforced Pavement on Soft Clay Grounds", *Geotextiles and Geomembranes*, Vol. 9, pp. 99-123.

Moghaddas-Nejad, F. and Small, J.C. (1996), "Effect of Geogrid Reinforcement in Model Track Tests on Pavements", *Journal of Transportation Engineering*, Vol. 122, No. 6, pp. 468-474.

Perkins, S.W. and Ismeik, M. (1997), "A Synthesis and Evaluation of Geosynthetic-Reinforced Base Layers in Flexible Pavements: Part I", *Geosynthetics International*, Vol. 4, No. 6, pp. 549-604.

Perkins, S.W., Ismeik, M., Fogelsong, M.L., Wang, Y. and Cuelho, E.V. (1998), "Geosynthetic-Reinforced Pavements: Overview and Preliminary Results", *Proceedings of the Sixth International Conference on Geosynthetics*, Atlanta, Georgia, Vol. 2, pp. 951-958.

Webster, S.L. (1993), *Geogrid Reinforced Base Courses For Flexible Pavements For Light Aircraft, Test Section Construction, Behavior Under Traffic, Laboratory Tests, and Design Criteria*, Technical Report GL-93-6, USAE Waterways Experiment Station, Vicksburg, MS, USA, 86 p.

MONOTONIC LOADING OF GEOGRID-REINFORCED FINITE DEPTH GRANULAR MATERIAL

D.L. WALTERS
GRADUATE STUDENT, DEPARTMENT OF CIVIL ENGINEERING, QUEEN'S
UNIVERSITY AT KINGSTON, ONTARIO, CANADA, K7L 3N6

G.P. RAYMOND
PROFESSOR, DEPARTMENT OF CIVIL ENGINEERING, QUEEN'S UNIVERSITY
AT KINGSTON, ONTARIO, CANADA, K7L 3N6

ABSTRACT

When granular supports are built on firm clay or silt subgrades, seasonal softening of a thin upper layer may be sufficient to permit a bearing capacity failure within the granular material. A small-scale model of a track-ballast system overlying artificial subgrades of different compressibilities, including a rigid subgrade, was subjected to a program of monotonic loading. The performance of test configurations reinforced with a single layer of geogrid was compared with unreinforced configurations. Test results indicate that the optimum depth for placing the geogrid reinforcement, for all subgrades, is close to the base of the footing. The compressibility of the thin upper subgrade layer had the greatest influence on the load-settlement response of the system. The geosynthetic geogrid produced a bearing capacity ratio in the range 1.9 to 4.3 while increasing the modulus of subgrade reaction measured at the surface.

INTRODUCTION

Ballasted tracks, roads and airfield pavements are examples of shallow foundations constructed using granular soils where the thickness of the layers are often relatively small in comparison with the width of the loaded area. These ballasted tracks, especially for large gantry cranes, built from granular material are commonly subjected to very heavy loads. When these granular track supports are built over clay or silt subgrades, even though these subgrades may be firm at the time of construction, seasonal softening of a thin subgrade layer may be sufficient to permit a bearing capacity failure within the granular material. Figure 1 shows the effect of seasonal softening on the Benkelman Beam rebound values for an affected subgrade. One method of increasing the load bearing capacity of the granular layer and also reducing the settlement of these tracks is the use of geogrid reinforcement within the track support.

OBJECTIVE

The inclusion of geosynthetic geogrid reinforcement within granular layers has been shown to improve the load-settlement resistance and ultimate bearing capacity (UBC) of the granular material due to the lateral restraint of the soil particles through friction and interlock between these particles and the geogrid (Raymond, 1992). In support of this major premise, this program of study will:

1. Compare the performance of geogrid reinforced and unreinforced granular support (representing ballast) with respect to the magnitude of the load-settlement resistance and UBC.

2. Examine the effect of non-failing subgrades of different compressibility, including that of a rigid subgrade, on the UBC and settlement of the surface footing (representing a continuous set of railroad ties or similar continuous footing).

3. Investigate the effect of a reducing thickness of the finite-depth granular layer on the UBC and settlement of the plane strain model footing when loaded monotonically.

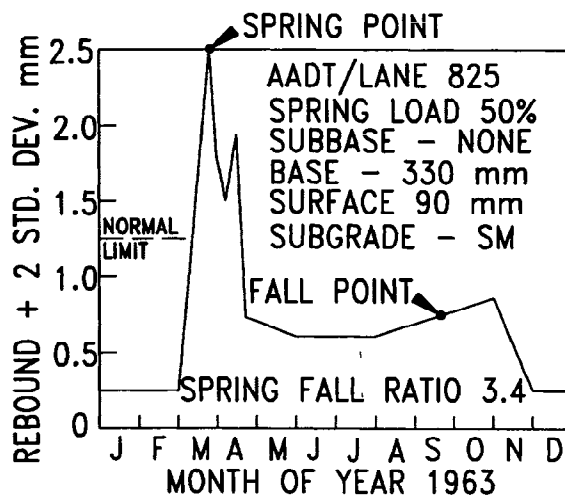4. Establish an optimum depth for placing the geogrid reinforcement below the footing.

Figure 1. Seasonal Effects on Benkelman Beam Rebound Values.

MODEL FORMULATION

In this study an experimental formulation based on an approximate one-tenth ($1/10^{th}$) scale for gantry cranes rail-track practice was used. Track with tie lengths of 2000 mm was modeled by a plane strain 200 mm wide footing. The No. 4 grading specification for ballast with an average size of 30 mm was modelled by spherical 3 mm diameter ceramic particles. The minimum geogrid placement depth below the footing was 12.5 mm. This represents a ballast depth of 125 mm typically required to prevent geogrid damage from the tamper ties. The non-failing flexible subgrades were scaled to represent thin layers of the top surface of the subgrade soil that may be disturbed in-situ down to a depth of 125 mm due to seasonal softening.

GENERAL TEST ARRANGEMENT

Figure 2 shows the general test arrangement. The testing tank 900 mm long, 200 mm wide and 330 mm deep was used to contain the granular soil on which the tests on the model plane strain footing were performed. The sides of the tank were made of 13mm thick Herculite

tempered glass, thereby minimizing the friction between the soil and the tank. The remainder of the tank was made of thick aluminum plates. Tests were performed with and without the geogrid reinforcement. For reinforced configurations, a single layer of geogrid was placed at variable depths below the base of the footing.

In order to simulate the softening of the subgrade a range of subgrade stiffness was included within the configurations. A rough rigid subgrade was simulated by placing a sheet of geotextile over the base of the tank thereafter placing the granular material directly over the geotextile. For compressible subgrades, a single rubber mat was placed between the soil and the base of the tank. Varying the stiffness of the rubber mat enabled the investigation of the effect of different underlying compressible subgrades.

The model footing was 200 mm wide (B) and extended over the entire width of the tank (200 mm) resulting in plane strain testing conditions. An air pressure activated loading piston controlled by a motorized regulator loaded the footing. The rate of average loading to the footing was maintained at 0.5 kPa per second.
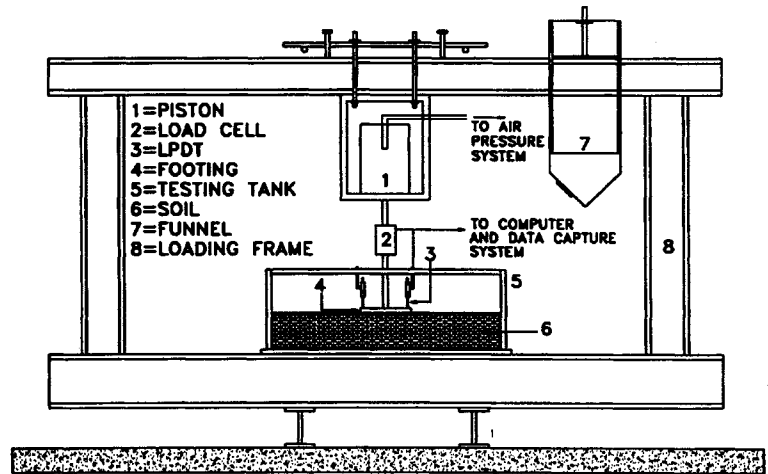
Figure 2. General Test Arrangement.

TEST DETAILS

Granular Material

All tests were performed using the single-sized 3 mm diameter rounded ceramic particles. Ismail (1994) determined that the specific gravity of these particles was 2.4 and the angle of internal friction was 33 degrees. Soil placement in 25 mm thick layers was accomplished by depositing the particles using the specially designed funnel. This layer thickness was halved whenever the depth for placing the geogrid necessitated this change. Ismail (1994) also determined that for each layer placed from an initial drop height of 330 mm, a placement density of 1.5 g/cm^3 (Relative Density of 90%) was attained.

Geogrid Reinforcement

The reinforcement used was a uniaxial geogrid manufactured from a high tenacity polyester fiber with PVC coating. The tensile strength (ASTM 4595) in the machine direction was 30.5 kN/m and 17.8 kN/m in the cross-machine direction. The aperture size in the machine direction

was 1.65 cm and 1.73 cm in the cross-machine direction. The reinforcement was cut so that its length and width were 25.4 mm less than the length and width of the tank. This clearance was provided to ensure that no contact friction was generated between the reinforcement and the walls of the tank. The sheet of geogrid was reused from test to test but was replaced whenever any of the strands became visibly overstressed.

Model Footing

The 200 mm (B) wide model footing was made from a "rigid" 19 mm thick aluminum plate to prevent deflection of the footing during testing. Four sets of thrust bearings, located on drill seats in the top of the footing, were used to ensure that the load always acted vertically on the footing.

Subgrade

Reinforced and unreinforced test configurations were assembled over artificial subgrades. Table 1 presents a summary of the subgrade properties used in this investigation. Three (3) different subgrade compressibilities, including the rigid base, were used.

Placing a single sheet of geotextile over the tank base simulated one option involving the rigid subgrade condition. This condition model a field situation in which the track overlies exposed bedrock, or where chemically stabilized stiff subgrade conditions occur.

One of the compressible subgrade conditions was modeled using a closed cell pure gum rubber mat as the artificial subgrade. Hammond (1997) determined a California Bearing Ratio (CBR) value of 28 for this material using the test procedure outlined in ASTM D 1883-73.

A very compressible subgrade condition was simulated using an open-cell neoprene rubber mat. A CBR value of 1 was determined for this material. This value indicates extreme subgrade compressibility that may occur during frost thaw or in marshy conditions.

Subgrade Type	Description	Thickness (mm)	CBR No.	General Rating
Rigid	Tank base covered with a single sheet of geotextile	0	∞	Excellent
Flexible	Closed Cell Pure Gum amber	12.5	28	Good
Very Flexible	Open Cell Neoprene Rubber	12.5	1	Very Poor

Table 1. Subgrade Properties.

A 193.5 cm^2 (30 in^2) air pressure activated bellofram-loading piston was used to apply the load to the footing. An air filter and a motorized regulator, in series, controlled the air pressure such that a loading rate of 0.5 kPa/s was applied to the footing. A load cell attached to the loading piston and four (4) linear displacement position transducers (LDPT) placed near each of the corners of the footing were used to monitor the load and vertical footing displacements throughout the testing program. The load cell and LDPT were connected to a computer running the data acquisition software at a sampling rate of 1 Hz.

TESTING PROGRAM

Figure 3 shows the general dimensional symbols and the schematic of the test configurations. Four (4) cases of tests were undertaken using granular thickness (H) of 150, 125, 100 and 75 mm.
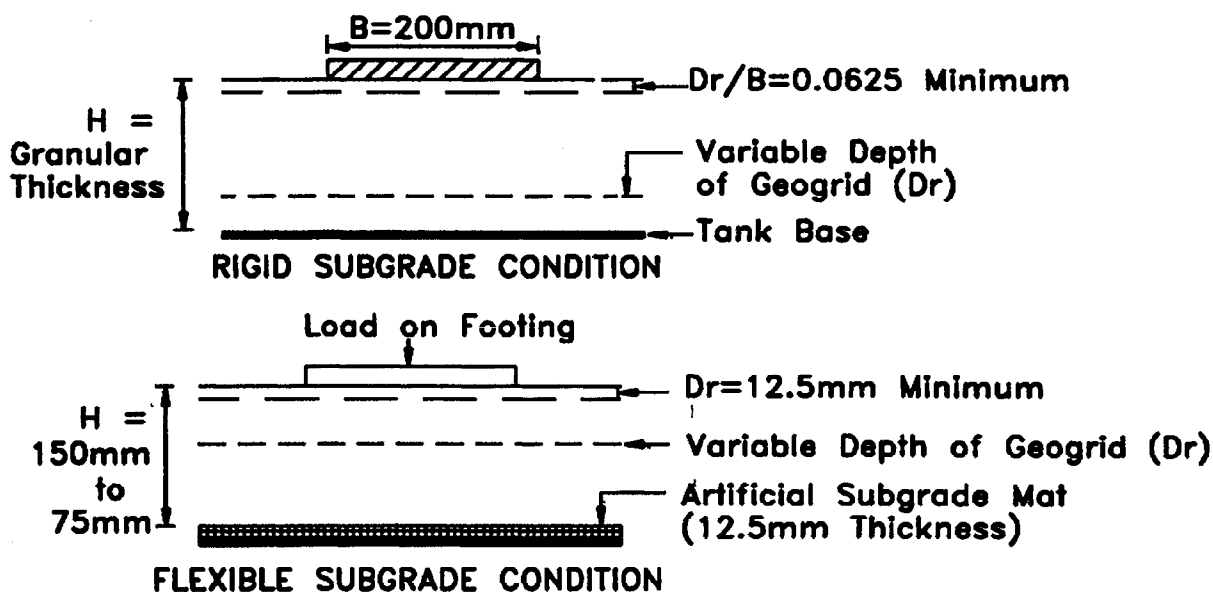
Figure 3. Dimensional Symbols for Test Configurations.

Case A

Test Case A consisted of three (3) series of tests, for the different subgrades in Table 1, using a granular thickness (H) of 150 mm, for a H/B ratio of 0.75. Within each of these series individual tests were performed with the geogrid placed at different depths. A total of twelve (12) different configurations comprising; no reinforcement (unrf'd), reinforcement at (Dr) 12.5, 25, 37.5, 50, 62.5, 75, 87.5, 100, 112.5, 125, and 137.5 mm depth below the surface, formed the tests within Case A for a total of thirty-six (36) tests.

<u>Case B</u>

Test Case B consisted of three (3) series of tests using a granular thickness of 125 mm, for a H/B ratio of 0.625. Ten (10) configurations were investigated. These comprised of a test with no reinforcement (unrf'd) and nine (9) tests with reinforcement at different depths of 12.5 to 112.5 mm below the surface. A total of thirty (30) tests were performed for this case.

<u>Case C</u>

Case C consisted of three (3) series of tests using a granular thickness of 100 mm, for a H/B ratio of 0.5. Twenty-four (24) tests were performed for this case.

<u>Case D</u>

Case D consisted of three (3) series of tests using a granular thickness of 75 mm, for a H/B ratio of 0.375. Eighteen (18) tests were performed for this case.

In total, 108 different test configurations were investigated for this program. In addition, duplicate tests were performed to ensure test repeatability and confirm or revise unexpected results.

RESULTS

<u>Effect of Reinforcement on Load-Settlement and UBC</u>

Figures 4, 5 and 6 show typical load settlement curves. The curves for the Rigid (assigned a CBR value of 100% for comparison purposes only) and Flexible (CBR = 28) subgrades follow the general trend of the typical non-linear bearing capacity curve for an infinite depth of medium dense sand. For the Very Flexible (CBR = 1) subgrade the curves are similar in trend with those of very loose sands. In all cases there was a stiffening of the soil resulting in a reduction of the settlement for any given footing pressure. This reduction was more pronounced after a settlement of about 1 mm for the Rigid and Flexible (CBR = 28) subgrades but only after 6 mm for the Very Flexible (CBR = 1) subgrade. It should be noted that the placement density of the soil remained constant throughout the testing program and so the change observed in the load-settlement response is attributable to the compressibility of the subgrade.

The UBC for the test configurations can be seen to increase with the inclusion of the geogrid reinforcement, which is in agreement with the findings of Raymond (1992). For each test case the UBC increased with a decrease in Dr/B (placement depth of geogrid/footing width). The soil's UBC could be increased by a minimum of 90% by placing one (1) layer of geogrid at the optimum placement depth.
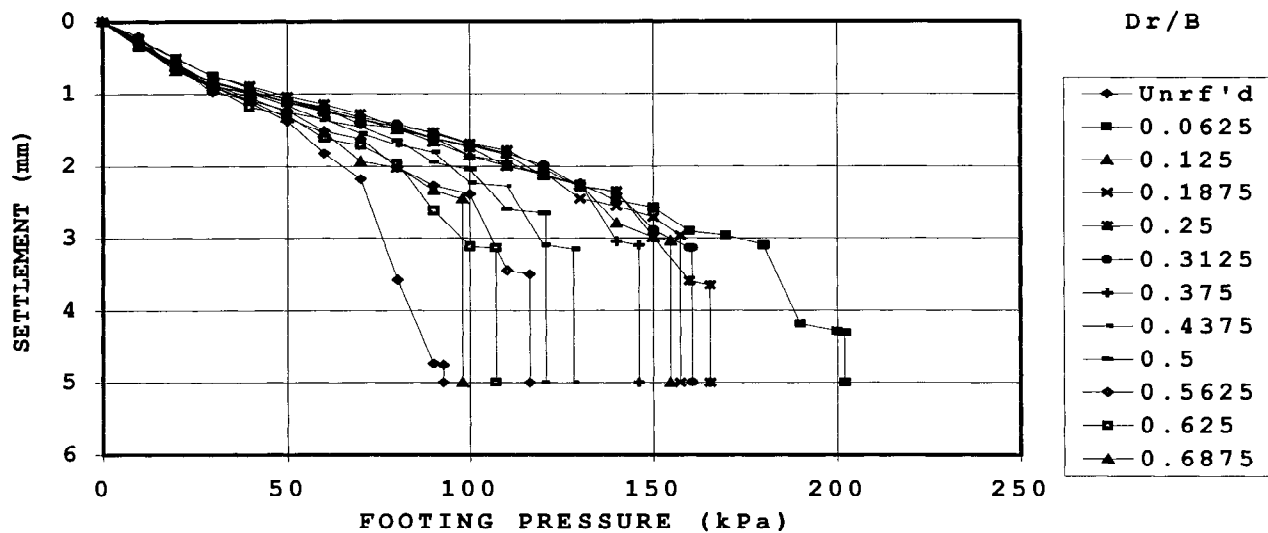
Figure 4. Load-Settlement Curves for Rigid Subgrade at H/B=0.75.
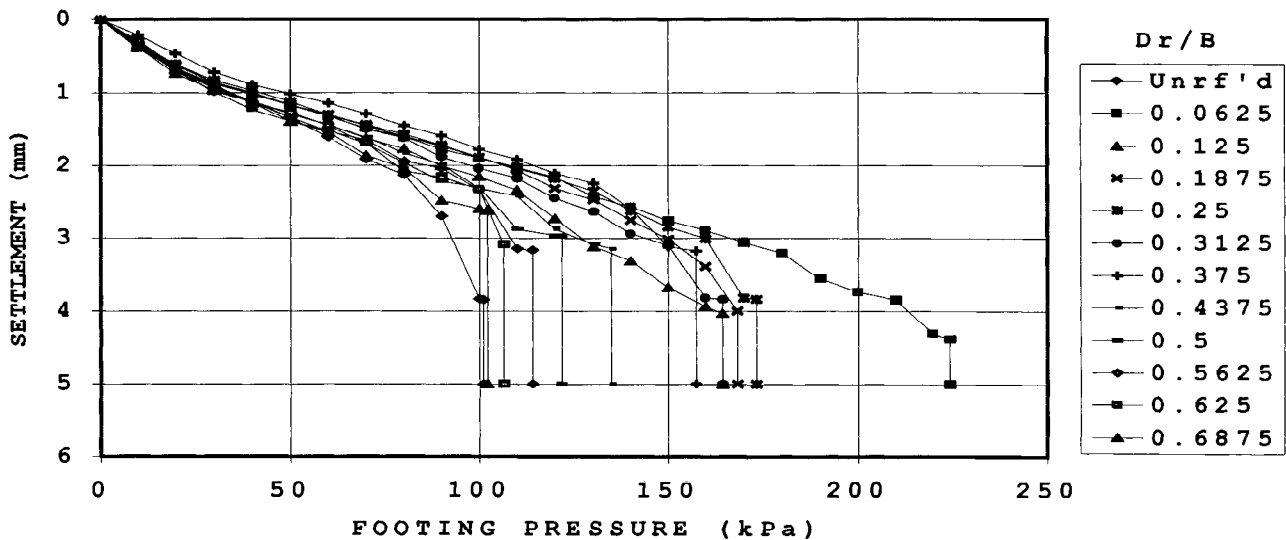
Figure 5. Load-Settlement Curves for Flexible Subgrade (CBR=28) at H/B=0.75.

Effect of Subgrade Compressibility on UBC and Settlement at Failure

Figure 7 is a typical plot of the influence of subgrade compressibility on the UBC of the model track-ballast system. The results indicate that the UBC was only slightly affected by the compressibility of the underlying subgrade when the Dr/B ratio remained constant. The UBC increased with a decrease in Dr/B but became more prominent after Dr/B became less than 0.5. This is in agreement with the findings of Raymond (1992).

There is a clear performance benefit due to the inclusion of the geogrid within the granular layer overlying the Very Flexible (CBR = 1) subgrade. A plateau of high values was obtained between Dr/B = 0.0625 to 0.25. This contrasts with peak values for the UBC for the other subgrade conditions.

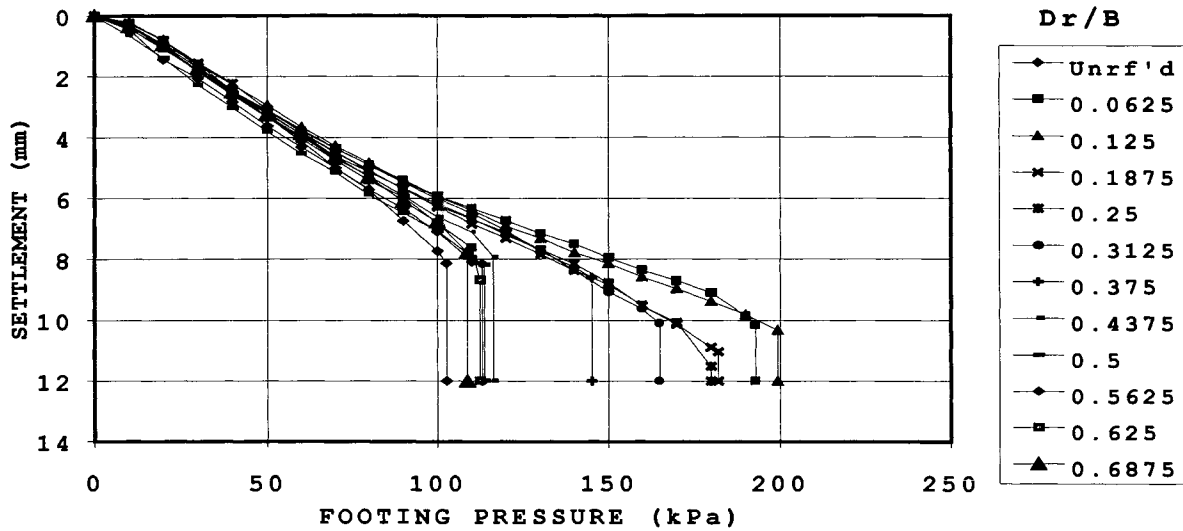Figure 6. Load-Settlement Curves for the Very Flexible Subgrade (CBR=1) at H/B=0.75.
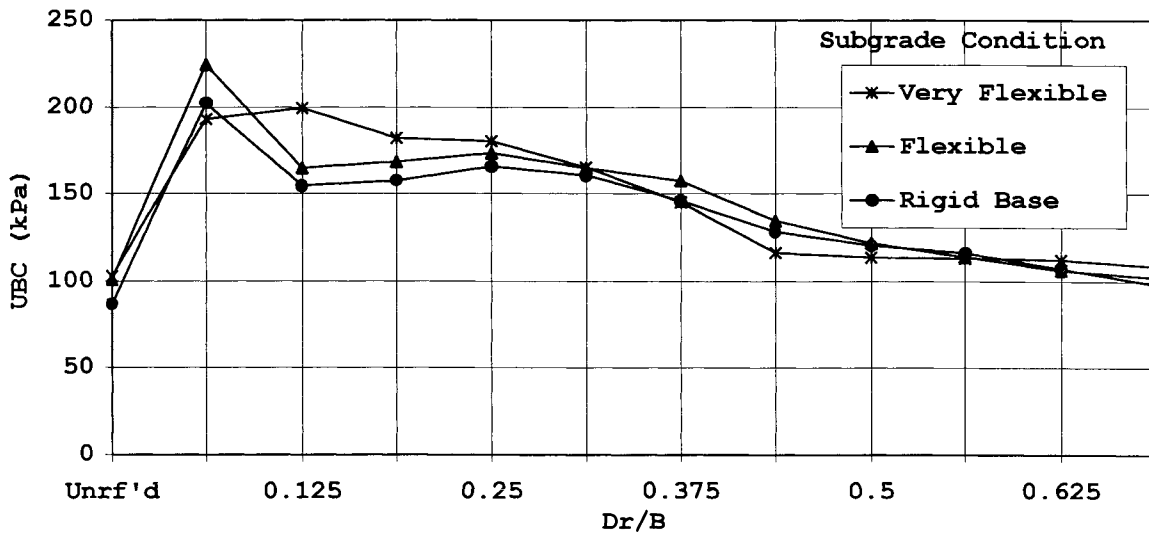
Figure 7. Influence of Subgrade Compressibility and Reinforcement on UBC at H/B=0.75.

Figure 8 shows that subgrade compressibility has a significant influence on the settlement at failure (Sf). The settlement at failure was fairly constant in the range 1.5 to 2.0% of the footing

width for the Rigid and Flexible (CBR=28) subgrades. However, for the Very Flexible (CBR=1) subgrade the settlement was in the range of 4 to 6% of the footing width.

Effect of H/B ratio on UBC and Settlement at Failure

Figures 9 and 10 show the effect of H/B ratio and reinforcement on the UBC and settlement at failure (Sf) for the Very Flexible (CBR = 1) subgrade. These responses are typical for all the subgrade conditions.

The results indicate that a reduction in the H/B ratio will produce a greater increase in the UBC of the reinforced test configuration when compared with the unreinforced test configurations. The reduction in the H/B ratio also increased the optimum Dr/B ratio from 0.0625

Figure 8. Influence of Subgrade Compressibility and Reinforcement Depth on Settlement at Failure at H/B=0.75.

Figure 9. Effect of H/B ratio on UBC for the Very Flexible Subgrade (CBR = 1).

Figure 10. Effect of H/B ratio on the Settlement at Failure (Sf) for the Very Flexible Subgrade (CBR = 1).

and 0.125 for the Flexible and Very Flexible subgrades respectively, found for the thicker granular depths with larger H/B ratios. This change in the buried depth is due to the compressible subgrades having a greater influence in the UBC of the system, as the soil layer became thinner and thinner.
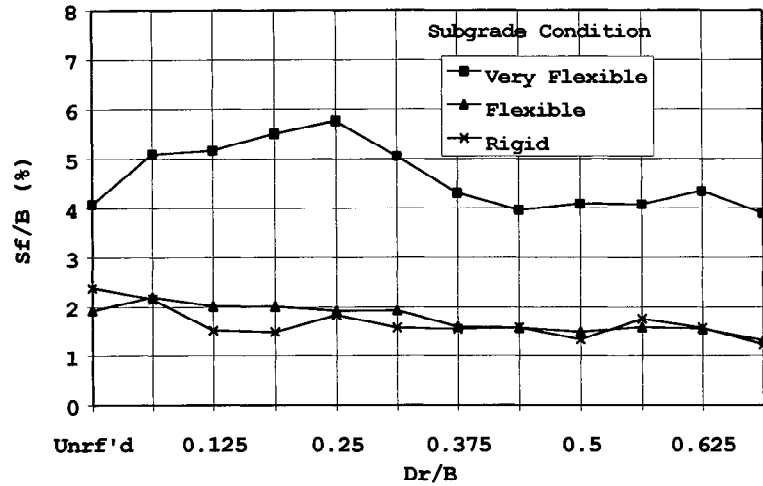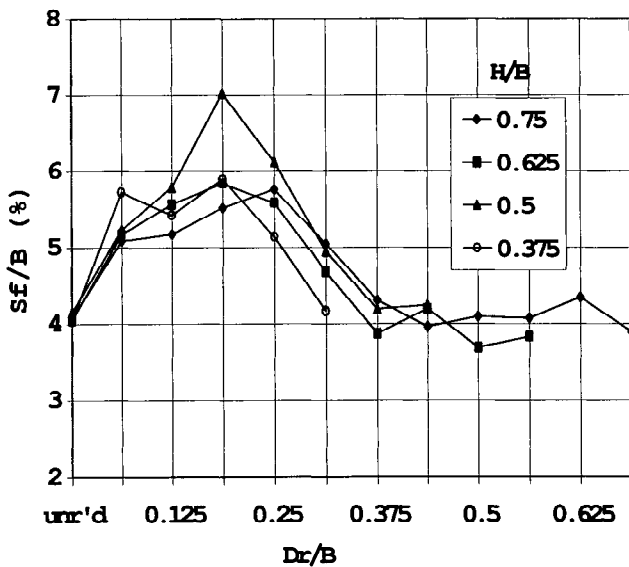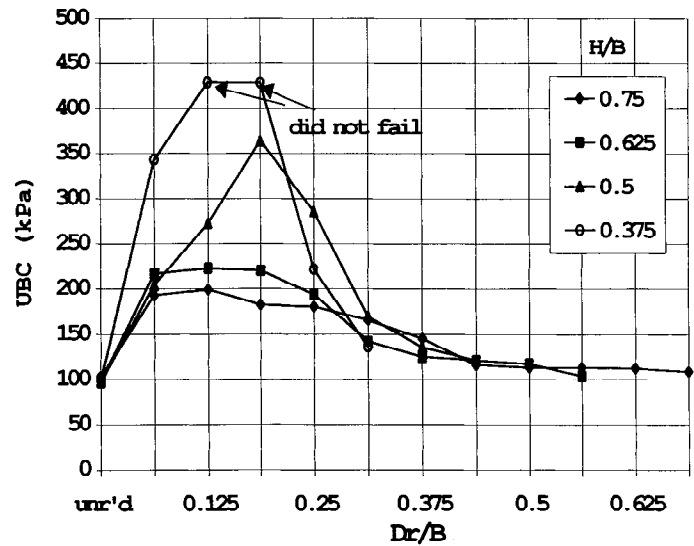
Optimum Depth for Placing the Reinforcement

The optimum depth for placing the geogrid was influenced by both the subgrade compressibility and H/B ratio. For the Rigid subgrade the optimum depth remained constant at Dr/B = 0.0625 for all the test cases. An optimum depth of Dr/B = 0.0625 was also determined for the Flexible (CBR = 28) subgrade for H/B = 0.75 to 0.5. At H/B = 0.375 the optimum depth changed to Dr/B = 0.125. For the Very Flexible (CBR = 1) subgrade the optimum depth was found to be at Dr/B = 0.125 for H/B = 0.75 to 0.625. The optimum depth then increased to Dr/B = 0.1875 for the thinner granular depths of H/B = 0.5 to 0.375.

Bearing Capacity Ratio

The inclusion of the geogrid reinforcement, at the optimum depth, has been shown to be very effective in improving the load-settlement resistance and UBC as compared with the bearing capacity for the same condition in the unreinforced tests. Binquet and Lee (1975) used the term bearing capacity ratio (BCR) at failure to compare the data from the reinforced and unreinforced tests. The BCR was defined as:

$$ BCR = \frac{q_r}{q_u} \tag{1} $$

in which q_u is the footing pressure on the unreinforced soil and q_r is the footing pressure on the reinforced soil; both measured at the UBC.

Figure 11 shows the results of this program when the geogrid was placed at the optimum depth and indicated that the BCR values will follow the same trend as those from the study published by Binquet and Lee (1975) and Omar et al. (1993). Reductions in the H/B ratio resulted in increases in the BCR values, ranging from about 1.9 to 4.3. It may also be seen that the greatest increase in the BCR was associated with the Very Flexible (CBR = 1) subgrade, indicating that the greatest
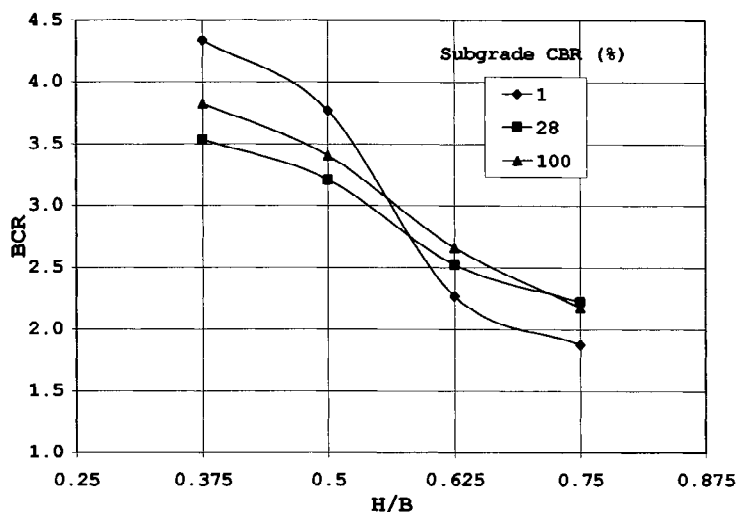
Figure 11. Bearing Capacity Ratio for all Subgrade Conditions with the Geogrid at the Optimum Depth for maximum UBC.

performance benefits, with respect to the UBC, could be derived when using compressible subgrade conditions.

Figure 12 shows the secant modulus of subgrade reaction (ks) at the loaded surface taken between 25 to 75% of the ultimate load. The increase in the modulus of subgrade reaction, for each different subgrade condition, was an indication of the stiffness added to the granular track support with the inclusion of the geogrid. It may also be seen that the modulus of subgrade reaction will decrease with an increase in the compressibility of the subgrade. This would suggest that while the geogrid would increase the modulus of subgrade reaction, increasing the rigidity of a compressible subgrade would have a greater effect.
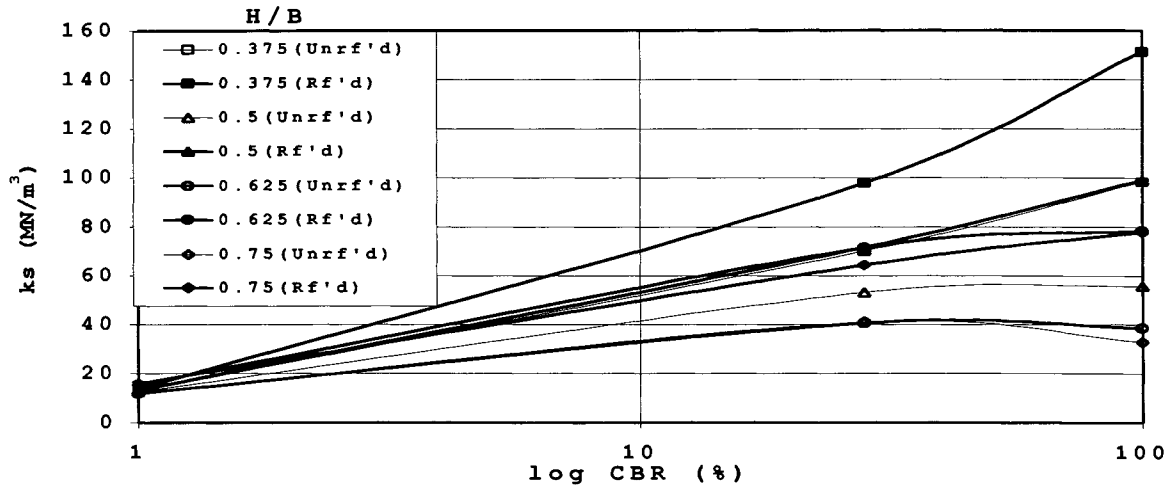
Figure 12. Percent Reduction in Settlement (S) due to the inclusion of the Geogrid at the Optimum Depth for maximum UBC.

DISCUSSION

During the loading of the footing, it may be seen from the load-settlement curves that "seating" of the footing had affected the initial segment of the curves up to about a contact footing pressure of 10 kPa. The secant modulus of subgrade reaction was taken between 25 to 75% of the ultimate load to avoid this initial segment which could have distorted the results obtained.

The optimum depth for placing the geogrid in order to maximize the UBC of the track support was shown to be as close as 6 to 12% of the footing width below the base of the footing. For a typical track tie of 2000 mm wide, the placement depth would then lie between about 120 to 240 mm. These placement depths are approximate multiples of the standard specified compacted lift thickness of 100 to 200mm (AREA, 1975) for granular material, and should not pose a serious concern for construction crews.

Previous studies at Queen's University (Ismail, 1994, and Hammond, 1997) using small-scaled geogrids with stiffness ranging from about one-half to greater than 10 times that of this uniaxial grid have report similar observed behaviour of the track-grid-ballast system as presented in this paper. Current studies are underway to compare the performance benefits derived from using geosythetic geogrids with that obtainable from high strength/modulus geotextiles.

CONCLUSION

It is concluded from the model tests performed that for non-failing subgrades with a granular thickness/footing width (H/B) ratio in the range $0.375 \leq H/B \leq 0.75$:

1) The load-settlement resistance of the track support was significantly increased with the inclusion of the reinforcing geogrid within the granular layer. The bearing capacity ratio increased with a decrease in the granular thickness/footing width ratio and was in the range 1.9 to 4.3.
2) The ultimate bearing capacity was only slightly affected by the compressibility of the underlying subgrade when the geogrid placement depth/footing width ratio remained constant.
3) Reducing the granular thickness/footing width ratio showed a trend of greater increases in the ultimate bearing capacity when the reinforcement was placed at the optimum depth as compared with the unreinforced test configuration.
4) Settlement at failure was not greatly affected by reducing the thickness of the granular layer but mainly by the compressibility of the subgrade.
5) The optimum depth for placing the geogrid to produce the maximum ultimate bearing capacity was close to the base of the footing and occurred at a geogrid placement depth/footing width of 0.0625 for the Rigid subgrade; between 0.0625 to 0.125 for the Flexible (CBR = 28) subgrade; and between 0.125 to 0.1875 for the Very Flexible (CBR = 1) subgrade.

RECOMMENDATIONS

The results of this study have supported the premise that the inclusion of geogrid reinforcement within a granular support for ballasted tracks will reduce the settlement while increasing the UBC of the soil. This statement holds true for all subgrade conditions. It is recommended that the geogrid should be placed close to the base of the track, Dr/B = 0.0625 to 0.1875, where B is the track width, in order to create a stiffer granular soil mass. On soft subgrades, this stiffening of the soil could be expected to increase the maintenance cycles and allow for increased axle loads. It was also shown that the compressibility of the subgrade had a greater influence on the settlement of the track than the inclusion of the geogrid. It is also recommended that subgrade softening should be prevented or mitigated by the adherence to correct engineering internal drainage design principles and maintenance practice.

APPLICATION BENEFIT

Figures 13 and 14 show applications of this research. In Figure 13, geosynthetic cells were placed within the track support of a ballast gantry crane track. These cells reduced the vertical settlement and confine the lateral movement of the ballast that resulted from the reinforcement of the track support. The decrease in track movement at the reinforced sections resulted in a reduction of the maintenance costs.

Walls and Galbreath (1987) have also included geogrid reinforcement in ballasted railway track rehabilitation. The inclusion of the geogrid reduced the three (3) monthly maintenance cycle to a cycle of over three (3) years. These case studies are clear indications of the performance benefit to be expected by including geogrid reinforcement in ballasted track support.

ACKNOWLEDGEMENTS
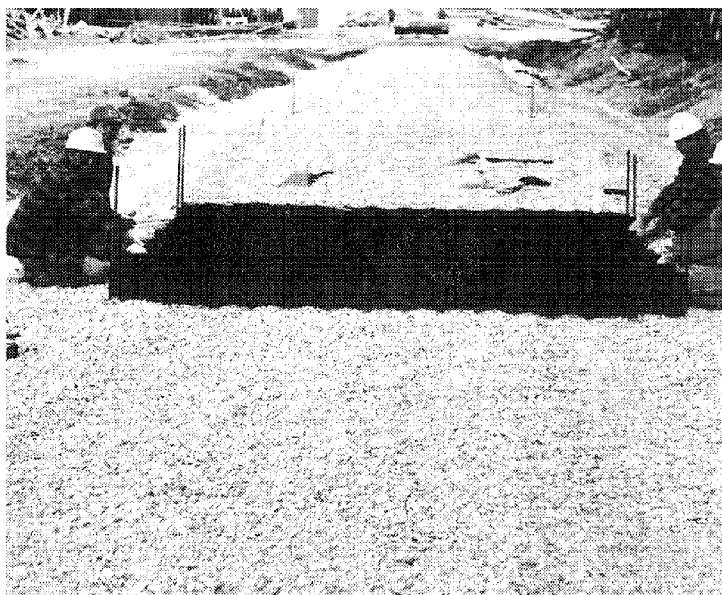
Figure 13. Application of Geosynthetic Reinforcement to a Ballasted Track.

Figure 14. Geogrid Reinforcement of a Ballasted Railway Track.

REFERENCES

Bathurst, R.J., Raymond, G.P. and Jarrett, P.M. (1986), "Performance Of Geogrid-Reinforced Ballast Railroad Track Support", 3rd International Conference on Geotextiles, Vienna, Austria.

Binquet, J., and Lee, K.L, (1975), "Bearing Capacity Analysis of Reinforced Earth Slabs", Journal of the Geotechnical Engineering Division, ASCE, Vol. 101, No. GT12, pp. 1257-1276.

Hammond, M.E., (1997), "Reinforcement of Shallow Granular Layers Overlying Bases of Different Compressibilities", M.Sc. Thesis, Queen's University, Kingston, Ontario.

Ismail, I., (1994), "Geosynthetic Reinforcement of Granular Layered Soils", Ph.D. Thesis, Queen's University, Kingston, Ontario.

American Railway Engineering Association, (1975), Manual for Railway Engineering.

Omar, M.T, Das, B.M., Puri, V.K., and Yen, S.C., (1993), "Ultimate Bearing Capacity of Shallow Foundations on Sand with Geogrid Reinforcement", Canadian Geotechnical Journal, Vol. 30, pp. 545-549.

Raymond, G.P., (1992), "Reinforced Sand Behaviour Overlying Compressible Subgrades", Journal of Geotechnical Engineering, ASCE, Vol. 118, No. 11, pp. 1663-1680.

Walls, J.C., and Galbreath, L.L., (1987) "Railroad Ballast Reinforcement using Geogrids", Proceedings Geosynthetics Conference, Vol. 1, pp. 38-45.

LABORATORY TESTS TO DETERMINE THE DIRECTION OF MOVEMENT OF PARTICLES ON A HORIZONTAL PLANE IN A ROAD DURING LOADING

THOMAS C. KINNEY, Ph.D., P.E.
SHANNON & WILSON, INC., USA

ABSTRACT

This paper hypothesizes that in order for a geogrid to be effective in base reinforcement, it must be placed in a position where there is significant particle movement and it must be able to resist the motion of the particles. This paper presents a series of tests to show the direction of particle movement on the plane of the geogrid under a rutting wheel load. During passing of the wheel, the particles move in a generally elliptical path but do not quite return to their initial positions. The major axis of the ellipse changes with distance from the center of the wheel path. The permanent movement of the particles is generally at an angle to the wheel path, not straight outward. Therefore, geogrids must resist a rotational particle movement during loading to resist fatigue cracking and an overall diagonal particle movement to resist rutting.

INTRODUCTION

Geogrids are being used in paved roads for base reinforcement. There is an ongoing controversy over the importance of the rigidity of the aperture structure in this application. The hypothesis of this paper is that to stabilize a road, a geogrid must resist the movement of the particles on the plane of the geogrid. This motion is generally elliptical during loading and, overall, is at an angle to the direction of the wheel movement. This paper presents the results of a series of tests that determine the direction of movement of the particles on the geogrid surface.

Under some circumstances, geogrids placed between the base and subgrade or in the base reduce both the plastic deformation (rutting) and the elastic deformation (fatigue cracking) (Webster, 1993; Fu, 1998; and Kinney, 1998). Rutting is developed through a combination of compaction (or consolidation) of the soils in the wheel path, and movement of soil particles out

from under the wheel path. In a properly designed system, the compaction of the base material should be minimal, and any rutting of the base would come through an outward migration of base materials. For a geogrid to be effective it must be placed in a zone where this outward migration is relatively large, and the geogrid must have sufficient stiffness to resist the particle motion.

There is evidence that geogrids with a stable grid aperture perform the base reinforcement function most efficiently. The Torsional Rigidity Test (Kinney and Yuan, 1995; and Yuan, 1993) was developed to help explain why certain geogrids performed better than others in full-scale tests on base reinforcement performed by the Waterways Experiment Station (Webster, 1993). The Torsional Rigidity Test consists of holding a node and twisting it in the plane of the geogrid. The aperture stability is defined as the torque divided by the rotation. The Torsional Rigidity Test correlated well with geogrid performance for the conditions tested, which infers that aperture rigidity is an excellent indicator of geogrid performance, at least for the conditions tested.

TEST FACILITY

The two different test apparatuses used were significantly different in the size, shape, and materials used, and the method of loading; however, the results are very similar. Most of the tests were performed with the second one, so that one is described herein. It is interesting to note that the results are not critically dependent on any of the dimensions or other attributes described.

The test apparatus was a box with a glass bottom. The box was filled with sand and a wheel was moved over the surface of the sand. The particle movements on the glass bottom were recorded with a camera and later digitized. The particle movements on the upper surface were measured with scales and a micrometer caliper.

Test Apparatus

Photographs 1 and 2 show the test apparatus. Photograph 3 shows one of the pictures taken through the glass bottom of the box.

The inside of the box was 1.75 meters long, 0.46 meter wide and 0.11 meter deep. A 0.3-meter-square hole was cut in the bottom of the box, and a 6.4mm thick, tempered glass plate was placed on the bottom of the box. A transparency with a grid was taped to the bottom of the glass plate under the hole.

The loading mechanism consisted of a pneumatic wheel attached to a loading platform. The wheel was 230mm in diameter and 76mm wide with a nearly flat running surface. The load was applied by pushing the loading cart slowly over the surface and then lifting the wheel off
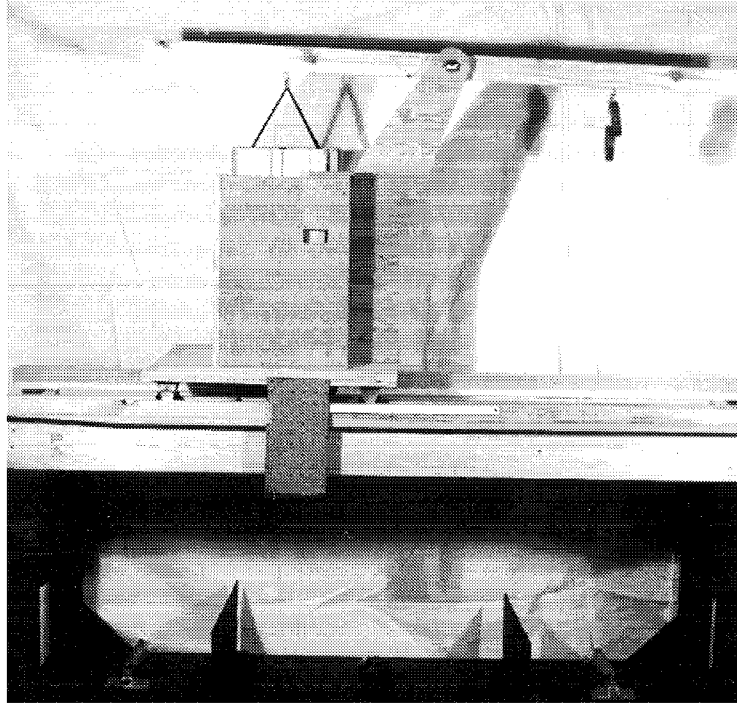
Photograph 1 – Test Apparatus
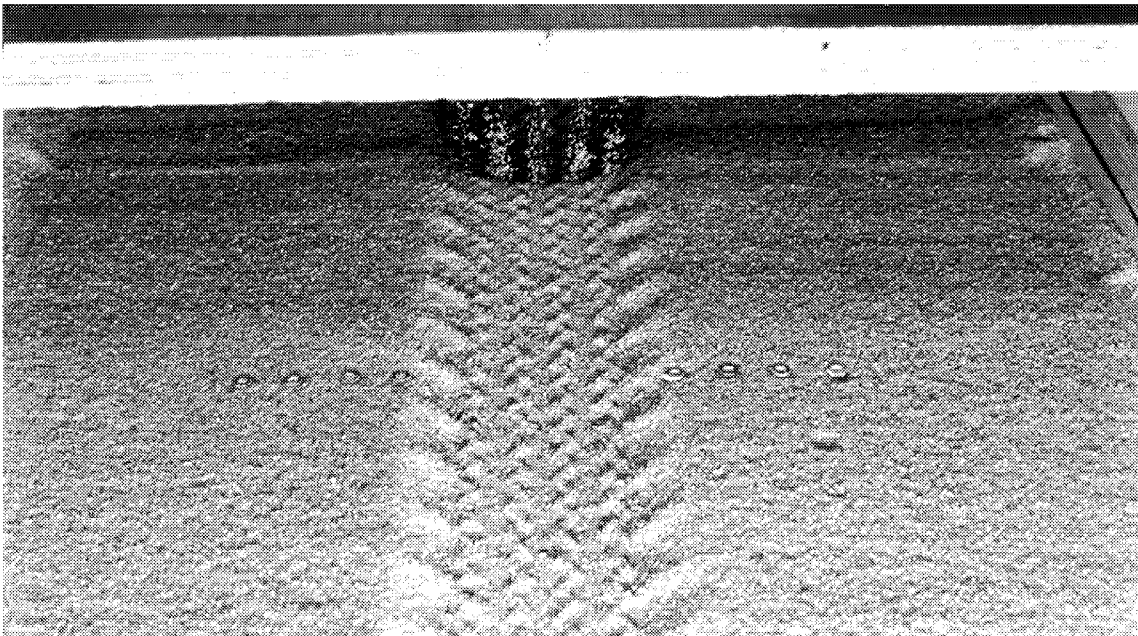
Photograph 2 - Surface of Sand During Testing

the surface for the return trip. Sometimes the load was pushed over the surface in one motion and others times it was stopped at strategic points to take still pictures as the wheel passed.
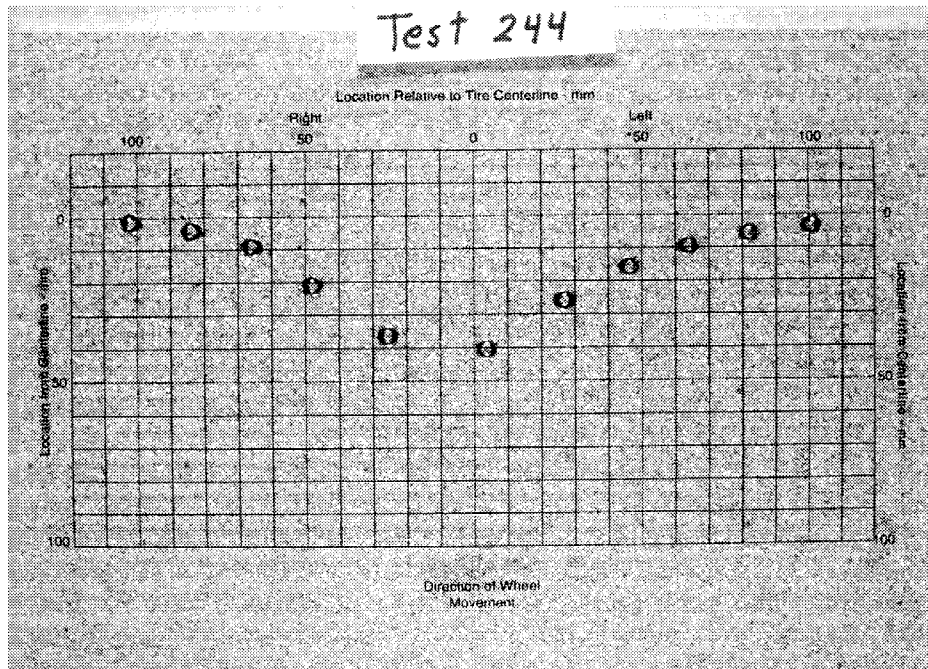
Photograph 3 - Movement of Markers on the Glass for Measurement

The sand used in the second test setup was a commercially available #20 quartz blasting sand. The first test used a laboratory standard Ottawa sand. Several types of markers were used throughout the testing. The ones used most often and most recently were small hex nuts. They show up well in the pictures, are easy to find in the sand, and do not seem to impact the motion of the sand.

A 35mm camera with slide film was used for most of the testing although print film was used on occasion. In addition, several tests were performed using a Super VHS video camera. The results described herein are based on measurements from the 35mm slide film. The other types of photography were used primarily for demonstration purposes.

The slides were projected on a white surface and measurements were made on the surface with a micrometer caliper. The measurement accuracy was about 0.2mm; however, using data reduction techniques this was improved to about 0.1mm.

Horizontal measurements were made on the surface, markers by looking vertically through a set of parallel grids attached to a platform about 10mm above the surface. There was about a 6mm spacing vertically between the grids. The accuracy of the horizontal measurements was

about 0.5mm. Vertical measurements on the surface were made with a micrometer caliper from a horizontal reference. This accuracy was about 0.3mm.

Test Setup

Markers were placed at intervals perpendicular to the centerline on the glass plate. Sand was then rained on the markers through a sieve to cover the markers without moving them. The desired amount of sand was placed loosely in the box and leveled while care was taken not to move the markers.

Compaction was done by striking the surface of the sand with the edge of a 200mm-long 2x4 (a piece of wood 38mm thick and 89mm wide). Enough force was used to make a 5 to 8mm deep mark on the surface of the sand with each blow. Two complete coverages were done in this manner. The surface was smoothed again and was struck with the side of the same piece of wood. Two complete coverages were made with smoothing between coverages. Sufficient force was applied during the last two coverages to leave 1 to 2mm deep marks on the surface. The minimum, maximum and test bulk specific gravity of the sand were 1.34, 1.60 and 1.48 respectively. The relative density of the sand in the test averaged 60%, but probably ranged from about 70% near the surface to about 50% on the glass plate.

The surface was smoothed a final time, and markers were placed on the surface directly above the markers on the glass.

Test Method

In general, the loading was done in two stages. The first stage was usually the first two passes. During each of these passes, the wheel was stopped for a picture at several points. The first point was 60mm before the wheel reached the centerline of the test section. Other stops were at 20mm intervals until the wheel was 60mm past the centerline.

When the wheel was directly over the markers, the rut depth was determined by measuring the distance between a fixed horizontal reference and the bottom of the wheel. After the wheel had passed, the horizontal and vertical positions of the markers on the surface were measured.

In the second stage, the wheel was stopped only at the center position to measure the rut depth, and pictures were taken only after the wheel had completely traversed the test area. In general, this was done at 3, 4, 5, 10, 15, 20, and 25 passes. The wheel was not stopped during traversing if measurements were not taken. This procedure was followed unless the markers moved too far to be of interest or there was no measurable movement.

<u>Tests Performed</u>

Several tests were performed to determine consistency between the apparatuses and several tests were performed to determine the variations in particle movement with variations in the test parameters. The basic test parameters were thickness of sand and load on the wheel. The primary variables between the two test apparatuses were type of sand, method of compaction, width of box, method of applying load to the wheel, method of moving the wheel, and size of the glass plate. The run matrix is shown in Table 1. The O's show tests performed with the original box, and the N's show the tests performed with the new apparatus.

Table 1. - Run Matrix

Load (kN)	Depth of sand (mm)		
	58	76	96
68.8	N		
78.6	N	O,N	
88.4	N	O,N,N	
98.2	N	O,N,N	
108.0		O,N	N
117.8			N
127.6			N

TEST RESULTS

The direction of particle movement on the horizontal plane at the bottom of the granular layer is the primary topic of this paper; therefore, only that portion of the data is presented.

Figure 1 shows the particle movement during the first two passes of the wheel in a test with 76mm of sand and a load of 98.2 kN on the wheel. Note the fishook shape to the direction of movement during the wheel passage. Data from the other tests show more or less movement and slightly different angles but they are all similar in shape.

The video pictures show this movement very definitively. It is possible to put a piece of tracing paper over the TV screen and trace the motion as the wheel passes. When this is done, the curves look very much like the ones shown above. It is difficult, however, to get accurate measurements using this method.
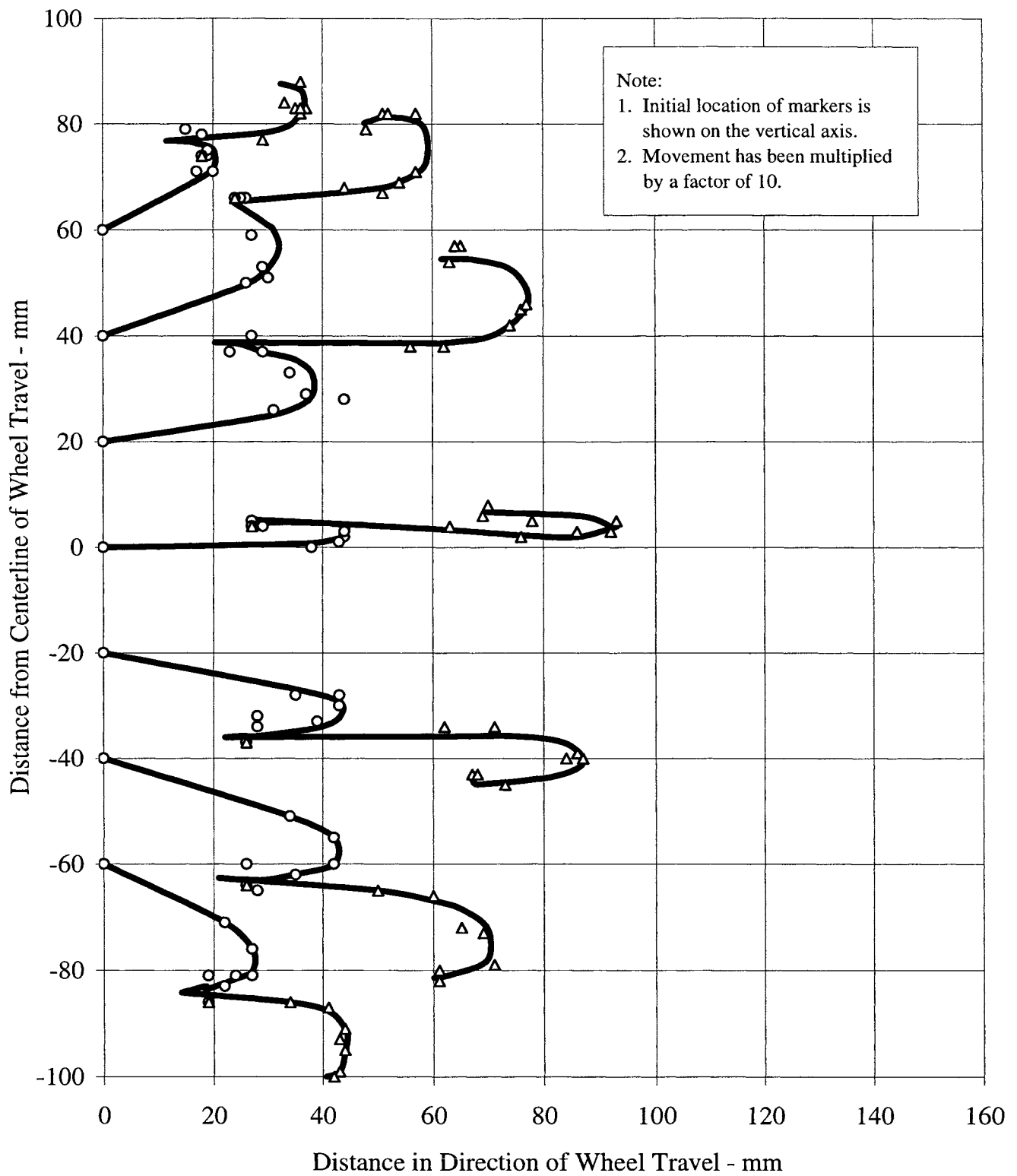
Figure 1. Movement of Markers on Glass During First Two Passes
76mm Sand - 98.2 kN load

Figure 2 shows the overall direction of marker movements for the same test. Note that markers near the centerline move nearly in the direction of wheel movement while other markers move at an angle to the direction of wheel movement. The angle becomes larger with distance from the wheel. Again, data from other tests show more or less movement per pass and somewhat different angles, but all test results show the same trends.

The purpose of this study was to demonstrate the trends and not to quantify the direction or magnitude of movement; hence, not all data is shown. Multiple tests using a range of variables were necessary to demonstrate that the results shown were not anomalous. The results from all the tests are interesting but do not add to the conclusions drawn in this paper.

Some preliminary tests were performed using a geogrid on the glass plate under the sand. The geogrid almost stopped the circular motion of the markers on the glass, and there was no measurable overall movement in a forward or outward direction. Surface rutting was also decreased, and the horizontal motion of the markers on the surface was less.

ANALYSIS

Theory of elasticity indicates that in an elastic system, a given marker would move in a somewhat elliptical pattern and return to its initial position. Calculations of the elastic movement for the points measured in the tests are shown on Figure 3. The shape of the movement shown was calculated using elastic theory (Poulus and Davis, 1974) considering the actual thickness of sand and size of wheel. The magnitude of movement was changed an arbitrary amount for plotting purposes by multiplying the movement in both directions by a constant. The elastic calculations shown are based on a homogeneous elastic half-space. In the author's opinion, this case fits the test conditions as accurately as any elastic solution and may therefore be used to demonstrate the general shape of the movement. The fact that the magnitude of the movement was changed arbitrarily does not alter the general shape of the movement.

The elastic movement is easy to visualize on the centerline. As the wheel approaches, the horizontal stresses increase and push the particles out in front of the wheel. As the wheel gets close, the horizontal stresses become more balanced and the particle returns to its original position when the wheel is directly overhead. As the wheel passes, the horizontal stresses are unbalanced, again pushing the particle backward. The particle returns to its initial position when the wheel has progressed outside the zone of stress influence.

In a system that ruts, there is plastic flow and at least some of the particles do not return to their original positions. Numerical analyses of this motion have been attempted (Fu, 1998) but to the author's knowledge, numerical methods have not adequately defined the motion. The soils are non-linear and plastic, the system is three-dimensional, and the wheel is moving. The theory is quite well developed, but the soil properties are not well known and computational ability is still lacking.

Note:
1. Data are shown for the end of each pass.
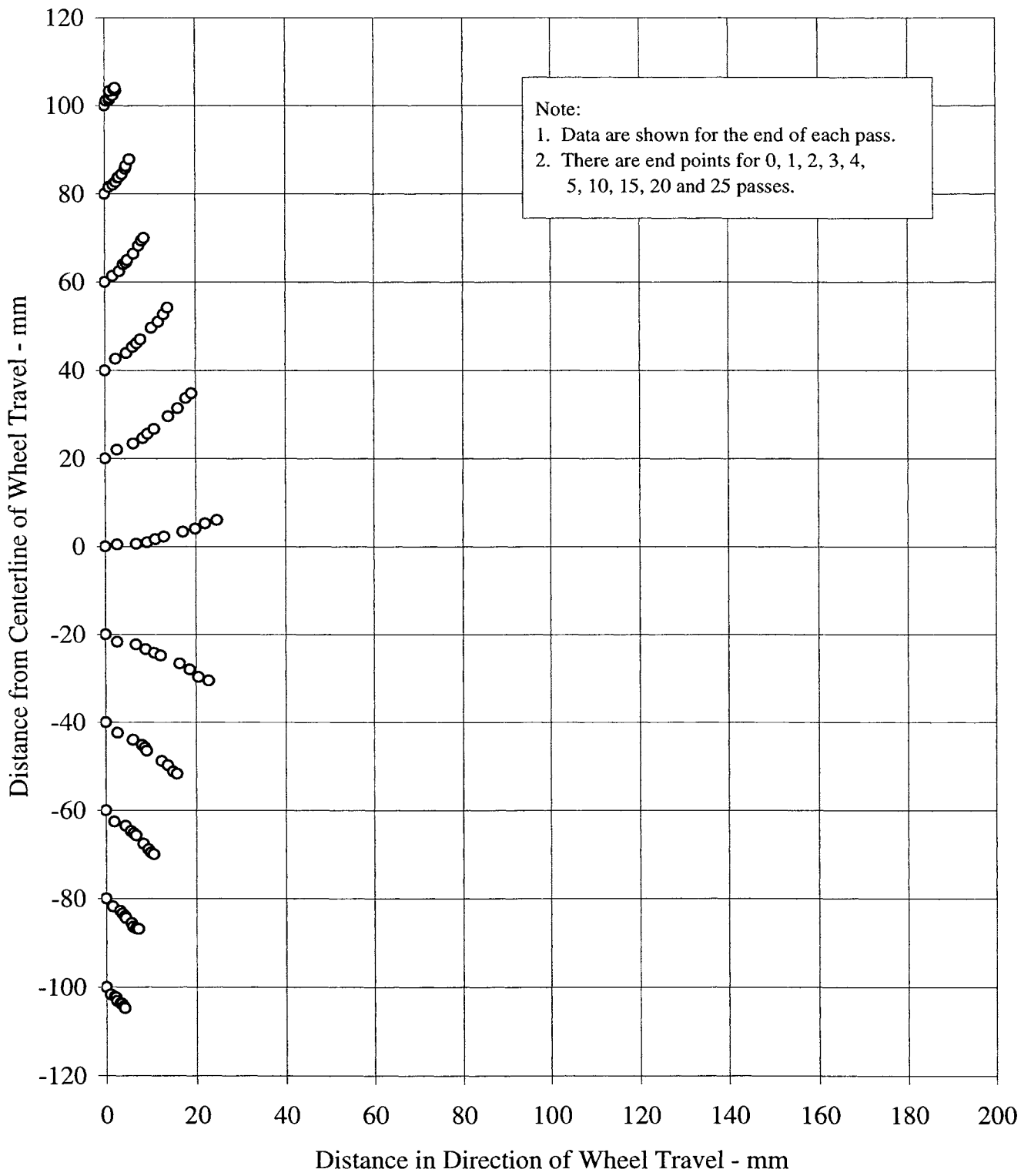2. There are end points for 0, 1, 2, 3, 4, 5, 10, 15, 20 and 25 passes.

Figure 2. Location of Markers on Glass During Loading
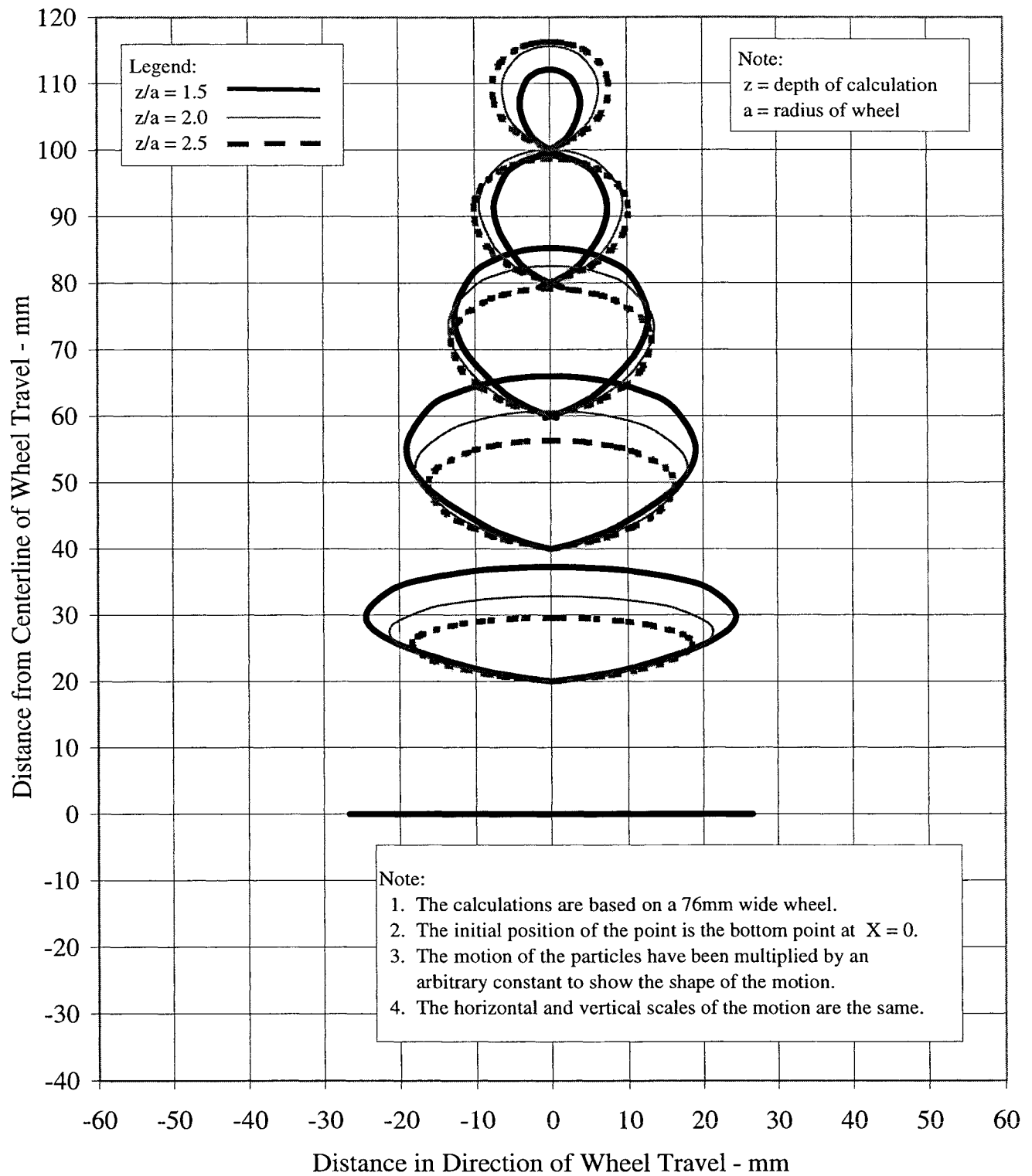76mm Sand - 98.2 kN load

Figure 3. Horizontal Movement of Particles in an Elastic System
During a Wheel Passage

It is the purpose of this study to show the general direction of particle motion on the plane of the geogrid in a base reinforcement application. The figures included herein show definite directions for one set of small-scale test conditions. The entire test matrix has established that these trends are valid for a variety of small-scale test conditions. All conditions tested are for an unbound granular layer on a relatively smooth horizontal subgrade under severe loading conditions. However, the same trends should hold for a variety of field conditions where there is a granular layer over a geogrid. In addition, these trends should also be evident in many flexible pavement sections. At the depths and in the sections where geogrids are typically used, the major principal stress and hence the particle motion on the plane of the geogrid would still have a similar shape.

If the system were elastic, the curved path of the each soil particle would return to its initial position. In systems such as the one tested here, where every pass of the wheel causes a significant amount of plastic deformation, the fishhook motion results. In a typical well-engineered road section, each pass of the wheel causes very little plastic deformation, and the path of each particle should return almost to its initial position.

Fatigue cracking is a result of repetitive elastic motions. In order for a geogrid to be effective in reducing fatigue damage, it must have sufficient stiffness to resist the elastic deformations, which are rotational in nature. Rutting is a result of plastic deformations. In order for a geogrid to be effective in reducing rutting it must resist the plastic deformations, which occur in a diagonal direction. The stresses involved on the plane of the geogrid in creating either the elastic or plastic deformations are relatively small in relation to the overall stiffness of most reinforcement geogrids. In addition, the total amount of movement is quite small. Only geogrids with high aperture stiffness at low strains can restrict particle motions to the very low values required to help reinforce the base.

CONCLUSIONS

This study shows that particle motion on a horizontal plane in the test section was fishhook shaped during passing of the wheel, and the overall movement was at an angle to the wheel path. Mathematical evidence suggests that a similar type of motion exists in actual roads but that the particle motion paths are quite small and they almost close on every pass. In order for a geogrid to be effective in base reinforcement, it must be placed where there is enough movement of the soil particles to mobilize the stiffness of the geogrid. The geogrid of most benefit will be the one that resists the direction of particle movement the best. It is likely that geogrids with a high degree of aperture stability will resist the twisting and diagonal motion most effectively.

ACKNOWLEDGEMENTS

Geosynthetics '95 Conference. The work was started and is ongoing because of the NAGS Award. Their contribution to this and many other research projects is greatly appreciated by the author as well as all others in the field.

REFERENCES

Fu, X., 1998, "Tests and Analysis of Geogrids as Base Reinforcing Materials," Ph.D. Dissertation, University of Alaska Fairbanks, School of Engineering, Fairbanks, Alaska.

Kinney, T.C., and Yuan, X., 1995, "Geogrid Aperture Rigidity by In-Plane Rotation," Proceedings, Geosynthetics 95, Industrial Fabrics Association International, St. Paul, MN, Vol. 2, p. 525-538.

Kinney, T.C., 1998, "The Effect of Tire Pressure on Pavement Performance," Research Report, Alaska Department of Transportation and Public Facilities, Research Section, Fairbanks Alaska.

Poulos, H.G., and Davis, E.H., 1974, "Elastic Solutions for Soil and Rock Mechanics," John Wiley and Sons, New York.

Webster, S.L., 1993, "Geogrid Reinforced Base Course for Flexible Pavements for Light Aircraft: Test Section Construction, Behavior Under Traffic, Laboratory Tests, and Design Criteria," Geotechnical Laboratory, Department of the Army, Waterways Experiment Station, U.S. Army Corps of Engineers, Technical Report GL-93-6.

Yuan, X., 1993, "Relating Index Tests to the Performance of Geogrids in Reinforced Aircraft Runway Pavement Systems," M. S. thesis, School of Engineering, University of Alaska Fairbanks.

GEOSYNTHETIC PREFABRICATED DRAINS BEHAVIOR DURING A THUNDER RAINFALL IN EXPERIMENTAL LASALLE MUNICIPALITY ROADWAY

J. MLYNAREK
SAGEOS, GEOSYNTHETIC TECHNOLOGY CENTRE, CANADA

E. BLOND
SAGEOS, GEOSYNTHETIC TECHNOLOGY CENTRE, CANADA

M. BOUTHOT
SAGEOS, GEOSYNTHETIC TECHNOLOGY CENTRE, CANADA

R. MARCIL
LASALLE MUNICIPALITY, QUEBEC

ABSTRACT

This paper presents an overall discussion on water behavior and the analysis of edge drain response to the heavy rainfall, in the experimental roadway in LaSalle Municipality in Quebec, Canada. Eight (8) experimental road sections, equipped with different types of edge drains were constructed in 1995. One section was not equipped with drain, and was monitored as a reference section. Each section was equipped with various monitoring instruments. The project was developed in collaboration between SAGEOS Geosynthetics Technology Centre, and three Canadian governing levels (Federal - Canada, Provincial - Quebec, and Municipal - LaSalle Municipality) under the 'Canada-Quebec Infrastructures Program (94)'.

It was found that edge drains are an excellent mean to stop water entry in the road foundation, by cutting the natural, preferential water flow paths. Drain response to rainfall was found to be rapid, and flow rates up to two liters per minute per linear meter of drain were recorded.

KEYWORDS

Geosynthetic, Edge-drains, Rain, Road, Water path

INTRODUCTION

Road quality is decreasing year after year. The main reasons of this deterioration is the combination of various factors, including a harsh climate, poor strength of in-situ subgrade soils, and, quite often, errors in roadway structure design. Our roadways are often designed without mitigation systems which can eliminate or, at least, partially eliminate the influence of harsh conditions. One of these mitigation solutions is roadway foundation drainage. Some estimation

of the potential influence of this solution has previously been proposed by Cedergren (1989) with a ratio of life expectancies of drained road structure compared to undrained ones varying between 1.5 and 6.

The purpose of this paper is not to give evidence of the influence of drainage on road durability, but to analyze the drainage efficiency given by either conventional techniques, or by geosynthetic edge drains. The project, developed in collaboration with the three Canadian governing levels (Federal - Canada, Provincial - Quebec, and Municipal - LaSalle Municipality) under the 'Canada-Quebec Infrastructures Program (94)', was initiated five years ago. Experimental road structures were constructed three years ago, followed by the installation of instrumentation. The monitoring of these road structures started two years ago.

Eight of the nine experimental road sections were designed with different types of geosynthetic edge drains and being installed in various configurations. The ninth section was not drained, and was monitored as a reference section.

This paper presents an overall discussion on water behavior in the experimental road and in the underlying soil as well as an analysis of the drain responses during a heavy rainfall in August 1998.

EDGE DRAINS AND THEIR FILTERS

Considering the importance of the filtration behavior of drainage systems, the materials were selected for filtration, retention and permeability. Then, the survivability criteria, e.g. the mechanical properties of the selected materials, were evaluated for strength requirements.

Filtration criteria

SAGEOS filtration criteria (Mlynarek, 1998) were used to determine the optimum filter properties for filtration and retention. The three-step methodology to design a geotextile filter for soil filtration and retention includes :

Step 1 : Determine site hydraulic conditions (type and direction of flow, as well as construction constraints).
Step 2 : Determine soil properties and soil's internal stability.
Step 3 : Select appropriate filter, based on the conclusions of step 1 and step 2.

For highways and roadways, bi-directional (dynamic) hydraulic and filtration conditions should be considered. The bi-directional analysis chart (presented in Figure 1) was thus used to select the filters. Taking bi-directional flow into consideration, soil properties such as particle size distribution, Atterberg limits and dispersion ratio were determined. The analysis of the roadbed soil (the particle size distribution is presented in Figure 2) lead to selection of a multi-layered

filter : 150 mm of fine sand filter was designed between the roadbed soil and the geotextile filter, which was designed with regard to the sand properties. The geotextile filters, selected for the drains, are listed in Table 1.

Soil Gradation
d_{10}, d_{20}, d_{30}, d_{50}, d_{60}, d_{85}, d_{90}, Cu

$d_{50} < 75\mu m$ — YES → $d_{30} < 2\mu m$ — NO

$d_{50} < 75\mu m$ — NO

$d_{30} < 2\mu m$ — YES → Determine Percentage Dispersion[1]

$d_{30} < 2\mu m$ — NO → Determine Plasticity Index[2]

$d_{50} < 60\mu m$ — NO

$d_{50} < 60\mu m$ — YES

Severe Hydraulic Conditions (Wave attack or Pumping)

Determine Plasticity Index[2] → Ip > 5 — YES → Select the multilayer geotextile filter[3]

Ip > 5 — NO

Determine Percentage Dispersion[1] → D% > 50% — YES → Select the multilayer geotextile filter[3]

D% > 50% — NO → $d_{90} < 60\mu m$ — YES → Select the multilayer geotextile filter[3]

$d_{90} < 60\mu m$ — NO → $d_{90} < 10d_{50}$

Severe Hydraulic Conditions — NO → Cu < 6

Severe Hydraulic Conditions — YES

Select the multilayer geotextile filter[3] → Filtration test of the selected geotextile/soil system is recommanded[4]

$d_{90} < 10d_{50}$ — YES → $d_{90} < 100\mu m$ — YES → END

$d_{90} < 10d_{50}$ — NO → $d_{50} < 10\mu m$

Cu < 6 — NO

Cu < 6 — YES → $d_{90} < 2.5d_{50}$

$d_{90} < 100\mu m$ — NO

$d_{50} < 10\mu m$ — NO

$d_{50} < 10\mu m$ — YES

$d_{90} < 2.5d_{50}$ — YES

$d_{90} < 2.5d_{50}$ — NO

$0.8d_{90}$ or $150\mu m^5 < FOS < d_{90}$

$80\mu m < FOS < 100\mu m$

$2d_{50}$ or $150\mu m^5 < FOS < 2.5d_{50}$

$8d_{50}$ or $150\mu m^5 < FOS < 10d_{50}$

d_{50} or $150\mu m^5 < FOS < d_{85}$

$0.8d_{50}$ or $150\mu m^5 < FOS < d_{50}$

END

[1]: ASTM D4221   [2]: ASTM D4318   [3]: If multilayer geotextile filter is not available, select 150mm thick fine sand filter and design the geotextile filter for this sand   [4]: SAGEOS method GX003/modified ASTM D5101   [5]: which ever is smaller

Figure 1 : SAGEOS filtration criteria for bi-directional flow

Table 1. List of edge-drains and their geotextile filter properties

Section	2	3	4	5	6	7	8	9
Product	French drain	Geocomp. Geotextiles 400mm	Mulit-pipes edge drain 450mm	Honey-combed core edge-drain 300mm	Honey-combed core edge-drain 450mm	Flatpipe edge-drain 450mm	Honey-combed core edge-drain 450mm	Perf. pipe 100 mm
General Properties								
Filter structure	NW-NP	NW-NP	NW-NP	NW-NP	NW-NP	NW-HB	NW-HB	Knitted
Core structure	Clean crushed gravel	NW-NP and perforated pipe	HDPE Multiple perf. pipe	Honey-combed HDPE sheet	Honey-combed HDPE sheet	HDPE Flat pipe	Honey-combed HDPE sheet	HDPE Perf. pipe
CGSB 148.1-3 Thickness[*]	1.4	1.56	1.11	2.65	2.65	0.45	0.55	0.73
CGSB 148.1-2 Mass p. unit area[*]		152.7	148.4	269.2	269.2	141.4	215.4	122.0
Hydraulic Properties								
ASTM D4491 Permittivity[*] (s^{-1})		2.6	2.1	1.4	1.4	1.6	0.37	11.0
Permeab[*] $(cm.s^{-1})$	2.8×10^{-1}	4.3×10^{-1}	2.9×10^{-1}	3.5×10^{-1}	3.5×10^{-1}	7.6×10^{-2}	2.0×10^{-2}	8.2×10^{-1}
ASTM D4716 Transmissivity (i=0.1) $(m^2.s^{-1})$ 65 kPa	N/A	(only NW-NP core) 5.4×10^{-5}	3.9×10^{-2}	2.9×10^{-2}	2.3×10^{-2}	6.1×10^{-2}	3.3×10^{-2}	
200 kPa		2.0×10^{-5}	3.3×10^{-2}	5.8×10^{-3}	1.6×10^{-3}	2.3×10^{-2}	1.4×10^{-2}	
400 kPa		8.3×10^{-6}	1.3×10^{-3}	7.0×10^{-6}	3.3×10^{-6}	6.9×10^{-4}	6.8×10^{-5}	
SAGEOS GX004 Wettability[*] (cm)		0.0	11.7	15.5	15.5	10.0	12.7	0.0
Mechanical properties [*]								
CAN 148.1-7.3 Tensile str. (N) machine direction	min: 755	437.8	584.8	496.1	496.1	608.4	929.6	215.3
cross direction	moy: 850	478.7	664.0	758.4	758.4	588.1	1007.0	168.7
CAN 148.1-7.3 Ext at break (%) machine direction	55 - 85	59.1	57.2	56.8	56.8	88.4	59.2	71.6
cross direction		74.5	63.6	45.6	45.6	70.8	65.1	115.9
ASTM D4833 Puncture (N)		333.6	352.6	466.8	466.8	219.3	382.0	158.8
CGSB 4.2 No 12.2 Tear (N) machine direction	min325	196.3	240.4	195.0	195.0	318.0	555.7	101.9
cross direction	moy: 415	208.2	321.0	390.9	390.9	431.7	552.8	107.5
Filtration properties [*]								
CGSB 148.1-10 FOS (μm)	55-80	107.4	115.1	85.6	85.6			321.8
SAGEOS GX-005 BBP (O_{98}) (μm)							114.1	83.7

NW-NP : needle punched non-woven ; NW-HB : heat bonded non-woven ; HDPE : high density polyethylene ;
BBP : Bubble-point - measured by Pore Size Distribution, as described by Vermeersch and Mlynarek (1996)
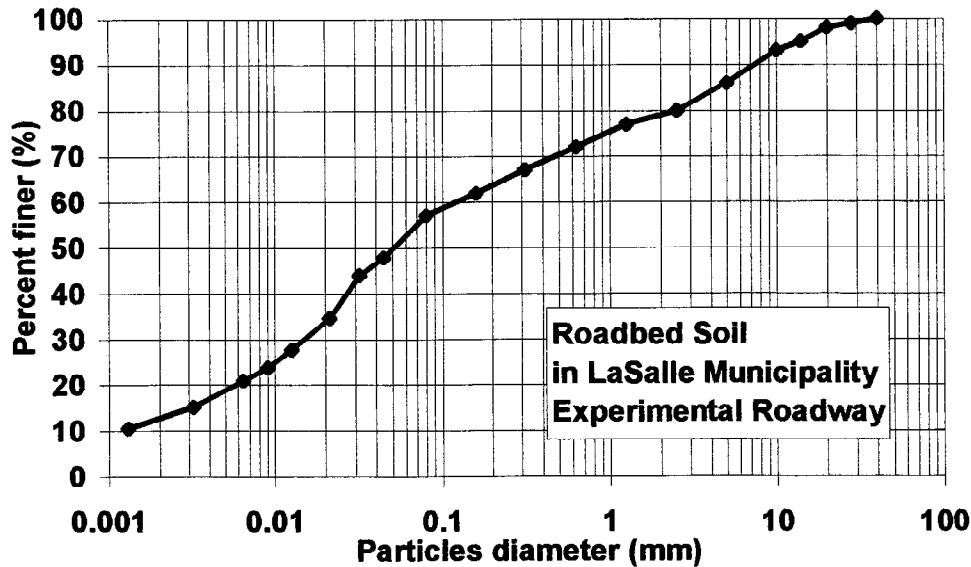[*] : Geotextile filter properties

Figure 2 : Roadbed soil particle size analysis

Survivability

The mechanical properties of the different products were compared to the AASHTO M288-96 specification for geotextiles (Table 2). No one geotextile filter met the AASHTO specifications, endangering the filters ability to survive installation. Observation of the drains lead the engineers to go ahead with the selected filters, and to pay great attention to all mechanical issues during handling and installation.

Table 2 : AASHTO M288-96 specification for geotextiles

ASTM	Test method ASTM	Unit	Geotextile type					
			Class 1		Class 2		Class 3	
			W < 50%	NW > 50%	W < 50%	NW > 50%	W < 50%	NW > 50%
Tensile strength	D4632	N	1400	900	1100	700	800	600
Tear resistance	D4533	N	500	350	400	250	300	180
Puncture resistance	D4833	N	500	350	400	250	300	180
Burst Strength	D3786	kPa	3500	1700	2700	1300	2100	950

NM : Non-woven geotextiles ; W : Woven geotextiles

Excavations, performed after two years of service, have shown that all products survived the installation and service mechanical stresses, excepted the light knitted product, which was found to have suffered of many tears. It is noted that the tear resistance of this product is only 101 N, while all other products have a tear resistance greater than 195 N.

EXPERIMENTAL ROADWAY STRUCTURES

A different drain was chosen for each experimental road section, in order to evaluate the response of a wide range of potential solutions. They are summarized in Table 3. Each experimental structures has a total thickness of 625 mm. Complete information regarding the site, roadway foundation and geosynthetic materials can be found in the project reports by Mlynarek et al. (1997, 1998a and 1998b).

INSTRUMENTATION

Each of the road sections was equipped with various monitoring instruments :
- TDR probes, installed to monitor the variations in foundation water content ;
- Open tube piezometers ;
- Frost tubes, used in winter to evaluate the frost penetration depth ;
- Manual flow-meters, to measure a discharge capacity of drains ;
- Level indicators, conventionally used for construction purpose to measure surface variation ;
- Rain-meter.

The frequency of instrument monitoring was dependent on the period of year, meteorological conditions, and some specific environmental events (additional construction works, predicted rainfalls etc.). This paper reports the results of one specific event, a heavy rainfall.

SITE CHARACTERIZATION

The experimental site was selected in 1994 to be representative of typical municipal roadways suffering from drainage problems. As long as the selected roadway was newly built on a uniform, horizontal land, it was assumed that soil conditions would be uniform. However, the piezometer readings were found to be very variable. Instead of the position of a water table, the analysis of these readings showed that the response of the piezometers was, in fact, the actual measurement of the water pressure in the in-situ soil. Additional observation of the site configuration as well as discussions with the local municipal engineers lead to a conclusion that the back-fill of about two meters thickness had been placed on the site location many years ago ! Non-uniformity of such back-fill results in the possibility of water circulating through preferential paths inside the back-fill structure.
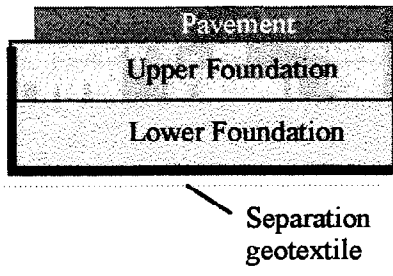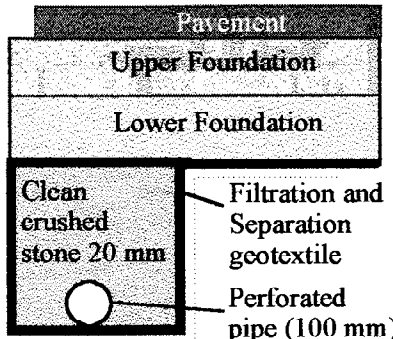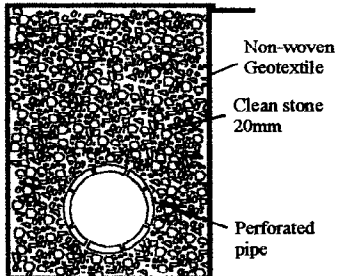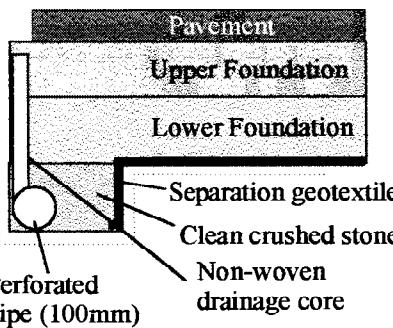
Table 3 (1/3) : Experimental sections properties
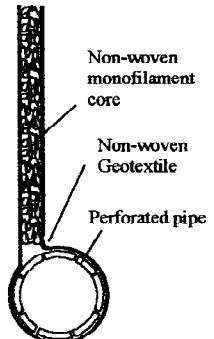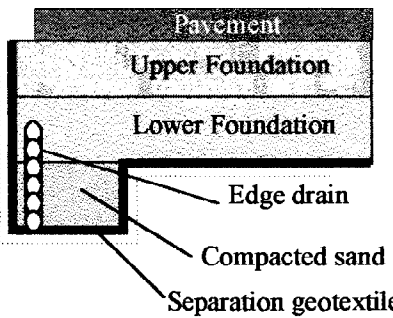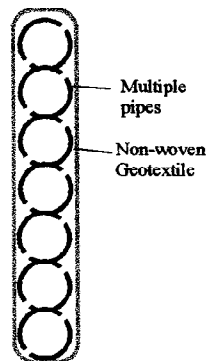
Section	Tested product	Product cost (CAN$/lm)	Typical cross-section	Drain section
1	None (reference section)	/	Pavement / Upper Foundation / Lower Foundation / Separation geotextile	None
2	French drain : Non-Woven Geotextile, FOS = 55-80 μm Clean crushed stone, perforated pipe to connect drains to outflow. Trench : 300 mm x 250 mm	Geotextile : 6.15 to 1.26	Pavement / Upper Foundation / Lower Foundation / Clean crushed stone 20 mm / Filtration and Separation geotextile / Perforated pipe (100 mm)	Non-woven Geotextile / Clean stone 20mm / Perforated pipe
3	Draincotex height : 400 mm with 100 mm perforated pipe Trench : 300 mm x 250 mm	5.90	Pavement / Upper Foundation / Lower Foundation / Separation geotextile / Clean crushed stone / Non-woven drainage core / Perforated pipe (100mm)	Non-woven monofilament core / Non-woven Geotextile / Perforated pipe
4	Multiflow height : 300 mm Trench : 300 mm x 250 mm	10.99 to 12.80	Pavement / Upper Foundation / Lower Foundation / Edge drain / Compacted sand / Separation geotextile	Multiple pipes / Non-woven Geotextile

Table 3 (2/3) : Experimental sections properties
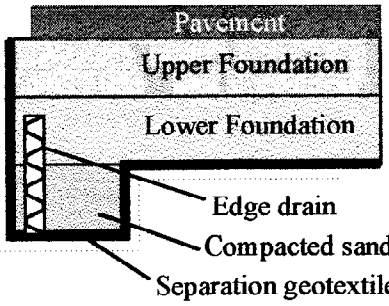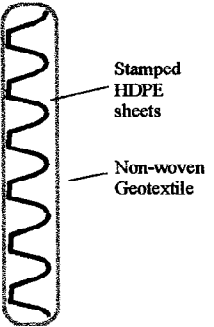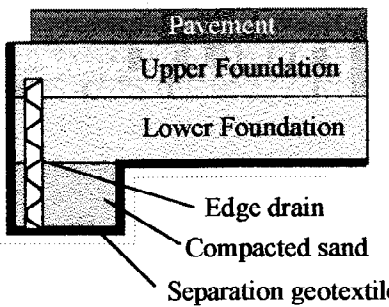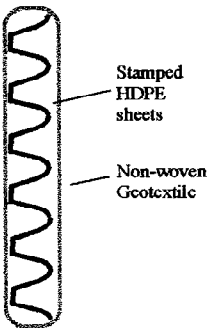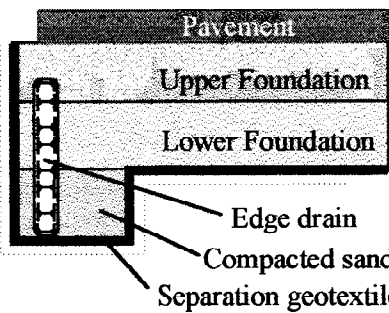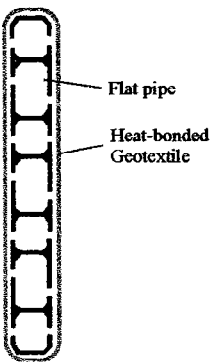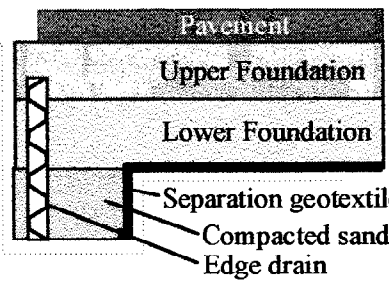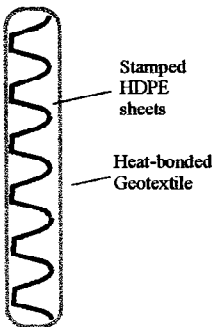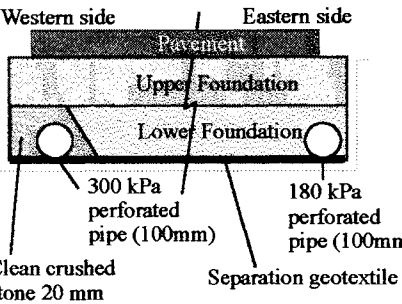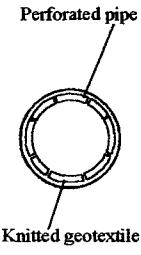
5	Soldrain 4000 height : 300 mm Trench : 300 mm x 250 mm	6.57 to 7.10	Pavement / Upper Foundation / Lower Foundation / Edge drain / Compacted sand / Separation geotextile	Stamped HDPE sheets / Non-woven Geotextile
6	Soldrain 4000 height : 450 mm Trench : 300 mm x 250 mm	6.83 to 7.59	Pavement / Upper Foundation / Lower Foundation / Edge drain / Compacted sand / Separation geotextile	Stamped HDPE sheets / Non-woven Geotextile
7	ADS Flatpipe height : 450 mm Trench : 300 mm x 250 mm	11.00	Pavement / Upper Foundation / Lower Foundation / Edge drain / Compacted sand / Separation geotextile	Flat pipe / Heat-bonded Geotextile
8	Alidrain height : 450 mm Trench : 300 mm x 250 mm	6.00	Pavement / Upper Foundation / Lower Foundation / Separation geotextile / Compacted sand / Edge drain	Stamped HDPE sheets / Heat-bonded Geotextile

Table 3 (3/3) : Experimental sections properties

9	Perforated pipe d = 100 mm East side : 180 kPa West side : 300 kPa	1.42 3.59	Western side — Eastern side; Pavement; Upper Foundation; Lower Foundation; 300 kPa perforated pipe (100mm); 180 kPa perforated pipe (100mm); Clean crushed stone 20 mm; Separation geotextile	Perforated pipe; Knitted geotextile

Observations of the piezometer readings at various time of the year, and particularly during the rainy days, confirms the above hypothesis that specific water circulation paths, in the in-situ soil, were developed. Water flows freely along these preferential paths and, in fact, most of the infrastructure soil is in unsaturated state. These paths may or may not cross piezometer heads, which explains the significant variations observed between two consecutive piezometers. A simplistic drawing of the possible water paths is presented in Figure 3.

With such critical hydraulic conditions, the use of edge drains appears to be the only mean to stop water access to the road foundation by 'cutting' the water flow path in the infrastructure.

● Piezometers placed on each road section
———— Probable flow channels (detected through analysis of piezometers response)
.... Probable flow channels (assumed)
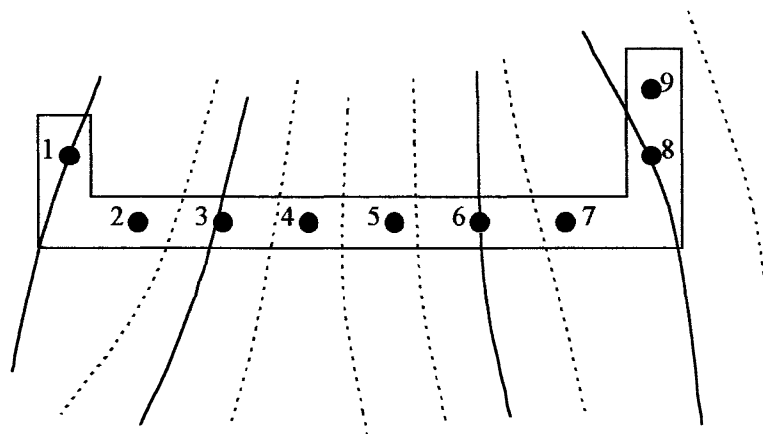
Figure 3. Hypothetical water circulation path in the roadbed soil

GEOSYNTHETIC DRAINAGE SYSTEMS BEHAVIOR DURING A THUNDER RAINFALL

The drains response to an intense summer rainfall was precisely monitored during a thunder rainfall on August 25th, 1998, on the experimental road area. The rain intensity and its total volume was measured with a rain-meter, installed on a flat surface next to the road. During the event, all the instrumentation was used to measure and analyze the time of response of the drains as well as the hydraulic behavior of the road foundations.

Thunder rainfall characteristics

56 mm of rain fell on the road structure and surrounding gardens 6.8 hours, with a mean intensity of 8.2 mm/h, and a recorded peak rain intensity of about 85 mm / hour. Rain data collected during this event are plotted in Figure 4.
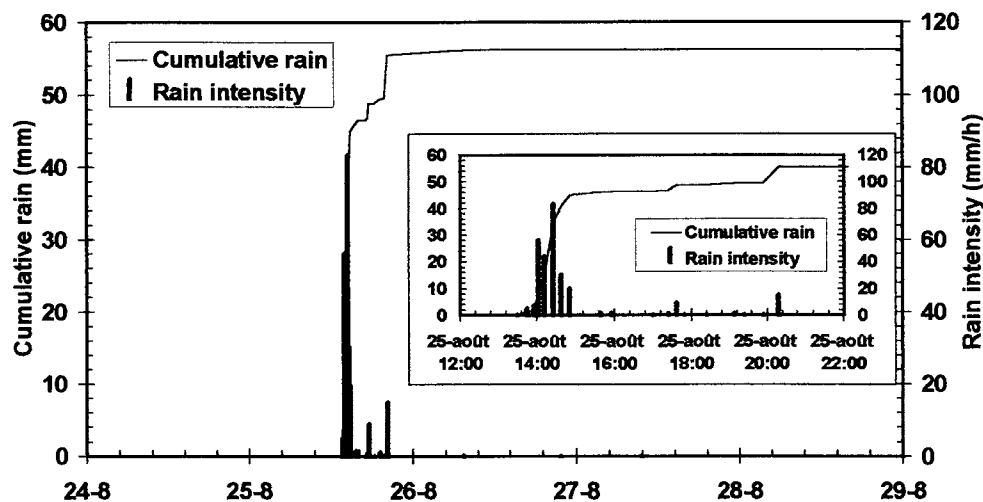
Figure 4. Recorded rain

Piezometers response

An example of piezometers response to the rain is illustrated in Figure 5. This Figure confirms a variable behavior of experimental roadway. It can be also noted that three days after the rainfall, some of the piezometers had still not reached their previous level, which is an indication of the extremly active water circulation in the underlying soilbed.

The response of piezometers to rainfall confirms the preferential paths of water movement in the road bed soil. The observed behavior depends on piezometer locations: most of the piezometers show a fast rise, followed by a decrease at various speeds. Some piezometers do not seem to be affected by the rainfall at all. Once more, it can be interpreted as the random water dispersion into the soil, and flow through the preferential water paths.
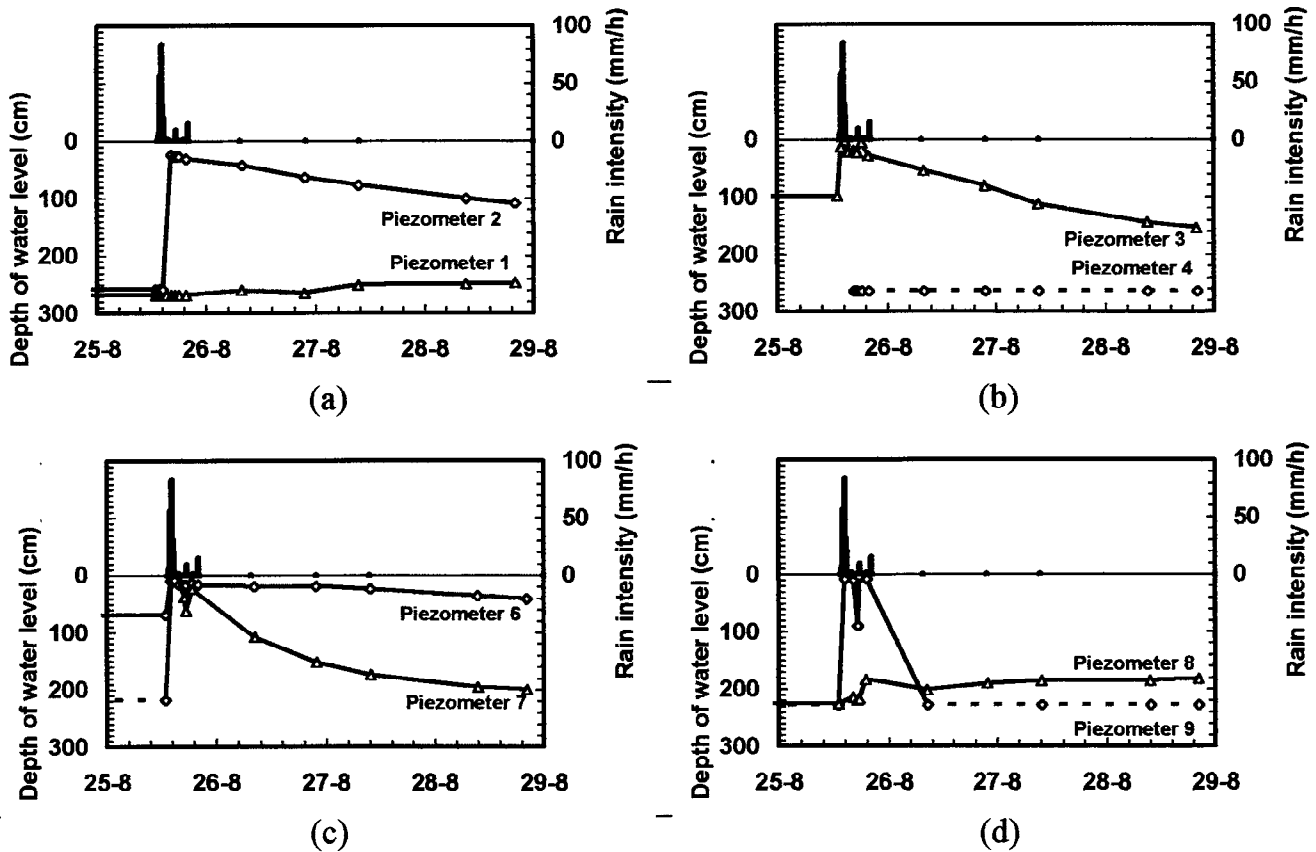
Figure 5: Example of recorded depth of water level (piezometer levels)

Flow rates

The drain responses were measured at the outlet of each section. Discharge up to 57 liters per minute was recorded in section 7, for a 30 meter long road section. It approaches 2 liters/minute/linear meter of drain for the rainfall described above.

All edge drains showed a good response to the water income, as presented in Figure 6. It is noted that the time response of drains relates to the rain intensity : a lap of time of about one hour separates a change in rain intensity and the related change in flow rate. This phenomenon can be observed at the beginning of the rainfall vs. the beginning of flow from drains, as well as for the recorded peak flow vs. the recorded rainfall peak.

Road foundation response

The water content variations measured by TDR cells in all nine sections are presented in Figure 7. These Figures show the relative variation compared to the water content recorded the day before the rain [$(w_f - w_i) \times 100 / w_i$].
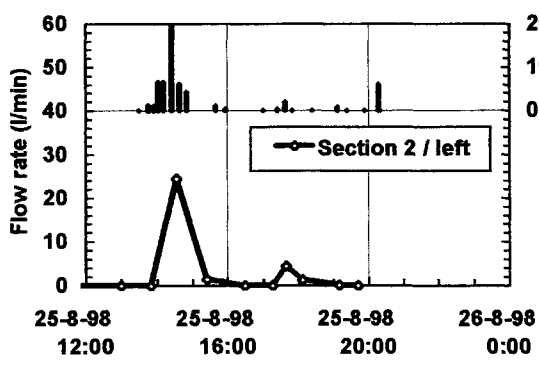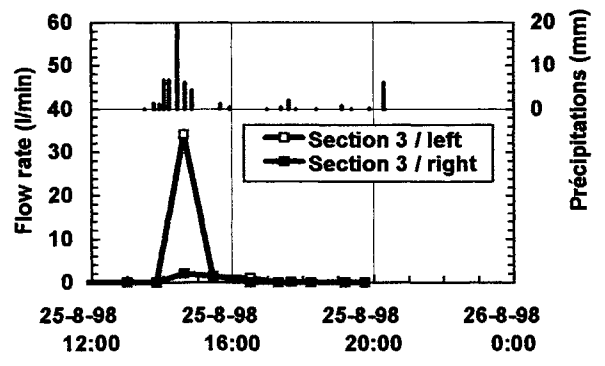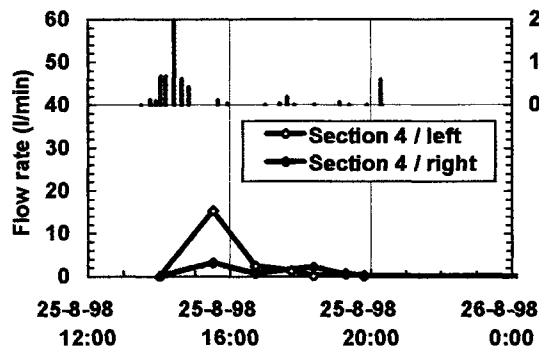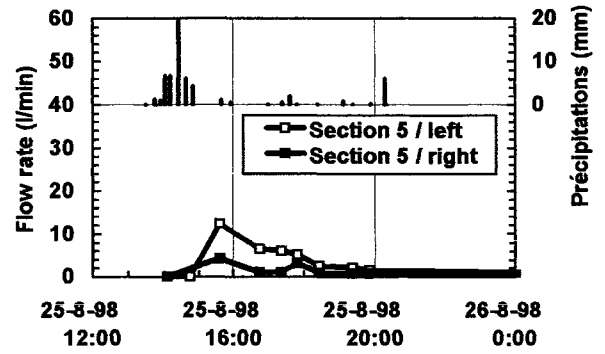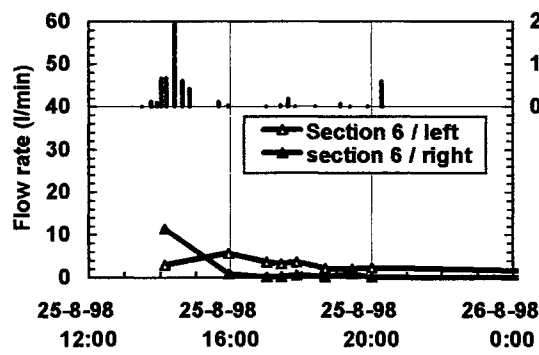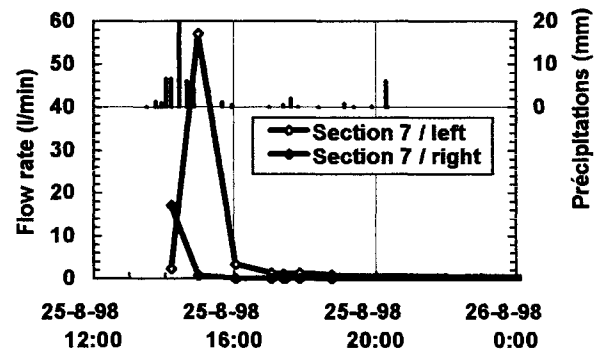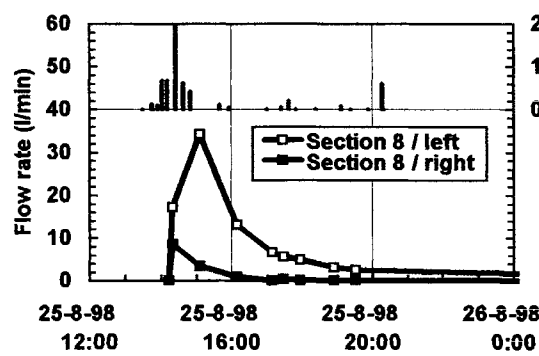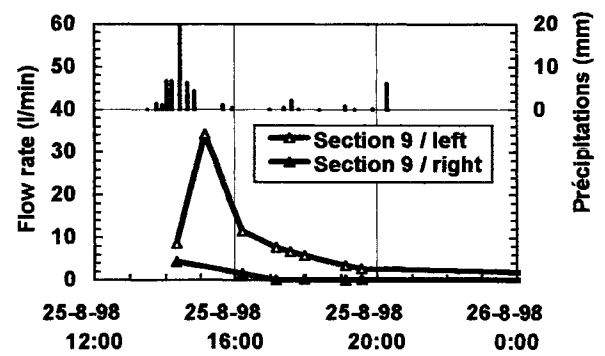
Figure 6: Recorded flow rates
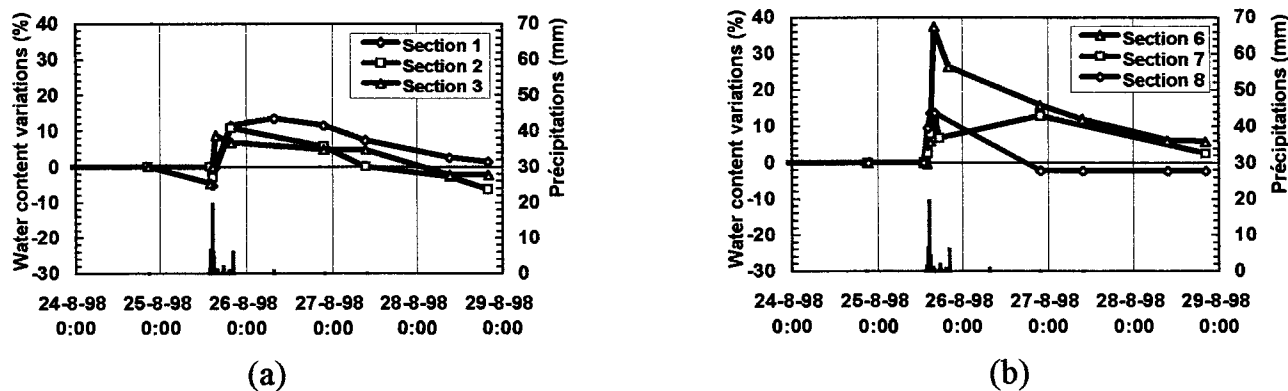
Figure 7: Recorded water content variations

Figure 7 shows an significant increase in water content in most experimental sections. Some sections did not show any water content variation (sections 4 and 9), and some drained sections (section 6, 7) show a slow decrease of water content with time.

DISCUSSION

After three years of service, no significant cracks could be observed on the pavement, either on the surface or on the shoulder concrete / pavement joint. Thus, almost all measured discharges and water content variations can be related to water entry from the in-situ soil, through the side or the bottom of the road structure.

Flow rates

Observation of the drain discharges show that flow rates are not related to the drain properties, but to the water entry from the soil. With the experimental section lengths of 30 meters, all drains were found to have a much higher discharge capacity than the one required during the monitored rainfall, and have enough efficiency to evacuate all incoming water. The water entry into drains varies among the test sections as could be expected from the piezometer readings.

Very high flow rates have been measured, which would not have been expected by a simple analysis taking in consideration the in-situ soil hydraulic conductivity. It confirms a presence of preferential paths within the soil, which convey very easily high volume of water into drains.

Road foundation response

Water content variation is dependent on water entry as well as soil drain-ability. The observed increase of water content should be analyzed in relation to the amount of water accessing the foundation, either through the edges or through the bottom of the road structure.

However, it appears that for a heavy rain like the one monitored here, the lack of horizontal drainage affects the road foundation water content.

In general, the drainage from sections equipped with edge-drains was found to be very good, and the water content decreases rapidly. It was found, however, that in some sections, in particular sections 6 and 7, time of water content decrease is quite slow, comparable to the time of response of the reference section with no drain. Two causes can be considered to explain this phenomenon. First, it could be due to an inappropriate installation of these drains, and non-uniform slope of the drains on their length. Second, it could be caused by a local lower drainability of the materials installed in the road foundation. To explain this unexpected behavior, an additional testing and analysis program is recommended.

CONCLUSIONS

It can be concluded that :

1. The water can flow in the soil through localized paths and channels, which are randomly distributed in soil discontinuities. These flow paths should be carefully considered in back-fills as well as in broadly graded soils, because they can create very critical drainage conditions for the road structures.

2. Maximum recorded flow rates related to a rain having a mean intensity of 8.2 mm/h for 6.8 hours were found to be as high as 2 liters / minute / linear meter of drain.

3. Drain response to rainfall was very rapid and is related to the intense water flows occurring during rainfalls in soil discontinuities. This behavior suggests the necessity to apply edge drains in every road structure, to avoid major water entries in the road foundation through roadbed flow paths or through road shoulders.

4. Edge-drains were found to be an appropriate mean to accelerate water evacuation from the road structure.

5. Although they did not meet all AASHTO survivability specifications, all filters have survived installation, except the light weight knitted geotextile installed on section 9, which dramatically suffered tearing.

REFERENCES

AASHTO (1996), Standard Specifications for Geotextiles - M 288, Standard Specifications for Transportation Materials and Methods of Sampling and Testing, AASHTO, Washington, D.C., pp.745-755.

ASTM (1994), Annual Books of ASTM Standards, ASTM, Philadelphia, Pennsylvania, Volume 4.08 (I), Soil and Rock, Volume 4.08 (II), Soil and Rock, Geosynthetics

CGSB (1998), Annual of CGSB Standards, Ottawa, Canada

Cedergren, H. (1989), Seepage, Drainage and Flow Nets, John Wiley & Sons Ed, New York, 465 pages.

Mlynarek J. (1998): Designing Geotextile Filters, Part 1 : Soil Filtration, Proc. 51th Canadian Geotechnical Conference, Edmonton, pp. 499-511.

Mlynarek J, Blond E, Vermeersch O (1997) : Étude in-situ du comportement et de l'efficacité de systèmes de drainage routier municipal utilisant les technologies géosynthétiques - Rapport d'étape #1.

Mlynarek J, Blond E, (1998) : Étude in-situ du comportement et de l'efficacité de systèmes de drainage routier municipal utilisant les technologies géosynthétiques - Rapport d'étape #2 : comportement observé après un an de suivi de performance.

Mlynarek J, Blond E, Bouthot M (1998) : Étude in-situ du comportement et de l'efficacité de systèmes de drainage routier municipal utilisant les technologies géosynthétiques - Rapport final.

SAGEOS (1995), Test Method Book, Method GX 004 , Wet-ability of Geotextiles, and Method GX 005, Pore Size Distribution of Geotextiles, SAGEOS, Saint Hyacinthe, Canada

Vermeersch, O. G. & Mlynarek J. (1996), Determination of the Pore Size Distribution of Nonwoven Geotextiles by a Modified Capillary Flow Porometry Technique, Recent Developments in Geotextile Filters and Prefabricated Drainage Geocomposites, ASTM STP 1281, Bhatia & Suits, Eds., ASTM, Philadelphia, PA, pp. 19-34.

TESTING AND INSTALLATION OF A GEOSYNTHETIC CLAY LINER CAPPING SYSTEM AT HIGH ELEVATION - A CASE STUDY AT THE SUMMITVILLE MINE

DONALD S. REIMER
ADVANCED TERRA TESTING, INC., USA
ALICE I. COMER
U.S. BUREAU OF RECLAMATION, USA
CHRISTOPHER J. WIENECKE
ADVANCED TERRA TESTING, INC., USA
WILLIAM E. BREWER
ADVANCED TERRA TESTING, INC., USA
RONALD K. FROBEL
R. K. FROBEL AND ASSOCIATES, USA

ABSTRACT

The Bureau of Reclamation (BOR), as the design organization to the United States Environmental Protection Agency and the State of Colorado, designed a 178,000 m^2 capping system for a heap leach pad at the historic Summitville Mine Superfund Site, located in southern Colorado. Several cap options were considered including a double flexible geomembrane separated by a drainage geocomposite, a double geosynthetic clay liner (GCL) separated by a drainage geocomposite, and a thick spray applied geomembrane. The prime contractor selected the GCL option and began construction during the summer of 1997. This paper will discuss the laboratory testing to verify the adequacy of the chosen cap system, design modifications required as a result of testing, and special installation techniques that were employed due to varying site conditions. The GCL product was configured specifically for this project and performance level testing was performed at an independent laboratory prior to acceptance of the product for final design. Quality control testing for the project materials was performed at the manufacturing facility and a conformance testing program was also undertaken at an on site laboratory at the Summitville site.

INTRODUCTION

The Summitville Mine Superfund Site is located at an elevation of 3,500 meters in the San Juan range of the Rocky Mountains, near Wolf Creek Pass in southwestern Colorado. The site is an abandoned gold mine that most recently operated as an open pit mine where gold was extracted using a cyanide solution sprinkled over a large volume of crushed latite ore placed onto a geomembrane lined heap leach pad. The site was last in operation in 1992 and ceased operations when the operating company, Summitville Consolidated Mining Co. Inc. (SCMCI),

declared bankruptcy. When the abandonment occurred there were numerous problems at the site, including a large 178,000 m² heap leach ore pile situated on top of an HDPE lining system installed in the 1980's that appeared to be breached in several areas, allowing cyanide leach solution to percolate down gradient into the groundwater system. In addition to the heap leach pad, numerous adits from previous mining operations were leaking acid mine drainage and the wastewater treatment dam was close to becoming over topped. Various remediation efforts have been implemented to mitigate these problems. The focus of this paper concerns the remediation of the heap leach pad.

A feasibility study was originally undertaken by the BOR in order to determine the potential effectiveness of a series of differing cap systems including a single layer of compacted clay, a single layer geomembrane system, and a double layer geomembrane and compacted clay system. The results of the infiltration tests performed indicated that a double layer cap would resist infiltration most effectively, and although the added cost would be significant, the overall long term benefits of increased stability and lower maintenance were sufficient to make this option the most appealing.

Photograph 1. The Summitville Mine Superfund Site heap leach
pad capping system under construction.

Three different geosynthetic capping options were proposed as a means to induce a cooperative effort between contractors and manufacturers in the belief that the final system would be cost effective and meet design criteria. These systems were all considered to be equal

in effectiveness with respect to permeability, durability, drainage, and water shedding characteristics. These systems were as follows: 1) Geomembrane cap composed of from bottom to top, a nonwoven geotextile, textured geomembrane (0.76 mm PVC, 1.0 mm PP, or 1.0 mm LLDPE), drainage geocomposite, the same textured geomembrane, and the same nonwoven geotextile, 2) GCL cap composed of two GCLs constructed with needle punched nonwoven geotextiles, on either side of a drainage geocomposite, 3) Thermoplastic spray applied 4.0 mm liner placed on a geotextile, followed by a second geotextile placed on top of the liner. The accepted bid was submitted by a contractor that chose the double GCL cap option. Factors involved in the selection of the GCL option included site weather conditions, high winds and the angular nature of the crushed ore being used as the subgrade and cover soil. The relative ease of installing a three layer system as in option 2, compared to the five layer system specified in option 1 was also a factor. At this point the GCL product to be used was selected, and the performance testing program was initiated.

PERFORMANCE TESTING PROGRAM

A modified GCL product was selected by the contractor for this project, consisting of (from top to bottom) a nonwoven needle punched 270 g/m² (8 oz/yd²) geotextile, a layer of sodium bentonite at low moisture content, and a composite of a light weight woven slit film geotextile needle punched to a 200 g/m² (6 oz/yd²) nonwoven geotextile. This product was modified by the manufacturer for the Summitville project. The 270 g/m² nonwoven geotextile is a dense mat of coarse and fine fibers. During the GCL composite manufacturing process, closely spaced barbed needles drive the fibers from the 270 g/m² geotextile through the composite into the lower geotextile. Fibers protruding through the woven/nonwoven composite side are then heat set to provide resistance to pullout and increased internal shear resistance. See Figure 1 for a
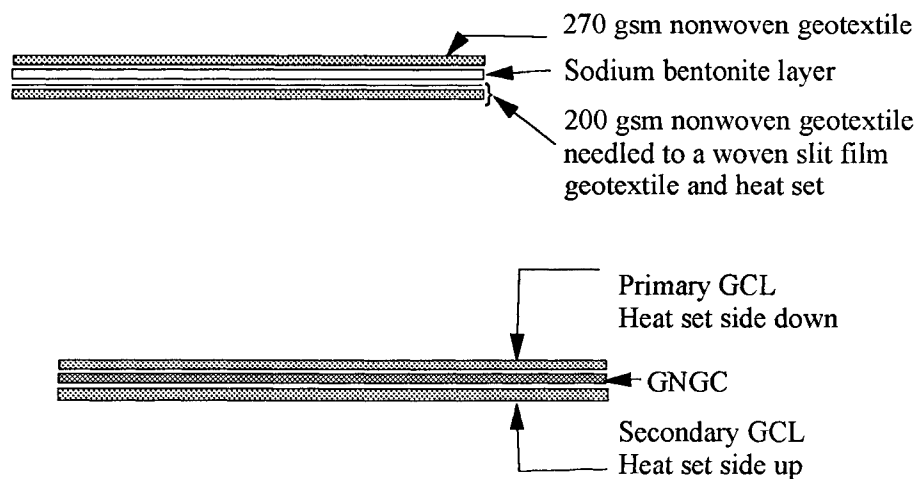
Figure 1. Schematic showing construction of GCL used at the site
and the deployment method selected.

detail of this composite GCL. The GCL manufacturer submitted five roll samples from the same production lot for this performance testing program.

The geonet geocomposite (GNGC) product selected for this site was composed of two 200 g/m² nonwoven needle punched geotextiles thermally bonded to both sides of a drainage net composed of high density polyethylene (HDPE). The GNGC manufacturer submitted one roll sample for the performance testing program.

Due to the location of the site and the extreme conditions that are often present at the site, as well as the desire to ensure that the leach pad would not become saturated and therefore unstable, a rigorous performance testing program was designed and conducted. This testing included GCL flux, free swell, fluid loss of bentonite, GNGC transmissivity, interface and internal shear, each performed using distilled water and a manufactured solution containing what was anticipated to be the site leachate following the amendments to the cover soil. Freeze/thaw testing was also performed, as the frost depth at the site has been known to reach 3.6 m. Conformance level index testing was also performed on the product, primarily to establish baseline values for field conformance testing. Tested parameters included mass per unit area, peel strength, wide width tensile strength, flux, free swell and fluid loss for the GCL, while the GNGC was tested for ply adhesion and mass per unit area.

Testing was also performed on the site ore material, primarily to establish values for Maximum Dry Density and Optimum Moisture Content for the purpose of compacting this material into the direct shear box for interface shear testing and internal shear testing of the GCL. The site soil was classified as a GM - clayey gravel with sand, according to the Unified Soil Classification System, and was used as both the subgrade and cover material for the project. The gravel portion of the soil caused numerous problems during the installation of the liner system, as there were often large angular cobbles and boulders in the soil that could not easily be removed or avoided.

Shear Testing Program

The shear testing program consisted of two differing types and series of tests, with varying test parameters, with the purpose of determining whether or not the site leachate and conditions would affect the shear properties of the lining system. Each series was performed in accordance with ASTM D 5321. The majority of the tests were performed using distilled water for hydration and immersion, while one series utilized a manufactured leachate that was to simulate water that would percolate through the amended cover soil. Interface shear testing was performed on each possible interface in the cover system, using site soils, the GNGC, and both sides of the GCL.

GCL Internal Shear Testing

Five GCL internal shear tests were performed on the samples utilizing distilled water, in order to establish a value to compare with the other test conditions. These internal shear tests were performed using a normal load of 19.2 kPa (400 psf), hydrated under 19.2 kPa load for 72 hours, with a machine strain rate of 10 mm/hour. The average maximum internal shear stress achieved under these conditions was 60.7 kPa with a standard deviation of 4.0 kPa. These maximum stresses occurred after an average of 2.1 cm of displacement, which is equivalent to approximately 6.8 percent strain based upon the sample size.

The two samples hydrated and tested in the leachate solution had an average maximum internal shear stress of 50.8 kPa at 6.5 percent strain. This value was slightly lower than that of the samples hydrated in distilled water, but was deemed to be acceptable for long term performance.

The final sample tested for GCL internal shear strength was tested following freeze thaw cycling. The sample was first hydrated under a load of 19.2 kPa for 72 hours using distilled water and then subjected to freezing (-9 degrees Celsius) conditions for a period of 24 hours, then elevated to room temperature (21 degrees Celsius) for a 24 hour period. This freezing and thawing continued for a total of six cycles. The maximum internal shear stress achieved in the freeze/thaw testing was 49.3 kPa, at 6.9 percent strain.

It should be noted that in each case, the shear failure of the material occurred by failing the woven geotextile of the heat set side of the GCL, and not internally shearing of the bentonite or by fiber pullout of the needle punched fibers. This indicated that internal shearing of the GCL was not going to be the controlling factor in the slope design angle, as long as the needle punching of the GCL was adequate to ensure proper internal shear strength.

Interface Shear Testing

The next series of shear testing was performed on each interface, with the purpose of determining at which interface the minimum shear angle occurred. The GCL was tested both with the heat set side and the nonwoven sides against the site soil, and achieved essentially the same shear angle (34 - 35 degrees). The nonwoven side reached a slightly higher adhesion, as the softer nonwoven side was more apt to lock the coarse particles of the subgrade into the GCL. The GCL was also tested against the GNGC geotextiles. As expected, the heat set side performed better against the nonwoven geotextile of the GNGC. The combination of the heat set side of the GCL and the nonwoven geotextile of the GNGC almost created a locking effect, such as is found with Velcro®, and a friction angle of 18 degrees. The nonwoven side of the GCL tested against the GNGC achieved a 15 degree friction angle, with minimal adhesion.

These results dictated that the most effective method of placement would be the secondary GCL placed with the nonwoven side down against the subgrade, the GNGC placed onto the heat set side of the secondary GCL, and then the primary GCL placed with its heat set side against the GNGC, allowing the cover soil to be placed against the nonwoven side. This configuration allowed the highest friction at each interface with the lowest friction angle being equal to 18 degrees, with an adhesion of 0.85 kPa.

Leachate - Bentonite Compatibility Testing

The GCL bentonite was tested for its compatibility with laboratory simulated site leachate. Because the crushed latite ore in the heap leach pad was also to be used as the cover soil, the question of whether the water percolating through the cover soil to the GCL would adversely affect the bentonite in the GCL had to be answered. To accomplish this, a series of GCL flux, free swell of bentonite and fluid loss of bentonite testing was performed, first with distilled water, then with generated leachate. The leachate was generated by percolating water through a column of the crushed latite ore cover soil, mixed with 9.0 kg/m^2 (1.84 lb/ft^2) of lime. Based upon a 1.2 m thickness, this percolation column was used to imitate the amended cover soil, following placement. The generated leachate had base values of pH equal to 4.6, with measurable levels of copper, magnesium, calcium, and sodium. Table 1 shows the chemical composition of this leachate solution. Prior to design of this test program, the latite ore in the heap leach pad had undergone an in place rinsing program in which the water in the pad was pumped out, treated, and then recirculated, such that much of the cyanide had been removed from the pad.

TABLE 1 - LEACHATE COMPOSITION

Test Parameter	Measured Value
pH	4.6
EC	2140 US/cm
Aluminum	6.4 mg/L
Calcium	556 mg/L
Copper	442 mg/L
Iron	13.4 mg/L
Potassium	5.4 mg/L
Magnesium	24.5 mg/L
Manganese	6.3 mg/L
Sodium	48.1 mg/L
Zinc	4.5 mg/L

The GCL flux testing was performed in accordance with ASTM D 5887. Five samples were tested, with individual samples of each being tested with distilled water and generated leachate. This testing was performed in flexible wall permeameters, under constant head conditions. The flux values and resulting permeabilities were both low, as is expected with GCL, for each set of samples. There was no obvious physical change between those samples tested with distilled water and those tested with leachate, indicating that at least for the short test duration, there was no apparent breakdown of the sodium bentonite in the GCL. The tests were terminated following stabilization to within the specifications outlined in ASTM D 5887. In each case, less than one pore volume had been passed through the sample upon termination.

The free swell testing of bentonite was performed in accordance with ASTM D 5890, with five specimens tested in distilled water, and five in generated leachate. With this test, there was a marked difference in the results generated. The Swell Index value is reported as milliliters of swell per two grams of dry, crushed bentonite. The average Swell Index for the samples tested in distilled water was equal to 39.8. The minimum acceptable value, per the site specifications, is equal to 24.0. The samples tested with the generated leachate achieved an average value of 27.6, which was acceptable according to specifications. It was apparent that the generated leachate was reacting with the bentonite in an adverse fashion, as evidenced by a cloudy yellow film coating the surface of the swelled bentonite and the lower swell values. As the minimum acceptance criterion was met, the material was accepted for the project.

The fluid loss of the bentonite was tested in accordance with ASTM D 5891, again with five samples each tested with distilled water and generated leachate. The purpose of this test is to determine how much fluid can be pressed out of a slurry and filter cake comprised of bentonite as an index measure of its hydraulic conductivity reduction in GCLs. The maximum allowable value for this test is 18.0 milliliters of filtrate loss, as delineated by the site specifications. Again, there was a noticeable difference between the value achieved by the distilled water samples and the leachate samples. The average for the distilled water samples was 9.6 ml, while the leachate samples attained an average of 12.1 ml. As was the case with the swell test, there were noticeable visual differences in the appearance of the specimens following the tests. The filter cakes appeared to have a gel like consistency and were not stratified when tested with distilled water, but were very stratified and had a thick, muddy density when mixed with leachate. Again, as the values achieved with the leachate were below the maximum acceptable value, the material was accepted for the project.

INDEX LEVEL CONFORMANCE TESTING

Several series of various index level tests were performed, both on the GCL and the GNGC, with the purpose of determining base line values for on site material conformance testing, as the GCL selected was a manufacturer modified product with no established baselines. Project specifications required that deployed material be tested at a frequency of one test per every 4,650 m² (50,000 ft²) of deployed material. As a full on site laboratory was to be set up, the

index level tests were selected based upon ease of testing in a field laboratory and effectiveness in proving material conformance. The tests selected for the GCL were mass per unit area, peel strength, wide width tensile strength and GCL flux, with fluid loss, swell index and moisture content being performed on the GCL bentonite. The GNGC was also conformance tested for ply adhesion and mass per unit area. The following sections describe some of the problems encountered in the test program, as well as the design considerations involved in choosing these specific tests as conformance tests.

Peel Strength

The peel strength of the GCL was determined using two different methods. The two methods were used because, at the time of this project, there was no industry wide standard for peel tests on GCLs. The American Society for Testing and Materials (ASTM) Committee D-35 is in the process of approving a method that will become the standard. At the time of this test program, however, the manufacturer certified its roll goods based upon one method (ASTM D 4632 modified - grab test), while the design engineer and testing laboratory used a different method (ASTM D 413 modified - wide width peel) to test for performance and material conformance. The manufacturer's quality control approach selected the single highest peak in grab peel to be the value reported as peak peel strength, whereas the engineer specified that an average of the five highest maximums and five lowest minimums of a wide width test should be the reported value. Figure 2 illustrates the differences in data interpretation between the two methods. In each case, a 10.2 cm wide by 20.3 cm long specimen size was used. The needle punched fibers of each specimen are cut for the first 7-9 cm, depending on gage length, allowing the two layers of geotextile to be peeled back from each other. Each specimen was tested in a calibrated tensiometer, under strain control at a rate of 30.5 cm per minute, with the data output recorded on a chart recorder. The minimum acceptance value was 8.3 N/cm width (4.75 lb/in), based upon original design conformance test data performed on roll samples submitted for that purpose.

A problem arose when the first rounds of material conformance testing began, approximately one month prior to the commencement of the installation. The project specifications required that every 4,650 m^2 (50,000 ft^2) of installed GCL was to be tested, however practicality required that the testing be performed prior to deployment, as the liner was also required to be covered by 0.6 to 1.2 m of cover soil on a daily basis. Based upon the roll dimensions of 45.7 m long by 4.72 m wide (150 ft by 15.5 ft), it was determined that approximately every twenty second roll should be randomly tested, which with passing results allowed the next twenty one rolls to be accepted based upon a sequential numbering of the roll goods. Following the testing of several rolls at the beginning of the project using ASTM D 413 method, it was discovered that roll goods were achieving failing results in peel strength. Samples were shipped back to the main laboratory for further tests, using the same equipment that was used in performing the initial conformance testing. This testing confirmed the results of the on site lab, which resulted in numerous rolls being initially rejected for use.
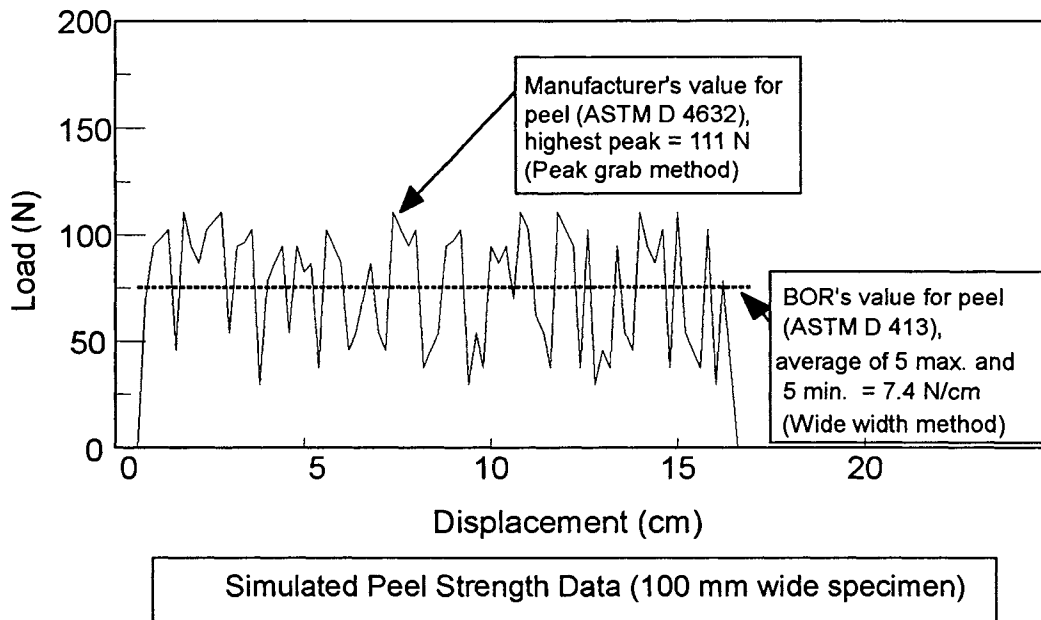
Figure 2. Comparison between methods of interpretation of the
results from peel strength testing.

In resolution following extensive retesting at both the manufacturer's and third party test laboratories, and based upon additional internal shear testing, the BOR decided that all rolls that achieved a minimum value of 6.67 N/cm (3.75 lb/in) tested by the ASTM D 413 wide width method would be accepted for use on all slopes. Those rolls that tested to a peak value of 66.7 N (15.0 lb/in)based upon the ASTM D 4632 grab method could only be used on slopes equal to 20:1. Rolls that failed to achieve either of these values were shipped back to the manufacturer or destroyed on site.

Moisture Content

At the time the project requirements were written, there was insufficient evidence to allay the designers concerns about freeze/thaw. Because of concerns over the high altitude effects of freezing of the bentonite, the GCL specified for the project was to have a low moisture content as received. Freezing may occur at any point during the year, and there was a lack of covered, heated storage at the site, a low moisture content GCL was specified in order to minimize the freezing, thawing, and water crystallization that could occur while the GCL was on the rolls, prior to deployment. Since that time, research has been undertaken that shows that freeze/thaw cycles do not have a detrimental effect on bentonite performance, but as the requirements specified low moisture content and this was not altered in successive amendments, the supplied GCL was required to have a low moisture content as received. Due to the rough nature of the subgrade, a low moisture content was also preferred to minimize the displacement of GCL upon

placement of cover soil, as it was thought that the wet bentonite would more easily displace when a large rock was placed on the GCL. The maximum value allowed was 12 percent moisture, based upon dry bentonite mass. Every sample tested yielded a value lower than the maximum acceptable value.

INSTALLATION CONCERNS

The extensive testing program was required in part due to the sensitive nature of the contaminated site, and also due to the rugged conditions that exist at Summitville. The ore material on the heap leach pad was very angular crushed latite ore containing varying proportions of clay, gravel, cobbles, boulders, and sand sized particles. The ore material was also to be used as the cover soil, so the geosynthetics involved had to be resistant to punctures and tears from cover soil placement as well as installation activities.

The installation subcontractor received permission to use a Positrack ASV low ground pressure vehicle with rubber tracks to facilitate deployment, which meant that the equipment would be operating directly on the geosynthetic materials and subgrade (see Photograph 2). This system of deployment was tested on the first day of deployment and demonstrated no advese effects on the GCL when the subgrade was in conformance. Thus, it was important that the subgrade conform to specifications which required that the subgrade be rolled tight with no loose material greater than 19 mm in diameter and no free standing water on the surface.

Photograph 2. Installation of capping system using rubber tracked low ground pressure vehicle operating directly on geosynthetics.

Rainstorms occurred on a regular basis throughout the project and were a frequent problem. These periodic rain events would wash away all fines that had been rolled into the surface creating pockets of exposed rocks. Even with repeated rolling with a vibratory roller, the rocks would not always roll back into the surface. When possible fresh material with additional fines was brought in to replace this material. When this was not possible, due to the nature of the material on the heap leach pad, these rock pockets were remediated by using scrap sections of GCL to cushion the area prior to deployment. On occasion, the rubber tracks of the vehicle would also tear up rocks out of the subgrade, which then had to be removed using hand labor. The main reason for concern with loose rocks on the subgrade was that equipment was constantly on the surface of the geosynthetics during the installation process. Even though the equipment exerted low ground pressure, a loose stone on the subgrade would create a hole in the GCL when it was run over by the tracked vehicle. One other problem associated with the frequent rainstorms involved the design of a perimeter ditch around the heap leach pad. The ditch was designed to divert storm water around the remediated pad. Unfortunately, this led to construction problems as the ditch was designed for a low gradient, which created ponding/wet conditions throughout the installation period. The engineer solved this problem by allowing the installer to place scrap lengths of GCL in the ditch, then deploying the liner system on top of it.

The relatively short construction season created another installation problem. The site is located at approximately 3,500 m in the Colorado mountains, and receives snow for almost the entire year. During the 1997 construction season, there was recorded snowfall on June 16 and September 21. The intervening three months were the rainy season, during which it could rain up to 25 mm on any given day. These issues required that the prime contractor and installation subcontractor work cooperatively to ensure that the subgrade was prepped just ahead of deployment, and that cover soil followed closely behind the deployment. Although precautions were taken, many times rolls of GCL were deployed and tarped, waiting for cover soil as the rains approached. Fortunately, with rapid tarping, removal of excessively hydrated GCL material was required on few occasions. Site specifications allowed the GCL to reach 20 percent moisture content prior to cover soil placement.

The 1997 construction season was halted in November of 1997, with about 40,500 m² remaining to complete the lining project. The reason for the stoppage was that the subgrade had finally frozen to the point that it would not thaw on a daily basis for subgrade preparation and anchor trench excavation. This cessation led to another problem: how to winterize and seal the edges of the in place GCL, so that construction could continue the following summer. This problem was solved by rolling out excess on site GNGC and placing it such that one half of the roll width covered the leading edges of the liner system, and one half went up the slope of the cover soil extents. The contractor then placed about 1.2 m of cover soil on top of this GNGC, which allowed the GCL, if it was to become hydrated during the spring runoff, to become hydrated under load. At the start up of the 1998 construction season, these winterization GNGC
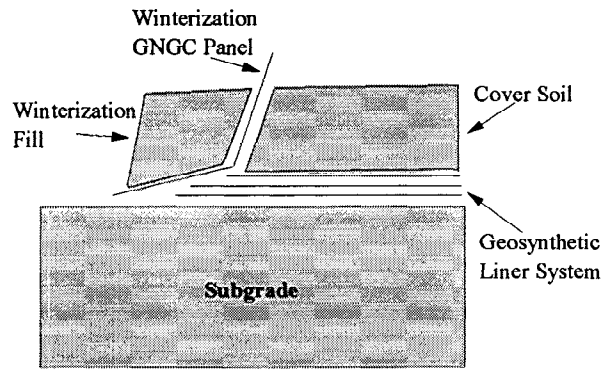
Figure 3. Schematic showing winterization of the leading edge of the installed liner system at the close of the 1997 construction season.

pieces were removed as the area was about to be lined, such that these areas would only be exposed for a minimal amount of time. For the most part, the efforts were a success with only minimal damage to the liner system upon removal. Following removal of the GNGC, the existing liner system was tied into by extending the new GCL layers all the way to the extents of the cover soil, then placing cover soil as rapidly as possible in order to ensure that hydrated GCL was exposed for as short a time as possible.

CONCLUSIONS

The Summitville Mine Superfund Site had numerous issues necessitating rapid, quality cleanup and remediation. The heap leach pad closure was among them and a geosynthetics system was determined to be the best possible method for capping the area to prevent future contamination. Although the remote location and extreme weather conditions present at the site created difficulties during the installation process, the end result was a quality installation that would prevent further contamination far into the future. The geosynthetics installation in the end proved itself to be the most cost effective method for remediation of the heap leach pad at the Summitville Mine Superfund Site.

ACKNOWLEDGMENTS

Company, Inc., Alamosa, Colorado was the prime contractor, and Simbeck and Associates Inc., Franktown, Colorado was the geosynthetics installation subcontractor.

EQUIVALENCY OF COMPOSITE GEOSYNTHETIC CLAY LINERS AS A BARRIER TO VOLATILE ORGANIC COMPOUNDS

Gary J. Foose
Florida State and Florida A&M Universities

Craig H. Benson
University of Wisconsin-Madison

Tuncer B. Edil
University of Wisconsin-Madison

ABSTRACT

Numerical and analytical models were used in this study to simulate contaminant transport of toluene in composite liners. Methods for demonstrating equivalency based on contaminant transport are also presented. Toluene was selected for this study because the transport properties of toluene are representative of those for volatile organic compounds (VOCs) commonly found in landfill leachate. Results from the model indicate that the mass flux of toluene through a GCL composite liner is as much as two orders of magnitude greater than that through a composite liner with a 61 cm thick soil liner (e.g. a Subtitle D liner) because a GCL composite liner is thinner. Performance of a GCL composite liner can be improved by adding an additional soil layer beneath the GCL, which reduces the concentration gradient across the base of the liner system. For the materials considered in this study, an additional 90 cm is sufficient to reduce the mass flux and increase the contaminant breakthrough time through the GCL composite liner to be comparable to that for a Subtitle D liner. A thinner layer can be used depending on the material properties of the soil and in particular, the porosity of the layer.

INTRODUCTION

Composite liners having a GCL are a popular alternative to the Subtitle D composite liner required in municipal solid waste landfills. A GCL composite liner typically consists of 5 to 6.5 mm of bentonite having low hydraulic conductivity overlain with a geomembrane liner. The Subtitle D liner consists of 61 cm of compacted clay having a hydraulic conductivity $< 1 \times 10^{-7}$ cm/s overlain with a geomembrane. Designers and owners are inclined to propose using GCL composite liners because suitable clayey soil may not be available, the GCL composite liner uses less air-space in the landfill, and building a composite liner with a GCL may be more economically viable.

Subtitle D of the Resource Conservation Recovery Act includes a provision that permits an alternative liner, provided that that the liner is equivalent to the Subtitle D liner. Traditionally, comparisons of liner systems have been made based on leakage rate through defects, with equivalency being defined as a liner system having a leakage rate less than or equal to that for the Subtitle D liner. However, leakage rates are not always indicative of performance of composite liner (Foose 1997). In fact, diffusion can be a significant mechanism of contaminant transport in soil liners and geomembranes (e.g. Shackelford 1990 and Park and Nibras 1993).

As shown in Fig. 1, VOCs can migrate through composite liners via advection and diffusion through defects in the geomembrane and subsequent advection and diffusion through the soil liner. Additionally, VOCs can diffuse through intact geomembranes (Park and Nibras 1993) and then diffuse through the soil liner (Fig. 1). In contrast to contaminant transport through defects, diffusion of VOCs can occur over the entire footprint of the liner system. Thus, mass flux of VOCs in the intact composite liner has the potential to be several orders of magnitude greater than that through defects, depending on the constituents of the leachate, the hydraulic conductivity of the soil liner, and the frequency, type, and size of defects.
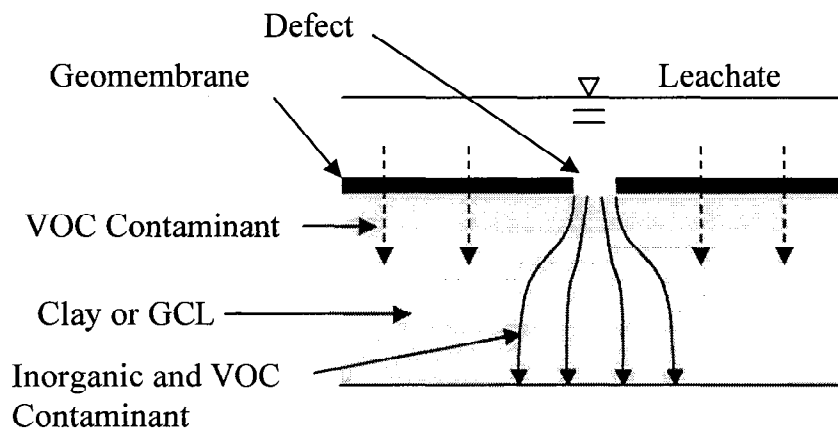
Figure 1. Contaminant Transport Processes in Composite Liners.

An analysis was conducted by Foose et al. (1996) using numerical models for predicting mass flux of a conservative inorganic contaminant in an EPA Subtitle D liner and composite liner having a GCL. Foose et al. (1996) found that the mass flux from defects in the composite liner having a GCL was greater than that in the EPA Subtitle D liner for the conditions analyzed.

A comparison of mass flux of cadmium and toluene through an EPA Subtitle D liner having few defects was performed by Foose (1997) using numerical models. The composite liner was assumed to be constructed with good quality control as defined by Giroud et al. (1992). The concentration of both cadmium and toluene were assumed to be the same. Results from analysis showed that the mass flux of toluene is nearly 5 orders of magnitude greater than that of cadmium. The reason that mass flux of toluene through the intact liner is much greater

than cadmium ion through defects is that the surface area over which transport of toluene occurs is approximately 5 orders of magnitude greater than the area of defects. Thus, provided that the flow rate through defects is small, the dominant pathway for transport of toluene is through the intact liner. Therefore, the remainder of this paper will focus on diffusive transport of VOCs through intact composite liners and transport through defects will not be considered further.

ASSESSING EQUIVALENCY

To compare alternative liner systems based on contaminant transport, the location at which the performance of the liner system will be evaluated must be selected. This location can be at some off-site monitoring well where the impact of the landfill is judged based on exceeding a particular maximum contaminant level (MCL) or immediately underneath the liner system. In many cases, however, the base of the liner system is used because it is usually at the same elevation regardless of the design of the liner. Ultimately, an analysis of groundwater contaminant transport should be conducted to assess how alternative liners impact groundwater quality.

Because a GCL composite liner is thinner than a Subtitle D liner, the contaminant breakthrough time through a GCL composite liner is less than that for a Subtitle D liner. Additionally, the mass flux from a GCL composite liner is greater than that from a Subtitle D liner because the location at which the flux is calculated is closer to the contaminant source for the GCL composite liner. Analyses demonstrating these conditions will be presented in a subsequent section.

When a GCL composite liner is being considered because sufficient clay is not available, the mass flux can be reduced and the breakthrough time increased by adding and additional layer of soil beneath the GCL. The additional layer of soil, which effectively is part of the liner, increases the distance between the source of the contaminant and the base of the liner. As a result, the concentration gradient at the base of the liner decreases and distance of travel increases. An appropriate thickness of the additional soil layer depends on the type of boundary condition existing at the base of the liner, characteristics of the additional soil layer, and the VOC being contained.

COMPOSITE LINER MODELS

Transient Models

Transport of VOCs through composite liners is different than that through porous media because the geomembrane component is not porous. VOCs diffuse through the interstitial spaces between polymer molecules in the geomembrane in a three-step process (Fig. 2): (1) partitioning into the geomembrane, (2) diffusing through the geomembrane, and (3) and partitioning out of the geomembrane (Park and Nibras 1993). After the VOC is transported

through the geomembrane, the contaminant diffuses through the soil liner in the same manner that diffusion occurs in porous media.
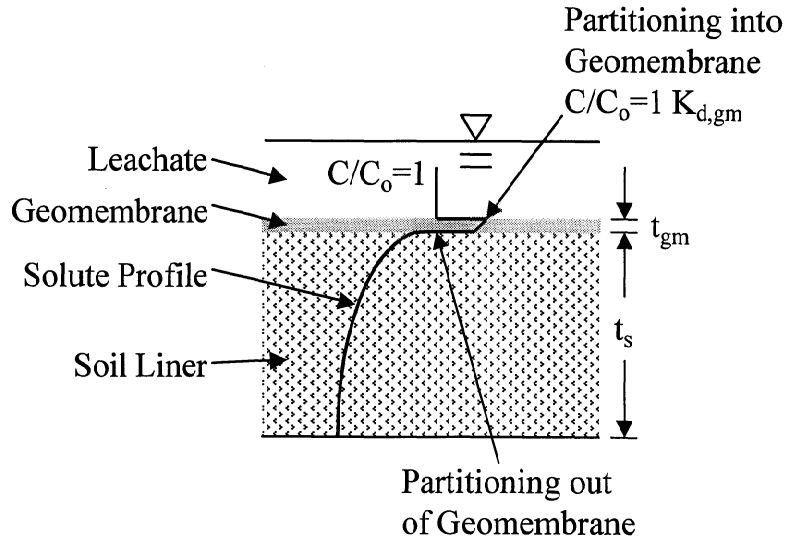
Figure 2. Transport Process for VOCs in Composite Liners.

Because of this multi-step transport process and combination of solid and porous media, application of analytical solutions is limited. Therefore, a numerical model was developed for analyzing transport of VOCs in composite liners. The numerical model includes the three-step process for diffusion of VOCs through geomembranes and maintains continuity of flux at the interface of the geomembrane and soil liner. Linear and reversible sorption and desorption are assumed for the geomembrane based on the findings of Park and Nibras (1993) who show that adsorption and desorption of VOCs onto geomembranes is approximately linear for aqueous concentrations < 100 mg/L.

If transport of VOCs is assumed to be spatially invariant, the governing equations for diffusive transport of VOCs through composite liners are:

$$\frac{\partial C}{\partial t} = D_{gm} \frac{\partial^2 C}{\partial z^2} \qquad 0 \le z \le t_{gm} \tag{1}$$

$$R_d \frac{\partial C}{\partial t} = D^* \frac{\partial^2 C}{\partial z^2} \qquad t_{gm} \le z \le t_{gm} + t_s \tag{2}$$

where C is the concentration of solute, t is time, D_{gm} is the diffusion coefficient of the solute in the geomembrane, z is the direction through the profile of the liner, R_d is the retardation factor, D^* is the effective diffusion coefficient of the solute in soil, t_{gm} is the thickness of the

geomembrane, and t_s is the thickness of the soil layer. Linear and reversible sorption and desorption were assumed to apply to the sorption of the solute onto the soil.

Continuity of mass flux at the interface between the geomembrane and soil liner is described by:

$$D_{gm} \frac{\partial C}{\partial z} = D^* n \frac{\partial C}{\partial z} \qquad z = t_{gm}, t \geq 0 \qquad (3)$$

where n is the porosity of the soil. In this study, it was assumed that the total porosity was equal to the effective porosity. Additional soil layers can be included by applying Eq. 2 for each soil layer and maintaining continuity of flux through the soil layers using equations similar to Eq. 3.

Initially, the solute concentration throughout the entire domain is assumed to be zero:

$$C = 0 \qquad z \geq 0, t = 0 \qquad (4)$$

and the concentration of the source was assumed to be a constant:

$$C = C_o \qquad z = 0, t \geq 0 \qquad (5)$$

where C_o is the concentration of the leachate. A constant source concentration was used because insufficient field data exist to support a more complicated boundary condition (Rowe 1987, Shackelford 1990).

Comparison of mass flux at the base of the liner requires proper characterization of the bottom boundary condition. Two bottom boundary conditions can be used to bracket the range of field conditions: (1) constant solute concentration at the base of the liner system and (2) a zero solute concentration and zero flux condition infinitely far from the base. The latter case corresponds to a liner system founded on a very thick saturated subgrade.

The bottom boundary was considered to be a constant concentration of zero in this study. The location of the bottom boundary was varied from immediately at the base of the composite liner system to 9 m from the base of the liner system. The latter case approximated a semi-infinite boundary for simulations of 100 years. For example, the concentration gradient at 100 years at a depth of 9 m is 3×10^{-15} mg/L/cm, for a Subtitle D liner, which results in a contaminant flux of essentially zero.

The governing equations were solved using a Crank-Nicholson node-centered finite-difference algorithm. Details regarding development of the composite liner model can be found in Foose (1997).

Steady-State Models

The steady-state diffusive mass flux (J_D) through composite liners in which the base of the liner system is maintained at a constant concentration can be calculated using Fick's first law:

$$J_D = D_{eq}\left(\frac{\Delta C}{t_{gm} + t_s}\right)$$ (6)

where D_{eq} is the equivalent diffusion coefficient for the composite liner, and ΔC is the difference in concentration between the solute source and the concentration at the base of the liner system. The equivalent diffusion coefficient (D_{eq}) can be obtained using an approach similar to that for determining the hydraulic conductivity of soil layers in series (Foose 1997). The equivalent diffusion coefficient is:

$$D_{eq} = \frac{t_{gm} + t_s}{\dfrac{t_{gm}}{D_{gm}K_{d,gm}} + \dfrac{t_s}{D^*n}}$$ (7)

where $K_{d,gm}$ is the partition coefficient for the contaminant and the geomembrane. The partition coefficient of the solute and the geomembrane appears in the denominator of the geomembrane term in the denominator because the solute diffuses in the geomembrane at a higher concentration than the solute source (Fig. 2). Additional soil layers can be incorporated by adding the thickness of the additional soil layer to the numerator and including another term for the additional soil layer in the denominator.

EQUIVALENCY OF COMPOSITE LINERS HAVING A GCL

The transport properties of liner systems and the constituents of leachate can vary significantly. In practice, equivalency comparisons between liners should be based on site-specific data whenever possible. In this study, however, representative material properties were selected (see Table 1) from a summary of material properties contained in Foose (1997). Toluene was the VOC analyzed because it is commonly found in landfill leachate and the properties of toluene are representative of other VOCs. Parameters for the compacted soil liner were taken from data compiled by Foose (1997) for compacted clays. The effective diffusion coefficient for toluene in the GCL is based off of measurements of apparent tortuosity by Shackelford (1989) for a smectitic clay and the porosity is representative of properties of GCLs reported by Ruhl and Daniel (1997). The total and effective porosity were assumed to be equal for all soils in this analysis.

The partition coefficient for toluene and the GCL was assumed to be equal to that for the compacted soil liner because there is a lack of data regarding sorption of VOCs onto GCLs.

Material properties for the additional soil layer are representative of a sandy soil (Foose 1997). The diffusion and partition coefficients for the geomembrane were taken from Park and Nibras (1993). The thickness of the geomembrane was assumed to be 1.5 mm. The thickness of the GCL was assumed to be 6.5 mm and the thickness of the compacted soil liner was 61 cm.

Table 1. Properties used in Analysis of Equivalency.

Material Property	Compacted Soil Liner	Geosynthetic Clay Liner	Additional Soil Layer	Subgrade Soil	Geomembrane
Effective Diffusion Coefficient (cm^2/s)	2.0×10^{-6}	2.0×10^{-6}	2.4×10^{-6}	2.0×10^{-6}	3.0×10^{-9}
Retardation Factor	3.3	1.7	1	1	-
Porosity	0.54	0.75	0.32	0.54	-
Partition Coefficient (mL/g for Soils)	0.7	0.82	0	0	135

Equivalency Based on Concentration at the Base of the Liner System

The numerical model was used to evaluate the concentration at the base of a liner as a function of time. Concentration at the base of the three liner systems founded on a thick subgrade versus time is shown in Fig. 3. As shown in Fig. 3, the concentration at the base of the GCL composite liner is greater than that for the Subtitle D liner for all times. If an additional layer of soil 80 cm thick is added beneath the GCL composite liner, the concentration is similar to that for the Subtitle D liner and, at 100 years is less than that for the Subtitle D liner (Fig. 3). For the concentration at the base of the GCL composite liner to always be less than that for the Subtitle D liner, an additional 120 cm of additional soil is required.

Concentration at the base of the liner is primarily a function of the diffusion coefficient of the soil and the retardation factor. These parameters can vary significantly with soil type. Hence, the thickness of soil required to maintain a lower concentration at the base of a GCL composite liner may vary considerably. This is particularly true if sorptive capacity of the Subtitle D liner is much greater than that for the GCL composite liner because the additional sorptive capacity will increase the contaminant breakthrough time.

Equivalency Based on Mass Flux

The steady-state mass flux, calculated using Eqs. 6 and 7 and a concentration of zero at the base of the liner is shown in Fig. 4 for the Subtitle D liner and the GCL composite liner. The mass flux from the GCL composite liner is nearly two orders of magnitude greater than that from the Subtitle D liner. However, adding an additional 50 cm of soil beneath the GCL results in comparable steady-state mass flux for the GCL composite and Subtitle D liners.
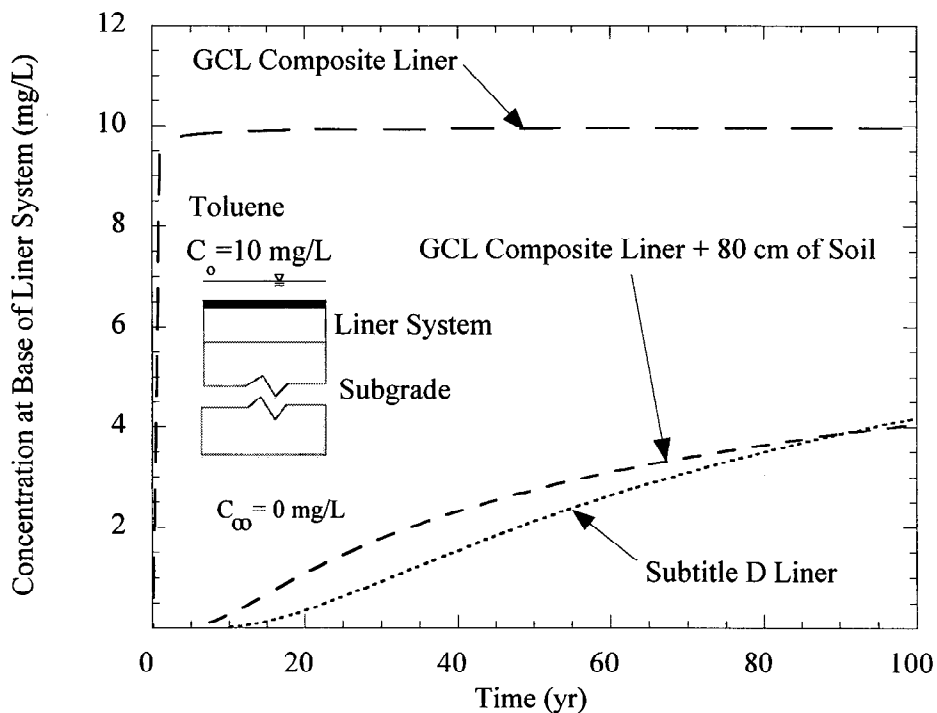
Figure 3. Concentration at Base of Liner Systems.
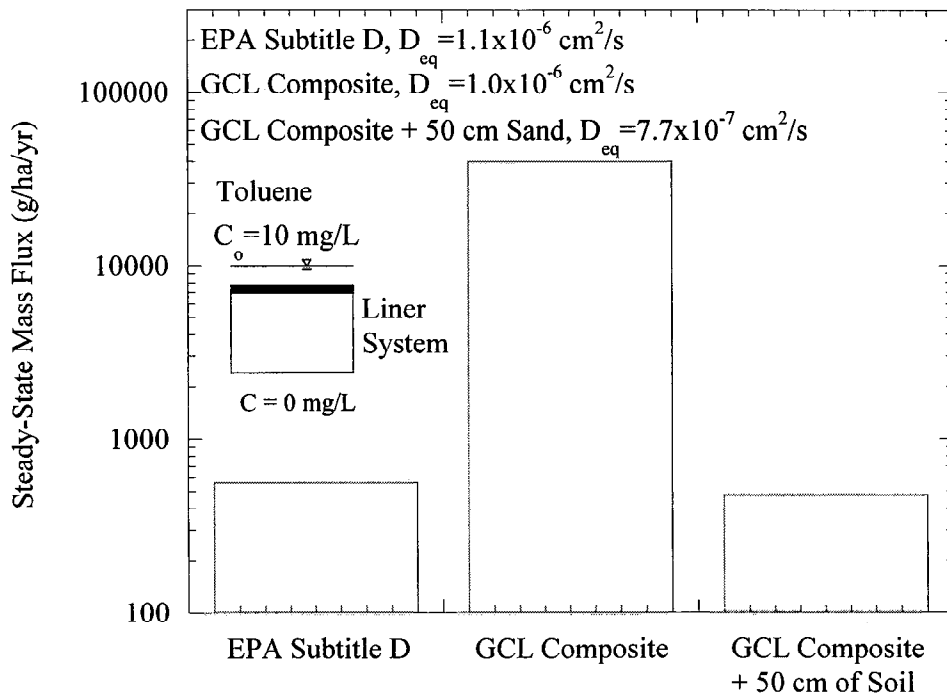
Figure 4. Steady-State Mass Flux through Liner Systems Analyzed.

The effective diffusion coefficient and the porosity of the soil impact the steady-state mass flux through the composite liner (Eq. 6). Decreasing the porosity of the additional soil layer decreases D_{eq} and reduces the mass flux. Thus, a thinner additional soil layer may be possible if the soil is more densely compacted. In addition, D^* of the soil should decrease as the pore space becomes smaller, which will also lower the mass flux.

Graphs of mass flux of toluene versus time for the two liner systems founded on a thick subgrade are shown in Fig. 5. The mass flux for the GCL composite liner is greater than that from the Subtitle D liner at all times. However, if an additional 90 cm of soil is added to the base of the GCL composite liner, the mass flux from the liners is similar for all times and at 100 years, mass flux from the GCL composite liner is less than that for the Subtitle D liner.
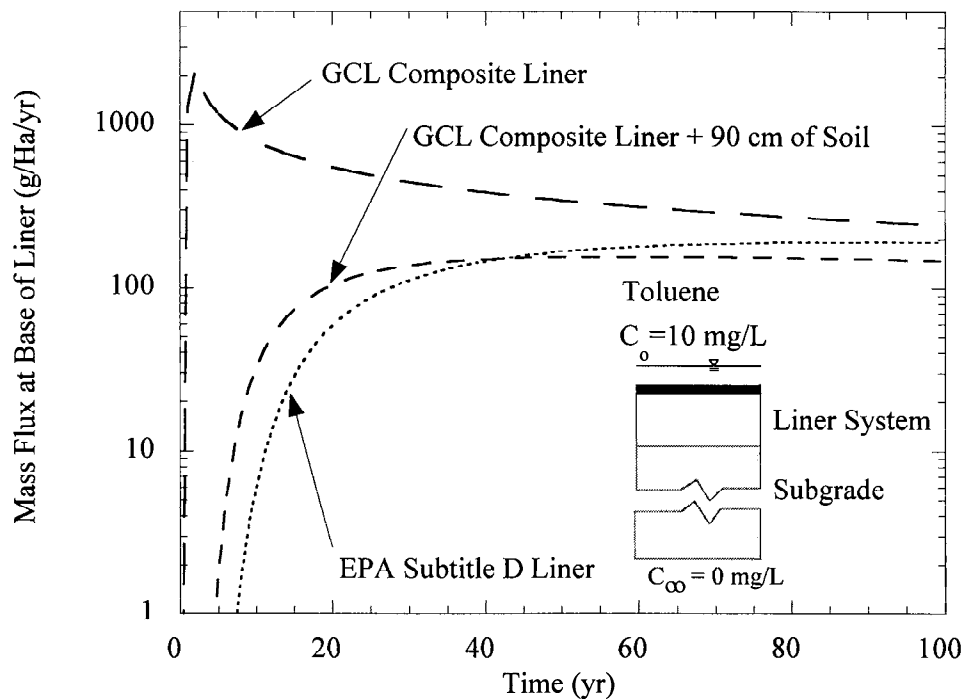
Figure 5. Mass Flux vs. Time through Liner Systems Analyzed.

Because of the peak in mass flux at early times for the GCL composite liner, comparisons based on cumulative mass discharged provide a better comparison. Cumulative mass discharged versus time for toluene for the GCL composite liner, Subtitle D liner, and the GCL composite liner with an additional layer of soil is shown in Fig. 6. The cumulative mass discharged from the GCL composite liner is the greatest because the mass flux during the first 20 years is much greater than that through the GCL composite liner with an additional layer of soil and the Subtitle D liner. Adding 90 cm of soil to the GCL composite liner results in slightly lower cumulative mass discharged at 100 years for the GCL composite liner than that for the Subtitle D liner.
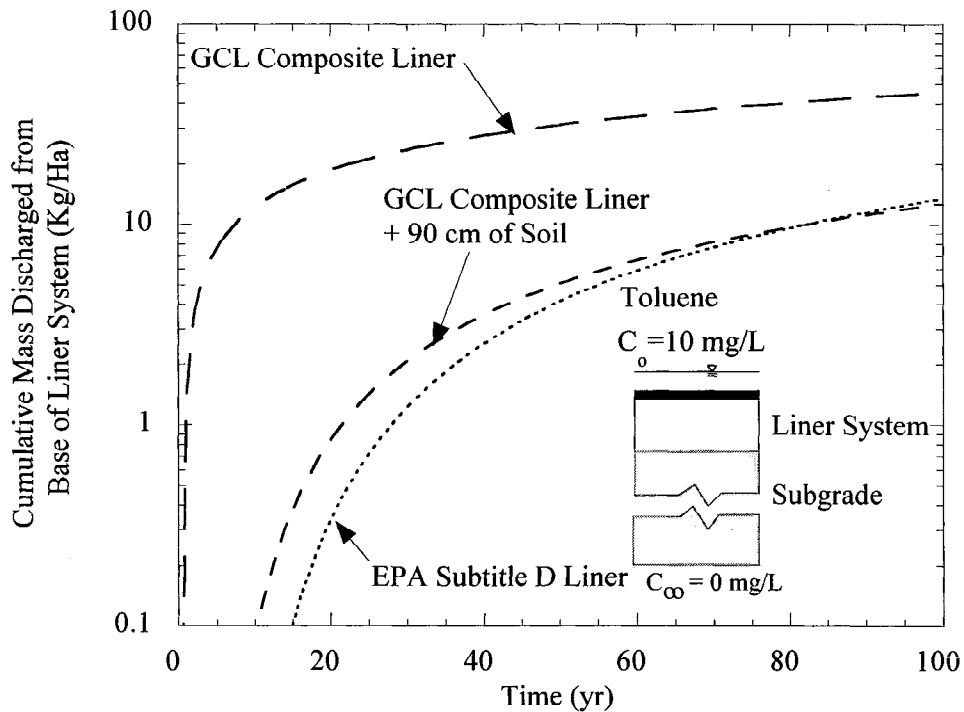
Figure 6. Cumulative Mass Discharged vs. Time through Liner Systems Analyzed.

The results in Figs. 3 through 6 show that an additional soil layer 50 to 90 cm thick is required for a GCL composite liner to be equivalent to a Subtitle D composite liner, with the different thickness corresponding to different equivalency criteria (50 cm based on steady-state mass flux, 80 cm based on contaminant breakthrough, and 90 cm based on mass flux). Thus, adding 90 cm of additional soil beneath the GCL will render the GCL composite liner equivalent or superior to the Subtitle D liner for the conditions that were modeled.

METHOD FOR EVALUATING EQUIVALENCY USING SITE-SPECIFIC MATERIAL PROPERTIES

The results presented in Figs. 3 through 6 are for the assumed material properties listed in Table 1. These properties do not represent the entire range of possible material properties and thus, the 90 cm of additional soil obtained from this analysis may be inadequate. Therefore, analyses should be conducted on a site-specific basis, using site-specific material properties. Unfortunately, there is a lack of tools applicable for analysis of transient transport of VOCs in composite liners. However, analyses of contaminant transport through composite liners using existing one-dimensional models, such as POLLUTE (Rowe and Booker 1983) or analytical solutions, can be conducted provided that the method of analysis is adjusted appropriately.

In the following analysis, an analytical solution to Eq. 2 for calculating mass flux at a particular distance from the contaminant source presented by Shackelford (1990) was used:

$$J_D = D^* n C_o \left[\frac{\exp\left(-\xi^2\right)}{\sqrt{\dfrac{\pi D^* t}{R_d}}} \right]$$

(8)

where ξ is:

$$\xi = \frac{t_s}{2\sqrt{\dfrac{D^* t}{R_d}}}$$

(9)

In a composite liner the geomembrane serves to limit the flow of liquid (i.e. advective transport). In terms of diffusion of VOCs, the geomembrane is relatively thin in comparison to the Subtitle D liner or GCL and thus can be neglected without significant error. Results shown in Fig. 7 for mass flux of toluene in a composite liner having a GCL are from an analytical solution to Eq. 2 and the material properties of the subgrade and a seepage velocity of zero. As shown in Fig. 7, the effect of neglecting the geomembrane and GCL in the analysis of diffusion of VOCs in composite liners having a GCL results in a slightly higher and earlier peak mass flux.
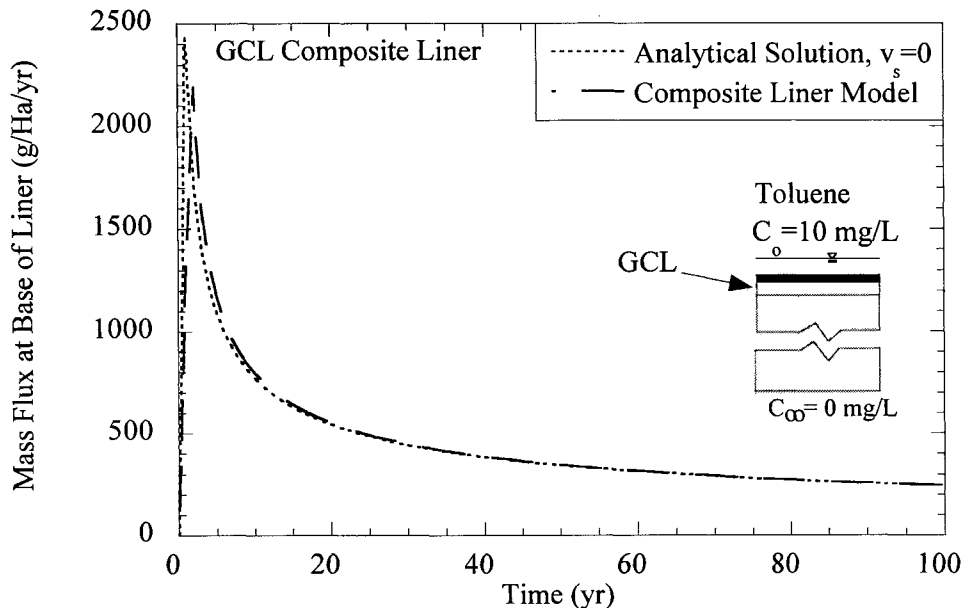
Figure 7. Mass Flux Predicted in a GCL Composite Liner using the Numerical and Analytical Models.

For the Subtitle D liner (Fig. 8), the comparison is not as favorable. The analytic solution for the case of zero seepage velocity and no geomembrane tends to over-predict the mass flux of toluene in the Subtitle D composite liner. The properties of the compacted clay were used in the analytical analysis. Results from Eqs. 8 and 9 tend to over-predict the mass flux in the EPA Subtitle D liner because the chemical gradient is overestimated. The chemical gradient is over estimated because the compacted clay liner is assumed to be semi-infinite and sorption beneath the composite liner (the subgrade) tends to reduce the solute concentration and hence, increase the chemical gradient. Nevertheless, the error from using Eqs. 8 and 9 is conservative in that the mass flux is over-predicted.
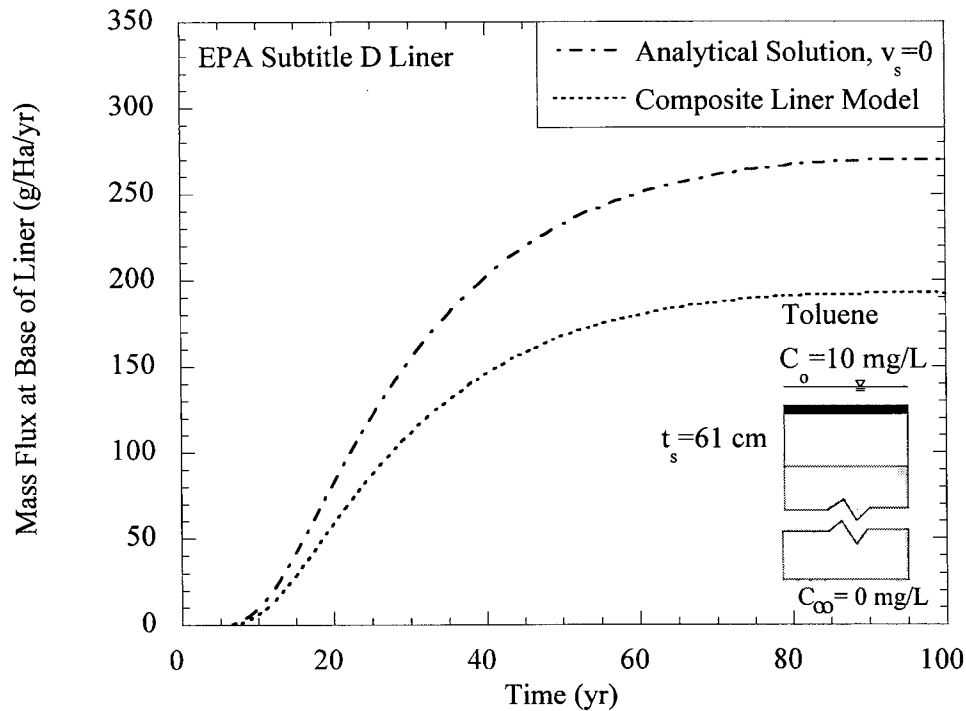
Figure 8. Mass Flux Predicted in an EPA Subtitle D Liner using the Numerical and Analytical Models.

A more detailed analysis can be conducted using POLLUTE (Rowe and Booker 1983) using a seepage velocity of zero. In addition, the geomembrane should not be included in the analysis. Because POLLUTE can be used for multiple layered systems, mass fluxes predicted using POLLUTE are likely to be closer to those from the numerical model because the profile of the liner and underlying soils can be represented in greater detail.

SUMMARY AND CONCLUSION

The current approach for evaluating equivalency of GCL composite and Subtitle D liners based on leakage rate through defects in the geomembrane is inadequate because VOCs can diffuse through intact composite liners. In fact, mass flux of VOCs through the intact liner can

be as much as 5 orders of magnitude greater than that through defects. A more appropriate approach is to employ numerical models and analytical solutions that simulate contaminant transport through intact composite liners.

Simulations conducted using a numerical model specifically developed to simulate VOC transport through composite liners showed that mass flux of toluene through a GCL composite liner can be two orders of magnitude greater than the mass flux through a Subtitle D liner. The mass flux is higher because the GCL composite liner is thinner than the Subtitle D liner and the concentration gradient near the base of the GCL composite liner is greater than that near the base of the Subtitle D liner.

Performance of GCL composite liners can be improved by adding an additional soil layer beneath the GCL. The additional layer reduces the concentration gradient across the base of the liner (which is the base of the additional layer of soil) and results in a decrease in mass flux. The additional soil layer does not have to meet the stringent requirements for compacted soil barriers with regard to hydraulic conductivity and compaction. For soils having diffusion coefficients, retardation factors, and porosity similar to those considered in this study, the additional thickness should be between 50 to 90 cm. In effect, the additional soil layer makes the GCL composite liner as thick as the Subtitle D liner.

The thickness of the additional soil layer needed varies with the diffusion coefficient, retardation factor, and porosity of the soil. The equation for steady-state mass flux (Eq. 6) in a composite liner using an equivalent diffusion coefficient can be used with site-specific material properties to determine a site-specific additional thickness. Additionally, traditional analytical and semi-analytical solutions (Eq. 8) for the advection-dispersion equation can be used to estimate the mass flux provided that the seepage velocity is set to zero. Such an analysis can be readily conducted on a personal computer using a commercially available spreadsheet program.

ACKNOWLEDGEMENT

REFERENCES

Foose G., Benson, C., and Edil, T. (1996), "Evaluating the Effectiveness of Landfill Liners," *Proceedings of Environmental Geotechnics*, Osaka, Japan, A. A. Balkema, Rotterdam, 217-221.

Foose, G. J. (1997), "Leakage Rates and Chemical Transport through Composite Landfill Liners," Ph.D. Dissertation, Dept. of Civil and Environmental Engineering, University of Wisconsin-Madison.

Giroud, J., Badu-Tweneboah, K, and Bonaparte, R. (1992), "Rate of Leakage Through a Composite Liner Due to Geomembrane Defects." *Geotextiles and Geomembranes*, 11(1), pp. 1-28.

Park, J. and Nibras, M. (1993), "Mass Flux of Organic Chemicals through Polyethylene Geomembranes." *Water Environment Research*, 65(3), Washington, D.C., pp. 227-237.

Ruhl, J. and Daniel, D. (1997), "Geosynthetic Clay Liners Permeated with Chemical Solutions and Leachates," *Journal of Geotechnical and Geoenvironmental Engineering*, ASCE, 123(4), 369-381.

Rowe, R., and Booker J. (1983), "Program POLLUTE, 1-D Pollutant Migration Analysis Program," SACDA, Faculty of Engineering Science, University of Western Ontario, London, Ontario.

Rowe, R. (1987), "Pollutant Transport through Barriers," *Geotechnical Practice for Waste Disposal*, GSP No. 26, ASCE, R. Woods, ed., 159-181.

Shackelford, C. (1990), "Transit-time Design of Earthen Barriers," *Engineering Geology*, 29, Elsevier Science Publishers, B.V., Amsterdam, pp. 79-94.

Shackelford, C. (1989), "Diffusion of Contaminants through Waste Containment Barriers," *Transportation Research Record 1219*, Transportation Research Board, National Research Council, Washington, DC, 177-217.

LONG-TERM MOISTURE MONITORING UNDER, IN AND OVER GCL LINERS

ALEX BRANDELIK AND CHRISTOF HUEBNER
INSTITUTE FOR METEOROLOGY AND CLIMATE RESEARCH,
KARLSRUHE RESEARCH CENTER / UNIVERSITY OF KARLSRUHE
POSTBOX 3640, D-76021 KARLSRHE, GERMANY

ABSTRACT

Control authorities, consulting and constructing engineers, are strongly interested in the moisture dynamics under and over a geosynthetic clay liner (GCL). The confirmation of a proper function can be achieved by a long-term water content monitoring on both sides of a liners. Manufacturers need to know the moisture distribution change inside the GCL during development of new products. For these demands a new moisture sensor is developed. It is 2 cm x 70 cm large, 2 mm thick, flexible, follows curved surfaces and is made for a life time longer than 20 years. Its measuring method is based on the determination of the dielectric coefficient (DK). The penetration depth of its measuring electromagnetic field can be adjusted to the material thickness of interest. It was proved in laboratory and test field measurements with an accuracy of ±5 % in the moisture range of 10 to 130 % without influence from neighboring materials. It can be used for desiccation warning. The sensor costs approximately $ 50 exclusive measuring device which can be multiplexed for several sensors. The sensor measures other thin sheet materials like fabrics, wood and plastics also.

KEY WORDS

Liner moisture, Moisture measurement, Liner moisture monitoring, Desiccation warning, GCL function control.

INTRODUCTION

Geosynthetic clay liners (GCLs) rely on bentonite with large intrinsic potential for shrinking and swelling. GCLs are widely used for moisture or gas isolation in civil engineering and landfill applications. The moisture content of the GCL determines its physical and chemical containment properties. A reliable and accurate moisture measuring method would provide confirmation of performance control during the construction and in the long-term function of sensitive sites. Manufacturers, suppliers, consulting engineers, plant operators and control authorities are deeply interested in the moisture dynamics under, in and over a GCL. Reliable and continuous quality control will promote the usage of GCLs

in new applications also (Richardson, 1997). Some GCLs will hold their long-term quality even when exposed to moisture that promotes ion exchange if a temporarily desiccation is avoided (Egloffstein, 1997). A common need is long-term and large area moisture monitoring where the GCL liner is interfaced between other materials. The long-term moisture measurement would provide possibility of an early warning in case of dangerous drying of the GCL.

Due to special problems that include the following:

volume expansion of the bentonite,
thin material sheet,
variable electric conductivity
non-plane surface,
aggressive environment,
different and closely attached neighboring materials,
long distance between sensor location and measuring device,
representative large area should be measured and
the need for a non-destructive long-term measurement

no suitable device was commercially available before.

After several years experience in soil moisture determination and development of three other soil moisture meters, the authors were able to develop a very simple, reliable and economic liner moisture measuring device, which in our opinion solves all the problems above.

Prior State Of The Art: Moisture Sensors

It is essential to distinguish between soil moisture measuring sensors for bulk materials, leakage detectors and liner moisture meters. Soil moisture sensors are designed to measure in large or bulk volumes. Their penetration depth are several centimeter or even some tenth of a meter. In most cases they are not suitable for thin layers like GCL liners. A good example for this bulk soil moisture sensors is the cryo-soil-moisture-sensor, LUMBRICUS.(Brandelik and Huebner, 1997). It measures the absolute water content in the field without any laboratory preparation. Its penetration depth is approximately 4 cm and is therefore too large in comparison to GCL liner thickness. Penetration depth using gamma ray absorption or neutron scattering is even greater. Electrical resistance blocks from porous gypsum can not be recommended for long-term operation because the resistance on the electrode surfaces changes unpredictably with time. In addition, they are small and fragile. The same problem occurs with sensors using the measurements of thermal conductivity. From a physical point of view, ultrasonic sensing would be suitable, but its applicator package (integrated transmitter and receiver) is still too big. Consequently, these soil moisture sensors are not suitable for GCL liner measurements.

Leakage detectors are developed to find leaks in plastic liners, especially when these liners are used to cover waste disposal sites. The largest group of them measures the electric conductivity or resistance through the liner. In case of a leak, the resistance drops from a very high level to a rather lower one. The position of a leak can be localized from many measurements on the periphery (Laine et al., 1997) or on grid like electrodes above and under the plastic liner. For this detection one has to suppose sufficient moisture at least on

one side of the liner. Another type of leakage detectors detects the diffusion of water in thin plastic tubes. The water travel time to the end of the tube gives the location of a leak.
Leakage detectors provide only an answer if there is any leak or not. They do not numerically measure the actual water content of the barrier. In most cases, plastic liners are used in combination with other sealing materials like clay liners or GCLs. It is not economical to repair a leak in the plastic liner if the other sheet is undamaged. Furthermore, for proper function of GCLs it is very important to sustain their optimal water content. Leak detectors can not verify this demand.

Liner moisture meters have to solve the specific problems listed in the introduction above. The small thickness and non plane position of GCLs often hindered the application of commercial available sensors.

There are reports on bench studies in which individually formed soil moisture sensors measured the GCL water content. One of the latest one was reported last year by Eberle and v. Maubeuge (1998). They inserted a 3-rod sensor probe in the middle of the GCL liner. This sensor measured the dielectric coefficient (DK) of the material between the rods by the use of the Time Domain Reflectometry (TDR).

The TDR technique is not a direct physical moisture measuring method as often called. The physical method is an indirect one where the DK of the moist material (e.g. soil as a mixture of solids, water and air) is measured and related to the water content. This method is very common and successful because of the great difference in the DKs of water (80), solids (3 to 8) and air (1). It is only a second order of interest how the DK is measured. It can be measured in the frequency or time domain. The measurement in the time domain is widely used in soil moisture determinations after Topp et al (1980) introduced it. The device is very handy and gives sufficient good results for common soils in common moisture ranges. Unfortunately, its general calibration is not adequate for clay, especially in high density and high moisture ranges. In this cases material specific moisture calibrations are needed. A further analysis of limitations of soil moisture determination using time and frequency domain measurements is reported by Brandelik and Huebner (1996).
However, the test bench of Eberle and v. Maubeuge (1998) represents the best prior attempt in GCL liner moisture determination. They use a sensor (3-rod) in combination with a TDR device which measures the travel time of an electric signal along the sensor rods. Its reading is converted into a dielectric coefficient DK of the GCL liner. Then the measured DK values were correlated to moisture contents based on a previous calibration. The problems and disadvantages of this solution are:

a. The measuring electric field is larger than the liner thickness. That means the materials above and under the liner will contribute to the measurement also. This disturbs the result.

b. It is complicated to place the 3-rod sensor in the middle of the thin GCL liner.

c. This sensor can only be a short one. In their case it is 6 cm long. It senses only a small surface which is not representative enough. The connection between the rods and transmission cable is a bulky one and disturbs the zone being measured.

d. Air gaps between sensor and material, in a drying phase during a longer monitoring time, lead to measurement errors and as a result that there is no chance for a sustainable calibration.

e. High density, highly saturated clay has a very high electrical loss, especially if salt water is in the material. This causes a very high electric signal attenuation along the sensor rods. The consequence is a significantly reduced electric signal which delivers inaccurate results.

f. The sensor and the measured material together determine the characteristic electric impedance of the measurement set-up. In order to get maximum sensitivity, this impedance has to be nearly the same as the characteristic impedance of the DK-measuring device, usually 50 Ohm. If ignored, the electric signal will be significantly reduced again, and the delivered moisture value will be inaccurate.

g. Up to now the hydraulic conductivity was regarded as function of **mean** water content and confining pressure in the GCL (Petrov et al., 1996). The authors do not have any information about cases where the water content gradient in the liner was the scope of investigations. GCLs are barriers to water which means that the moisture content on one side of the liner at proper operation is usually higher than that on the other. For adequate hydraulic conductivity at higher confining pressure, it may be sufficient to have a thinner fully hydrated zone while the remaining part of the GCL can be dryer. Consequently, it is not always sufficient to give the **mean** moisture content for the entire thickness. It is better to measure the water content and their changes from both liner sides.

THE NEW GCL LINER SENSOR

The authors have developed a soil moisture measuring system patent protected for water content determination in large areas (TAUPE). It consists of flexible, moisture sensitive radiofrequency flat band cables buried in the soil (Figure 1).
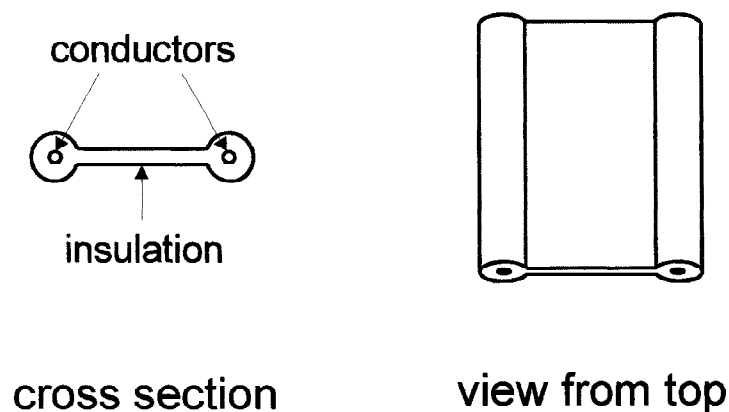
Figure 1. Design of the flat band cable

Redundant measurements of the complex signal propagation along the cable sections in time and frequency domains and the cross-talk between two cables provide the dielectric coefficient (DK) of the moist soil in an approximately. 10 cm neighborhood of the cables. Then the DK is converted to relative water content. In high density and high saturated clay, the cable length can be up to ~ 20 m. The cable is 6 cm wide and ~ 2 mm thick. It can detect 2% water content changes. After sufficient experiences on a 2000 m^2 dump site installation, (Brandelik and Huebner, 1998), the authors changed the design of the moisture sensitive cable for thin sheet measurements. The result is the liner sensor FORMI. It consists of a sensor and a DK measuring device. The sensor is again a moisture sensitive, flexible radiofrequency flat band cable. Its flexible metallic electrodes are embedded in LDPE isolation, which reduces the attenuation. Because of the proper thickness of the isolation it is possible to shield the measuring electric field on one side of the cable by a metallic foil (Figure 2).
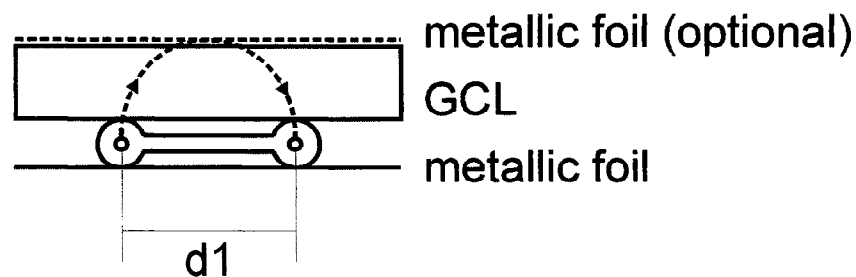
Figure 2. Liner measurement set-up

Now, the sensor is sensitive only one side which is faced to the GCL. By proper design of the electrode distance, d1, and the isolator thickness, one can adjust the expected set-up impedance to the optimal impedance range of the DK measuring device and to the GCL thickness. This way the measuring electric field is not deeper than the material sheet is thick. In case of uncertainty about material thickness (e.g. swelling), a second optional metallic foil can cover the measured GCL liner. If the sensor is to wide (due to the impedance adjustment), this second metallic foil can be perforated to enable the water transport to the GCL. d1 is approximately the measured material thickness. In a second step one selects the isolator thickness to a proper device impedance. The sensor is flexible. It lies **on the material** (not in it) and follows curved surfaces. The sensor doesn't disturb the material, doesn't provoke air gaps, its sensitivity and calibration remain constant. From these reasons it is suitable for long-term dessiccation warning also. A small pressure is sufficient to prevent an air gap between sensor and liner. All the failures caused by a sensor in the material are avoided. If we select the penetration depth of the measuring field smaller than the liner, only a part of the liner thickness will be measured. With a second sensor on the other liner side one can distinguish between the water content in the upper and lower parts of the liner. By continuous long time monitoring, one can directly determine the hydraulic conductivity from this measurement pair.

In order to reduce other disturbing electric fields, sensors are usually designed in a 3-line technique (e.g. 3-rod sensor) as shown in Figure 3.
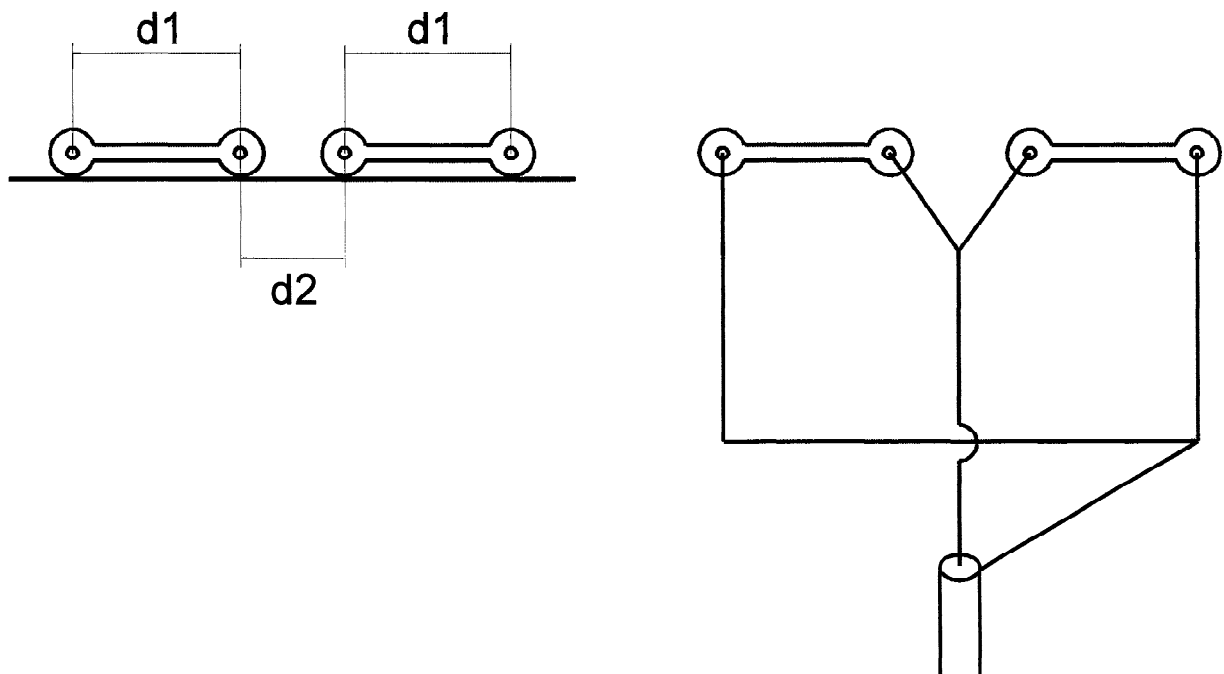
Figure 3. Three-line configuration from two line-pairs

The middle electrode is "hot" while the two outer ones are grounded. If the middle electrode is built from two neighboring electrodes of two parallel electrode pairs, the distance d2 gives a further possibility to adjust the system impedance in addition to the isolation thickness choice.

Of course, FORMI is a relative measuring device (in contrast to the soil moisture sensor LUMBRICUS). For absolute water content display it has to be calibrated by the help of gravimetric determination or by the soil moisture sensor LUMBRICUS.

The liner moisture sensor FORMI can be used for water content measurements of other non-metallic thin materials like textile, wood, foam and food also.

As the figure 3 shows, one can adjust the line with proper choice of the distance d2. In this case one can use commercial available flat band cable, too. The price of a sensor is approximately $ 50 where the price of the material itself is negligible. In time-domain measurements, we used the Metallic Cable Tester, Type 1502 from Tektronix. In order to reduce the future price of a DK measurement device, we measured in frequency-domain also. These measurements are carried out by the Vector Analyzer Type 8712C from Hewlett Packard.

LABORATORY TESTS

In our laboratory we measured the liners Bentofix produced by NAUE Fasertechnik, Germany and the RAWAMAT HDB Membrane by RAWELL Water Control Systems, England. We wetted a series of dry (ca. 8 % bound water content) GCL liners to produce an increasing water content. These samples were (6 x 70 cm) the same size as our sensor. This measuring surface provides a representative water content value. The sensor is ~ 2 mm thick and can be connected to the DK measuring device by a 20 m coaxial cable. Both TDR device and impedance analyzer were used. The shielding foil was a metallic tape. We measured in the water content range of 10 to 130 % with an accuracy of ±5 %.If the coaxial connecting cable is only 10 m long, the accuracy will be ±3 % as shown in Figure 4 where the radii of data circles correspond to the measurement uncertainty. This uncertainty is mostly due to the mechanical tolerances and to the uncertainty of the gravimetric calibration.

We could measure the moisture difference between the two sides of a GCL also. The liner was in this case approximately 8 mm thick (after swelling of the lowest sheet which was in a permanent contact with a water bath). The confinement pressure corresponded to a soil height of 1 m. After three week operation the water content difference became constant The water content on the lower side (to the water bath) was 94±5 % while it was 33±5 % on the upper side, (so called dry side). These measures correspond to material thickness' of approximately 3 mm.
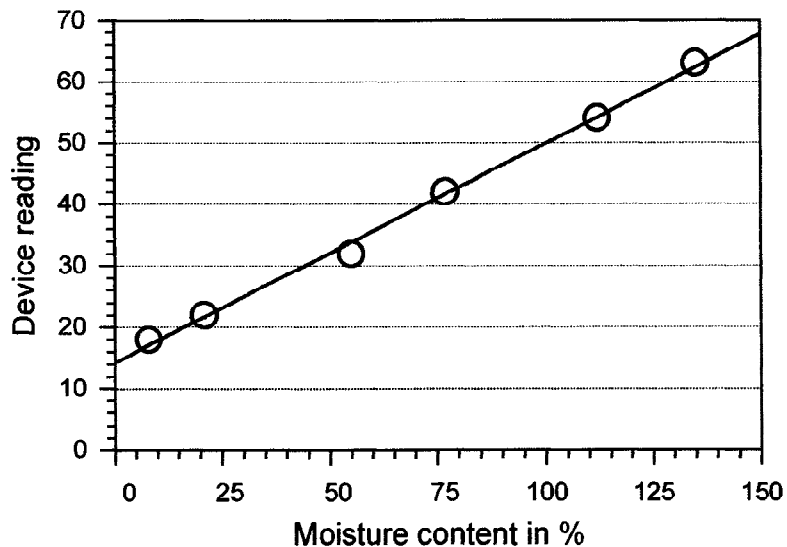
Figure 4. Set-up calibration

Figure 4 shows the device reading in relation to the gravimetrically determined water content. One can notice the very good linear character of the sensing. The GCL liners were about 6 to 10 mm thick. We changed the materials under and above the liner and sensor combinations. It was proved that the neighboring materials do not falsified the results even if the neighboring material was metallic.

FIELD TEST

Since spring 1996 we have cables buried in the field with the same material and sealing construction as FORMI. No degradation could be measured in the cable performance up to now. The cable is designed in our laboratory and produced by a firm with appropriate expertise for buried cables. So, we can expect, FORMI would be suitable for long-term monitoring as well.

NAUE Fasertechnik constructed six lysimeters in which several barrier designs will be tested. We already equipped these lysimeters with three sensors each. One FORMI under and a second one over the GCL liner. The third sensors (TAUPE) measure the vertical moisture distribution in a soil layer over the liners. The sensors are connected to an automaticaly multiplexed data acquisition. The measurements start in January 1999. In the 1999 conference we will be able to give results from this field project as well.

ACKNOWLEDGEMENTS

REFERENCES

Brandelik, A., and Huebner, C. (1996) „Distinguished Problems in Soil Aquametry" IEEE MTT-S Int. Microwave Symp., Workshop on Electromagnetic Wave Interaction with Water and Moist Substances. San Francisco, USA.

Brandelik, A. and Huebner C. (1997) „Long-term Monitoring of Clay-type Barrier Materials" Proc. Sardinia 97 Sixth Int. Landfill Symp Vol. III. pp. 85-91.

Brandelik, A. and Huebner, C. (1998) „Monitoring of Clay-type Surface Barrier on Dump Sites" Conf. Proc. Sixth Int. FZK/TNO Conference on Contaminated Soil, Edinburgh, UK. Vol. II. pp 1055-1056.

Eberle, M. A. and v. Maubeuge, K.P. (1998) „ Measuring the In-situ Moisture Content of Geosynthetic Clay Liners (GCLs) Using Time Domain Reflectometry (TDR)". Conference Proc. Sixth Int. Conference on Geosynthetics, Atlanta, USA, pp. 205-210.

Egloffstein, T. (1997) „Geosynthetic Clay Liners, Part Six: Ion Exchange", Geotechnical Fabrics Report. Vol. 15. No.5.

Laine, D.L., Binley, A.M. and Darilek, G.T. (1997) „How To Locate Liner Leaks Under Waste", Geotechnical Fabrics Report. Vol. 15. No.6.

Petrov, R.J., Rowe, R.K. and Quigley, R.M. (1996) „Selected Factors Influencing GCL Hydraulic Conductivity", Geotechnical Research Centre Report, GEOT-3-96. Geotechnical Res. Centre. Univ. of Western Ontario, Canada.

Richardson, G.N. (1997) „GCLs: Alternative Subtitle D Liner Systems", Geotechnical Fabrics Report. Vol. 15. No.4.

Topp, G.C., Davis, J.L., and Annan, A.P. (1980) „Electromagnetic Determination of Soil Water Content: Measurements in Coaxial Transmission Lines", Water Resources Research, Vol.16, No.3. pp 574-582.

NEEDLES IN NONWOVEN GEOTEXTILES – A LANDFILL CASE HISTORY

SCOTT PURDY, RG, CEG
VECTOR ENGINEERING, INC., USA
RAMIN YAZDANI, PE
YOLO COUNTY DEPARTMENT OF PUBLIC WORKS, USA

ABSTRACT

Engineers have been specifying geotextiles in liner systems for landfills for a number of years. While the physical properties of the geotextile are often addressed in great detail within the specifications, the engineer must also consider the manufacturing process when specifying a needle-punched, nonwoven geotextile. During the placement of the filter geotextile component of a landfill liner system in California, needles from the manufacturing process were discovered in the fabric. The potential effect of the needles on the integrity of the system was evaluated and procedures developed to determine the acceptability of the material. Following the successful completion of the project, language was developed for the specifications to minimize the potential for this problem in the future. The following paper describes the project in detail and provides the steps taken to obtain regulatory approval for the installation.

INTRODUCTION

Geotextiles have been an integral component of liner systems for landfills for a number of years. These products include woven and nonwoven fabrics composed of a variety of raw materials most typically polyester or polypropylene. In waste containment applications, nonwoven geotextiles are commonly utilized as a filter or a protective layer. While other manufacturing processes are available, mechanical needle punching is the standard process used to produce nonwoven geotextiles for landfill liner systems.

The engineer must consider the manufacturing process when specifying a needle-punched, nonwoven geotextile. As the geotextile is made, there is the potential for needles to break off and become embedded in the fabric. The specifications must require quality control procedures to be conducted at the manufacturing plant that reduce the potential of undetected needles in the geotextile. While all of the major producers of geotextiles conduct a high level of quality control, new or foreign manufacturers may not be as rigorous.

During the deployment of a composite liner system at the Yolo County Central Landfill near Davis, California, a large number of broken needles were found in the filter geotextile. Over the course of the project, testing was conducted to determine the effect of the needles on the integrity of the system. The evaluation included large scale hydrostatic puncture testing based on GRI Test Method GM3 and leakage rate calculations from potential punctures in the geomembrane. From this information, procedures were developed to inspect the on-site rolls of geotextile and determine the acceptability of the fabric. Following the successful completion of the project, language was developed for the specifications to minimize the potential for this problem to manifest itself in the future.

BACKGROUND

The Yolo County Central Landfill was opened in 1975 and has accepted over three million tons of nonhazardous solid wastes, construction debris, and nonhazardous liquid wastes. The site is designed as a Class III landfill in accordance with the California Code of Regulations, Title 27. Since opening, approximately 56.7 hectares (140 acres) of the 291 hectare (720 acre) site have been filled.

Landfilling activities at the Yolo County site presently involve the development of landfill cells using the area fill method. A composite liner system was designed by the County of Yolo for the Module B waste management unit (part of a 34.8 hectare [86 acre] expansion at the site). From bottom to top, the liner system was composed of the following components: 61cm (two feet) of clay with a hydraulic conductivity less than 1×10^{-7} cm/sec, a 1.5 mm high density polyethylene (HDPE) geomembrane, HDPE geonet, nonwoven, needle-punched geotextile, and 46 cm (1.5 feet) of protective cover soil. A detail of the liner system is shown in Figure 1.

Construction quality assurance (CQA) services were provided during construction of the liner system in accordance with the CQA Plan prepared by the County. The physical properties of the materials were tested in the field and laboratory to ensure conformance with the specifications. As the materials were placed, the contractor's work was observed and documented.

Since the liner system was being installed in late summer/early fall, high temperatures caused the HDPE geomembrane to wrinkle during the daylight hours. In order to avoid folding the liner and creating potential stress points, placement of the protective cover soil was conducted at night when cooler temperatures caused the liner to contract. Prior to placement of the protective cover soil over the geomembrane and geonet, a layer of 407 gm/m^2 (12 oz/yd^2) needle-punched, nonwoven filter/cushion geotextile was placed, overlapped, and sewn.

46 cm PROTECTIVE COVER

GEOTEXTILE

HDPE GEONET

1.5 mm HDPE GEOMEMBRANE

61 cm CLAY LINER
$K < 1 \times 10^{-7} cm/sec$

SUBGRADE
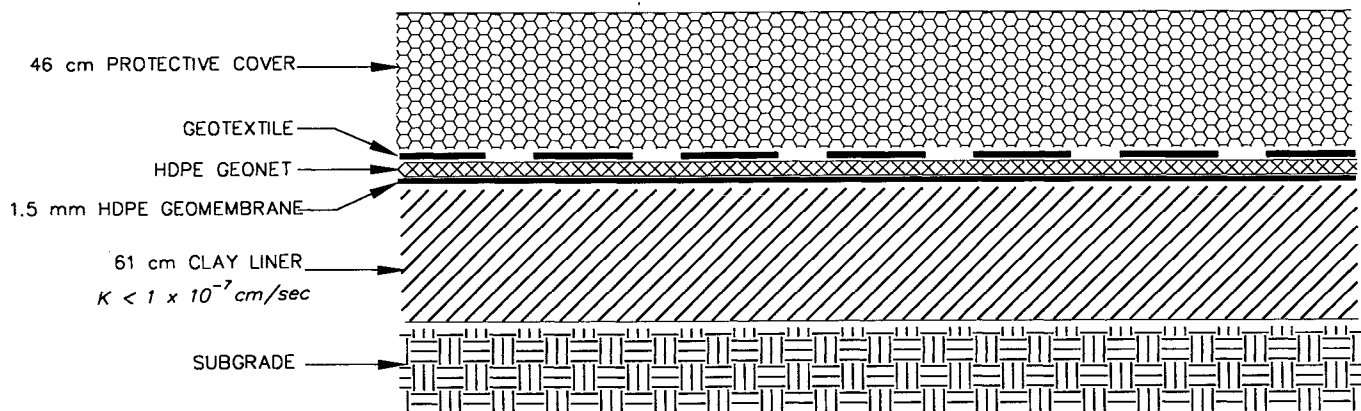
Figure 1. Detail of Liner System

PROBLEM

Since CQA personnel were monitoring the placement of the geotextile and protective soil materials at night, the identification of needles in the geotextile would be very difficult. Although they were not specifically looking for needles, CQA personnel monitoring the work being conducted in the daytime hours noticed broken needles in the geotextile at the edge of the protective cover soil. A more careful inspection of the immediate area resulted in finding broken needles and needle fragments in three additional areas.

A deficiency meeting was immediately held between the contractor, County, installer, and CQA firm. Two related problems were identified. First, approximately 3.2 hectares (8 acres) of the 8.1-hectare (20-acre) expansion area had already been covered with protective soil. Secondly, almost all of the remaining geotextile was already on-site with some of it deployed and ready to be covered with protective soil.

It was recognized that extensive evaluations would be necessary to determine the potential for damage to the geomembrane under the area already covered by protective soil. Of more immediate concern was what to do with the deployed but not covered geotextile and the rolls already on-site. As a result of the deficiency meeting, it was agreed that more rigorous inspection procedures would be implemented for the geotextile that had been previously deployed but not covered, and for geotextile yet to be deployed.

After the needles were identified, and in an attempt to determine the source of the needles, the CQA firm performed a plant visit to inspect the production facility and review the plant quality control program with respect to needles. The CQA Officer and County project manager attended the plant audit at the manufacturer's plant in Southern California.

During the audit, it was found that the production line used needling boards at two locations and that the needles from the plant matched those found in the field. Regarding quality control, the facility used a magnet over the geotextile to remove loose needles. The magnet was cleaned of needles every two days with about 200 needles typically recovered (100 needles per day). No inventory was taken to compare needles recovered with those lost from the boards. Furthermore, no metal detector was used in the production line to identify broken needles that bypass the magnet.

From this audit, it was concluded that the needles were most likely from the plant and that plant practices were insufficient to prevent needles from being incorporated into the geotextile in significant quantities.

INSPECTION OF EXPOSED GEOTEXTILE

Due to significant delays associated with obtaining new rolls of geotextile, procedures/criteria were quickly developed by the CQA firm to accept or reject the existing on-site materials. Different procedures were developed for rolls of geotextile that had not been deployed and rolls that had been deployed but not covered.

For the rolls of geotextile that had not been deployed, the inspection procedures were as follows:

1.   Six contractor personnel wearing cotton gloves standing shoulder to shoulder were utilized for the inspection of each roll.

2.   The personnel slowly unrolled the geotextile on a flat surface and visually and physically inspected the roll over its entire surface. Any needles found were marked and removed.

3.   Once the geotextile was unrolled, the six personnel knelt down and inspected the other side of the roll.

4.   After both sides of the geotextile were inspected, the roll was opened to expose the inner sides of the geotextile [each roll consisted of two rolls of geotextile factory seamed together, folded over, and re-rolled]. These two sides were also inspected.

5.   An approved metal detector was employed during the inspection process. The Contractor proposed the type of detector and the procedure to be used, which was approved by the Engineer.

6.   Any geotextile roll with four or more needles found was rejected and not used on the project. Rolls with three or less needles were used after the needles had been removed.

7. The CQA firm continuously monitored the inspection of the geotextile. A log was kept on each roll documenting the roll number, amount of needles found, and acceptance/rejection of the roll. No rolls were used on the project unless the CQA Monitor released them.

The geotextile that had already been deployed, but not covered with protective soil material was inspected as described below:

1. To enable adequate inspection, the sewn seam for each double roll of geotextile was cut and the thread removed. Six Contractor personnel inspected each half of the double roll by kneeling and visually and physically inspecting the geotextile.

2. After one side of one panel of the double roll had been approved, the material was folded over and the other side inspected.

3. After folding the material back, the geonet was inspected by kneeling and visually observing the geonet for the presence of needles. After the geonet was inspected and determined to be free of needles, the inspected geotextile was folded back on top of the geonet.

4. The opposite side of the double roll was then inspected. The geonet was also inspected as described above in No. 3.

5. A metal detector was used on the geotextile in addition to the manual inspection using the approved method.

6. If four or more needles were found, the roll was rejected and removed from the project. If three or less needles were found, they were marked and removed and the geotextile utilized for the project.

7. The CQA firm provided continuous monitoring of the inspection and kept a log of each roll. The rolls were not used unless kept by the CQA Monitor.

For rolls of geotextile that were already deployed, if only one side of the double roll was found to have excessive needles, it was removed and the other side utilized. For new rolls of geotextile, the entire double roll was rejected if four or more needles were found.

The above inspection procedures were performed on 111 panels (individual rolls of geotextile) and needles were identified in 74 of the 111 panels (67%). All identified needles were removed, and panels with more than four needles were rejected and removed. The total number of needles found averaged 59 needles per 0.4 hectare (1 acre). The attitude of the needles was randomly oriented and ranged from horizontal and sub-horizontal to vertical and sub-vertical.

Based on the rigorous inspection procedures developed for identifying and removing needles in the geotextile, rolls were later accepted for use at the site that contained more than four needles. This procedure was only allowed after the contractor demonstrated that all the needles could be removed with the inspection process.

In addition to collecting and removing the needles, Vector performed a size distribution analysis on 353 broken needles and needle fragments found. The results of this analysis are shown in Table 1.

Table 1. Needle Size Distribution

Size Range, cm (inch)	Occurrence, %
1.6 – 1.9 (5/8 – 3/4)	17
1.3 – 1.6 (1/2 - 5/8)	24
.95 – 1.3 (3/8 – 1/2)	17
.64 - .95 (1/4 – 3/8)	31
.32 - .64 (1/8 – 1/4)	10
< .32 (<1/8)	<1

Attempts to correlate panel location with needle occurrence were not successful. The needles seemed to occur randomly.

DISPOSITION OF COVERED GEOTEXTILE

Because of the pervasive frequency of needles throughout the exposed geotextile, the CQA firm concluded that the 3.2 hectares (8 acres) of covered geotextile also contained needles. It was assumed that the needles were at the same frequency as identified by the modified quality control procedures, or 59 needles per 0.4 hectare (1 acre).

Because the needles underlying the 3.2-hectare (8-acre) covered area in the western portion of the module could not be easily located and removed, the CQA firm was asked by the County to perform laboratory puncture testing and to qualitatively estimate the leakage threat posed by the needles. Laboratory puncture tests were performed at the CQA firm's geosynthetics laboratory. In order to obtain collaboration with the results, an additional independent geosynthetics laboratory conducted concurrent testing. The testing was performed in general conformance with GRI Test Method GM3.

The GRI Test Method GM3 places a geomembrane test specimen on the proposed installation materials within a high-pressure test vessel. Once the membrane and other materials are placed within the vessel, hydrostatic pressure is applied to an intended value, typically, to a pressure that simulates the anticipated field conditions. Pressures in the field are induced in two

modes; one mode is during construction by foot and equipment traffic and the second is during the operational life applied by the vertical loading on the liner from refuse and soil. Based on these anticipated field conditions, an ultimate pressure of 689.5 kilo Pascals (100 pounds per square inch) was used in the performance of the test.

The test apparatus consists of a two-piece pressure vessel. The inlet pressure is applied to the upper half connected to a regulated nitrogen tank and the bottom of the tank has a pressure relief outlet valve. Steel flanges that are welded to each section fasten the two halves to each other.

The lower unit of the pressure vessel was filled partially with free-draining pea gravel and the remaining portion was filled with the soil proposed for use as an operations layer at the site. The native protective soil consists of mostly sandy and silty clays with some gravel material. A layer of geotextile was placed between the operations material and the pea gravel to prevent cross contamination.

Once the soil was in-place, representative samples of the geotextile and the geonet were cut to fit the inside diameter of the pressure vessel. They were then taped together along the edges so that they would not move around during test assembly. Eleven broken needles, which were retrieved from geotextile materials at the site, were placed within the central portion of the test geotextile sample. Each needle location was noted with a white circle marked on the geotextile. These needles were oriented with their points essentially perpendicular to the HDPE liner which would be placed on top of these materials during the test. The geonet and geotextile were placed against the compacted operations material in a "floating" position (i.e. they were not fixed in-place by the flange of the vessel).

The geomembrane was then cut and holes drilled to fit the general configuration of the outside flanges of the pressure vessel. Neoprene rubber gaskets were placed along the flanges and the geomembrane was placed against the underlying materials. Once the materials were set, the upper section of the vessel was placed and bolted to the lower half. The lower (outlet) valve was kept open at all times during the test so that no buildup of pressure could occur below the test sample.

The upper section was then filled with water through the top portal valve. Once filled, the system was gradually pressurized at a prescribed rate of 70 kilo Pascals (10 psi) per minute to an initial target value of 414 kilo Pascals (60 psi). This pressure was held constant for a dwell time of approximately 48 hours. The test pressure was then increased at the rate indicated to a final value of 689.5 kilo Pascals (100 psi), at which time the test was completed. Once the test was started, the pressure was monitored periodically to ensure that the proper pressure was maintained. At the completion of the test, the condition of the geomembrane was noted.

As mentioned previously, each test was performed using two samples of the geotextile. In the first test, the geomembrane had been penetrated and partially damaged by seven of the

eleven needles placed in the geotextile. Two of these needles remained embedded in the liner and one of the needles had completely perforated the geomembrane. Similar conditions were noted on the second specimen with nine needles damaging the geomembrane and no needles embedded in the liner. However, four needles had perforated the geomembrane in the second sample. The independent testing firm's results were similar with five needles perforating the geomembrane in one sample and none in the other.

The results of the puncture testing demonstrated that the potential existed for broken needles present within the geotextile materials to penetrate and damage the liner materials. In order to simulate a worst-case orientation of the needles, they were placed vertically in the geotextile perpendicular to the HDPE liner. It should be noted that only a very small percentage of vertically oriented needles were detected at the site in the existing geotextile.

Following the above testing that demonstrated the potential for liner puncture, the County, CQA firm, and contractor developed a new testing program in conjunction with another independent consulting firm. The purpose of the new program was to more realistically assess the potential for leakage by mimicking the actual field conditions as closely as possible and increasing the testing database.

The new testing program included the following modifications:

1. **The number of tests performed was increased to include more needle fragment orientations.** The new puncture tests were performed with needle fragments oriented at 30, 45, 60, and 90 degrees from the horizontal. It was generally agreed that needles oriented less than 30 degrees from the horizontal would not pose a serious puncture risk. Tests were also conducted with bent needle fragments placed both vertically and horizontally with the points allowed to settle in place.

2. **The number of tests performed was increased to include two loading patterns.** Two loading mechanisms were identified which could cause punctures in the geomembrane. The first was the loading from a scraper running over the protective layer fully loaded. This was modeled by quickly loading the sample to 414 kilo Pascal (60 psi), unloading it, reloading it, and unloading it again. Each cycle took approximately three minutes. The second loading mechanism modeled the forces due to the final build-out of the landfill (up to 61 meters [200 feet]). The waste load for full build-out was 689.5 kilo Pascals (100 psi). Each loading type was performed on each needle fragment orientation and type.

3. **The protective soil layer was placed at 90 percent of the ASTM D-1557 maximum dry density within two percent of the optimum moisture.** Although there were no compaction requirements for the protective soil layer, this density was reasonable following scraper traffic and refuse loading.

4. **Needle fragment lengths met the distribution of fragments noted in Table 1.** This distribution was not available during the initial round of testing.

5. **Half of the fragments were placed with their points toward the geomembrane and half were placed with their points away from the geomembrane.** Due to the factory seaming of two rolls of geotextile together, there was no way to determine the direction of the needle fragments. Therefore, it was agreed that half of the fragments could be assumed to be in each direction.

6. **More needle fragments were used for each test.** To improve the statistical significance of the testing, more needle fragments than utilized in the first round of testing were used in each of the tests.

Based on the above criteria, a total of ten puncture tests were conducted using a total of 192 needle fragments. None of the tests with straight needle fragments showed any punctures or partial penetrations of the geomembrane. One of the tests using bent needles under a simulated scraper loading showed a penetration of the liner.

Based on the observed puncture, a leakage rate determination was conducted. A formula for calculating leakage rates through composite liners from a puncture in the geomembrane was developed by Giroud (1989).
That formula was:

$$Q = 0.21 \ h_w^{0.9} a^{0.1} k_s^{0.74}$$

where: Q = the leakage rate in cubic meters per day
h_w = the head on the liner in meters
a = the area of the hole in square meters
k_s = the hydraulic conductivity of the underlying clay in meters/sec

For this application, a leachate head of 0.003 m (per Giroud and Bonaparte, 1989) for geocomposite liners with geonet drainage layers was used. This assumes that the leachate collection and removal system was designed, constructed, and will be operated to minimize leachate head buildup. The diameter of the hole from the puncture testing was measured and the area was calculated to be 1.6×10^{-7} square meters. The hydraulic conductivity of the underlying compacted clay layer was determined to be 1×10^{-9} m/sec. Using these values in the above-noted formula resulted in a calculated leakage rate of 0.0045 liters (0.0012 gallons) per day per puncture.

Of the needle fragments found in the area of the landfill which had not been covered by the protective soil layer, 28 percent were bent. The additional testing indicated that 5 percent of the bent fragments could cause punctures of the geomembrane. Using these percentages on the

59-fragment/0.4 hectare (1-acre) value results in 0.8 punctures per 0.4 hectares (1-acre) or 6.5 punctures for the 3.2-hectare (8-acre) area.

Using this calculated potential puncture rate of 0.8 punctures per 0.4 hectares (1 acre) and the leakage rate of 0.0045 liters (0.0012 gallons) per day per puncture, an area leakage rate of 0.029 liters (0.008 gallons) per day was calculated. This translates to less than 11 liters (2.8 gallons) per year from the entire 3.2-hectare (8-acre) area.

Included in the leakage formula used is an inherent assumption that a puncture is a hole in the geomembrane and it will likely remain as such. If a needle fragment causes a puncture, the fragment will remain in the hole acting as a barrier to liquid until it is removed or rusts away. It could be removed by degradation caused by the leachate, but some metal fragments would remain. Factors such as tensile stresses induced by settlement of the foundation soils could elongate holes. However, soils, microorganisms and other suspended material within the leachate would tend to settle in low spots on the geomembrane and plug small holes. Under the pressure of increased loading and elongation from increased temperature in the presence of leachate, the HDPE geomembrane could expand laterally a small amount and act to either seal or elongate a hole.

CONCLUSIONS

Based on the extensive puncture testing conducted on samples of the geotextile containing needle fragments, it was determined that the potential exists for needles present in a geotextile to puncture an underlying geomembrane. While the leakage rate through the punctures will be minimal, it does represent an increase over and above the standard leakage rate from a 1-cm diameter hole that would be expected from a well-constructed composite liner system (U.S. EPA 1987, 1992). High groundwater levels (within 1.5 meters [5 feet] of the ground surface) at the Yolo County site also required any leakage to be seriously considered.

After evaluating the amount of potential leachate that could be generated along with other site specific factors at the landfill, it was determined that the composite liner system in-place would adequately protect the waters of the State. This information was presented to the regulatory agencies and the facility was permitted to accept refuse.

For subsequent phases of construction at the Yolo County Central Landfill, the specifications were amended to specifically address the potential for needles in the geotextile. Included in the amended specifications was the following: "Prior to delivery, submit to the Engineer and CQA Monitor a letter of certification from the geotextile supplier stating that the geotextile products are in conformance with the requirements of these Specifications. The manufacturer shall provide documentation stating that the plant quality control includes magnets and continuous metal detectors to detect manufacturing needle fragments, and shall certify that the geotextile provided is "needle-free". Also included in the specifications was a statement that

the geotextile shall be free of foreign objects or debris, including manufacturing needle fragments.

It should be noted that all major manufacturers of geotextile in the United States currently follow rigorous quality control procedures that include both magnets and metal detectors. However, by using the above specification language and conducting a plant audit of manufacturers, the engineer can minimize the potential for needles in the geotextile component of liner systems.

REFERENCES

Giroud J.P., and Bonaparte, R. (1989) "Leakage Through Liners Constructed with Geomembranes – Part I. Geomembrane Liners." Geotextiles and Geomembranes, Vol. 8, No. 1, pp. 27-67.

U.S. EPA (1987) Background Document on Proposed Leak Detection Rule, IPA/530-SW-87-015, Washington, DC.

U.S. EPA (1992) Action Leakage Rates for Leak Detection Systems Supplemental Background Document for the Final Double Liners and Leak Detection Systems Rule for Hazardous Waste Landfills, Waste Piles, and Surface Impoundments." EPA/530-R-92-004, Washington, DC.

SIMPLIFIED DESIGN CHARTS FOR GEOMEMBRANE CUSHIONS

STEPHEN N. VALERO, P.E. – SYNTHETIC INDUSTRIES, INC. (USA)
DERON N. AUSTIN, P.E. – SYNTHETIC INDUSTRIES, INC. (USA)

ABSTRACT

Recent and ongoing research indicates that use of a properly selected nonwoven, needle-punched geotextile cushion adjacent to (above and/or below) a geomembrane can effectively protect it from construction and operational damage. The current practice selects an appropriate geotextile cushion using the Geosynthetic Research Institute (GRI) method (Koerner, et. al. 1996). This method was used to develop simplified design charts allowing quick, conservative selection of an appropriate geotextile cushion. Charts are provided for typical applications including solid waste landfills and liquid impoundments with varying load, subgrade and cover/subgrade soil conditions. In addition, a brief discussion of the design procedure is provided with completed numerical examples.

INTRODUCTION

Most solid and hazardous waste landfills, lagoons and reservoirs built today incorporate geomembranes to contain liquids. Although these low permeability liners have demonstrated excellent performance, they are susceptible to damage when drainage stone or alternate drainage media (such as shredded tires, crushed glass, etc.) are placed over them (Figure 1). In addition, geomembranes are prone to damage from isolated protrusions present in the subgrade onto which they are deployed.

Figure 1. Stone Placement over a Geomembrane

Figure 2 illustrates the typical components of modern landfill liner system and Figure 3 represents a typical liquid impoundment liner system. Of these components, the geomembrane is the most prone to

damage. Protecting the geomembrane from tearing or puncturing during construction and operation is critical. Recent and ongoing research indicates that deployment of a properly selected nonwoven, needle-punched geotextile cushion adjacent to (above and/or below) a geomembrane provides effective protection against damage.
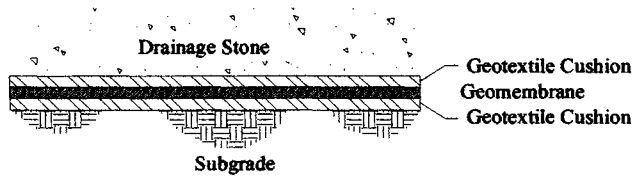
Figure 2. Typical Municipal Landfill Liner System
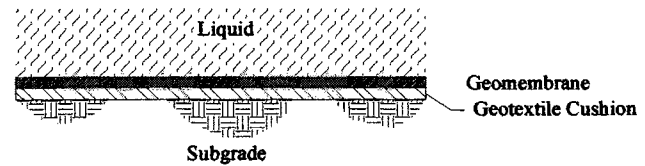
Figure 3. Typical Liquid Impoundment Liner System

STATE OF GEOMEMBRANE CUSHION DESIGN PRACTICE

State of geomembrane cushion design practice suggests using the generalized procedure developed by Koerner, et. al (1996) at the Geosynthetic Research Institute (GRI). The GRI method couples theoretical (Wilson-Fahmy, et. al., 1996) and empirical (Narejo, et. al., 1996) puncture protection analysis through use of a global factor of safety. The method directly applies to 1.5 mm (60 mil), smooth, high density polyethylene (HDPE) geomembranes protected by virgin polymer, nonwoven, needle-punched geotextiles. However, early work by Hullings and Koerner (1991) and field research by Richardson and Johnson (1998) indicate that the method may be conservative for geomembranes manufactured from more flexible polymers. Koerner, et. al. (1996) also suggest that the GRI method may be extended to other types of cushion materials.

The governing equation (Equation 1) incorporates several simplifying assumptions. For extrapolation to field design, (at least partially) subjective modification/reduction factors are required. In addition, laboratory testing used to develop the model did not incorporate dynamic loading. Therefore, the GRI method is considered adequate in cases where uniform, normal, static loading controls the design (i.e. moderate to high waste fills and most liquid impoundments) and may be under-conservative in cases where construction (dynamic) loading controls (i.e. shallow waste fills, poor construction practices, etc.). Based on field evaluation of geosynthetic cushions under construction loading, Richardson (1996) recommends modification of the GRI method such that the minimum nonwoven geotextile cushion mass selected is 405 g/m^2 (12 oz/yd^2) for 2.5 cm (1 in) maximum gravel over smooth HDPE geomembranes. This recommendation was later extended to 1.3 cm (0.5 in) gravel through additional field testing (Richardson and Johnson, 1998). Reddy et. al. (1996) performed similar field evaluations and concluded that a lighter 270 g/m^2 (8 oz/yd^2) geotextile is capable of providing adequate protection against construction loading. Based on laboratory testing, Reddy and Saichek (1998) also concluded that a 270 g/m^2 (8 oz/yd^2) may provide acceptable long-term protection under specific conditions.

Although a comprehensive review of previous research is beyond the scope of this paper, the reader is encouraged to read and understand the referenced literature prior to application or modification of the GRI method. This methodology (that forms the basis for the simplified design charts presented later in this paper) is summarized in the following steps.

Step 1:   Estimate the Allowable Pressure on the Geomembrane (in terms of M_A)

$$P'_{allow} = \left(450 \cdot \frac{M_A}{H^2}\right)\left(\frac{1}{MF_S \cdot MF_{PC} \cdot MF_A}\right)\left(\frac{1}{FS_{CR} \cdot FS_{CBD}}\right)$$ (Equation 1)

Where:

P'_{allow} = Allowable pressure on geomembrane (kPa)
450   = Empirical constant (kPa·mm^2/(g/m^2))
M_A = Required mass per unit area of nonwoven, needle-punched geotextile (g/m^2)
H   = Effective height of protrusion (mm)
MF_S = Modification factor for protrusion shape (dimensionless)
MF_{PC} = Modification factor for protrusion configuration (dimensionless)
MF_A = Modification factor for overburden arching effect (dimensionless)
FS_{CR} = Factor of safety for geotextile creep (dimensionless)
FS_{CBD} = Factor of safety for geotextile chemical/biological degradation (dimensionless)

Equation 1 should be solved in terms of M_A. The effective height of protrusion (H) represents the maximum height of any object in contact with the geomembrane extends relative to the overlying/underlying media. In cases where protection is sought from uniformly packed stones (such as landfill leachate collection/drainage media), H may be estimated as one-half the maximum particle diameter of the stones. However, when protection is sought from isolated protrusions (such as stones encountered in a hastily prepared subgrade), H may be estimated as the maximum particle diameter of the protrusions. In the later case, the value of H may be based on observed conditions, or specified by restricting the largest particle size allowed to remain on the prepared subgrade during geosynthetic deployment. Modification Factors for protrusion shape, protrusion configuration, and overburden arching effect may be selected based on guidelines presented by Narejo, et. al (1996):

Table 1. Recommended Modification Factor for Protrusion Shape
(Adapted from Narejo, et. al., 1996, page 647)

Protrusion Shape	Modification Factor, MF_S
Angular	1.00
Subrounded	0.50
Rounded	0.25

Table 2. Recommended Modification Factor for Protrusion Configuration
(Adapted from Narejo, et. al., 1996, page 647)

Protrusion Configuration	Modification Factor, MF_{PC}
Isolated Protrusions	1.00
Uniformly Packed Surface	0.50

Table 3. Recommended Modification Factor for Overburden Arching Effect
(Adapted from Narejo, et. al., 1996, page 648)

Anticipated Arching Effect	Modification Factor, MF_A
None (i.e. Liquid Overburden)	1.00
Moderate	0.50
Maximum	0.25

Through limited creep testing, Narejo, et. al. (1996) indicated that geotextile cushion creep is primarily a function of H and M_A. Since M_A is unknown at this point, Equation 1 may be solved by assuming a reasonable value for FS_{CR} based on the anticipated M_A required. Following completion of the required calculations, the assumed value of FS_{CR} must be checked for validity. Table 4 provides recommended FS_{CR} values in the form of unique linear equations for several commonly available nonwoven, needle-punched geotextiles. It is interesting to note that the recommended upper limit with respect to H, is in general agreement (probably by coincidence) with construction limits established by Richardson (1996) and Reddy and Saichek (1996). The equations for FS_{CR} and their range of validity were interpolated/extrapolated from available geotextile cushion creep test data (Narejo, et. al., 1996).

Table 4. Factor of Safety for Geotextile Creep
(Adapted from Narejo, et. al., 1996, page 644 - 648)

Nonwoven, Needle-punched Geotextile Mass per Unit Area	Factor of Safety, FS_{CR}
270 g/m^2 (N/R for H > 12 mm)	$\geq 0.0417 \cdot H + 1.25$
405 g/m^2 (N/R for H > 19 mm)	$\geq 0.0292 \cdot H + 1.18$
540 g/m^2 (N/R for H > 25 mm)	$\geq 0.0166 \cdot H + 1.11$
675 g/m^2 (N/R for H > 29 mm)	$\geq 0.0139 \cdot H + 1.08$
745 g/m^2 (N/R for H > 31 mm)	$\geq 0.0129 \cdot H + 1.07$
810 g/m^2 (N/R for H > 32 mm)	$\geq 0.0119 \cdot H + 1.06$
945 g/m^2 (N/R for H > 35 mm)	$\geq 0.0100 \cdot H + 1.03$
1015 g/m^2 (N/R for H > 36 mm)	$\geq 0.0089 \cdot H + 1.02$
1080 g/m^2 (N/R for H > 38 mm)	$\geq 0.0080 \cdot H + 1.00$

NOTE: N/R = Not recommended

The factor of safety for chemical and biological degradation (FS_{CBD}) should be selected based on the aggressiveness of the anticipated chemical environment and the geotextile polymer composition. Table 5 provides general recommendations:

Table 5. Recommended Factor of Safety for Chemical and Biological Degradation
(based on Koerner, 1994, page 151 and Synthetic Industries, 1997)

Chemical Environment	Factor of Safety for Chem/Bio Degradation, FS_{CBD}	
	Polyester (PET) Geotextiles	Polypropylene (PP) Geotextiles
Normal (i.e. 3 < pH < 10)	1.0	1.0
Aggressive (pH <3 or pH > 10)	1.5 – 2.0	1.0 – 1.5

Step 2:   Estimate the Anticipated Pressure on the Geomembrane

$$P_{actual} = \gamma \cdot h$$ (Equation 2)

Where:

γ = Unit weight of overburden material or liquid (kN/m^3)
h   = Design height of overburden material or liquid depth (m)
P_{actual} = Estimated maximum pressure on geomembrane (kPa)

The parameters required to complete Equation 2 may be assumed or specified based on site specific considerations. The unit weight of typical municipal solid waste may be estimated to equal 12.56 kN/m^3 (80 lb/ft^3) in the absence of site specific data. Likewise, the unit weight of most liquids can be approximated by the unit weight of water, 9.81 kN/m^3 (62.4 lb/ft^3).

In some cases (i.e. shallow waste fills, poor construction practices, etc.), the dynamic forces associated with construction loading may exceed those associated with long-term static loading. The exact point at which this occurs is dependent on multiple variables and difficult (if not impossible) to estimate. Therefore, caution should be exercised in selection of a geotextile cushion having a mass per unit area less than 405 g/m^2 (12 oz/yd^2), the construction limit recommended by Richardson and Johnson (1998).

Step 3:   Calculate the Required Mass per Unit Area of the Cushion Geotextile

$$P'_{allow} \geq FS_{g\,min} \cdot P_{actual}$$ (Equation 3)

Where:

P'_{allow} = Allowable pressure on geomembrane in terms of M_A (Equation 1)
FS_{gmin} = Global Factor of Safety (dimensionless)

Equation 3 may be solved for M_A through substitution (Equation 1 and 2 results) and algebraic manipulation. The global factor of safety (FS_{gmin}) should be selected based on the protrusion configuration and H. Recommendations are provided in Table 6.

Table 6. Recommended Global Factor of Safety
(Adapted from Koerner, et. al., 1996, page 648)

Protrusion Configuration	Global Factor of Safety, FS_{gmin}
Isolated Protrusions	$= 0.22 \cdot H + 1.77$ (≥ 3.0)
Uniformly Packed Surface	3.0

Step 4:   Select Appropriate Geotextile Cushion

Select a nonwoven, needle-punched geotextile having a minimum average roll value (MARV) M_A greater than or equal to that calculated in Step 3. It should be noted that the method presented herein is based on limited testing (Narejo, et. al, 1996) using virgin polymer, nonwoven, needle-punched geotextile and may not apply to all types of geotextiles and cushion materials.

Step 5:   Check Assumed Value of FS_{CR} and Construction Limits

In Step 1, FS_{CR} was assumed to allow solution of Equation 1. Check Table 4 to ensure that the assumed value is valid for the geotextile selected in Step 4 (If not, revise FS_{CR} and repeat Steps 1 through 4).

In cases where solid material (i.e. rock, solid waste, etc.) will be placed on top of the geomembrane with heavy equipment, construction loading must be considered. Based on field experimentation, the minimum M_A geotextile should be between 270 g/m^2 (8 oz/yd^2) (Reddy, et. al., 1996) and 405 g/m^2 (12 oz/yd^2) (Richardson and Johnson, 1998) to prevent construction damage. The reader should review and understand both documents prior to selecting a geotextile having M_A less than 405 g/m^2.

SIMPLIFIED GEOMEMBRANE CUSHION SELECTION CHARTS

A series of simplified design charts have been developed for the most common geomembrane cushioning applications based on the methodology presented. These charts allow the user to quickly and conservatively select an appropriate virgin polymer, nonwoven, needle-punched geotextile cushion. The applicability and assumptions associated with these charts are provided in the notes section of each figure. In addition, the reader is encouraged to review and understand the limitations of the GRI method (discussed in the referenced literature) prior to application the charts on the following pages. Figures 4 through 7 present charts for landfill applications while Figures 8 and 9 relate to liquid impoundment applications.

Y-axis: Maximum Landfill Height (m)

X-axis: Maximum Overlying Stone Diameter (mm)

NOTES:
1. Charts are applicable for selection of polypropylene, nonwoven, needle-punched geomembrane cushion geotextiles.
2. Assumed unit weight of waste = 12.56 kN/m^3
3. Assumes no significant subgrade protrusions & uniformly packed overlying stones.
4. Assumes moderate arching effect in overburden material.
5. Global Factor of Safety = 3.0, Creep Factors of Safety interpolated from Narejo, et. al. (1996)
6. Assumes that long-term loading controls the design.

270 g/m^2 - Note: May not be adequate to protect against construction damage (See Reddy, et. al., 1996; Richardson and Johnson, 1998)

Contact Geotextile Manufacturer

405 g/m^2

540 g/m^2

675 g/m^2

745 g/m^2

810 g/m^2

945 g/m^2

1015 g/m^2

1080 g/m^2

Figure 4. Geomembrane Cushion Selection Chart - Landfill Application, Rounded Overlying Stones (SI Units)
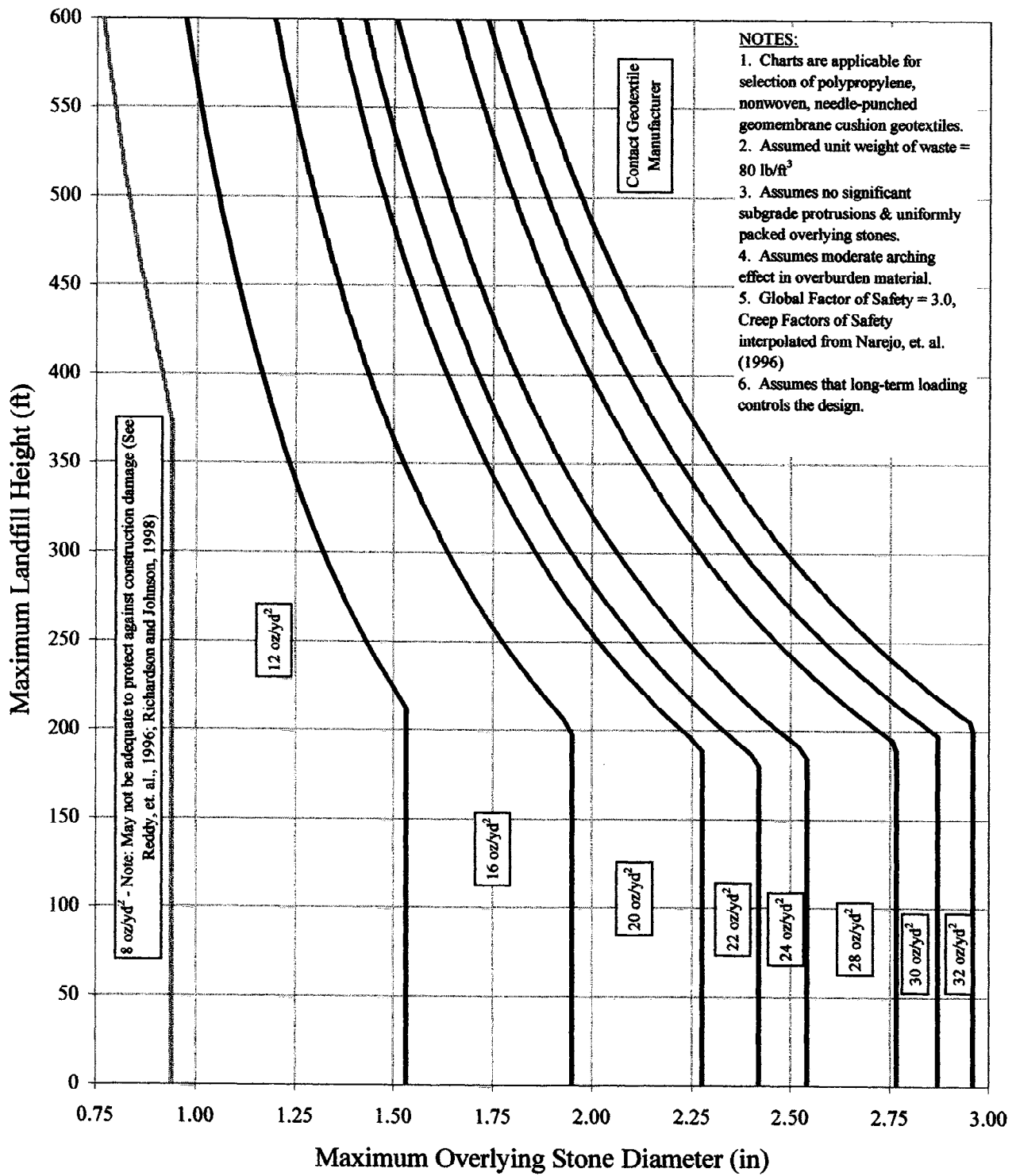
Figure 5. Geomembrane Cushion Selection Chart - Landfill Application,
Rounded Overlying Stones (US Units)

NOTES:
1. Charts are applicable for selection of polypropylene, nonwoven, needle-punched geomembrane cushion geotextiles.
2. Assumed unit weight of waste = 12.56 kN/m³
3. Assumes no significant subgrade protrusions & uniformly packed overlying stones.
4. Assumes moderate arching effect in overburden material.
5. Global Factor of Safety = 3.0, Creep Factors of Safety interpolated from Narejo, et. al. (1996)
6. Assumes that long-term loading controls the design.

Figure 6. Geomembrane Cushion Selection Chart - Landfill Application,
Angular Overlying Stones (SI Units)

NOTES:
1. Charts are applicable for selection of polypropylene, nonwoven, needle-punched geomembrane cushion geotextiles.
2. Assumed unit weight of waste = 80 lb/ft³
3. Assumes no significant subgrade protrusions & uniformly packed overlying stones.
4. Assumes moderate arching effect in overburden material.
5. Global Factor of Safety = 3.0, Creep Factors of Safety interpolated from Narejo, et. al. (1996)
6. Assumes that long-term loading controls the design.

Figure 7. Geomembrane Cushion Selection Chart - Landfill Application,
Angular Overlying Stones (US Units)

NOTES:
1. Charts are applicable for selection of nonwoven, needle-punched geomembrane cushion geotextiles.
2. Assumed unit weight of liquid overburden = 9.81 kN/m^3
3. Assumes isolated, subangular subgrade protrusions.
4. Global Factor of Safety = f(subgrade stone diameter) after Koerner, et. al. (1996), Creep Factors of Safety interpolated from Narejo, et. al. (1996).

Figure 8. Geomembrane Cushion Selection Chart - Liquid Impoundment
Application, Subangular Subgrade Stones (SI Units)

NOTES:
1. Charts are applicable for selection of nonwoven, needle-punched geomembrane cushion geotextiles.
2. Assumed unit weight of liquid overburden = 62.4 lb/ft^3
3. Assumes isolated, subangular subgrade protrusions.
4. Global Factor of Safety = f(subgrade stone diameter) after Koerner, et. al. (1996), Creep Factors of Safety interpolated from Narejo, et. al. (1996).
5. Assumed that long-term loading controls the design.

Figure 9. Geomembrane Cushion Selection Chart - Liquid Impoundment Application, Subangular Subgrade Stones (US Units)

EXAMPLES

The following simple design examples illustrate application of the charts and GRI method to three common geomembrane cushion applications. Examples 1 and 2 illustrate selection of a geotextile cushion using Figures 4 through 9. Example 3 depicts selection of a geotextile cushion for conditions other than those represented by the charts.

Example 1: Municipal Landfill Liner Cushion

A municipal solid waste (MSW) landfill cell is to be constructed over a carefully prepared subgrade (no significant isolated protrusions). The leachate collection media (to be placed above the geomembrane) is angular crushed stone with a maximum diameter of 38 mm (1.5 in). The maximum design height of the cell is 80 m (262.5 ft). Select an appropriate geotextile to protect the geomembrane.

Solution 1:

Using the design charts in Figures 4 or 5 select a needle-punched, nonwoven, polypropylene geotextile having a MARV M_A of at least 540 g/m^2 (16 oz/yd^2).

Example 2: Liquid Impoundment Liner Cushion

A liquid impoundment is to be constructed over a subgrade containing isolated, angular stone protrusions. The impoundment is to be lined with a geomembrane underlain by a 540 g/m^2 (16.0 oz/yd^2) needle-punched, nonwoven, polypropylene geotextile for protection against the subgrade stones. No stone or other solid material will be placed on the geomembrane. Therefore, construction loading is not a concern. It is anticipated that the maximum li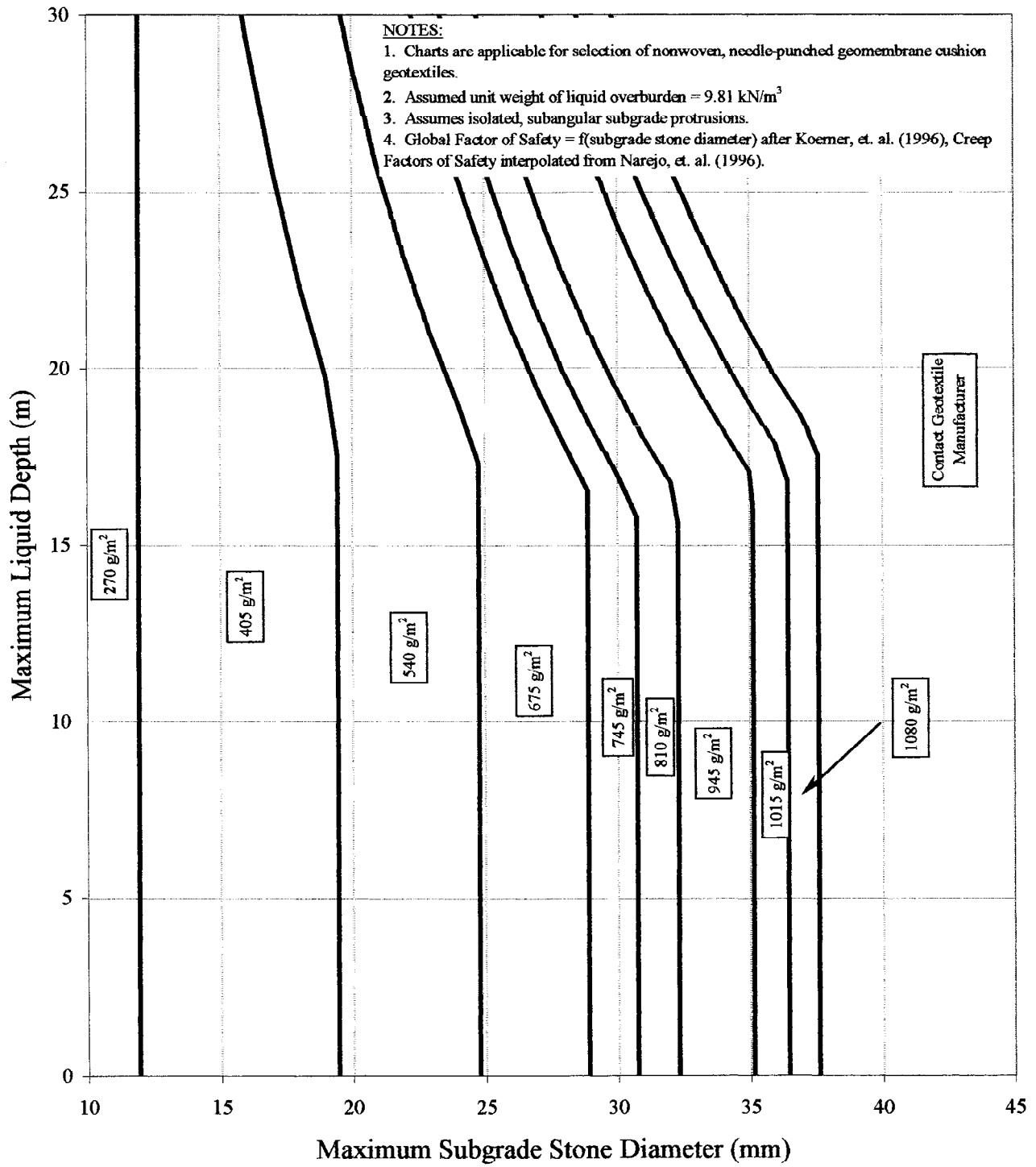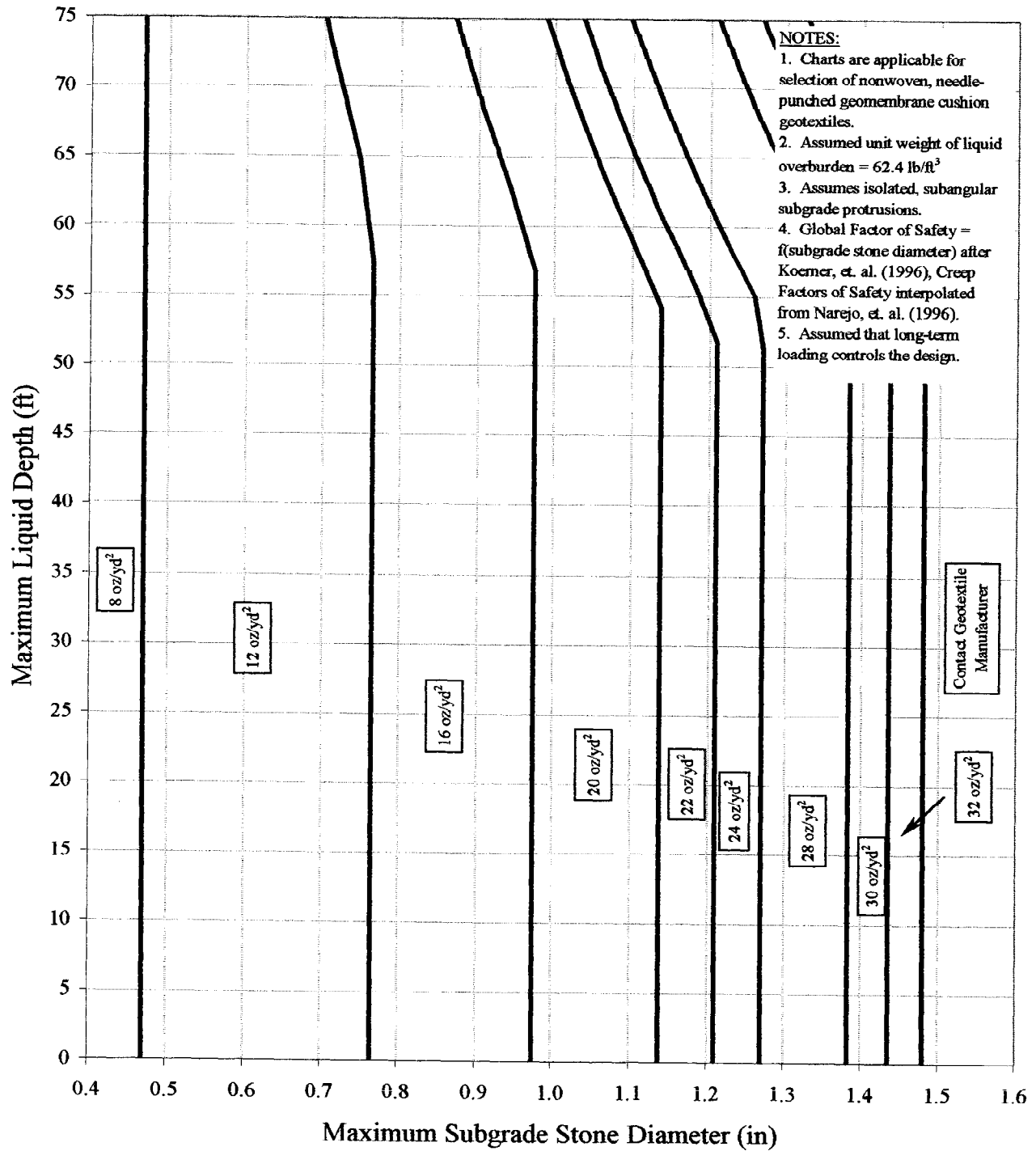quid depth will be 20 m (65.6 ft). For specification purposes, determine the largest stone which may safely remain on the subgrade without damaging the geomembrane.

Solution 2:

Based on the design charts in Figures 8 or 9, stones larger than 23 mm (0.9 in) in diameter might damage the geomembrane. Thus, the construction specification could be written to require removal of all protruding subgrade stones larger than approximately 25 mm (1 in).

Example 3: Industrial Landfill Liner Cushion

A portion of the cell described in Example 1 is to be used as a monofill for automobile shredder fluff (average unit weight equal to 10.2 kN/m^3 (65 lb/ft^3)). This portion of the cell is design to be filled to a height of 25 m (82 ft). In addition, a finer 25 mm (1 in) angular, crushed stone will be used for leachate collection media. Assuming all other liner components (except the cushion) remain unchanged, select an appropriate geotextile to protect the geomembrane.

<u>Solution 3:</u>

The design charts are not applicable to this problem since $\gamma \neq 12.6$ kN/m^3 (80 lb/ft^3). In addition, construction loading may control geotextile selection given the relatively shallow fill height and low unit weight of waste. Consequently, the problem must be solved by equation.

A.   Determine P'$_{allow}$ in terms of M$_A$, where:

H   = ½ of maximum overlying particle diameter = 12.5 mm
MF$_S$ = 1.0 (Table 1 - angular stone)
MF$_{PD}$ = 0.5 (Table 2 - uniformly packed surface)
MF$_A$ = 0.75 (Table 3 - moderate arching of waste materials)
FS$_{CR}$ = 1.6 (assumed, corresponds to 270 g/m^2 - to be checked against Table 4)
FS$_{CBD}$ = 1.2 (Table 5 - polypropylene geotextile in waste application)

$$P'_{allow} = \left(450 \cdot \frac{M_A}{12.5^2}\right)\left(\frac{1}{1.0 \cdot 0.5 \cdot 0.75}\right)\left(\frac{1}{1.6 \cdot 1.2}\right) = 4.0 \cdot M_A$$

B.   Determine anticipated pressure on geomembrane, where:

γ = 10.2 kN/m^3 (given)
h   = 25 m (given)

$$P_{actual} = 10.2 \cdot 25 = 255 \cdot kPa \quad \text{(Equation 2)}$$

C.   Solve for minimum geotextile M$_A$ through manipulation of Equation 3, where:

FS$_{gmin}$ = 3.0 (Table 6 – uniform packed stones, no isolated subgrade protrusions)
P'$_{allow}$ = 4.0· M$_A$ (Equation 1)

$$4.0 \cdot M_A \geq 3.0 \cdot 255 \quad \text{(Equation 3)} \qquad \text{or:} \quad M_A \geq \frac{3.0 \cdot 255}{4.0}$$

Thus, M$_A$ ≥ 191.3 g/m^2 (5.7 oz/yd^2)

D.   Check result against Creep limits established in Table 4 and Construction Limits:

From Table 4, the minimum acceptable M$_A$ = 405 g/m^2 (12 oz/yd^2). Coincidentally, this agrees with the construction limits recommended by Richardson and Johnson (1998). Thus, select a nonwoven, needle-punched geotextile having a MARV M$_A$ of at least 405 g/m^2. Although, FS$_{CR}$ was selected based on a 270 g/m^2 (8 oz/yd^2) geotextile, the problem need not be reevaluated in this case since a 405 g/m^2 (12 oz/yd^2) geotextile is the minimum acceptable material based on creep limits (Table 4).

SUMMARY AND APPLICABILITY

The design charts and methodology provided herein are intended to provide a quick and conservative method to select an appropriate geomembrane cushion. Prior to applying the design charts or method, the reader should review and understand the limitations and assumptions discussed in the referenced literature. In circumstances where site specific conditions deviate significantly from the research forming the basis for the charts and GRI method, it is recommended that a project specific testing program be conducted and evaluated by a qualified professional. Geosynthetic materials, testing parameters, etc. should be modeled after anticipated field conditions.

REFERENCES

Hullings, D. and Koerner, R.M., 1991, "Puncture Resistance of Geomembranes Using a Truncated Cone Test", Geosynthetics '91 Conference Proceedings, IFAI: Roseville, MN, pp. 273-285.

Koerner, R.M., 1994, "Designing with Geosynthetics", 3rd ed., Prentice-Hall, Inc.: Englewood Cliffs, New Jersey.

Koerner, R.M., Wilson-Fahmy, R.F. and Narejo, D., 1996, "Puncture Protection of Geomembranes Part III: Examples", Geosynthetics International, vol. 3, no. 5, pp. 655-675.

Narejo, D., Koerner, R.M. and Wilson-Fahmy, R.F., 1996, "Puncture Protection of Geomembranes Part II: Experimental", Geosynthetics International, vol. 3, no. 5, pp. 629-653.

Reddy, K.R. and Saichek, R.E., 1998, "Performance of Protective Cover Systems for Landfill Geomembrane Liners Under Long-Term MSW Loading", Geosynthetics International, vol. 5, no. 3, pp. 287-307.

Reddy, K.R., Bandi, S.R., Rohr, J.J., Finy, M., and Siebken, J., 1996, "Field Evaluation of Protective Covers for Landfill Geomembrane Liners Under Construction Loading", Geosynthetics International, vol. 3, no. 6, pp. 679-700.

Richardson, G.N. and Johnson, S., 1998, "Field Evaluation of Geosynthetic Protective Cushions: Phase 2", Geotechnical Fabrics Report, vol. 16, no. 8, Oct.-Nov., pp. 44-49.

Richardson, G.N., 1996, "Field Evaluation of Geosynthetic Protection Cushions", Geotechnical Fabrics Report, vol. 14, no. 2, Mar., pp. 20-25.

Synthetic Industries, 1997, "The Durability of Polypropylene – Nonwoven Geotextiles for Waste Containment Applications - SMART SOLUTIONS® Technical Note, SM-404", Synthetic Industries, Chattanooga, Tennessee.

Synthetic Industries, 1998, "Design and Selection of GEOTEX® Ultra Heavy Weight Nonwoven Geotextiles for Geomembrane Cushioning - SMART SOLUTIONS® Technical Note, SM-116", Synthetic Industries, Chattanooga, Tennessee.

Wilson-Fahmy, R.F., Narejo, and D., Koerner, R.M., 1996, "Puncture Protection of Geomembranes Part I: Theory", Geosynthetics International, vol. 3, no. 5, pp. 605-628.

TIE-IN OF GEOSYNTHETIC SYSTEMS FOR PHASED CONSTRUCTION OF AREA FILL WASTE CONTAINMENT FACILITIES

MARTEN J. CIESLIK, P.E., DEE
FOTH & VAN DYKE, USA

MICHAEL E. DOWNS
FOTH & VAN DYKE, USA

ABSTRACT

Waste contaminant facilities which incorporate geosynthetic materials are often designed to be constructed in phases. This phased construction usually requires the connection or tie-in of the geosynthetic materials.

This paper describes the general types of tie-in details the authors have encountered and provides commentary on their constructability aspects. The paper concludes with a few general recommendations to designers from field personnel.

INTRODUCTION

The authors have observed construction of geosynthetic tie-ins on over 30 different solid waste containment facility projects involving polyethylene geomembranes throughout the Midwest over the last 15 years. The projects include both municipal solid waste and hazardous waste landfill liner and final cover system construction. This experience, with relatively short intervals (less than five years) between phases of construction of liner and final cover systems, forms the basis of our discussion of geosynthetic tie-ins presented here.

Working on these tie-ins often doing field engineering to ensure performance during their design life, has lead us to conclude that there is a lack of consistency throughout the engineering community on the design of tie-in details. It is our perception that on too many projects the tie-in detail does not receive necessary attention during the design stage. It is our intention to provide the engineering community with feedback from the field perspective, regarding important constructability aspects of effective tie-ins.

We will discuss the general types of tie-in designs we have encountered. We will then provide a commentary of what worked in the field.

LINER SYSTEM TIE-IN DESIGNS

The United States Federal regulations referred to as Subtitle "C" and Subtitle "D" which provides baseline regulation of the design of hazardous waste and municipal solid waste landfills respectively, are generally considered the catalyst which spurred the design and construction of landfills which incorporate geosynthetic elements, particularly geomembranes, in liner and final cover systems. Usually, these landfills are designed and permitted to be constructed in phases over a period of years. The containment systems of these phases (i.e., the liner and cover systems), are typically designed to be connected or tied-in.

The designs of tie-ins of area fill landfill liner systems, which the authors have experience with, generally fall into one of two types. In one there is a permanent phase separation berm that is an integral component of the liner system and in the other, the phase separation berm is not part of the liner system. The phase separation berm which is an integral part of the liner system is always a permanent berm. It is almost always incorporated into the liner system. Figure 1 illustrates the concept of a permanent phase separation berm. The geomembrane liner is placed over the berm constructed of the same material as the clay liner.

Figure 2 by contrast shows a phase separation berm which is not an integral component of the liner system. Note that the phase separation berm is above the liner system and the geosynthetic elements extend beneath and beyond the phase separation berm.

The ease of making the geosynthetic tie-in from one phase to the next is largely dependent on location of the end of the geosynthetics relative to the location of the phase separation berm.

The phase separation berm is a key element in the tie-in detail because of its role in landfill operation rather than its role during future construction. The phase separation berm is the landmark landfill operators use during filling operations to identify the edge of the fill. The phase separation berm therefore determines the proximity of the waste mass when the tie-in is made. Thus, the location and configuration of the phase separation berm is a primary design consideration of a tie-in detail.

There are a few other design considerations for tie-in details. These include:

- Protection of the edge of geosynthetics, particularly the geomembrane for effective future tie-in.
    - Geotextile wrap
    - Plywood protective layer
    - Soil cover

GEOMEMBRANE

PHASE 2 | PHASE 1

GEOTEXTILE

DRAINAGE LAYER

TOP OF CLAY
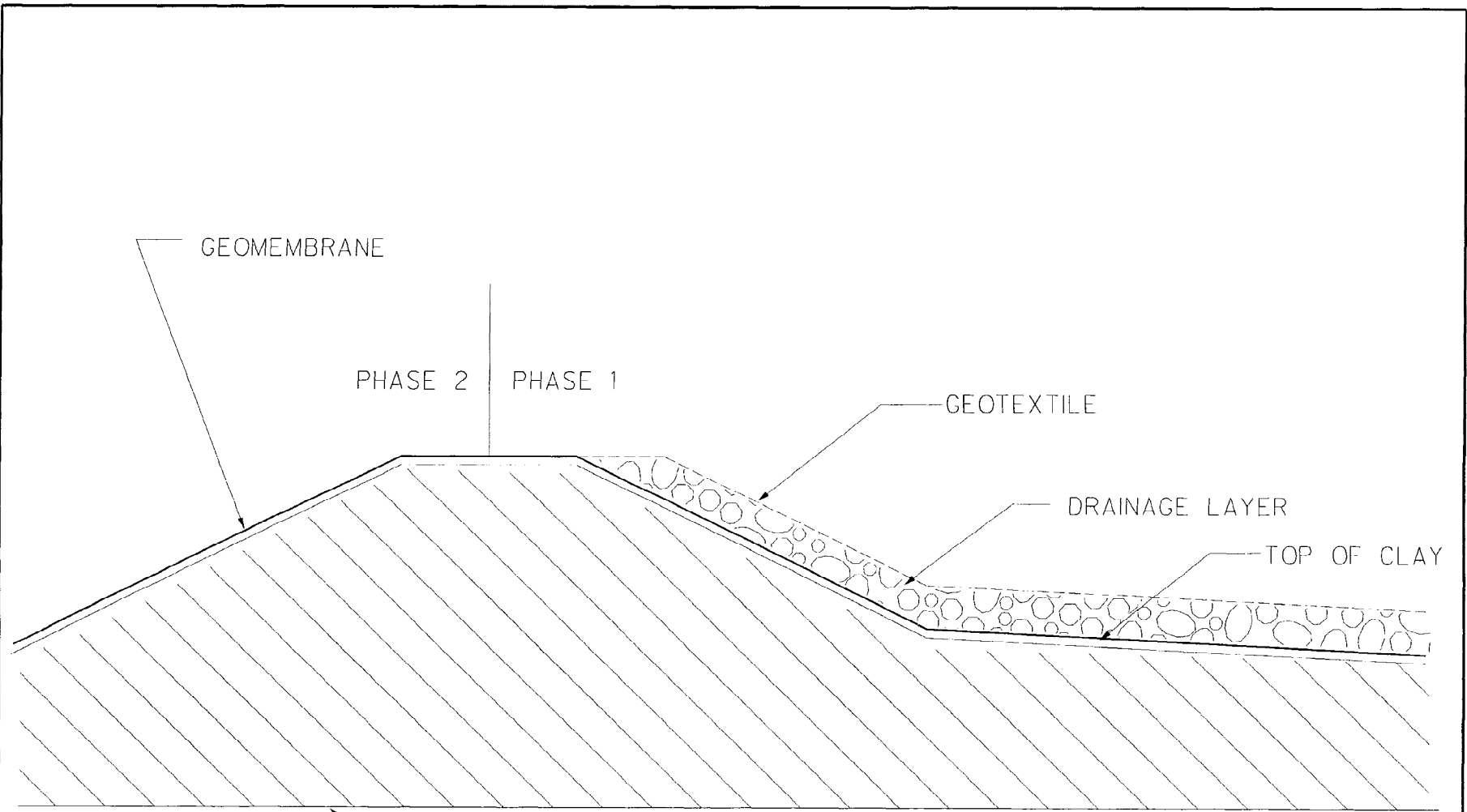
BOTTOM OF CLAY

| FIGURE 1 |
| PHASE SEPERATION BERM AS AN INTERGRAL COMPONENT TO THE LINER SYSTEM |
| Scale: NOT TO SCALE |
| Date: JULY 1998 | By: BJSI |

PHASE 2 | PHASE 1

GEOTEXTILE

GEOTEXTILE
CUSHION

PHASE
SEPERATION
BERM

SLOPE

SLOPE

LINER

GEOMEMBRANE

DRAINAGE LAYER

APPROX. 20'
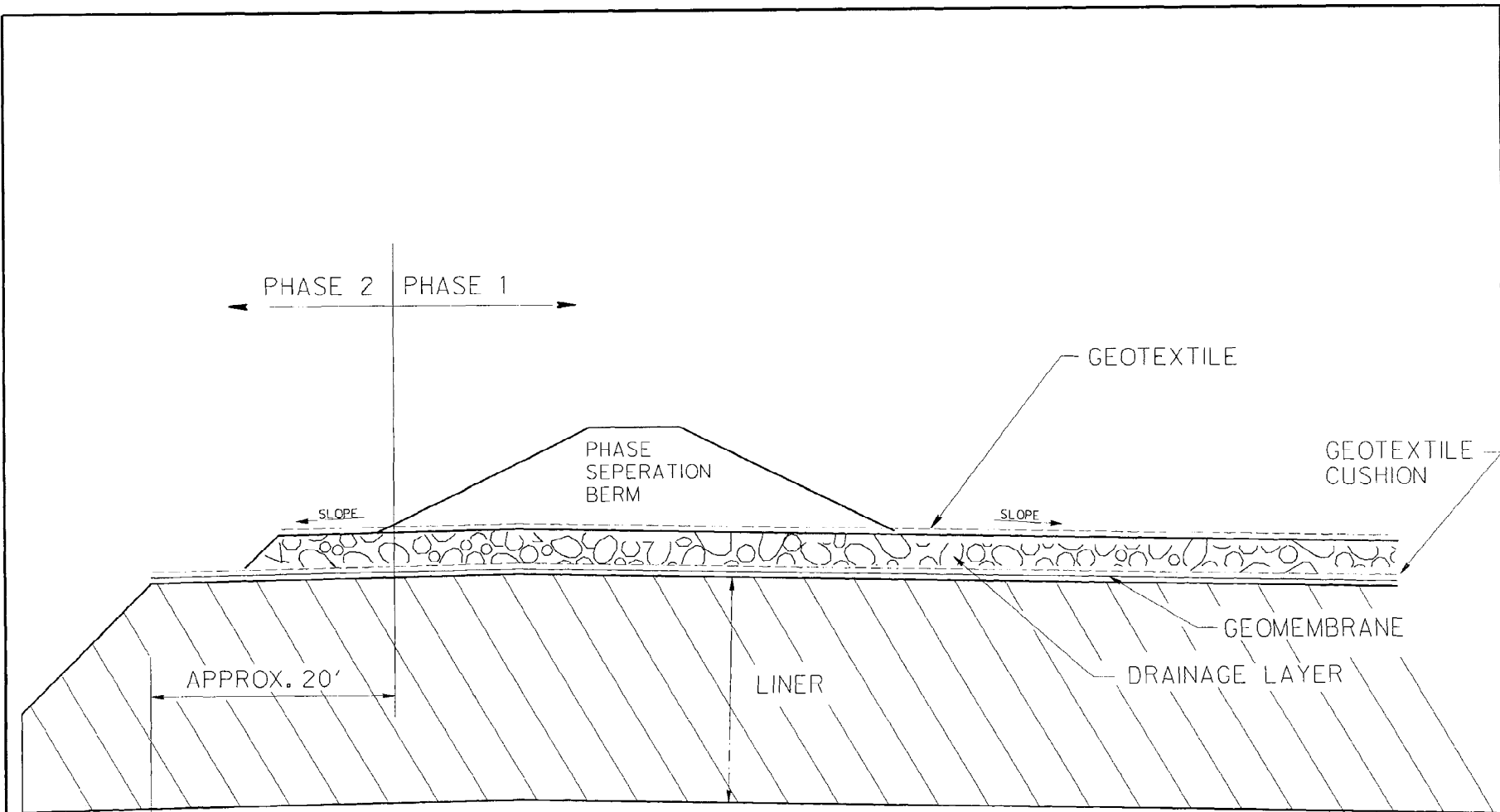
DOCUMENTED END OF CLAY LINER CONSTRUCTION

FIGURE 2

NON INTREGAL PHASE SEPERATION BERM

Scale: NOT TO SCALE

Date: JULY 1998 | By: BXJ

- Anchor trenches at the tie-in
- Surface water drainage
- Subsurface leachate drainage
- Types of geosynthetic elements
- Time separation between phase construction.

The protection of the geomembrane tie-in edge has been accomplished in a variety of ways. The authors have dealt with sites where plywood was placed over the geomembrane edge followed by a layer of soil. Figure 3 illustrates the use of plywood on the tie-in edge. The intent of the plywood is to:

1. Protect the geomembrane from damage when the edge is dug up during the construction of the subsequent phase.

2. Serve as a marker for the edge of the geosynthetics.

Geotextiles have also been used as an alternative for protection and serve as a marker along the edge of a tie-in area.

Soil cover is generally used when the time between construction of adjacent phases exceeds one year. The use of soil cover to protect a tie-in edge dictates the need for careful operation of backhoe during the subsequent exposure of the geosynthetics. Careful operation will minimize damage to the geosynthetic components.

We have dealt with designs which called for the geosynthetics to be placed in an anchor trench where there will be a subsequent tie-in. Figure 4 illustrates this type of detail. The purpose of this type of anchoring is to hold the geosynthetics in place between construction phases.

Surface water drainage is an important consideration for tie-in designs. It is important that surface water be directed away from the tie-in. Usually surface water drainage will be away from the tie-in because phases are usually separated by divides in the leachate collection drainage basins. However, surface water drainage patterns are very site specific so one cannot ignore the consideration of them, especially when designing a final cover tie-in detail.

Subsurface drainage must also be considered when locating the tie-in. The tie-in should be a at or near a high point in the leachate drainage pattern.
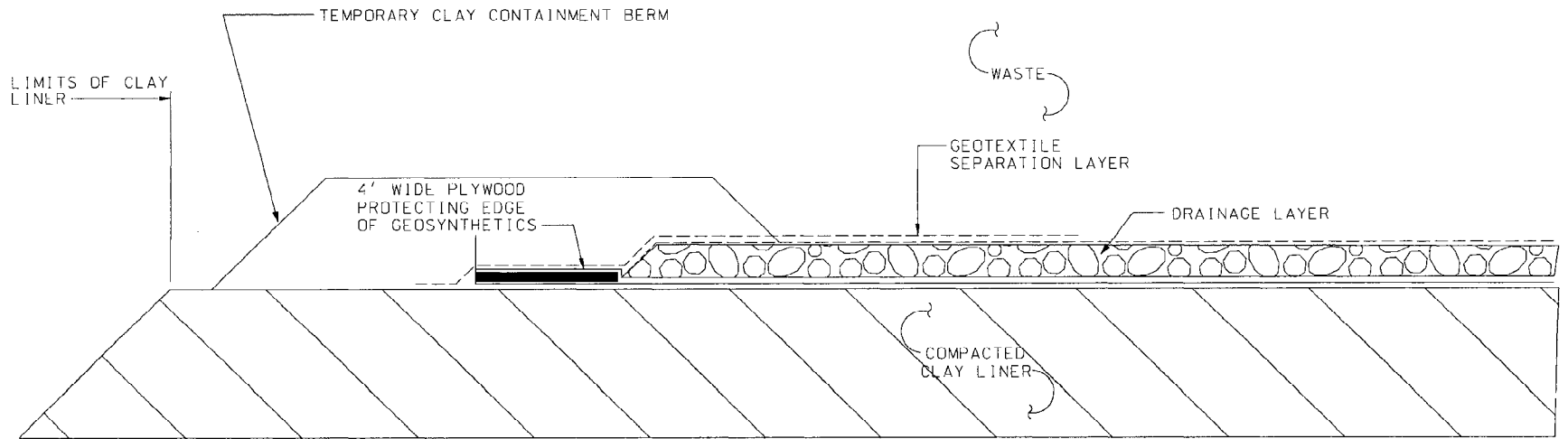
TEMPORARY CLAY CONTAINMENT BERM

LIMITS OF CLAY LINER

WASTE

GEOTEXTILE SEPARATION LAYER

4' WIDE PLYWOOD PROTECTING EDGE OF GEOSYNTHETICS

DRAINAGE LAYER

COMPACTED CLAY LINER

FIGURE 3
PLYWOOD PROTECTION
Scale: NOT TO SCALE
Date: JULY 1998	By: BJS1

PROTECTIVE LAYER

PROTECTIVE LAYER

PHASE 2 PHASE 1

GEOTEXTILE

GEONET

WASTE

GEOMEMBRANE

2'

ACTIVE PHASE

SOIL INNER LAYER

1

3

COMPACTED FILL/

IN-SITU MATERIAL

GEOTEXTILE DRAINAGE STRIP

FIGURE 4
RECORD DRAWING ANCHOR TRENCH ON PHASE SEPERATION BERM
Scale: NOT TO SCALE
Date: JULY 1998	By: BJS1

The types of geosynthetics used in a design need to be considered. Usually all of the geosynthetic elements of the design are continuous. The tie-in detail should take into account not only the geomembrane, but also the geonet, geotextiles, geosynthetic clay liners and other elements.

Finally, the layout of the tie-in needs to consider the expected time lapse between the construction of adjacent phases. If the expected time is less than one construction season, then rather minimal efforts at protecting and planning for the tie-in are needed.
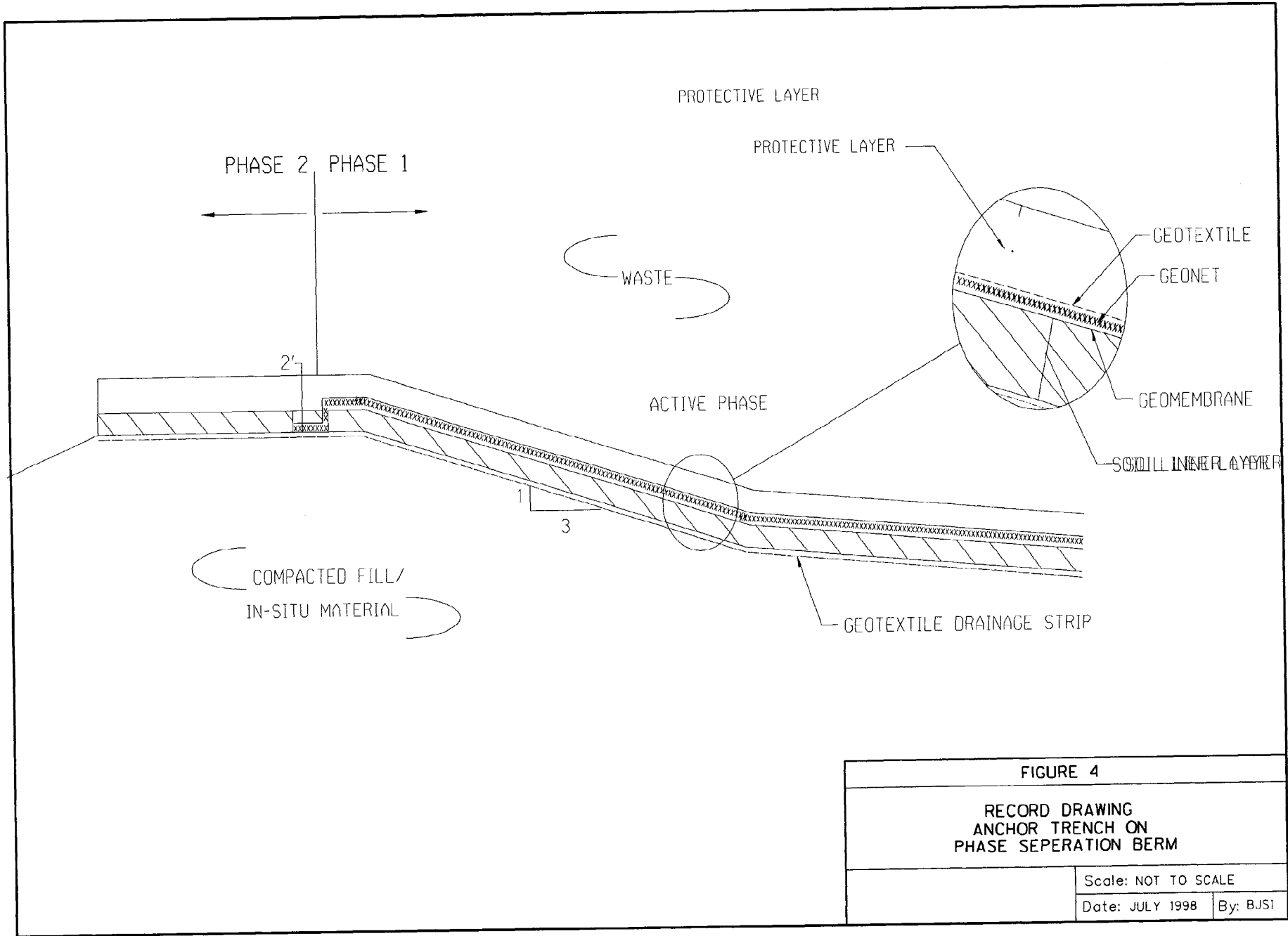
Tie-ins which will be made a year or more after the initial construction require more protection and planning.

Tie-ins which may occur decades after the initial construction are beyond the scope of this paper and the authors' experience.

FIELD EXPERIENCE COMMENTARY

The authors wish to stress that the one overriding consideration for the design community for design of the tie-in is to locate the splice some distance away from the operational area. Most of the other complications can be handled in the field if the tie-in is to occur away from the placed waste.

We have had experience at too many sites where waste had to be excavated or otherwise moved in order to expose the tie-in edge of the existing phase during the construction of the adjacent phase.

The location of the edge of the tie-in relative to the location of the phase separation berm is the single most important element of a straight-forward (meaning less costly) tie-in construction. The phase separation berm is the landmark landfill operations personnel use to identify the edge of the constructed area. Operations personnel will tend to want to fill right to the top inside edge of the phase separation berm. Thus the closer the tie-in edge is to the inside top edge of the berm, the greater the effort required to expose the edge.

We have found that from the perspective of constructability of the geosynthetic tie-in, it does not matter how the phase separation berm is built. The berm can be an integral part of the liner system as shown in Figure 1 or it can be above the geosynthetics as shown in Figure 2.

The second most important consideration for a good tie-in detail is how the geosynthetics are protected. We have found that both the use of plywood and the use of the geotextile wraps have been successful. We do not have data which indicates which type of protection is more cost effective. The effectiveness of the protection afforded by the plywood and the geotextile is

largely dependent on the care used by the backhoe operator when exposing the geosynthetics. As long as the teeth of the backhoe bucket are somehow accounted for, either by changing to a bucket without teeth or by attaching a plate or bar over the teeth either the plywood or the geotextile wrap method can be successful. We define success as minimal damage to the in-place geosynthetics caused by the act of exposing the geosynthetics.

Our experience with soil cover over the tie-in edge is that it is virtually always done. Soil is needed to keep the plywood or the geotextile wrap from blowing away. We have seen it applied to all but extremely short periods of time such as one month or less between construction of adjacent phases. We have no reason at this time to go against this conventional approach to protection of the tie-in edge.

We cannot comment on the long duration (in the decades long time frame) tie-in as we have not had experience observing the construction of phases separated by more than five years.

We do not believe that anchor trenches should be used where a subsequent tie-in will be made. We cannot say that an anchor trench is never to be needed, but we think it is the very rare case where site conditions warrant it. We take this position because we have observed that the material placed in the anchor trench is almost certainly wastes when the tie-in is made. The material in the anchor trench will either be covered over, cut off or so badly damaged by the effort to remove it from the trench that it will be worthless.

Generally, surface water drainage has not been a significant issue for liner system tie-ins. However, we have noticed surface water drainage to be an issue with final cover system phased construction. We have seen a few cases where the lower portion of the final cover slope has been constructed several years ahead of the landfill reaching its maximum height. Efforts have been lacking on the diversion of surface water drainage away from the tie-in area. Figure 5 shows the three slopes of a landfill that received final cover during the 1994 construction season. The remaining top area reached final cover in 1997. This site is an example of what we believe is an emerging tie-in construction difficulty, namely the phasing of final cover construction.

Generally, the authors have not had difficulties with leachate seepage from drainage layers during tie-in construction. We have been fortunate that the designers to have placed the phase breaks on the high points of leachate drainage basins or in upslope positions. Occasionally we have encountered situations where there is leachate seepage which must be controlled operationally.

PREVIOUSLY CAPPED
PORTION OF LANDFILL
(CAPPED IN 1994)

NEWLY CAPPED
PORTION OF LANDFILL
(CAPPED IN 1997)
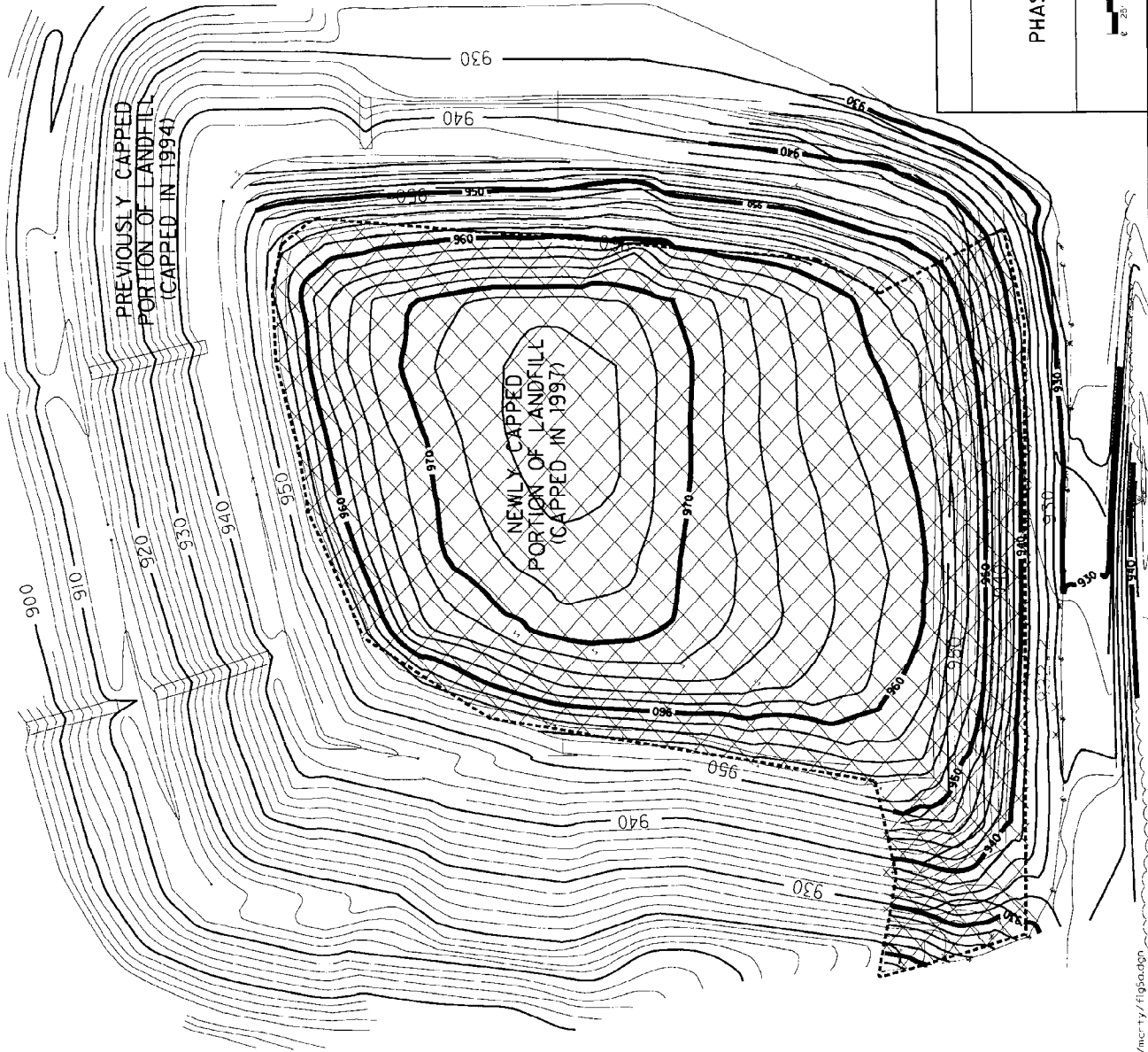
NEWLY CAPPED PORTION

TIE-IN LOCATION

FIGURE 5

PHASED FINAL COVER CONSTRUCTION

Scale: 1" = 100'
Date: NOV 1998   By: BXJ

Scale:
0 25 50 100 150

h/98dC09/mcrty/fig5a.dgn
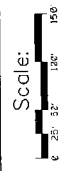
Our experience regarding the time between construction of adjacent phases is limited to several years (up to five years) and less than one year. Generally, we believe that protection schemes should be used if delay before construction of the adjacent phase is one or more years. We do not have any specific recommendations on the need for a better protective system for a one year versus a five year intervening period between construction of adjacent phases. Plywood, geotextiles and soil will be the main elements in the protective system. A tie-in protective system designed to last five years versus one year may need to have more permanent surface water and erosion control features but the essence of the geosynthetics protection will be the same and should include:

- a location marker
- protection from damage during exposure and
- a weighted edge (i.e., soil) to keep the protection in place

SUMMARY

Based on our experience spanning probably the entire time period of HDPE installation in Midwestern U.S., we would suggest the following points for consideration by landfill designers and contractors:

- Tie-in designs should be well thought-out and address site operation specifics.

- The geosynthetics should be extended some distance from the operational edge of any phase requiring tie-in with a future phase. We suggest as a starting point that designs call for the liner systems to extend 10 to 15 feet beyond the expected end of the operational areas.

- If construction of adjacent phases will extend longer than a few months, then the tie-in edge needs to be protected using plywood and/or geotextiles. Soil as a cover will also usually be needed.

- Avoid using anchor trenches on top of phase separation berms.

REFERENCES

Donohue and Associates, (January 1991) "Construction Documentation, Countywide Recycling and Disposal Facility, Cell 1".

Foth & Van Dyke, (December 1992) "Construction Documentation Module 2A, Madison Prairie Landfill".

Foth & Van Dyke, (September 1993) "Construction Documentation Module 2B, Madison Prairie Landfill".

Foth & Van Dyke, Golder Associates, Gershman, Brickner & Bratton, Inc., FEH Associates, KJWW Engineering Consultants, Inc. (January 1995). "Construction Drawings Cells 1 and 2 for Scott Area Solid Waste Landfill".

Foth & Van Dyke, (September 1996) "Record Drawings Scott Area Sanitary Landfill, Cell 1".

Foth & Van Dyke, (December 1997) "Record Drawings Scott Area Sanitary Landfill, Cell 3".

Foth & Van Dyke, (January 1998) "Record Drawings, Final Phase of Final Cover and Landfill Gas Management System, Metropolitan Refuse District New Landfill 107."

Montgomery Watson (February 1998) "1998 Project Manual, Deer Track Park Landfill."

Warzyn, (January 1992) "Construction Observation Report, Module 1B Site Preparation, Madison Prairie Landfill".

Woodward - Clyde Consultants, (March 1995) "Record Drawings, Final Cover and Landfill Gas Management System, Metropolitan Refuse District New Landfill 0107."

Rationale and Background for the GRI-GM13 Specification for HDPE Geomembranes

Y.G. Hsuan
and
R.M. Koerner
GRI, Drexel University, Philadelphia, PA

ABSTRACT

The Geosynthetic Research Institute (GRI) test method GM13 "Test Properties, Testing frequency and Recommended Warrant for High Density Polyethylene (HDPE) Geomembranes" sets forth a set of minimum properties that must be met, or exceeded, by both smooth and textured high density polyethylene (HDPE) geomembranes upon being manufactured. In some of the properties, a range is specified. In the context of quality systems and management, this specification is targeted toward manufacturing quality control (MQC).

The properties listed in this specification were obtained by testing in according to the latest standard test methods established by either the American Standard Testing and Materials (ASTM) or GRI. The unique aspect of this specification in comparison to previous HDPE specification is the requirement for long-term performance testing of the geomembranes. Three different tests are specifically designated to challenge the antioxidant package, which acts in an essential role in assurance the long-term performance of HDPE geomembranes.

This paper describes the rationale of selecting the relevant test methods and the background for establishing the specified values. Also discussed is the frequency of performing the tests and the logic of including a recommended warranty.

INTRODUCTION

High density polyethylene (HDPE) geomembranes have been used as liquid and gas barriers in geoenvironmental applications for more than 20 years. The only *generic* specification available to aid engineers was published in 1983 by the National Sanitation Foundation (NSF) as Standard No. 54. The standard provided a list of tests together with their corresponding minimum values. Although four revisions were carried out in the intervening years, the standard was still lagging behind the state-of-practice of the HDPE geomembrane industry. For example,

only smooth HDPE geomembranes were listed, and many of the specified test methods did not reflect current practice. Some of the tests were even generally considered irrelevant or inappropriate for currently manufactured HDPE material. Most importantly, the long-term performance of the material was never addressed. For a number of interrelated issues, NSF decided to withdraw from the geosynthetic industry by terminating the publication of Standard No.54 as of the end of 1997.

Considering the above situation, a completely new HDPE specification was needed. In 1996, a technical task group was formed within GRI consisting of HDPE resin suppliers and geomembrane manufacturers. The group decided that the purpose of the specification was to be directed at manufacturing quality control (MQC) of HDPE geomembranes. This infers that if an owner or specifier has unique or extenuating circumstances for a particular project, modifications in the form of a project specification can be made, however, such changes should be communicated accordingly to the manufacturer.

The new specification covers MQC considerations for both smooth and textured HDPE geomembranes. However, it does not include properties that are related to installation, such as field construction and seaming procedures, seam testing and strength, seam sampling frequency, etc. The specification also presents a recommended warranty, which is focused on the geomembrane material itself, i.e., not the installation. In addition to basic physical and mechanical properties of geomembranes, long-term performance properties are required. On the other hand, tests that were considered as being irrelevant to MQC or outdated are not included. The majority of the required properties are evaluated by test methods established by the ASTM D35 Geosynthetics Committee. In cases, where no ASTM standards are available, GRI test methods are used.

This paper explains the GRI-GM13 Specification, its rationale and background, and its uniqueness with respect to the earlier specification, i.e. NSF Standard No.54. This is particularly the case for tests that are oriented toward evaluation of the long-term performance of the geomembranes. Also, test data that support the specified value are presented. The minimum physical, mechanical, and chemical properties are listed. In a few cases, a range is specified. Finally, the reason of the recommended warranty is presented along with the actual document.

OVERVIEW OF THE SPECIFICATION

The specification covers HDPE geomembranes with a formulated sheet density of 0.940 g/ml, or greater, in the thickness range of 0.75 mm to 3.0 mm. Tables 1 and 2 are the actual specification tables with test methods, limiting values, and testing frequencies. Table 1 is for smooth HDPE geomembranes, and Table 2 is for single and double sided textured HDPE geomembranes. The respective values are presented according to seven different sheet thicknesses. The minimum testing frequencies are also defined for each required property. Most of the testing frequencies are based on the weight in units of kilograms. The reason for using kilograms instead of number of rolls is to achieve a consistent value between different sheet thicknesses and sheet widths. There are nine notes in each of the tables to further clarify the test conditions and specific requirements.

DISCUSSION OF TEST METHODS INCLUDED IN THE SPECIFICATION

Many test methods and procedures have been considered incorporation in this specification. The rationale for including/excluding specific test methods/procedures is presented below.

Excluded Tests. There are as many as sixteen tests that are occasionally included in HDPE specifications, which are omitted from this standard because they are either irrelevant, or not appropriate to be used in routine MQC testing. In this section, these tests are presented together with the reason for excluding them. Following are the tests that are *irrelevant* to the MQC of HDPE geomembranes:

- Volatile Loss – This test is performed according to ASTM D 1203, by measuring the volatile loss at 70 °C after 24 hours. However, there are no components in HDPE geomembranes that will evaporate below 100 °C. Thus, this test is irrelevant. In a thermogravimetric analysis (TGA), the onset of the weight loss at 470 °C corresponds to the decomposition of the polymer chains. Prior to that temperature, no weight loss can be measured, as shown in Halse, et al., (1991).
- Water Absorption – The test is performed according to ASTM D 471 to evaluate rubber characteristics. Due to the high crystallinity and non-polar characteristics of polyethylene, HDPE geomembranes have a hydrophobic characteristic, which has relatively low water absorption.
- Water Vapor Transmission - This test is performed according to ASTM E 96. The test is not designed to measure sheet materials with thickness like geomembranes, particularly HDPE materials. Both the thickness and relatively high rigidity of the material leads to leakage around the seal, leading to large errors in test results. In addition, the true mechanism for studying the liquid transmission through HDPE geomembrane should be diffusion, as described by Rowe et al. (1996).
- Dimensional Stability - The purpose of this test is to assess the presence of residual stress in the geomembrane. The test is conducted according to ASTM D 1204. The dimensional changes of the specimen before and after incubation in a forced air oven at 100 °C for one hour are measured. The changes are always found to be less than 1% regardless the type of manufacturing process. This indicates that the magnitude of residual stresses is relatively small in currently produced HDPE geomembranes. Such stress probably does not impose impact on either the short term or long term performance of the geomembrane. Thus, the test was felt not to be relevant.
- Coefficient Of Linear Expansion – The test is performed according to ASTM D 696 to determine the coefficient of linear expansion between –30 °C and +30 °C. The coefficient value is an intrinsic property of the HDPE material; it increases as density of the material decreases and vice versa. Furthermore, for polymeric materials, such value varies with temperature. It is important for designers to specify the temperature range and then perform the test accordingly. Under such circumstances, the test is no longer

an index test, but a performance test. Most importantly, this value has no relevance to the quality of the geomembrane.

- Resistance to Soil Burial – This test is conducted according to ASTM D 3083 to evaluate "Flexible Polyvinyl Chloride (PVC) Plastic Sheeting for Pond, Canal and Reservoir Lining". The purpose of the test is to evaluate the biodegradation of the geomembrane, specifically for the plasticizer component of PVC geomembranes. There is no plasticizer in HDPE geomembranes. Furthermore, HDPE geomembranes are made from high molecular weight polymers. The test has no relevance to the performance of HDPE geomembranes and should not be included.
- Hydrostatic Resistance – This test is conducted according to ASTM D 751 for "Coated Fabrics". The test is designed to evaluate the burst strength of reinforced geomembranes. The test is not applicable to evaluate HDPE geomembranes due to the lack of a scrim and its high strength.
- Tensile Impact – The test is conducted according to ASTM D 1822, for determining "The Tensile Impact Energy to Break Plastics and Electrical Insulating Materials". This is another index test meant to evaluate the tensile strength of the geomembrane. The unique difference between this test and other mechanical index tests is the high speed of the impacting pendulum. However, geomembranes are seldom subjected to such impacts, hence the test is irrelevant in a MQC specification.
- Brittleness Temperature – This property is measured according to ASTM D 746 to determine "The Brittleness Temperature of Plastics and Elastomers by Impact". HDPE geomembranes are not very sensitive to cold brittle fracture due to their high crystallinity. The brittleness temperature is below -100 °C. Thus, the test does not have relevance to the general usage of HDPE geomembranes. However, if extremely low temperature is to be encountered at a specific site, a complete evaluation on the mechanical behavior of the geomembrane should be performed at the lowest temperature that the site will encounter, not only the brittleness temperature.
- Various Toxicity Tests – This suite of tests is only applicable if the HDPE geomembrane is used in contact with drinking water. If such application is encountered, the geomembrane should be evaluated accordingly. (See NSF Standard No.61 in this regard.)

Following are tests that were considered to be *not appropriate* as routine MQC tests:
- Ozone Resistance – This property is required in very select applications, e.g., in possibly railroad applications. Thus, it should not be included in a general MQC specification. However, if the property is required, the test should be included as an additional requirement.
- Modulus of Elasticity – This value can be readily obtained from the tensile test according to ASTM D 638, Type IV. However, due to the nonlinear behavior of HDPE geomembranes, the measurement of elastic modulus is always subjective. A large variation can result even when using an extensiometer; hence, it was considered to be not appropriate.

- Wide Width Tensile – This test is performed according to ASTM D 4885, using a strain rate of 1 mm/min. For HDPE geomembranes, break stress and break strain are generally unable to obtain due to the height limitation of most tensile testing machines. Furthermore, the testing time is very long due to the required slow strain rate. The test should be considered as a performance test to investigate the behavior of geomembranes under plane strain conditions.
- Multi-axial Tension – This test is performed according to ASTM D 5617, and is considered to be a performance test to model out-of-plane deformation of geomembranes.
- Field Seam Strengths (Shear and Peel) – As stated in the previous section, this specification is for MQC of the manufactured sheet. It does not include any field installation related requirements.

Revised Tests. There are several tests that are considered relevant in an HDPE specification, but need to be *updated and revised* to the current ASTM standards. They are as follows:

- Environmental stress crack resistance (ESCR) – Many HDPE geomembrane specifications, have ESCR evaluated according to ASTM D 1693, the bent strip test. This test has many disadvantages, such as undefined testing stress, stress relaxation, large standard deviation, etc. Subsequently, a new stress crack resistance test, the notched constant tensile load (NCTL) test according to ASTM D 5397, was developed and adopted by the industry (Hsuan, et al. 1993). In this specification, the abbreviated version of the NCTL test, the single point-NCTL test (ASTM D 5397-Appendix), is specified to assess the material's ESCR behavior.
- Puncture Resistance – The usual test used to assess puncture resistance of HDPE geomembranes has been Federal Testing Material Standard (FTMS 101, Method 2065). The method has been depreciated since federal agencies are encouraging the use of consensus standards. ASTM D 4833 is the replacement test for the evaluation of the puncture resistance of HDPE geomembranes.
- Carbon Black Dispersion – This property has traditionally been evaluated using ASTM D 1765 for "Carbon Black Used in Rubber Products". However, the type and amount of carbon black used in rubber products are very different than those used in geosynthetics. The function of carbon black in rubber is for reinforcement as well as ultraviolet resistance, and the amount of carbon black content can be as high as 30%. Thus, the applicability of this test to the geosynthetic products is questionable. Recently, a new carbon black dispersion test was developed to evaluate geosynthetic products. It uses microtome sections viewed under a transmission light microscope at 100 magnification, and compares with reference images. This replacement test is ASTM D 5596, which is required in this specification.

New Tests. Several tests are included in this specification because they are essential in the context of current manufacturing processes, or to assess the durability of the material. The following *new tests* have been incorporated in the specification:

- Core thickness of textured sheet – A new test, ASTM D 5994, was adopted to measure the core thickness of textured HDPE geomembranes. The test uses a pair of tapered gage points, as shown in Figure 1, to probe into the valley of the texturing in order to measure the core thickness.
- Asperity height of textured sheet – For ensuring that there is a minimum roughness on the surface of textured HDPE geomembranes, an asperity height is measured. An index test, GRI-GM 12, was developed to measure the height of textured profile using a depth gauge, as shown in Figure 2.
- Oxidative induction time (OIT) – Both the standard (Std-OIT, ASTM D 3895) and high pressure (HP- OIT, ASTM D 5885) tests are included in the specification. The purpose of including two OIT tests is to provide options for manufacturers to choose the appropriate test to evaluate their specific antioxidant package. Since some of the antioxidant packages have an evaporation temperature lower than 200 °C, the Std-OIT test is not the suitable method. For those antioxidant packages, the HP-OIT test is the proper method (Hsuan and Guan, 1997).
- Oven aging – The purpose of oven aging is to challenge the long-term thermal oxidation behavior of the HDPE geomembrane. The incubation procedure is conducted according to ASTM D 5721 in forced air ovens at 85 °C for 90 days. Since the initial part of the lifetime of HDPE geomembranes is governed by the antioxidant package, use of oven aging coupled with OIT measurements provides insight into the long-term performance of antioxidant package. This directly reflects on the duration of the geomembrane, Husan and Koerner, 1998.
- Ultraviolet (UV) Resistance – For HDPE geomembranes that are exposed to sunlight during their service life, UV resistance is a major property that must be evaluated. The exposure procedure used to assess UV resistance is conducted according to GRI-GM 11 using an UV-fluorecent weatherometer. The exposure is for 1600 hours, with alternating 20 hour of UV at 75 °C followed by 4 hour condensation at 60 °C. Similar to oven aging, the stability of the antioxidant package is assessed using the OIT test. However, only the HP-OIT test should be used. A detailed discussion will be presented in the later section of the paper.

SPECIFIED MATERIAL PROPERTIES

The properties specified in Tables 1 and 2 can be divided into three categories: physical, mechanical, and endurance. Individual properties will be discussed according to each category. In addition, the frequency for conducting the tests is also defined in the tables. Testing frequency for the majority of the properties is based on weight. This is designed to make the

required testing consistent for the manufacturer regardless of the thickness, length or width of the geomembrane.

Physical Properties. This category includes thickness, asperity height, density, and melt index. It should be noted that melt index (MI) is not included in the table, but is described in the main text of the specification.

- Thickness – For all geomembranes, the nominal thickness of the geomembrane is the obvious target value. For smooth sheet, the average thickness must be the nominal value; however, the lowest individual of 10 values can be –10% due to variation of the material and testing. For textured geomembranes, the average core thickness can be 5% less than the nominal thickness of the sheet. This was a difficult decision to make and attests to the variation in blown film process, which is relatively difficult to control when aggressive texturing is required. Based on the ASTM interlaboratory test data, the coefficient of variation of core thickness for double sided textured geomembranes was ±3.6%. Regarding the lowest individual value, the lowest for eight out of ten values can be -10%, and the lowest for any of the ten values can be –15%. The ASTM interlaboratory test data showed that the lowest individual was -19% for double-sided textured geomembranes. The test frequency for this property is every roll of geomembrane.

- Asperity Height – This is an index property, and is only applicable to textured geomembranes. The property has no known correlation to the interfacial shear strength behavior of the geomembrane, e.g., as determined using ASTM D 5321 direct shear testing. Similar to the thickness test, ten measurements are required across the width of the geomembrane. The minimum average value should be 0.25 mm. Since this is new test, details of the lowest value within the ten measurements have not been established. The test frequency of this property is every second roll. If the sheet has double sided texturing, the measurement side is performed on an alternating basis.

- Density – A minimum value of 0.940 g/ml is required for the manufactured geomembrane. It should be recognized that the virgin opaque resin has a lower density value than the formulated material. An appropriate equation used to estimate resin density from formulated sheet density is listed in ASTM D 3350, and is given in Equation (1). The test frequency for density is per every 90,000 kg of resin.

$$D_r = D_p - 0.0044*C \qquad\qquad (1)$$

Where: D_r = density of resin (g/ml)

D_p = density of product (g/ml)

C = carbon black content (%)

- Melt Index – The difference between melt flow index values per ASTM D 1238 for HDPE geomembrane made from blown film versus flat extrusion methods is significant. Since both manufacturing methods are appropriate, a range was considered,

but it is so broad as not to be meaningful. Thus, a specific value is left off the tables, but included as a comment in the text of the specification.

Mechanical Properties. This category includes tensile properties, tear resistance, and puncture resistance.

- Tensile properties – The test is performed according to ASTM D 638 Type IV using dumbbell shaped specimens. Four test parameters are required: yield stress, break stress, yield elongation, and break elongation. The minimum average value of these four parameters refers to both machine and cross machine directions with 5 test specimens being required in each direction. The minimum yield stress for both smooth and textured geomembranes is 15,000 kN/m^2 and the break stress is 27,000 kN/m^2. In the specification, these values are presented in units of "kN/m" by multiplying the stress by the nominal thickness of the geomembrane. Regarding the elongation, the minimum yield elongation for smooth and textured sheets is 12% using a gage length of 33 mm. The break elongation for smooth and textured geomembranes is 700% and 100%, respectively. The gage length used to determine the break elongation is 50 mm. The relatively low break elongation for textured geomembranes is for textured sheet manufactured by blown film co-extruded texturing process. The test frequency for these tensile properties is every 9,000 kg
- Tear resistance – The minimum average tear resistance is 125 kN/m for both smooth and textured geomembranes. Data in the tables are presented in units of "N" by multiplying the above value by the nominal thickness of the geomembrane. The test frequency is every 20,000 kg.
- Puncture resistance – This value is evaluated according to ASTM D 4833. The minimum average puncture resistance is 320 kN/m. Data in the table are presented in units of "N" by multiplying the above value by the nominal thickness of the geomembrane. The test frequency is every 20,000 kg.

It should be noted that the required value for the above three mechanical properties varies linearly with thickness. It is assumed that the thickness of the geomembrane has no influence on the fundamental stress, or strength, of the geomembrane. Generally, the strength of the bulk material increases slightly with thickness due to the increase in crystallinity in bulkier products. However, the actual correlation is not well defined, and is strongly dependent on the processing method. As a conservative approach, strength values obtained from thinner geomembranes are used in the calculation for greater geomembrane thicknesses.

Endurance Properties. This category includes stress cracking resistance, carbon black content and dispersion, OIT, oven aging, and UV resistance. The majority of the properties in this category are new with respect to previous specifications. They are essential in assuring the long-term performance of the geomembrane.

- Stress cracking resistance – This property is evaluated using the SP-NCTL test. The pass/fail criterion is indicated in Table 3, according to GRI-GM10.

Table 3 – Specification for SP-NCTL test according to GRI-GM10
(F_t = failure time)

Test Condition	Yield Stress (ASTM D 638)	Number of Test Specimens	Passing Criteria	Action if Failure Criterion is not Reached
A	manufacturer's mean value via MQC testing	1	1 out 1 with $F_t > 200$ hr	Retest using condition B
B	manufacturer's mean value via MQC testing	5	4 out of 5 with $F_t > 200$ hr (noncomplying specimen with $F_t > 100$ hr)	Perform full NCTL test via ASTM D 5397 with $T_t > 100$ hr
C	Average value of five tests from the sheet sample under consideration, e.g., from MQA testing	5	4 out of 5 with $F_t > 200$ hr (noncomplying specimen with $F_t > 100$ hr)	Reject sheet(s)

The 200 hours failure time of the SP-NCTL test defined in Table 3 was deduced from data which included fourteen commercially available virgin geomembranes and seven field cracked geomembranes (Hsuan et al., 1993; Hsuan and Koerner, 1995).

- Carbon black content – The test is performed according to ASTM D 1603, with a specified range from 2 to 3 %. The 3% carbon black value is the maximum opacity level above which no significant improvement in ultraviolet resistance occurs, Accorsi. and Romero (1995). The specification also allows other testing methods, such as ASTM D 4218 (muffle furnace) or the microwave technique to evaluate carbon black content if an appropriate correlation to D 1603 can be established.
- Carbon black dispersion – The specification for this property is based on viewing ten microtome slides, which are taken from various locations along of the width geomembrane. The image that is observed under 100x of a transmission light microscope is compared with patterns that are shown on the reference chart. All ten views should be in Category 1 or 2 to assure the uniformity of the carbon black in both dispersion and distribution.
- OIT – Either the Std-OIT test or the HP-OIT test can be used to evaluate this property. The purpose of permitting either test is to allow for the selection of the appropriate test for the particular antioxidant package used in the formulation. Certain antioxidant packages are not suitable to be evaluated by Std-OIT (Thomas and Ancelet, 1993; Hsuan and Guan, 1997).

Since these two OIT tests are relatively new, a GRI interlaboratory test program was undertaken in order to establish the variability of the test and to determine the typical OIT values for current commercially available geomembranes. Eight HDPE geomembranes were included in the test program. Three were smooth and five were textured geomembranes. They all contained different antioxidant packages. The thickness of the geomembranes was 1.0 mm. Five laboratories participated in the testing. The result of the Std-OIT testing is shown in Table 4. Samples A to F, show a Std-OIT value range from 115 to 183 minutes. The coefficient of variation of these six samples ranges from 6% to 16%. It should be recognized that this percentage incorporates the variability of the material, test and equipment. Since the majority of the tested geomembranes (the notable exceptions being G and H) shows a Std-OIT value above 100 minutes, the value of 100 minutes was selected to be the minimum required value for Std-OIT. For perspective, an antioxidant package of a HDPE geomembrane with Std-OIT value of 80 minutes was predicted to have a lifetime of 200 years at 20°C under soil burial conditions (Hsuan and Koerner, 1998). Thus, the 100 minute seems to be acceptable for a screening test, although the long-term performance of the antioxidant must be assessed using an aging procedure, which will be discussed later.

Table 4 – Std-OIT values (in minutes) obtained from different laboratories

Sample	Std-OIT Value from Different Laboratories					Average OIT	Variation Coefficient (%)
	Lab. 1	Lab. 2	Lab. 3	Lab. 4	Lab. 5		
A (S)	132	126	116	134	127	127	6
B (T)	134	108	99	117	119	115	11
C (T)	187	126	162	167	194	167	16
D (S)	202	175	174	201	165	183	9
E (T)	198	129	176	199	189	178	16
F (S)	182	176	162	156	184	172	7
G (T)	64	42	54	73	60	59	20
H (T)	61	45	52	70	57	57	17

Note: S = smooth sheet
T = textured sheet

For Samples G and H, their Std-OIT values are well below 100 minutes. There are two possibly reasons causing such low values. One is an insufficient amount of antioxidant. The other is the particular type of antioxidant package, which may not be suitable to be evaluated by the Std-OIT test. Under this situation, the HP-OIT test should be performed on these materials to verify the cause.

For the HP-OIT test, there were only two laboratories involving in interlaboratory testing. The results are shown in Table 5. The two sets of data are very similar, however, the variability of the test and material cannot be quantified based on the sparse data. Samples A to F show the HP-OIT value ranging from 334 to 1068 minutes. The

HP-OIT to Std-OIT ratio for five out of six geomembranes is in the range of 2.5 to 3.3, not considering samples C, G, and H. This seems to suggest that the five geomembranes may contain similar antioxidant types but of different proportions. The antioxidants are probably a blend of phosphites and hindered phenols, since similar ratio values were observed in HDPE geomembranes that contain similar antioxidant packages (Hsuan and Guan, 1997). In contrast, a high HP/Std-OIT ratio is obtained in Samples C, G, and H, due to their high HP-OIT values. Thus, these three geomembranes are most likely to contain different types of antioxidant package than the other five, but not necessary the same among them.

Table 5 – HP-OIT values (in minutes) and HP/Std OIT ratio

	HP-OIT Value		Average HP-OIT	Average Std-OIT	HP/Std Ratio
	Lab. 1	Lab. 4			
A (S)	331	336	334	127	2.6
B (T)	335	333	334	115	2.9
C (T)	1195	940	1068	167	6.4
D (S)	520	512	516	183	2.8
E (T)	593	575	584	178	3.3
F (S)	436	428	432	172	2.5
G (T)	269	292	281	59	4.8
H (S)	275	258	267	57	4.7

Note: S = smooth sheet
        T = textured sheet

Before establishing the minimum HP-OIT value, the purpose of including the HP-OIT test should be clarified. It is to provide an alternative test for evaluating antioxidant packages that are sensitive to the high testing temperature used in the Std-OIT test, e.g., the situation occurring in Samples C, G, and H. The minimum required value must be higher than the HP-OIT value that is obtained from the antioxidant package with Std-OIT of 100 minutes. Thus, the HP-OIT value was determined by multiplying 100 minutes by the average HP/Std-OIT ratio of five geomembranes that contain phosphites and hindered phenols. The average HP/Std-OIT ratio is 2.8, which results in a HP-OIT value of 280 minutes. Since the specification value must be higher than that, it was arbitrarily agreed to use 400 minutes. Geomembranes that pass Std-OIT test most likely will not pass the HP-OIT test. Furthermore, there is no known correlation between the proposed Std-OIT and HP-OIT values. However, geomembranes must pass one of the two OIT requirements. Based on the specified value, geomembrane samples G and H do not fulfill the OIT requirement due to an insufficient amount of antioxidants. The frequency of OIT testing (by either method) is every 90,000 kg same as the density.

- Oven aging – The OIT value discussed above is designed as an index test to verify the existence of the amount of antioxidant. In itself, it does not reflect on long-term performance of the antioxidant insofar as the lifetime of the geomembrane. A performance challenge to the antioxidant package is required to ensure the durability of the geomembrane. For assessing the thermal-oxidation of the antioxidants, the forced air oven aging is a simple and consistent incubation environment, although it is recognized that such environment does not simulate true field conditions. The temperature of the oven is elevated to 85°C in order to shorter the testing duration. Incubated samples are retrieved after 90 days for OIT measurement. The percent-retained value cannot be less than 55% for Std-OIT or 80% for HP-OIT testing. These values are established based on data from the GRI interlaboratory test program described in the previous section. Four laboratories participated in the 90 day incubation study for the Std-OIT test. The results are shown in Table 6. The average OIT retained value is 65% regardless the type of antioxidant package. The lowest measured value is 56%. Thus, the specification value was set at a minimum retained value of 55%.

Table 6 – Std-OIT retained percent values in 85°C forced air oven after 90 days

Sample	Std-Retained Values form Different Labs (%)				Average Retained (%)
	Lab. 1	Lab. 2	Lab. 3	Lab. 4	
A (S)	68	54	47	54	56
B (T)	61	54	60	56	58
C (T)	75	58	63	60	64
D (S)	70	57	67	60	64
E (T)	75	84	67	55	70
F (S)	66	56	71	53	62
G (T)	83	94	73	75	81
H (T)	75	56	61	72	66
Note: S = smooth sheet			Average Retained (%)		65
T = textured sheet			Coefficient of Variation		12%

For the HP-OIT test, only one laboratory was involved. The results are shown in Table 7. The average value is 85%. However, since only one laboratory participated, a more conservative value was set in the specification, i.e., 80% minimum OIT retained. It should be noted that the Sample C is below the specified HP-OIT value, but passes the Std-OIT value. The antioxidant package of this geomembrane probably contained thiosynergists (sulfate compounds) which exhibit a rapid decrease of HP-OIT value in the early stage of incubation, but then stay constant (Hsuan and Guan, 1997) For this antioxidant package, a Std-OIT is the more appropriate test method.

Table 7 – HP-OIT retained percent values in a 85oC forced air oven after 90 days

Sample	HP-OIT Retained (%)
A (S)	89
B (T)	88
C (T)	50
D (T)	95
E (T)	89
F (S)	91
G (T)	89
H (S)	91
Average	85

Note: S = smooth sheet
T = textured sheet

Ultraviolet (UV) resistance – For exposed geomembranes, the material's UV resistance is obviously a critical property. The UV-fluorescent weatherometer was selected to simulate UV degradation of the geomembrane. Such devices are simple to use, small in size, require little maintenance and are relatively inexpensive, e.g. with respect to the Xenon arc weatherometer. The incubation condition per GRI-GM11 requires 20 hours UV cycle at 75°C followed by 4 hours condensation at 60°C. The incubation duration of the exposure is 1600 hour elapsed machine time. Three laboratories completed the Std-OIT test, and two the HP-OIT test. The results indicate that the Std-OIT gives extremely variable percentage retained values, as shown in Table 8. In contrast, (with the exception of C) the HP-OIT retained values are more well behaved. It is suspected that antioxidants may have their structure altered under UV exposure, subsequently becoming more sensitive to the high testing temperature used in the Std-OIT test. A detailed investigation on the chemical structure of the antioxidants is required to fully understand the mechanisms involved. In the meantime, only the HP-OIT is recommended to be used in the UV resistance test. The average HP-OIT retained value was initially set at 60%, however, there is a large different in each of the tested geomembranes between the two sets of data. The variability is probably caused by the inconsistency of UV incubation. Thus, the minimum retained percentage is redefined at 50%. Similar to the oven aging, Sample C shows a very low HP-OIT value,17%. The value remained unchanged even after 2400 hr incubation. This unique HP-OIT response of the thiosynergist type of antioxidants must be carefully examined. Geomembranes that contain this type of antioxidant package typically show a HP-OIT/Std OIT ratio ranging from 6 to 9. If this type of geomembrane could not pass the specification, a long-term mechanical test should be provided to indicate the performance longitivity of the material.

Table 8 – Std-OIT and HP-OIT percent retained values after incubation
in the UV weatherometer for 1600 hours.

Sample	Std-OIT Retained Value (%)			HP-OIT Retained Value (%)	
	Lab. 1	Lab. 2	Lab. 3	Lab. 1	Lab. 2
A (S)	46	57	15	86	84
B (T)	9	13	12	64	44
C (T)	10	12	6	17	18
D (S)	29	16	9	73	67
E (T)	37	13	14	75	62
F (S)	20	13	11	80	64
G (T)	7	12	19	39	52
H (S)	14	34	16	71	91
Average	22	21	13	63	60

Note: S = smooth sheet
T = textured sheet

WARRANTY

The issue of material warranties accompanying a geomembrane specification is somewhat adopted from the roofing industry. Roofing membranes in flat roofs are usually exposed to the site-specific environment. As such, UV light, coupled with high temperature, must be accommodated. These two factors are arguably the most aggressive actions that cause the degradation of polymeric materials. Clearly, a 20-year warranty on a roofing membrane (and by logical extension to exposed geomembranes in applications like uncovered reservoir liners, canal liners, and floating covers) is a worth pursuit. The vast majority of geomembranes, however, are covered and backfilled. Twenty year warranties do not even begin to challenge the potential lifetime for HDPE geomembrane durability. Depletion of antioxidants alone should reach 200 years depending on site temperature, and this is only the first stage in the aging process, e.g., see Hsuan and Koerner, 1998. Thus, to request a 20 year warranty from a HDPE geomembrane manufacturer is clearly within the materials capability and represents a questionably relevant document at best. Quite possibly, it also represents a financial burden to the manufacturer from an insurance perspective.

(Far better than a material warranty would be an extended installation warranty which places a emphasis on both construction quality control (CQC) and construction quality assurance (CQA) organizations and personnel.) Nevertheless, owners/specifiers/regulators continue to request material warranties, and the GRI-GM13 specification contains a recommended material warranty in its appendix. The suggested time period is for 5-year, which represents a compromise between having a document for archieval purposes and a minimum financial burden with respect to insurance costs on the part of the manufacturer.

SUMMARY AND CONCLUSION

With HDPE geomembranes (as with all geosynthetics) material modifications and upgrading by the manufacturing/resin/additive community is an ongoing process. As such, any specification must be reviewed and modified (as required) on a regular basis. GRI-GM13 requires such a review every 24-months, or earlier. The information presented in this paper represents the original document dated June 1997, as well as the first review (15 months later) in September, 1998. This first review resulted in six relatively minor changes from the original.

To the authors' knowledge, all North American (and most worldwide) HDPE geomembrane manufacturers can produce HDPE geomembranes in accordance with this specification. In order for the specification to be fully effective, however, the owner/specifier/regulatory communities must adopt and require its use. To be sure, the relative rigidity of the test methods, test values, and frequency of testing is more stringent than past generic specifications or even individual manufacturers specifications. However, if the balance of relevant test methods, achievable property values, and appropriate long-term performance is the goal of a HDPE geomembrane user, GRI-GM 13 should be seriously considered for adoption and use.

ACKNOWLEDGMENTS

This specification represents the combined efforts of the HDPE resin and HDPE geomembrane manufacturer organizations over the course of 4-years during which numerous meetings were held. The authors sincerely appreciate the participant's efforts and congratulate them in the development of this specification. Sincere appreciate is also extend to all of the GRI members, in particular owners/consultants/government agencies, and test laboratories, for reviewing and commenting upon the specification. The authors would like to thank Mr. Rick Thiel, Thiel Engineering for providing the thickness data of textured geomembranes from the ASTM interlaboratory program, of which he is the task group leader.

REFERENCES

Accorsi, J. and Romero, E. (1995) "Special Carbon Black for Plastics", Plastics Engineering, April'95, pp. 29-32.

Halse, Y., Wiertz, J., Rigo, J-M. and Cazzuffi, D.A. (1991), "Chemical Identification Methods used to Characterize Polymeric Geomembranes," Geomembranes Identification and Performance Testing, Report of Technical Committee 103-MGH, *Mechanical and Hydraulic testing of Geomembranes*, RILEM, Edited by Rollin, A. and Rigo, J-M., Chapman and Hall, pp. 316-336.

Hsuan, Y. and Koerner, R.M. (1993), "Stress Cracking Resistance of High Density Polyethylene Geomembranes," ASCE, Journal of Geotechnical Engineering, Vol. 119, No. 11, pp. 1840-1858.

Hsuan, Y. and Koerner, R.M. (1995), "The Single Point-Notched Constant Tension Load Test: A Quality Control Test for Assessing Stress Crack Resistance," Geosynthetics International, Vol. 2, No. 5, pp. 831-843.

Hsuan, Y. and Koerner, R.M. (1998), "Antioxidant Depletion Lifetime in High Density Polyethylene Geomembranes," Journal of Geotechnical and Geoenvironmental Engineering, Vol. 124, No. 6, pp. 532-541.

Hsuan, Y. and Guan, Z. (1997), "Evaluation of the Oxidation Behavior of Polyethylene Geomembranes Using Oxidative Induction Time Tests," Oxidative Behavior of Materials by Thermal Analytical Techniques, ASTM STP 1326, A.T. Riga and G.H. Patterson, eds., ASTM, pp. 76-90.

Thomas, R.W. and Ancelet, C.R. (1993), "The effect of Temperature, Pressure, and Oven Aging on the high-pressure Oxidative Induction Time of Different Types of Stabilizers", Geosynthetics '93 Conf. Proc., IFAI, St. Paul, Minn, pp. 915-924.

Rowe, R.K., Hrapovic, L. and Armstrong, M.D. (1996) "Diffusion of Organic Poluutants Through HDPE Geomembrane and Composite Liners and Its Influence on Groundwater Quality", *proceedings 1st European Geosynthetics Conference*, Maastricht, Oct., pp. 737-742.